ALFRED-WEGENER-INSTITUT
HELMHOLTZ-ZENTRUM FÜR POLAR- UND MEERESFORSCHUNG

703
2016

Berichte
zur Polar- und Meeresforschung

Reports on Polar and Marine Research

The Expedition PS94 of the Research Vessel POLARSTERN to the central Arctic Ocean in 2015

Edited by
Ursula Schauer
with contributions of the participants

HELMHOLTZ GEMEINSCHAFT

Die Berichte zur Polar- und Meeresforschung werden vom Alfred-Wegener-Institut, Helmholtz-Zentrum für Polar- und Meeresforschung (AWI) in Bremerhaven, Deutschland, in Fortsetzung der vormaligen Berichte zur Polarforschung herausgegeben. Sie erscheinen in unregelmäßiger Abfolge.

Die Berichte zur Polar- und Meeresforschung enthalten Darstellungen und Ergebnisse der vom AWI selbst oder mit seiner Unterstützung durchgeführten Forschungsarbeiten in den Polargebieten und in den Meeren.

Die Publikationen umfassen Expeditionsberichte der vom AWI betriebenen Schiffe, Flugzeuge und Stationen, Forschungsergebnisse (inkl. Dissertationen) des Instituts und des Archivs für deutsche Polarforschung, sowie Abstracts und Proceedings von nationalen und internationalen Tagungen und Workshops des AWI.

Die Beiträge geben nicht notwendigerweise die Auffassung des AWI wider.

Herausgeber
Dr. Horst Bornemann

Redaktionelle Bearbeitung und Layout
Birgit Reimann

Alfred-Wegener-Institut
Helmholtz-Zentrum für Polar- und Meeresforschung
Am Handelshafen 12
27570 Bremerhaven
Germany

www.awi.de
www.reports.awi.de

The Reports on Polar and Marine Research are issued by the Alfred Wegener Institute, Helmholtz Centre for Polar and Marine Research (AWI) in Bremerhaven, Germany, succeeding the former Reports on Polar Research. They are published at irregular intervals.

The Reports on Polar and Marine Research contain presentations and results of research activities in polar regions and in the seas either carried out by the AWI or with its support.

Publications comprise expedition reports of the ships, aircrafts, and stations operated by the AWI, research results (incl. dissertations) of the Institute and the Archiv für deutsche Polarforschung, as well as abstracts and proceedings of national and international conferences and workshops of the AWI.

The papers contained in the Reports do not necessarily reflect the opinion of the AWI.

Editor
Dr. Horst Bornemann

Editorial editing and layout
Birgit Reimann

Alfred-Wegener-Institut
Helmholtz-Zentrum für Polar- und Meeresforschung
Am Handelshafen 12
27570 Bremerhaven
Germany

www.awi.de
www.reports.awi.de

Titel: Rückkehr zum Schiff nach der Installation von Atmosphären-, Eis- und Ozeanobservatorien auf einer Eisscholle (Foto: Mario Hoppmann, AWI)

Cover: Return to the ship after installing atmosphere, sea ice, and ocean observatories on an ice floe (Photo: Mario Hoppmann, AWI)

The Expedition PS94 of the Research Vessel POLARSTERN to the central Arctic Ocean in 2015

Edited by

Ursula Schauer

with contributions of the participants

Please cite or link this publication using the identifiers
hdl:10013/epic.48723 or http://hdl.handle.net/10013/epic.48723 and
doi:10.2312/BzPM_0703_2016 or http://doi.org/10.2312/BzPM_0703_2016

ISSN 1866-3192

PS94

17 August 2015 - 15 October 2015

Tromsø - Bremerhaven

Chief Scientist
Ursula Schauer

Coordinator
Rainer Knust

Contents

1. ZUSAMMENFASSUNG UND FAHRTVERLAUF

Ursula Schauer (AWI)

Die Expedition PS94 diente der Erfassung der physikalischen, biologischen und chemischen Veränderungen im Arktischen Ozean und war damit ein „Trans-Arctic survey of the Arctic Ocean in transition“ (TransArc II). Der seit Jahrzehnten andauernde Rückgang des mehrjährigen Meereises ist verknüpft mit Änderungen in der Ozeanzirkulation und damit mit Änderungen im Wärme- und Süßwasserhaushalt, mit Folgen für den Gasaustausch zwischen Ozean und Atmosphäre, für die biogeochemischen Stoffumsätze und für das Leben von Organismen im Eis, in der Wassersäule und am Meeresboden.

Um Prozesse mit mehrjähriger Variabilität von langfristigen Trends unterscheiden zu können, erfassen wir im Abstand von mehreren Jahren die regionale Verteilung der wichtigsten Komponenten des Systems Arktischer Ozean. Acht Jahre nach dem Internationalen Polarjahr IPY 2007/2008 und vier Jahre nach TransArc (I) wurde mit TransArc II die dritte großskalige Zustandsaufnahme des eurasischen Sektors der Arktis durchgeführt.

Konkretes Ziel unseres Messprogramms war es festzustellen, ob die Advektion von immer wärmerem Wasser aus dem Atlantik und dem Pazifik weiter anhält und inwieweit dies im Zusammenhang mit dem Eisrückgang steht; ob die Akkumulation von Süßwasser in der Arktis, die über Jahrzehnte andauerte, und die damit verbundene Strukturänderung der Deckschicht jetzt einen Wendepunkt erreicht haben; ob neben der Ausdehnung auch die Dicke des Meereises weiter zurückgeht. Parallel wurden die Veränderungen in der Zusammensetzung des Phytoplanktons in Eis und Wasser untersucht und eine Bestandsaufnahme des Zooplanktons vorgenommen. PS94 stellte auch einen zentralen Beitrag zum internationalen Programm GEOTRACES dar, das zum Ziel hat, weltweit die Verteilung von Spurenstoffen und von ihren Isotopen im Ozean zu bestimmen um ihren Kreislauf zu verstehen. Die Arbeiten von GEOTRACES waren eng verknüpft mit Untersuchungen zu Prozessen, die biogeochemische Stoffkreisläufe in Eis und Wasser bestimmen. *In situ*-Messungen der Beschaffenheit und der Dicke des Meereises dienten auch der Validierung von Fernerkundungsdaten, u.a. der CryoSat2-Mission.

Wir haben dazu Messstationen entlang von mehreren langen Transekten im eurasischen Teil der Arktis durchgeführt, die von der Barentssee, bzw. dem Gakkelrücken bis ins Makarowbecken reichten (Abbildung 1.1). Auf Schiffs-, Helikopter- und Eisstationen haben wir *in-situ*-Messungen durchgeführt und Eis-, Wasser- und Bodenproben gewonnen. Um die räumliche und die zeitliche Abdeckung über die reine Forschungsfahrt hinaus zu erweitern brachten wir zahlreiche autonome Messsysteme aus. Auf Eisschollen installiert, driften diese mit dem Eis und nehmen dabei über die kommenden Monate bis Jahre eine Vielzahl von Eis-, Wasser- und zum Teil auch atmosphärischen Parametern auf und übertragen die Informationen per Satellit an Land. Zwei am Boden verankerte Messsysteme werden die saisonale Entwicklung von Zirkulation, Hydrographie und Partikelfluss registrieren und zum ersten Mal in der zentralen Arktis oberflächennah Wasserproben in wöchentlicher Abfolge gewinnen, die nach der Aufnahme der Verankerung im Sommer 2016 im Labor auf die saisonale Nährstoffentwicklung untersucht werden.

Während der gesamten Fahrt außerhalb nationaler ausschließlicher Wirtschaftszonen wurde mit dem Fächerlot der Meeresboden vermessen, um die bathymetrische Datenlage in der Arktis zu verbessern.

Neben GEOTRACES (www.geotraces.org/), war TransArc II ein Beitrag zu den internationalen Programmen IABP (http://iabp.apl.washington.edu/index.html), ASOF (http://asof.awi.de/), Arctic ROOS (http://arctic-roos.org/), Transdrift (www.transdrift.info) und ART (http://oceanrep.geomar.de/10151/), sowie zum nationalen Programm RACE (http://race.zmaw.de/). Darüber hinaus trug TransArc II zur Implementierung des Infrastrukturprogramms FRAM (Frontiers in Arctic Monitoring) der Helmholtz-Gemeinschaft Deutscher Forschungszentren (HGF) bei.

Während der gesamten Fahrt in der zentralen Arktis behinderten schwierige Eisbedingungen durch bis zu 100%ige Eiskonzentration und Neueisbildung, kombiniert mit einer zunehmend dicken Schneedecke, das Fortkommen; zusätzlich schränkten der häufige Schneefall und schlechte Sicht die helikoptergestützten Arbeiten stark ein.

Ein Höhepunkt der Fahrt war das Treffen mit dem US-amerikanischen Küstenwachschiff *Healy* am Nordpol am 7. 9. 2015. Auch die *Healy* war für das GEOTRACES-Programm unterwegs und durch das Treffen konnten wir eine Interkalibrationsstation genau am Nordpol durchführen.

Die Reise war gegenüber der ursprünglichen Planung durch zwei weitere Faktoren beeinflusst:

1. Die Transekte waren eigentlich bis in die Kara- und Laptewsee geplant, um den Austausch zwischen Schelfmeeren und tiefen Becken zu erfassen. Da uns die russischen Behörden keine Genehmigung zur Forschung in der russischen ausschließlichen Wirtschaftszone erteilten, konnten wir unser Forschungsprogramm in der Kara- und Laptewsee gar nicht und im Nansenbecken nur eingeschränkt durchführen.

2. Durch einen medizinischen Notfall musste das Programm vor Ostsibirien am 24.9. 2015 abgebrochen und durch ein Alternativprogramm ersetzt werden.

TransArc II begann am 17. August 2015 in Tromsø. In der zentralen Barentssee begann die Benthosgruppe mit zwei Multicorerstationen einen Schnitt entlang 30°E, der nach Norden mit einer Folge von CTD/Rosettenstationen fortgesetzt wurde. Zwischen den Stationen wurde vom fahrenden Schiff aus kontinuierlich eine Underway-CTD eingesetzt, mit der auch ein kurzer zonaler Schnitt über den Viktoria-Trog gefahren wurde. Auf dem Kontinentalhang bei 81°N versuchten wir, eine Verankerung für das Norwegian Polar Institute aufzunehmen. Da wir kein akustisches Signal empfingen, lösten wir die Verankerung nicht von ihrem Grundgewicht und brachen die Aufnahme ab.

Bei 81°N erreichten wir die Eiskante, aber erst bei 83°43'N war das Eis stabil genug für eine Eisstation. Ein anhaltendes Hoch am Nordpol und niedrige Temperaturen mit Neueisbildung sorgten schnell für erste Eispressungen. So entschlossen wir uns bei 84°24'N, den Schnitt auf 30°E abzubrechen und nach Osten zu dampfen um bei 60° E unseren Kurs nach Norden wieder aufzunehmen. Allerdings wurden die Eisbedingungen nicht viel besser und in der Folge mussten auch weitere Schnitte verkürzt werden.

Am 29.8. setzten wir im Amundsenbecken bei 85°18'N die erste von zwei Verankerungen aus. Am 2.9. folgte die zweite Aussetzung in der Spalte des Gakkelrückens bei 87°1'N, 59°15'E in unmittelbarer Nähe einer hydrothermalen Quelle. Den Ausstrom aus dieser Quelle beprobten wir für alle Parameter des GEOTRACES-Programms. Auf den folgenden Eisstationen setzten wir nun auch verschiedene Messsysteme aus, die mit dem Eis driftend über das ganze Jahr Daten aus Atmosphäre, Eis und Ozean liefern.

Dem Nordkurs entlang 60°E folgend, erreichten wir am 7. 9. 2015 den Nordpol. Einige Tage zuvor hatte sich herausgestellt, dass gleichzeitig auch die US-amerikanische *Healy* im Rahmen ihres wissenschaftlichen Programms am Nordpol arbeiten würde, so dass wir das große Glück hatten, uns dort zu begegnen. *Polarstern* machte an der gleichen Eisscholle wie die *Healy* fest, Wissenschaftler und Mannschaft besuchten mit großem Interesse das jeweils andere Schiff und wir nutzten diese einmalige Chance, um am Nordpol synchron eine Interkalibrationsstation für GEOTRACES durchzuführen.

Nach dem Treffen folgten wir dem Kurs auf 120°W ein Stück weit ins Makarowbecken hinein, um hier das untere Ende der sogenannten Transpolaren Drift zu beproben, die Eis und Flusswasser aus den sibirischen Schelfmeeren quer durch die Arktis in Richtung Nordatlantik transportiert. Aber wegen zu starken Eisdrucks änderten wir am 11. 9. den Kurs nach Westen in Richtung Sibirien. Der nächste Wegpunkt, 87°30'N 180°E, war eine weitere, diesmal weit im Voraus geplante Interkalibrationsstation für GEOTRACES im Makarowbecken; danach ging es zurück zum Gakkelrücken, um von dort die Aufnahme des eurasischen Teils der Arktis auf einem Schnitt im sibirischen Teil des Amundsenbeckens und am Lomonossowrücken abzurunden.

Ein Schnitt über den Kontinentalhang der Ostsibirischen See und anschließend auf dem Schelf westwärts in die Laptewsee sollte das Programm im Quellgebiet der Transpolaren Drift abschließen. Diesen Plan mussten wir wegen eines medizinischen Notfalls an Bord aufgeben und unmittelbar nach Tromsø aufbrechen.

Nachdem der Patient in Tromsø abgeliefert worden war, starteten wir in Richtung Grönlandsee um zwei Gleiter zu bergen. Die Gleiter sollten ursprünglich von dem Forschungsschiff *Heincke* aufgenommen werden, was aber aufgrund eines Sturmtiefs und der durch Abwettern bedingten Zeitknappheit für die *Heincke* mit großem Risiko behaftet war. Ohne die Bergung durch *Polarstern* wären die Gleiter möglicherweise verloren gewesen. Anschließend konnten wir zwischen Norwegen und Spitzbergen einen Schnitt durchführen, der ein essentieller Beitrag zum internationalen GEOTRACES-Programm ist, aber eigentlich für PS100 im Sommer 2016 geplant war. PS100 steht aber unter hohem zeitlichem Druck, sodass das Vorziehen des Schnittes diese Komponente des GEOTRACES-Programms sicherstellen konnte.

Am 14. Oktober 2015 machte *Polarstern* in Bremerhaven fest.

SUMMARY AND ITINERARY

The expedition PS94 Trans-Arctic survey of the Arctic Ocean in transition ("TransArc II") aimed at capturing the physical, biological, and chemical changes of the Arctic Ocean. The retreat of the multi-year sea ice over the last decades, and the changes in ice and ocean circulation are tightly linked to changes in the heat and fresh water distribution with consequences for the gas exchange between ocean and atmosphere, for biogeochemical cycling and for organisms and ecosystems in the sea ice, in the water column and on the sea floor.

To distinguish processes of multiyear variability from long-term, maybe anthropogenic, trends we capture in a distance of several years the regional distribution of the key components of the Arctic Ocean. Eight years after the International Polar Year (IPY 2007/08) and four years afte TransArc (I), TransArc II constituted the third large-scale survey of the Eurasian sector of the Arctic Ocean.

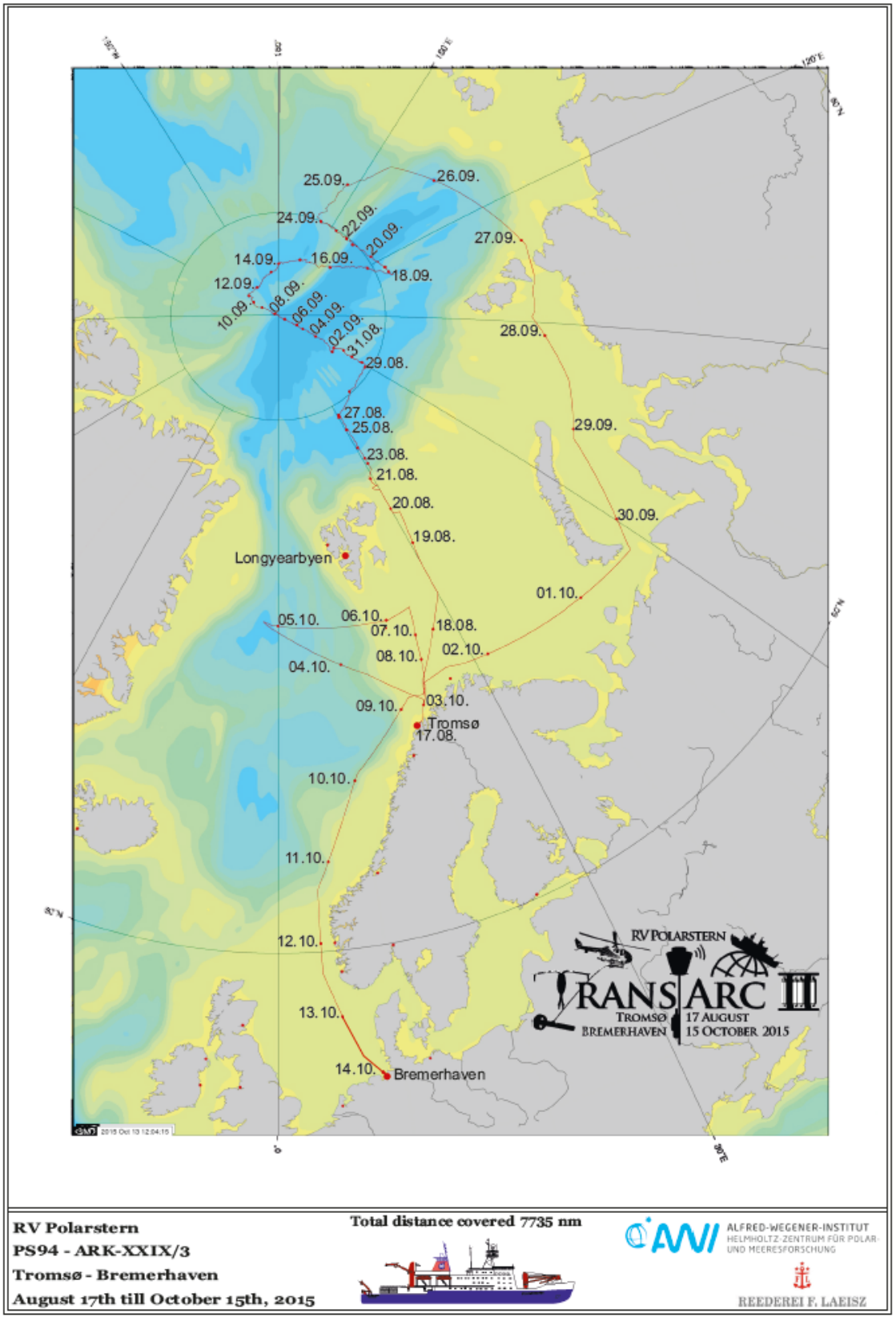

Abb. 1.1: Kursplot der Polarstern-Expedition PS94 (17.8. - 15.10.2015)
Fig. 1.1: Course plot of Polarstern expedition PS94 (17.8. - 15.10.2015)

Specific goals of our programme were to determine if the water that is advected from the Atlantic and Pacific oceans continues to become warmer and whether this development has an impact on the sea ice decrease; whether the accumulation of fresh water in the Arctic that lasted over the past decades, as well as the related change of the upper ocean stratification has reached a turning point; whether besides the extent also the thickness of the sea ice continues to decrease. We also studied changes in the composition of phytoplankton in ice and water, and investigated the state of zooplankton. In the same time, PS94 was a central contribution to the international programme GEOTRACES which aims at determining the distribution and

cycling of trace substances and their isotopes in the global ocean. *In-situ* measurements of the structure and the thickness of the sea ice served also as validation for remote sensing products, among them from the CryoSat2 mission.

To follow these goals, we conducted a number of long transects through the Eurasian part of the Arctic which extended from the Barents Sea and the Gakkel Ridge, respectively, into the Makarov Basin (Fig. 1.1). From the ship, the helicopter and on ice stations we conducted *in-situ* measurements and sampled sea ice, water and sediment. We deployed a suite of autonomous platforms: observation systems installed on ice floes will record atmospheric, sea ice and water properties over the next months and – hopefully - years and send the data ashore while drifting with the host floes through the Arctic; two moorings were mounted at the sea floor to measure the seasonal cycle of hydrography, currents and vertical particle flux, and for the first time we will get once per week near-surface water samples from the central Arctic which will be analyzed for their nutrient content after successful recovery in summer 2016.

When operating in international or Norwegian waters, we recorded the sea floor topography with the multibeam echosounder to extend the still poor Arctic Ocean data coverage.

Besides GEOTRACES (www.geotraces.org/), TransArc II contributed to the international programmes IABP (iabp.apl.washington.edu/index.html), Arctic ROOS (arctic-roos.org/), ASOF (asof.awi.de/), Transdrift (www.transdrift.info), and ART (oceanrep.geomar.de/10151/), as well as to the national programme RACE (race.zmaw.de/). Furthermore, TransArc II participated in implementing the infrastructure initiative FRAM (Frontiers in Arctic Monitoring) of the Helmholtz Society of German Reseach centers (HGF).

During the entire cruise, difficult ice conditions with concentration up to 100 % and new ice formation, as well as a continuously thickening snow layer on the ice hampered the sailing. In addition, the frequent snow fall and bad visibility limited the use of the helicopters.

A highlight of the cruise was the meeting with the US coastguard ice breaker *Healy* at the North Pole on September 7, 2015. Also the *Healy* conducted a GEOTRACES programme and during the meeting an inter-calibration station right at the North Pole was conducted.

The cruise was further affected by two incidents:

1. The original planning contained the extension of the transects to the Kara and Laptev Sea for capturing the exchange between shelf seas and deep basins. Since no clearance for research in the Russian Exclusive Economic Zone was granted, the Kara Sea and Laptev Sea and part of the Nansen Basin were excluded from the survey.
2. Due to a medical emergency we had to cancel our work on September 24 north of the East Siberian Sea.

TransArc II started on August 17, 2015 in Tromsø. With two multi-corer stations in the central Barents Sea, the benthos group started a section along 30°E which then continued northwards with a suite of CTD/Rosette casts. Between the station stops an Underway CTD was run continuously with which also a short section across the Viktoria Trough was conducted. On the continental slope at 81°N, we tried to recover a mooring for the Norwegian Polar Institute. However, after not being able to get in touch acoustically we stopped the procedure without releasing the mooring.

At 81°N we reached the ice edge, but only at 83°43'N the ice was stable enough for a first ice station. Continuous high pressure around the North Pole and low temperatures with new ice formation brought us the first ice press. Hence we decided to brake off the 30°E section at 84°24'N and try to get northward along 60°E. However, the ice conditions did not improve and we had to shorten sections throughout the cruise.

On August 29, we deployed our first mooring in the central Amundsen Basin at 85°18'N. On September 2, the second mooring was deployed in the trench of the Gakkel Ridge at 87°1'N, 59°15'E, in the immediate vicinity of a hydrothermal vent. We succeeded in conducting a rosette cast in the plume of this vent and took samples for all GEOTRACES parameters. We also started finally deploying a variety of observation systems on ice floes that will capture air, ice and water properties year-round.

Sailing along 60° E, we reached the North Pole at September 7, 2015. Only a couple of days before, it had turned out that the US American Coastguard ship *Healy* which was also conducting research in the framework of GEOTRACES happened to work at the North Pole in the very same time. Hence *Polarstern* went alongside on the same floe as *Healy*, and there was enthusiastic mutual visiting by crew members and scientists. Both parties took the unique chance to conduct a GEOTRACES intercalibration station at the North Pole synchronously.

After this event we continued the direction, now along 120°W, into the Makarov Basin in order to study the downstream end of the so-called Transpolar Drift which carries ice and freshwater from river inflow through the Arctic towards the Atlantic Ocean. Once more, heavy ice forced us to change our plans and to turn westwards to our next milestone, a planned GEOTRACES intercalibration station in the deep Makarov Basin at 87°30'N 180°E. From there we headed back to the Gakkel Ridge in order to comprehend the survey of the Eurasian Arctic by sampling the eastern Amundsen Basin and Lomonosov Ridge.

The survey should have been completed by a section across the East Siberian continental slope and along the shelf edge to capture the upstream part of the Transpolar Drift. However, we had to cancel this plan due to a medical emergency onboard and head towards Tromsø.

After the patient had been evacuated in Tromsø a compensating programme was conducted: Two gliders were recovered in the Greenland Sea and a section was conducted between Norway and Svalbard. The gliders had been planned to be recovered through RV *Heincke*, but due to bad weather and the thereby shortage of time for the *Heincke*, the recovery was at risk. Without the recovery through *Polarstern* the gliders might have been lost. The section between Norway and Svalbard is an essential contribution to the international GEOTRACES programme which was originally scheduled for PS100 in summer 2016. PS100 has however, large temporal and berths constraints, and by anticipating the section during PS94 this important component of the GEOTRACES programme was secured.

Polarstern arrived in Bremerhaven on October 14, 2015.

2. WEATHER CONDITIONS

Max Miller, Juliane Hempelt DWD

On August 17, 2015, 4:45 pm when *Polarstern* left Tromsø, sunshine, 20° C and light winds were observed. On our way north we steamed between a high over the White Sea and a low over north-eastern Greenland. Already during the night to Tuesday (Aug. 18) we reached its frontal zone with rain and freshening westerly winds which peaked at Bft 6 on Wednesday. The low moved to Franz-Josef-Land and *Polarstern* got at its west side. Winds abated temporarily but veered north on Thursday evening (Aug. 20) and increased up to Bft 5 to 6 again.

From Saturday (Aug. 22) on a high north of the New Siberian Islands built a ridge towards Franz-Josef-Land and moved itself to North Pole. First we observed only light and variable winds, but from Monday (Aug. 24) on north-easterly winds at force 4 to 5. Only sometimes the subsidence temperature inversion could dissipate the moist ground layer. Often low stratus, mist or fog were prevailing.

On Thursday (Aug. 27) a low trough extended between Norway and northern Fram Strait where a secondary low formed and moved towards Franz-Josef-Land. Easterly winds at Bft 4 to 5 veered north on Sunday (Aug. 30) after the low had departed eastwards. A small low north of Bering Strait moved across the Pole and merged with another low near Novaya Zemlya. Occasionally winds peaked at force 5.

From Sunday (Sep. 06) on a low over Jan Mayen moved north and southerly winds increased Bft 5 to 6. Crossing North Pole on Monday evening (Sep. 07) wind direction switched from south to north. The low also reached the Pole and from Thursday (Sep. 10) on we operated in its centre. Therefore light winds often changed their direction.

A high north of Bering Strait extended a ridge across North Pole towards a high over Eastern Europe. Until Tuesday (Sep. 15) only light and variable winds were prevailing and skies cleared, but on the other hand shallow fog patches formed.

A new low near Svalbard rounded-up North Pole eastwards and stopped north of the Queen-Elizabeth-Islands on Sep. 16. After weakening a bit it intensified again and moved back and we got wind force 5. But at the Taymyr Peninsula a small high formed temporarily and strengthened the pressure gradient. During the night to Sunday (Sep. 20) northerly winds peaked at Bft 8 for short times and abated rapidly afterwards.

On Monday (Sep. 21) another low over Fram Strait moved towards the New Siberian Islands via Laptev Sea. It passed south of *Polarstern* and only on Thursday (Sep. 24) winds from north increased up to force 5. Out of a trough near Severnaya Zemlya a strong low formed and moved east, too. Meanwhile we had left the ice. On Sunday (Sep. 27) and Monday northerly winds freshened up to Bft 7 and caused a sea of 2 to 3 m.

On Monday (Sep. 28) a low formed west of Ireland, deepened rapidly to a storm and arrived at Svalbard on Wednesday (Sep. 30) with a centre pressure of only 960 hPa. Over Kara Sea it caused southerly winds around Bft 8 and waves up to 4 m, but observation stations around

Barents Sea often reported higher wind forces (up to 11). After passing Kara Strait during the night to Thursday winds abated clearly and veered west to northwest around Bft 5 until we arrived off Tromsø on Saturday morning (Oct. 03). A swell of 4 m decreased soon, too.

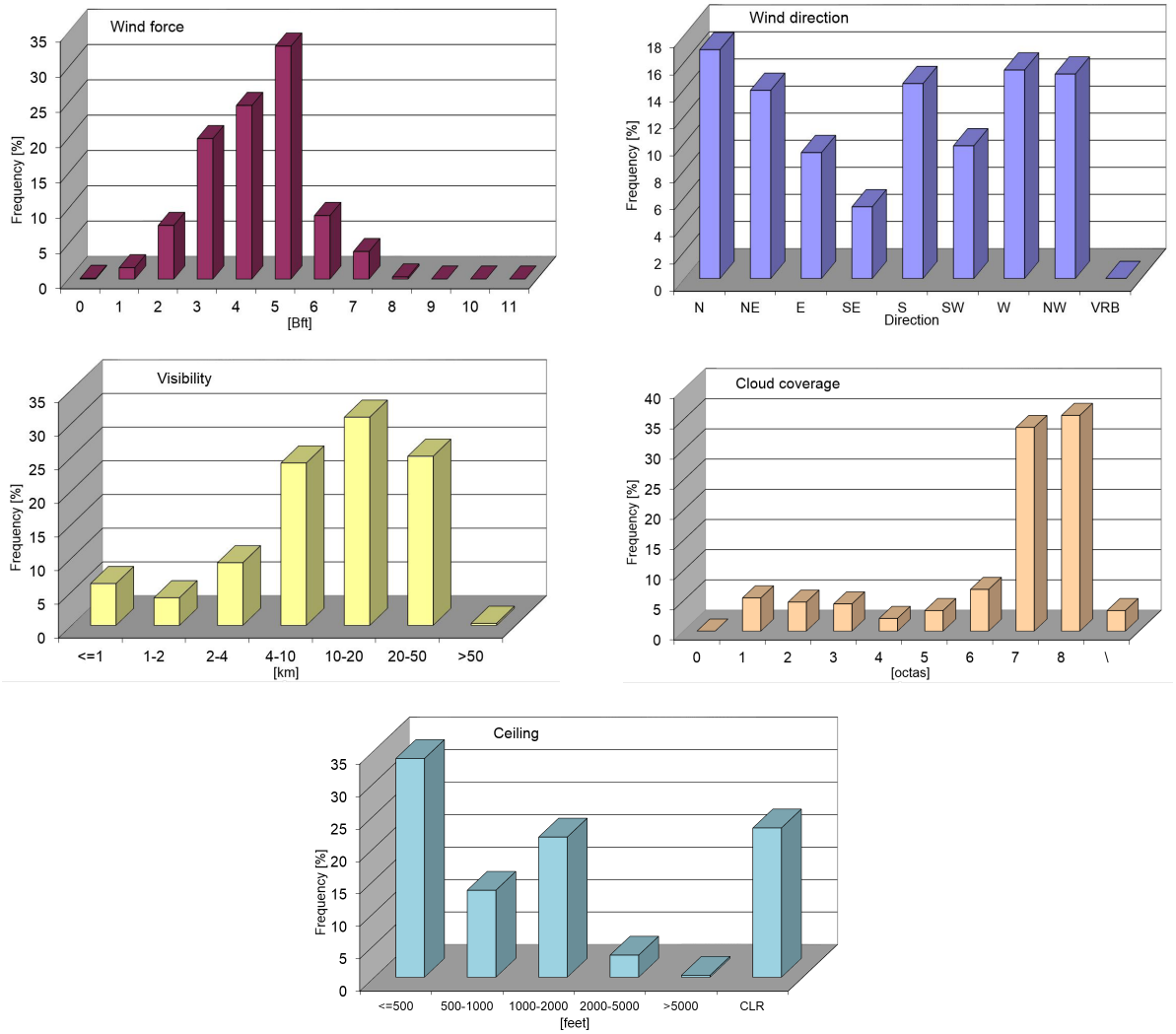

Fig. 2.1 Statistics of weather parameters

While we were steaming towards the Greenland Sea easterly winds increased during the night to Oct. 4 and peaked at Bft 7. A small low had formed southeast of Svalbard and moved towards the Kola Peninsula. On Sunday noon, while we were entering a large area of weak pressure gradient winds abated. On Oct. 5, a small high had arrived over northern Norway. During the following days this high developed to a strong anticyclone over Scandinavia. Together with several lows near Iceland southerly winds were forced. From Oct. 8 until Oct. 12 winds along the Norwegian coast changed between Bft 4 to 5 and Bft 7 to 8 depending on the intensity of the lows. Wave heights did not exceed 3 m.

Meanwhile the high had moved to Russia but build a ridge towards Great Britain. At its southern side over North Sea, north-easterly winds were prevailing and peaked for short times at Bft 7 during the night to Wednesday (Oct. 14). *Polarstern* reached Bremerhaven at fresh winds from northeast to east.

Statistics of the weather during the cruise are shown in Fig. 2.1.

3. PHYSICAL OCEANOGRAPHY

Benjamin Rabe[1], Rainer Graupner[1], Hendrik Hampe[1], Mario Hoppmann[1], Myriel Horn[1], Meri Korhonen[2], Sven Ober[6], Sergey Pisarev[3], Jean-Philippe Savy [4], Ursula Schauer[1], Daniel Scholz[1], Nicolas Villacieros-Robineau[5]

[1]AWI,
[2]FMI
[3]SIO
[4]LEGOS
[5]LOCEAN
[6]NIOZ

Grant No. AWI_PS94_00

Background and objectives

Next to the dramatic retreat of sea ice, the strongest climatic signal of the Arctic Ocean and the Nordic Seas in the past decade are changes in temperature and salinity. A strong accumulation of fresh water has been observed in the past decades in the Arctic Ocean; the waters advected from the Atlantic became much warmer and saltier, and there is high multi-year variability in temperature and salinity of the Pacific Water inflow. Concurrently, there is a multi-decadal positive trend in continental runoff into the Arctic and decadal changes in the atmospheric circulation. The aim of the physical oceanography part of this cruise is to document and quantify the present state of the water mass distribution and circulation in the Eurasian and Makarov basins. The observations will be fundamental to understand the time-mean state of the Arctic Ocean from basin-scales to individual ice floes. They will allow us, in the context of appropriate modelling, to identify variability on seasonal to decadal timescales and long-term trends. Waters imported to the Arctic Ocean are subject to cooling, freezing and melting, altering the properties of these water masses. The warm inflow of waters of Atlantic origin occurs via two pathways: the eastern Fram Strait and the Barents Sea. These two branches are subject to transformation by surface processes and lateral mixing before and after entering the Nansen Basin. Continental runoff enters the Eurasian and Makarov basins via the extensive shelf regions north of Eurasia, before being advected within the Transpolar Drift and, at times, the Beaufort Gyre. At slightly lower salinity than Atlantic Water, Pacific Water enters the Amerasian Basin via the Bering Strait and even reaches into the Eurasian Basin in certain years. This water mass is sandwiched between the warmer waters of Atlantic origin and the fresher, colder waters near the surface. In the central Arctic, stratification due to fresh water in the mixed layer and the halocline inhibits the release of heat from underlying waters to the atmosphere and affects vertical fluxes of dissolved chemical components, such as nutrients. The strong stratification is maintained by continental runoff, and ice or meltwater. However, the variable distribution of fresh water may facilitate the release of some of this heat in certain areas; for example, the recent convergence of fresh water in the central Arctic may, for dynamical reasons, lead to a weakening of the stratification along the warm boundary current at the rim of the basins. Changes may also occur from the different wind mixing with and without ice cover, and the transition from perennial to seasonal ice cover in much of the Arctic.

To address these questions we conducted physical measurements in the Eurasian and Makarov basins. Several hydrographic sections were intended to give a quasi-synoptic view of the Eurasian and central Arctic during late summer and early autumn 2015. Furthermore,

the observations lie in regions covered by earlier cruises conducted since the early 1990s with the icebreakers *Polarstern* and *Oden*, and within the NABOS (Nansen-Amundsen Basin Observation System) project. These observations were augmented by upper-water-column hydrography perpendicular to the sections to capture horizontal gradients in all directions. To aid the interpretation of the hydrographic data and estimate transports we conducted continuous and on-station measurements of current velocity. We deployed autonomous, ice-based buoys, and bottom-moored observatories to extend the observational range of the ship survey in space and time. We used a turbulence profiler from sea-ice to obtain estimates of fine structure and turbulent energy dissipation in the upper water column. This will improve our understanding of vertical mixing processes in the context of large scale hydrography. Our work is part of the Helmholtz strategic investment Frontiers in Arctic Marine Monitoring (FRAM) and contributes to several projects on a national (Bundesministerium für Bildung und Forschung, RACE and TRANSDRIFT; AWI strategy fund, ISO-ARC) and international (International Arctic Buoy Program, IABP; Forum for Arctic Modelling and Observational Synthesis, FAMOS; French equipex IAOOS, http://www.iaoos-equipex.upmc.fr and http://iaoos.ipev.fr; EU FP7 Ice Arc project, http://www.ice-arc.eu).

Work at sea

The work of the Physical Oceanography group on-board entailed measuring vertical profiles of temperature, salinity and ocean current velocity. To study variability and distribution of temperature and salinity in regions and time not covered by our expedition, we deployed instrumentation moored at the seafloor, and deployed drifting buoys in sea ice for autonomous measurements. Details of buoy deployments are described in chapter 5.

To obtain temperature and salinity profiles we used several different Conductivity Temperature Depth (CTD) systems operated from the ship and from ice floes reachable by helicopter. For on-station work CTD sondes were mounted on two different rosettes with 24 bottles each for water sampling. The regular rosette (AWI rosette) bottles each could hold 12 l whereas the large rosette (NIOZ-large rosette) had Niskin-type watersamplers manufactured by Ocean Test Equipment, USA, each with a volume of 25 l. The stainless steel frame of the NIOZ-large rosette was manufactured by Royal NIOZ. The main part of the electronics in each rosette was manufactured by Seabird Electronics (USA), a central unit, model SBE911+. All sensors on the rosettes, except the lowered Acoustic Doppler Current Profiler (LADCP) system, were connected to the SBE911+. This unit communicated via a winch cable with a conducting core (coaxial) with a SBE11plus (S\N 11P16392-0457) deck-unit in the winch control room of *Polarstern*. The deck-unit was connected via an RS-232 serial connection to a standard PC, which was also connected to an NMEA data stream giving time and geographic position in real-time. The logging software ‘Seasave’ was running on this PC under Windows 7 (64 bit).

The CTD on both rosettes contained double sensors for temperature and conductivity, one sensor for pressure and one for oxygen. A fluorometer for chl a fluorescence, a beam transmissometer and a downward looking altimeter were also attached to the frame and connected to the SBE911+. A fluorometer for yellow substance was mounted on both rosettes for part of the expedition, to derive concentrations of Coloured Dissolved Organic Matter (CDOM). The altimeter was mostly working well throughout the cruise except for one station which lead to the rosette hitting the bottom requiring the cable to be cut and newly terminated. Hence, a bottom detector with a rope and 8 kg weight was installed on the NIOZ-large rosette, to give a signal 10 m from the bottom. Further details of the sensors on both rosettes can be found in tables 3.1 and 3.2. The primary conductivity sensor on the NIOZ-large rosette was changed once during the cruise due to a broken cell. The cables of the oxygen, and the secondary conductivity and temperature sensors on the NIOZ-large rosette were changed several times during the cruise due to erratic data at high pressure. The oxygen sensor

was eventually replaced as it most likely suffered from a broken membrane. We determined the salinity of 61 water samples, taken at selected stations, using the Optimare Precision Salinometer on-board *Polarstern* and standard seawater from Ocean Scientific International. These measurements will be used after the expedition to calibrate the conductivity sensors. Likewise, the GEOTRACES group determined oxygen in water samples from 89 stations (see chapter 7) to calibrate the oxygen sensors after the expedition. A third “ultra-clean” CTD-rosette (UCCTD) was operated by a group from NIOZ and is described in chapter 7.

During a few casts a SBE35 reference-thermometer (S\N 0019) was used on the NIOZ-large rosette. It appeared that the difference between this thermometer and the 2 profiling thermometers (SBE3, S\N 03P5115 and S\N 03P2929) depends more or less linearly on pressure. Assumed is that the more robust SBE35 is not or at least less pressure dependent than the fragile needle of the SBE3’s. An example of this is shown in Fig. 3.2.

An Underway CTD (UWCTD) system (UCTD 10-400) from Oceanscience (Oceanside, USA) was used from the stern of *Polarstern*, mounted on the reiling at the stern portside, to obtain temperature, salinity and pressure profiles while underway. The system contains a Seabird CTD measuring at 16 Hz. The profile depth is limited by the speed of the ship and the length of the cable. The nominal profile depth at a ship speed of 10 kn is 400 m. However, the deepest profile only reached to about 250 m depth in water more than 400 m deep. The tailspool rewinder system, capable of extending the profile depth to about 1,000 m, was found to be broken at the beginning of the expedition due to moisture inside the system.

An XCTD-1, by Tsurumi-Seiki Co. Ltd. (Yokohama, Japan) was used to obtain CTD profiles up to 1,100 m water depth, some while underway from the ship and some from ice floes reachable by helicopter. The system consisted of a launcher for expendable CTD probes and a mobile deck-unit (MK-150) for data acquisition. The probe sinks down with constant velocity measuring temperature and conductivity.

All three rosette systems were used to obtain stations from the ship along different sections throughout the Eurasian and central Arctic (Fig. 3.1). A total of 125 CTD profiles were taken, 56 of which with the NIOZ-large rosette, 41 with the AWI-rosette and 28 with the UCCTD on the ultra-clean rosette (see A.4, station list PS94). We used the UWCTD to obtain 139 profiles in the Barents Sea along 30°E (Table 3.3). We continued to increase the resolution of the CTD stations by using the XCTD to obtain 94 profiles once *Polarstern* reached the ice until the end of the scientific work in the Barents Sea. Furthermore, we obtained 17 XCTD profiles from ice floes reached by helicopter (Table 3.4).

Two moorings were deployed in the Eurasian Basin: one is located in the Nansen Basin, south of the Karasik Seamount, the other further north in the deep trench of the Gakkel Ridge (Table 3.5). Both moorings are meant to observe the near-surface physical, biological and biogeochemical environment, as well as sedimentation to deeper parts of the water column. The mooring in the trench was co-located with a CTD profile showing hydrothermal vent signal in the deep part of the water column. Several recording CTDs, current profilers and meters, sediment traps and a water sampler were mounted on the mooring line. An additional acoustic recorder is meant to monitor marine environmental sound. A list of deployed moorings with devices is given in. We attempted to recover one mooring for the Norwegian Polar Institute, (Tromso, Norway), northeast of Svalbard. However, we were not able to establish acoustic communication with the releases and abandoned the recovery due to dense ice cover.

We used a turbulence profiler (MSS90L, Sea & Sun Technology) to obtain profiles of fine-scale motion by measuring temperature, salinity, pressure, current shear and light transmission. The profiler is free-falling with a 400 m long data cable attached to an electrical winch. We operated the system through a hole in the sea-ice for several hours during ice stations. In total, sets of between 11 and 49 profiles were obtained at seven ice stations.

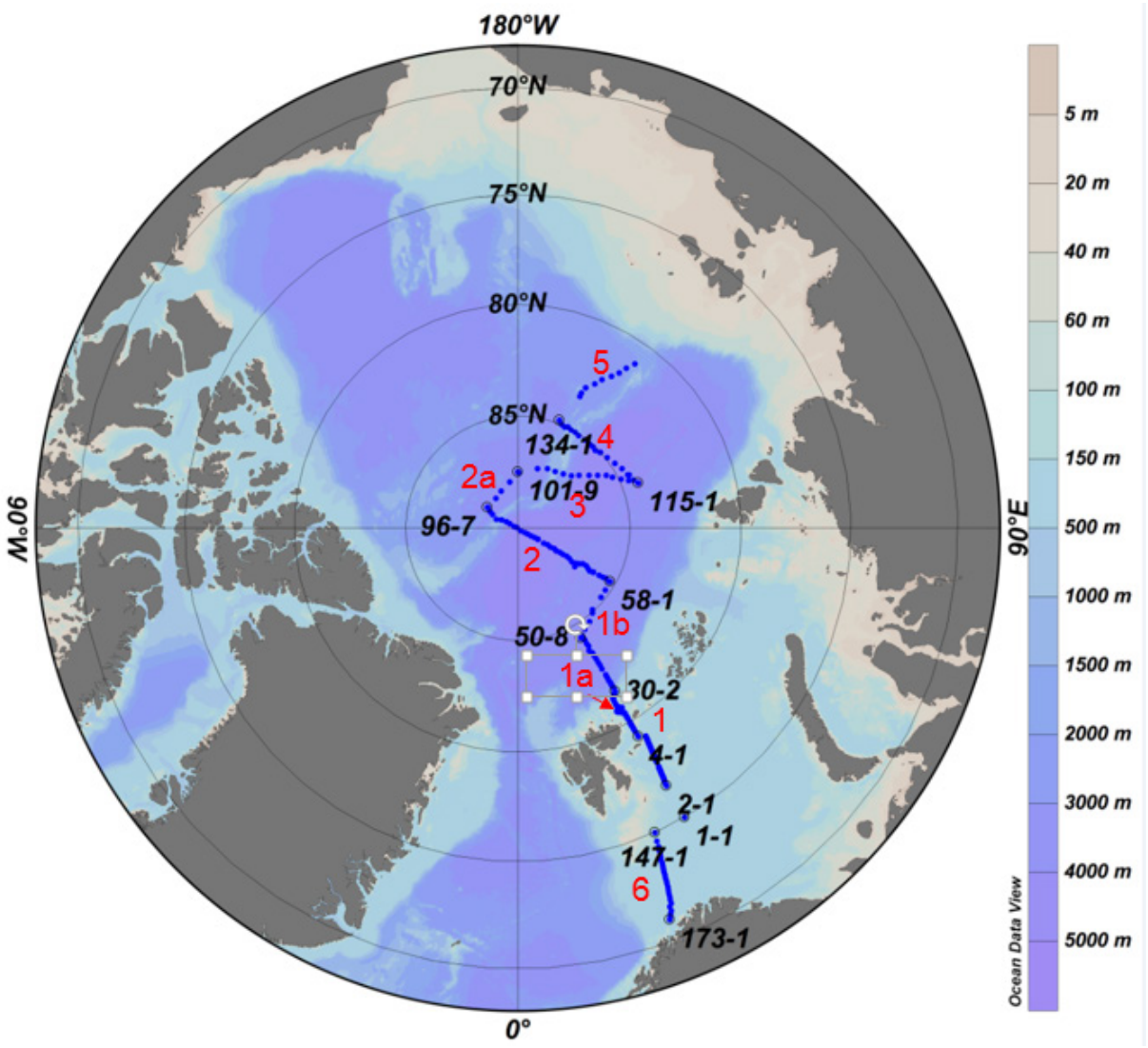

Fig. 3.1: Map of stations (blue) with station number in black and section numbers in red

We measured profiles of ocean current velocity in the upper 300 m while underway with a vessel-mounted Acoustic Doppler Current Profiler (VMADCP). The RDI Ocean Surveyor instrument (150 kHz) was mounted at an angle of 45° to the forward along-ship direction in the 'Kastenkiel' of FS *Polarstern*. The instrument was configured in narrowband mode and set up to use 4 m bin size covering a range from 15m to 500 m. The actual range in Arctic waters is about 200 - 300 m depending on sea state, ice conditions, ship's speed and backscatter signals. The ADCP was set to ping as fast as possible (parameter TP000000). The software VmDas (Teledyne RD Instruments) was used to set the ADCP's operating parameters and to record the data. Finally the Ocean Surveyor data conversion was done using Matlab (Mathworks) routines last changed by Tim Fischer (Geomar, Kiel, Germany) in February 2015 (osheader.m, osdatasip.m, osrefine.m). Our setup allows standard calibrations for misalignment angle and scaling constants (Joyce, 1989) as well as an evaluation of the instrument's performance after calibration coefficients are derived. Preliminary analysis using this method gave a misalignment angle of 1.3362° and a velocity scaling factor of 1.0178. Problems to resolve velocities occurred due to low backscatter and shallow water depths. Post-cruise analysis will focus on analysing any interference of other acoustic devices with the

velocity measurements. Interfering signals may originate in the vessel's Doppler log (79 kHz), the multibeam echosounder HYDROSWEEP (15.5 kHz) and acoustic signals to release.

The ship's pumped seawater system measured temperature and salinity underway at depths of 6 m (in open water only) and 11 m (ice and open water). The electronic engineer responsible for scientific laboratories on *Polarstern* took regular samples to calibrate the conductivity sensor near the intake of the underway pumped system.

To support the oceanographic programmes and increase the amount of topographic data in the central Arctic, which are rare, we conducted multibeam surveys with the Hydrosweep DS-3 system (Atlas Hydrographic). The system is permanently installed on *Polarstern* and ensured spatially highly resolved depth information throughout the expedition. We used the ATLAS Hydromap Control (AHC) software version 2.6.6.0 with the following relevant parameter settings: beam spacing 'Equal Footprint', desired number of beams '920', C-Keel source 'System C-Keel', and transmission sequence 'equidistant transmission'. We adjusted the swath width portside/starboard side permanently during the expedition in order to get the optimum data quality. In shallow regions with water depth less than 1,000 m the swath width was mainly set to 150 to 200 %, at water depths of 1,000 to 3,000 m to 100 to 150 %, and at deeper depths than 3,000 m to 50 to 100 %. For online visualization of the raw data, the HYPACK software package versions 12.0.8.12, 13.0.9.17, and 15.0.9.71 were used. Raw data was stored in *.asd-format and *.hsx-format in 30 minute blocks. No water column data was collected. The multibeam survey was started on August 19, 2015 at 9:37 am in the Barents Sea and was continued until September 26 at 7:56 pm, before we entered the Russian EEZ. When leaving the Russian EEZ on October 2 at 10:04 pm the data acquisition was continued until October 9 at 04:52 am, when starting the transit to Bremerhaven. During station work, the data recording was stopped except during ice stations, where we drifted with the ice floe. Eight CTD profiles were used to derive the sound velocity for different parts of the survey. The data processing will be done after the cruise by the Bathymetry group of the AWI. Although continuous data recording was possible throughout most of the cruise, some system errors appeared during the cruise, causing gaps in the data acquisition. These could only be resolved by a total system shut down and restart. Unfortunately the HYPACK software broke down several times and could not be restarted easily. Hence, we had to change between different versions of the software during the surveys.

During CTD casts, we tested a new LADCP system to obtain full-depth profiles of ocean current velocity in an environment of low horizontal magnetic field intensity in the vicinity of the North Pole. The new system by SubCtech (Kiel, Germany) contains a Subsea MicroDI datalogger in a titanium housing (rated to 6,000 m water depth). The logger is connected to a gyro (XSENS MTi-300 AHRS), a pressure sensor (Keller PA-35X), also contained in the same housing. The system is connected to external upward and downward looking LADCP heads (RDI-Teledyne 300 KHz Workhorse) and an external battery pack. The gyro allows for detection of the change in orientation of the rosette independent of the magnetic field. To obtain the geographic heading a GPS is temporarily mounted on the rosette connected to the logger system before the rosette is deployed in water. All measurements except those by the ADCP are saved to a micro-SD memory card within the titanium housing. The whole system was mounted on the AWI rosette with specially designed fittings and cables to allow all 24 bottles being mounted at the same time as the LADCP system. The two LADCP heads were set to ping every second. We encountered problems during system startup of the logger due to the quality of the GPS acquisition. The GPS signal quality was generally only "1", but the system expects a minimum of "2". The LED signal on the titanium housing of the logger was blinking green, indicating a problem with one of the devices in the system. However, we were informed by SubCTech during the expedition that the system is supposed to work and acquire data even if the GPS quality criterion is not met. The initial profiles around the southern margin

of the Nansen Basin were complemented by running the system during the final transect in the Barents Sea. Further problems were encountered when downloading the logger data (which currently excludes the ADCP data, downloaded directly from the RDI workhorse systems) using a terminal and the RS-232 connection on the titanium housing. However, it was possible to open the housing and reading the data directly from the micro-SD card. Further analysis of this prototype system will be done after the cruise.

We recovered two autonomous gliders, deployed during PS93.1, that had been operating in the Greenland Sea from July to October 2015 and one autonomous profiling drifter (”ARGO float“) was deployed (Table 3.6). The measurements contribute to the hydrographic monitoring of the Nordic Seas with Argo floats that started in 2001.

A Picarro water vapour isotopic analyser was used during PS94 as a contribution to the ISO-ARC Project. This analyser performed continuous measurements of water vapour isotopic composition in the surrounding air, focusing on the isotopic fingerprint of the eastern Arctic Water Cycle. The instrument was running properly during the entire expedition. The calibration device underwent one minor liquid standard water delivery issue, which was easily solved by the scientists responsible for the instrument on-board, following the standard procedure. The instrument showed a strong robustness during the entire Arctic season in 2015 and restarted easily after being switched off in the Russian EEZ.

The automatic programme sending a daily diagnostic report to AWI PIs suffered a breakdown, which had no effect on the recording itself. Bug-fixes and adaptations will be provided during the maintenance of the instrument before the Antarctic field season. To fill the information gap caused by this loss, a new simple automatic programme was established and installed to transfer part of the metadata by email, and allow this daily diagnostic. Data were acquired between 17 August and 12 September 2015, with the exception of the period 27 September to 03 October 2015, when we crossed the Russian EEZ. Preliminary results suggest that isotopic parameters δ18O and δD evolved similarly, and are correlated with humidity. An important latitudinal gradient was identified as the main source of variability for humidity level and isotopic composition (δ18O and δD), decreasing towards the pole, and for the second order parameter deuterium excess (d-excess = δD – 8 * δ18O), increasing towards the pole. On top of this latitudinal gradient, a significant synoptic variability was observed linked with large scale meteorological variations. In addition, we took daily samples from the *Polarstern* underway pumped system. The isotopic composition of those samples will be determined after the cruise, and compared with the measurements obtained by Picarro. It has to be noted however that the water throughflow next to the ships high-precision salinometer (intake at 6 m depth) was switched off in moderate ice conditions. The sampling procedure was therefore adapted during PS94, using a valve on the working deck, connected to the 11 m intake.

Preliminary results

Preliminary temperature and salinity profiles show the transition between the warm and saline Atlantic Water inflow into the Barents Sea and the colder, less saline waters in the section along approximately 30°E (section 1, Figs 3.3ff). In the southern Nansen Basin we see the signature of the inflow from the Fram Strait as a subsurface warm core hugging the continental slope underneath fresher surface waters. Further north the ocean is covered by sea-ice and surface waters are colder. At the transect 2, along 60 E / 120 W (Figs 3.1), we gradually encountered fresher and slightly warmer waters (Figs 3.3 and 3.4), in particular in the northern Amundsen Basin and the Makarov Basin close to the Lomonosov Ridge. Freezing occured until the end of transect 5 (Figs 3.5 and 3.6) at air temperatures below -10°C.

Data management

Data from the rosette-mounted CTDs, XCTD, UWCTD, MSS as well as LADCP and VMADCP data collected during PS94 will be delivered after post-cruise calibration to the PANGAEA database and to the appropriate national data centres. The gliders are piloted from AWI in real time. The uncalibrated data will be provided in near-real time to the Coriolis data centre for use in operational applications. The calibration and final processing will take place after completion of the mission, and the data will be delivered to the PANGAEA database. The ARGO float data will be provided in near-real time to the Coriolis data centre and replaced by delayed mode quality controlled data afterwards.

Tab. 3.1: Sensors used on the small AWI rosette with serial numbers (right column). The AWI rosette was used during stations 001-01 to 036-02, 046-04 to 50-08 and 147-01 to 173-01.

CTD-sonde	SBE 911+	7396
CTD-sensors Temperature	SBE3	pri. 5101 / sec. 5112
Conductivity	SBE4	pri. 3570 / sec. 3597
Pressure	Digiquartz 410K-134	0937
altimeter	Benthos PSA-916 (until stn. 031-01) (from stn. 032-02)	 1229 51533
oxygen	SBE43	0467
transmissiometer	WET Labs C-Star	1220
fluorometer chlorophyll a	WET Labs ECO-AFL/FL	1853
fluorometer CDOM	Dr. Haardt (stations 004-1 to 050-8)	03
rosette sampler	SBE 32	0718

Tab. 3.2: Sensors used on the NIOZ large rosette with serial numbers (right column). The NIOZ large rosette was used during stations 038-01 to 046-03 and 054-02 to 134-01

CTD-sonde	SBE 911+	09P865-0321
CTD-sensors Temperature	SBE3	pri. 5115 / sec. 2929
Conductivity	SBE4 (until stn. 068-01) (from stn. 069-04)	pri. 3290 / sec. 3585 pri. 1199 / sec. 3585
Pump	SBE5	pri. 4316 / sec. 5258
Pressure	Digiquartz 410K-134	0321
Altimeter	Benthos PSA-916	47766
oxygen	SBE43 (until stn. 059-01) (from stn. 061-01)	1605 0743
transmissiometer	WET Labs C-Star	1198DR
fluorometer chlorophyll a	WET Labs FLRTD	1670
fluorometer CDOM	Dr. Haardt	03
rosette sampler	SBE 32 (until stn. 046-03) (from stn. 054-02)	32176773-0202 3249818-0657

Tab. 3.3: Details of UWCTD profiles

Station	Date	Time [UTC]	Latitude	Longitude	UWCTD depth [m]	Water depth [m]
003-01	19/08/15	06:34:00	76° 45.45 N	30° 02.79 E	178	262
003-02	19/08/15	07:25:00	76° 53.51 N	30° 07.79 E	220	266
003-03	19/08/15	07:35:00	76° 55.10 N	30° 08.72 E	203	259
003-04	19/08/15	07:44:00	76° 56.53 N	30° 09.58 E	194	256
003-05	19/08/15	07:53:00	76° 57.97 N	30° 10.54 E	202	250
003-06	19/08/15	08:03:00	76° 59.57 N	30° 11.51 E	195	246
003-07	19/08/15	08:12:00	77° 01.00 N	30° 12.31 E	212	247
003-08	19/08/15	08:22:00	77° 02.58 N	30° 13.35 E	200	240
003-09	19/08/15	08:31:00	77° 04.00 N	30° 14.20 E	204	238
003-10	19/08/15	08:40:00	77° 05.43 N	30° 15.11 E	182	225
003-11	19/08/15	08:47:00	77° 06.54 N	30° 15.74 E	187	213
003-12	19/08/15	08:56:00	77° 07.96 N	30° 16.68 E	153	209
003-13	19/08/15	09:02:00	77° 08.91 N	30° 17.26 E	139	206
003-14	19/08/15	09:08:00	77° 09.86 N	30° 17.80 E	140	205
003-15	19/08/15	09:14:00	77° 10.80 N	30° 18.40 E	168	210
003-16	19/08/15	09:22:00	77° 12.06 N	30° 19.17 E	165	202
003-17	19/08/15	09:28:00	77° 13.00 N	30° 19.74 E	168	206
003-18	19/08/15	09:35:00	77° 14.10 N	30° 20.39 E	165	192
003-19	19/08/15	09:41:00	77° 15.04 N	30° 21.08 E	163	199
003-20	19/08/15	09:47:00	77° 15.99 N	30° 21.67 E	161	191
003-21	19/08/15	09:54:00	77° 17.10 N	30° 22.32 E	165	191
003-22	19/08/15	09:59:00	77° 17.89 N	30° 22.84 E	170	198
003-23	19/08/15	10:06:00	77° 19.01 N	30° 23.55 E	174	201
003-24	19/08/15	10:13:00	77° 20.16 N	30° 24.22 E	171	198
003-25	19/08/15	10:19:00	77° 21.13 N	30° 24.78 E	161	202
003-26	19/08/15	10:26:00	77° 22.28 N	30° 25.54 E	162	201
003-27	19/08/15	10:32:00	77° 23.25 N	30° 26.21 E	157	197
003-28	19/08/15	10:38:00	77° 24.21 N	30° 26.75 E	164	211
003-29	19/08/15	10:45:00	77° 25.31 N	30° 27.52 E	166	192
003-30	19/08/15	10:51:00	77° 26.25 N	30° 28.07 E	163	206
003-31	19/08/15	10:59:00	77° 27.48 N	30° 28.84 E	173	210
003-32	19/08/15	11:06:00	77° 28.55 N	30° 29.56 E	173	210
003-33	19/08/15	11:13:00	77° 29.61 N	30° 30.25 E	174	218
003-34	19/08/15	11:22:00	77° 30.97 N	30° 31.11 E	168	218
003-35	19/08/15	11:29:00	77° 32.03 N	30° 31.72 E	179	226
003-36	19/08/15	11:37:00	77° 33.24 N	30° 32.47 E	188	223
003-37	19/08/15	11:45:00	77° 34.45 N	30° 33.25 E	210	227
003-38	19/08/15	13:09:00	77° 47.26 N	30° 41.53 E	223	234
003-39	19/08/15	13:21:00	77° 49.12 N	30° 42.72 E	190	248
003-40	19/08/15	13:29:00	77° 50.37 N	30° 43.61 E	195	242

Station	Date	Time [UTC]	Latitude	Longitude	UWCTD depth [m]	Water depth [m]
003-41	19/08/15	13:38:00	77° 51.77 N	30° 44.55 E	195	241
003-42	19/08/15	13:46:00	77° 53.04 N	30° 45.29 E	199	234
003-43	19/08/15	13:54:00	77° 54.29 N	30° 46.10 E	196	263
003-44	19/08/15	14:04:00	77° 55.88 N	30° 47.16 E	208	268
003-45	19/08/15	14:14:00	77° 57.47 N	30° 48.28 E	209	243
003-46	19/08/15	14:22:00	77° 58.74 N	30° 49.04 E	211	256
003-47	19/08/15	14:32:00	78° 00.32 N	30° 50.11 E	214	261
003-48	19/08/15	14:41:00	78° 01.76 N	30° 51.07 E	212	248
003-49	19/08/15	14:50:00	78° 03.18 N	30° 51.99 E	208	219
003-50	19/08/15	14:59:00	78° 04.61 N	30° 52.94 E	186	235
003-51	19/08/15	15:07:00	78° 05.87 N	30° 53.77 E	193	234
003-52	19/08/15	15:14:00	78° 06.96 N	30° 54.57 E	194	242
003-53	19/08/15	15:23:00	78° 08.36 N	30° 55.49 E	192	243
003-54	19/08/15	15:31:00	78° 09.62 N	30° 56.38 E	190	232
003-55	19/08/15	15:39:00	78° 10.88 N	30° 57.13 E	193	240
003-56	19/08/15	15:47:00	78° 12.12 N	30° 58.06 E	200	242
003-57	19/08/15	15:55:00	78° 13.36 N	30° 58.84 E	195	272
003-58	19/08/15	16:04:00	78° 14.76 N	30° 59.77 E	191	256
003-59	19/08/15	16:12:00	78° 16.02 N	31° 00.58 E	195	249
003-60	19/08/15	16:21:00	78° 17.44 N	31° 01.57 E	199	260
003-61	19/08/15	16:30:00	78° 18.86 N	31° 02.62 E	205	258
003-62	19/08/15	16:39:00	78° 20.28 N	31° 03.60 E	200	251
003-63	19/08/15	16:48:00	78° 21.73 N	31° 04.50 E	202	259
003-64	19/08/15	16:57:00	78° 23.15 N	31° 05.54 E	203	257
003-65	19/08/15	17:06:00	78° 24.57 N	31° 06.54 E	205	271
003-66	19/08/15	17:16:00	78° 26.17 N	31° 07.57 E	206	281
003-67	19/08/15	17:26:00	78° 27.73 N	31° 08.70 E	201	300
003-68	19/08/15	17:35:00	78° 29.16 N	31° 09.66 E	206	299
003-69	19/08/15	17:45:00	78° 30.73 N	31° 10.74 E	216	306
003-70	19/08/15	17:56:00	78° 32.46 N	31° 11.96 E	220	312
003-71	19/08/15	18:07:00	78° 34.18 N	31° 13.06 E	221	315
003-72	19/08/15	18:19:00	78° 36.05 N	31° 14.34 E	222	312
003-73	19/08/15	18:29:00	78° 37.59 N	31° 15.49 E	215	305
003-74	19/08/15	18:39:00	78° 39.12 N	31° 16.60 E	212	311
003-75	19/08/15	18:50:00	78° 40.83 N	31° 17.75 E	219	287
003-76	19/08/15	19:00:00	78° 42.37 N	31° 18.86 E	208	270
003-77	19/08/15	19:10:00	78° 43.92 N	31° 19.88 E	183	257
003-78	19/08/15	19:19:00	78° 45.30 N	31° 20.90 E	109*	242
003-79	19/08/15	19:29:00	78° 46.84 N	31° 21.93 E	100*	238
003-80	19/08/15	19:38:00	78° 48.23 N	31° 22.92 E	107*	148
003-81	19/08/15	19:47:00	78° 49.60 N	31° 23.97 E	93*	134

Station	Date	Time [UTC]	Latitude	Longitude	UWCTD depth [m]	Water depth [m]
003-82	19/08/15	19:56:00	78° 50.97 N	31° 24.86 E	60*	124
003-83	19/08/15	20:03:00	78° 52.02 N	31° 25.64 E	105*	108
003-84	19/08/15	20:13:00	78° 53.53 N	31° 26.69 E	102*	151
003-85	19/08/15	20:21:00	78° 54.73 N	31° 27.60 E	65*	177
003-86	19/08/15	20:28:00	78° 55.79 N	31° 28.33 E	114*	202
003-87	19/08/15	20:35:00	78° 56.83 N	31° 29.08 E	48*	202
003-88	19/08/15	20:41:00	78° 57.74 N	31° 29.72 E	91*	229
003-89	19/08/15	20:48:00	78° 58.78 N	31° 30.52 E	137*	251
003-90	19/08/15	21:00:00	79° 00.53 N	31° 31.73 E	185	181
003-91	19/08/15	21:07:00	79° 01.55 N	31° 32.51 E	116	160
003-92	19/08/15	21:12:00	79° 02.28 N	31° 33.00 E	130	138
003-93	19/08/15	21:17:00	79° 03.01 N	31° 33.60 E	131	136
003-94	19/08/15	21:22:00	79° 03.74 N	31° 34.07 E	110	120
003-95	19/08/15	21:26:00	79° 04.34 N	31° 34.47 E	110	119
005-01	20/08/15	10:23:00	79° 16.42 N	30° 02.51 E	97*	253
007-01	20/08/15	12:58:00	79° 34.11 N	30° 00.01 E	224	263
007-02	20/08/15	13:08:00	79° 35.80 N	29° 59.95 E	195	257
007-03	20/08/15	13:20:00	79° 37.82 N	29° 59.97 E	206	263
007-04	20/08/15	13:32:00	79° 39.86 N	30° 0.05 E	195	256
007-05	20/08/15	13:42:00	79° 41.57 N	29° 59.95 E	195	270
009-01	20/08/15	15:14:00	79° 47.45 N	29° 59.97 E	145	152
009-02	20/08/15	15:23:00	79° 48.85 N	29° 59.95 E	135	142
009-03	20/08/15	15:29:00	79° 49.80 N	30° 00.06 E	171	210
009-04	20/08/15	15:36:00	79° 50.90 N	30° 00.05 E	199	264
009-05	20/08/15	15:46:00	79° 52.44 N	30° 00.08 E	195	243
009-06	20/08/15	15:55:00	79° 53.81 N	29° 59.94 E	194	245
009-07	20/08/15	16:04:00	79° 55.19 N	29° 59.98 E	194	252
009-08	20/08/15	16:13:00	79° 56.55 N	29° 59.96 E	201	245
009-09	20/08/15	16:22:00	79° 57.92 N	29° 59.94 E	214	273
011-01	20/08/15	19:32:00	80° 09.01 N	30° 00.03 E	103	298
011-02	20/08/15	19:37:00	80° 09.82 N	29° 59.98 E	222	284
011-03	20/08/15	19:50:00	80° 11.93 N	29° 60.00 E	257	299
013-01	20/08/15	20:40:00	80° 16.03 N	30° 00.05 E	202	234
013-02	20/08/15	20:51:00	80° 17.86 N	30° 00.06 E	170	205
013-03	20/08/15	21:00:00	80° 19.34 N	30° 00.05 E	145	150
013-04	20/08/15	21:06:00	80° 20.31 N	29° 59.96 E	199	194
013-05	20/08/15	21:18:00	80° 22.30 N	29° 60.00 E	183	198
013-06	20/08/15	21:27:00	80° 23.81 N	29° 59.92 E	200	236
013-07	20/08/15	21:37:00	80° 25.47 N	30° 00.02 E	172	175
013-08	20/08/15	21:45:00	80° 26.81 N	30° 00.07 E	158	338
015-01	20/08/15	22:52:00	80° 31.57 N	29° 46.99 E	216	501

Station	Date	Time [UTC]	Latitude	Longitude	UWCTD depth [m]	Water depth [m]
015-02	20/08/15	23:06:00	80° 32.94 N	29° 35.46 E	207	314
015-03	20/08/15	23:18:00	80° 34.07 N	29° 25.94 E	140	174
015-04	20/08/15	23:26:00	80° 34.82 N	29° 19.66 E	187	258
015-05	20/08/15	23:36:00	80° 35.75 N	29° 11.76 E	169	191
015-06	20/08/15	23:44:00	80° 36.48 N	29° 05.48 E	192	326
015-07	20/08/15	23:54:00	80° 37.39 N	28° 57.69 E	195	261
015-08	21/08/15	00:03:00	80° 38.24 N	28° 50.79 E	191	305
015-09	21/08/15	00:13:00	80° 39.14 N	28° 42.95 E	219	485
015-10	21/08/15	00:27:00	80° 40.45 N	28° 32.13 E	218	444
016-01	21/08/15	01:26:00	80° 45.02 N	28° 28.47 E	75	80
016-02	21/08/15	01:31:00	80° 45.00 N	28° 31.78 E	106	121
016-03	21/08/15	01:35:00	80° 44.99 N	28° 34.62 E	186	191
016-04	21/08/15	01:50:00	80° 45.00 N	28° 49.89 E	216	492
016-05	21/08/15	01:58:00	80° 44.99 N	28° 58.32 E	218	501
019-01	21/08/15	08:01:00	80° 47.35 N	29° 33.84 E	250	423
019-02	21/08/15	08:17:00	80° 49.86 N	29° 26.69 E	256	399
019-03	21/08/15	08:35:00	80° 52.68 N	29° 20.02 E	236	431

Tab. 3.4: Details of XCTD profiles. Those profiles taken from the ship are listed by station number from the station list PS94 (A.4), those taken from sea-ice are listed as ‘Heli’ with incrementing cast number for each profile.

No	Station	Date Time [UTC]	Latitude	Longitude	Water depth [m]	XCTD s/n	XCTD depth [m]	Filename
1	017-01	21/08/15 02:22	80° 45.01 N	029° 23.58 E	480	14078062	480	XCTD-000308212015
2	017-02	21/08/15 02:43	80° 45.01 N	029° 47 E	286	14078065	280	XCTD-000408212015
3	017-03	21/08/15 02:52	80° 45.01 N	029° 55.44 E	247	14078069	240	XCTD-000508212015
4	017-04	21/08/15 03:00	80° 45.01 N	029° 03.91 E	256	14078068	250	XCTD-000608212015
5	017-05	21/08/15 03:07	80° 44.99 N	029° 12.31 E	224	14078063	210	XCTD-000708212015
6	017-06	21/08/15 05:28	80° 45.66 N	030° 06.69 E	252	14078060	240	XCTD-000808212015
7	017-07	21/08/15 03:52	80° 45.41 N	029° 44.27 E	304	14078066	290	XCTD-000908212015
8	020-01	21/08/15 08:58	80° 56.24 N	029° 09.75 E	411	14078059	506	XCTD-001008212015
9	022-01	21/08/15 10:51	80° 04.45 N	029° 03.49 E	373	14078036	471	XCTD-008108212015
10	023-01	21/08/15 11:36	81° 10.02 N	029° 07.01 E	355	14078035	496	XCTD-008208212015

No	Station	Date Time [UTC]	Latitude	Longitude	Water depth [m]	XCTD s/n	XCTD depth [m]	Filename
11	024-01	21/08/15 12:14	81° 14.65 N	029° 10.02 E	333	14078034	403	XCTD-008308212015
12	026-01	21/08/15 14:44	81° 22.02 N	029° 41.90 E	299	14078038	559	XCTD-001108212015
13	027-01	21/08/15 15:29	81° 25.75 N	030° 04.02 E	201	14078039	297	XCTD-001208212015
14	028-01	21/08/15 16:11	81° 29.05 N	030° 24.33 E	646	14078037	400	XCTD-001308212015
15	033-01	23/08/15 07:26	81° 57.81 N	030° 53.65 E	3193	14078042	1085	XCTD-001408232015
16	035-01	23/08/15 11:39	82° 07.65 N	030° 46.81 E	3304	14078040	116	XCTD-001508232015
17	035-01	23/08/15 11:55	82° 08.08 N	030° 50.74 E	3300	14078044	793	XCTD-001608232015
18	037-01	23/08/15 18:23	82° 17.98 N	030° 54.23 E	3400	14078045	1085	XCTD-001708232015
19	039-01	23/08/15 23:28	82° 32.95 N	030° 54.79 E	3597	14062658	369	XCTD-001808242015
20	041-01	24/08/15 15:19	82° 53.63 N	030° 54.19 E	3802	15062662	790	XCTD-001908242015
21	Heli-01	24/08/15 15:52	82° 55.47 N	032° 09.17 E		15062663	1085	XCTD-002008242015
22	Heli-02	24/08/15 16:23	82° 54.64 N	029° 43.77 E		15062659	1085	XCTD-002108242015
23	043-01	24/08/15 22:10	83° 12.79 N	030° 57.31 E	3956	15062660	391	XCTD-002208252015
24	045-01	25/08/15 05:45	83° 32.71 N	030° 58.11 E	4030	15062661	533	XCTD-002308252015
25	Heli-03	25/08/15 12:16	83° 42.10 N	034° 06.91 E		15062635	1085	XCTD-002408252015
26	Heli-04	25/08/15 12:38	83° 42.27 N	033° 13.20 E		15062638	1085	XCTD-002508252015
27	Heli-05	25/08/15 13:00	83° 42.62 N	032° 18.58 E		15062634	1085	XCTD-002608252015
28	Heli-06	25/08/15 13:20	83° 42.60 N	031° 21.69 E		15062641	1085	XCTD-002708252015
29	Heli-07	25/08/15 13:51	83° 42.03 N	027° 14.26 E		15062644	1085	XCTD-002808252015
30	Heli-08	25/08/15 14:15	83° 42.26 N	028° 17.83 E		15062642	1085	XCTD-003008252015
31	Heli-09	25/08/15 15:10	83° 40.57 N	029° 20.36 E		15062640	1085	XCTD-003108252015
32	047-01	25/08/15 21:15	83° 53.01 N	031° 00.37 E	4051	15062639	109	XCTD-003208252015
33	049-01	26/08/15 04:37	84° 12.91 N	030° 54.40 E	4056	15062637	287	XCTD-003408262015
34	Heli-10	26/08/15 08:21	84° 34.02 N	031° 03.74 E		15062633	1085	XCTD-003508262015
35	051-01	27/08/15 15:30	84° 37.22 N	033° 30.81 E	4048	15062468	246	XCTD-003608262015

No	Station	Date Time [UTC]	Latitude	Longitude	Water depth [m]	XCTD s/n	XCTD depth [m]	Filename
36	052-01	27/08/15 21:48	84° 46.80 N	037° 29.44 E	4230	15062657	235	XCTD-003708262015
37	053-01	28/08/15 12:37	84° 58.81 N	041° 14.35 E	4224	15062664	113	XCTD-003808262015
38	055-01	29/08/15 21:12	85° 05.06 N	046° 57.72 E	4004	15062665	1085	XCTD-000008282015
39	056-01	29/08/15 01:30	85° 12.32 N	050° 20.34 E	3986	15062668	1085	XCTD-003908262015
40	057-01	29/08/15 07:14	85° 14.34 N	054° 49.07 E	3964	15062435	366	XCTD-004008262015
41	Heli-11	30/08/15 13:11	85° 13.66 N	059° 06.54 E		15062438	1085	XCTD-004108262015
42	Heli-12	30/08/15 08:23	85° 31.62 N	060° 17.53 E		15062442	1085	XCTD-004208262015
43	060-01	30/08/15 20:16	85° 39.05 N	060° 01.77 E	3936	15062667	490	XCTD-004308262015
44	Heli-13	31/08/15 02:22	85° 59.93 N	060° 00.15 E		15062443	1085	XCTD-004408262015
45	063-01	01/09/15 02:53	86° 17.65 N	059° 25.58 E	2583	15062444	44	XCTD-004508262015
46	063-01	01/09/15 03:03	86° 17.80 N	059° 30.18 E	2512	15062441	125	XCTD-004608262015
47	065-01	01/09/15 12:10	86° 33.29 N	061° 21.78 E	2554	15062433	317	XCTD-004708262015
48	067-01	02/09/15 00:05	86° 51.04 N	061° 01.77 E	3279	15062440	163	XCTD-004808262015
49	071-01	03/09/15 20:32	87° 10.85 N	057° 56.08 E	3627	15062437	1085	XCTD-004908262015
50	073-01	03/09/15 03:46	87° 31.41 N	060° 00.55 E	4180	15062436	1085	XCTD-005008262015
51	075-01	04/09/15 10:37	87° 51.64 N	060° 16.01 E	4449	15062463	656	XCTD-005108262015
52	077-01	04/09/15 21:43	88° 10.15 N	060° 44.99 E	4422	15062466	861	XCTD-005208262015
53	079-01	05/09/15 06:23	88° 30.23 N	060° 47.09 E	4420	15062439	1085	XCTD-005308262015
54	Heli-14	05/09/15 11:47	88° 51.90 N	060° 01.41 E		15062467	1085	XCTD-005408262015
55	082-01	06/09/15 22:07	89° 09.83 N	060° 28.92 E	4391	15062464	411	XCTD-005508262015
56	084-01	07/09/15 05:52	89° 30.12 N	060° 04.52 E	4351	15062465	1085	XCTD-005608262015
57	086-01	07/09/15 16:25	89° 50.10 N	046° 55.03 E	4306	15062434	211	XCTD-005708262015
58	088-01	08/09/15 12:06	89° 48.47 N	113° 15.86 W	4251	15062460	131	XCTD-005808262015
59	090-01	09/09/15 05:21	89° 24.17 N	119° 17.57 W	2313	15062457	1085	XCTD-005908262015
60	092-01	09/09/15 18:12	88° 57.21 N	112° 42.91 W	1375	15062461	1085	XCTD-000109092015

No	Station	Date Time [UTC]	Latitude	Longitude	Water depth [m]	XCTD s/n	XCTD depth [m]	Filename
61	095-01	10/09/15 17:08	88° 32.29 N	121° 02.01 W	3994	15062462	1085	XCTD-006009102015
62	097-01	12/09/15 11:41	88° 19.32 N	143° 33.31 W	3798	15062458	1085	XCTD-006109102015
63	Heli-15	13/09/15 08:26	87° 56.87 N	158° 56.48 W	3979	15062459	1016	XCTD-006209102015
64	Heli-16	13/09/15 09:10	88° 05.37 N	167° 08.14 W		14078047	1085	XCTD-006409102015
65	100-01	13/09/15 11:09	87° 54.40 N	170° 00.11 W	3979	14078048	1085	XCTD-006509102015
66	103-01	15/09/15 09:34	87° 12.33 N	162° 09.81 E	4006	14078057	1085	XCTD-006609102015
67	104-01	15/09/15 15:53	87° 02.64 N	153° 57.16 E	1796	14078056	247	XCTD-006709102015
68	106-01	16/09/15 05:57	86° 50.50 N	140° 14.10 E	2160	14078055	1085	XCTD-006809102015
69	107-01	16/09/15 11:14	86° 39.90 N	134° 46.53 E	3413	14078054	1085	XCTD-006909102015
70	108-01	16/09/15 17:22	86° 24.69 N	131° 07.29 E	4282	14078053	1085	XCTD-007009102015
71	109-01	16/09/15 22:39	86° 03.23 N	126° 47.56 E	4379	14078051	1085	XCTD-007109102015
72	110-01	17/09/15 04:05	85° 44.09 N	123° 37.85 E	4399	14078052	1085	XCTD-007209102015
73	111-01	17/09/15 09:24	85° 24.73 N	120° 53.61 E	4406	14078049	746	XCTD-007309102015
74	112-01	17/09/15 13:16	85° 12.90 N	118° 23.61 E	4410	14078050	1085	XCTD-007409102015
75	113-01	17/09/15 19:24	84° 54.42 N	115° 30.32 E	4425	15062656	1085	XCTD-007509102015
76	114-01	17/09/15 23:36	84° 38.24 N	113° 24.68 E	4222	15062655	1004	XCTD-007609102015
77	116-01	18/09/15 11:36	84° 24.90 N	112° 43.19 E	3135	15062654	1085	XCTD-007709102015
78	120-01	20/09/15 17:56	84° 55.56 N	128° 22.50 E	4358	15062653	385	XCTD-007809102015
79	Heli-17	21/09/15 06:36	84° 29.73 N	115° 41.58 E		15062649	1085	XCTD-007909102015
80	122-01	21/09/15 12:30	85° 06.81 N	135° 13.63 E	4282	15062652	1085	XCTD-008009102015
81	124-01	22/09/15 02:52	85° 04.84 N	140° 00.14 E	3911	15062650	471	XCTD-008109102015
82	126-01	23/09/15 06:16	85° 03.86 N	142° 56.05 E	3402	15062646	1085	XCTD-008209102015
83	127-01	23/09/15 07:57	85° 04.49 N	144° 37.98 E	2715	15062647	402	XCTD-008309102015
84	129-01	23/09/15 16:45	85° 00.88 N	149° 13.02 E	1725	15062651	1085	XCTD-008409102015
85	131-01	24/09/15 04:40	84° 58.17 N	153° 48.90 E	1667	15062645	1085	XCTD-008509102015

No	Station	Date Time [UTC]	Latitude	Longitude	Water depth [m]	XCTD s/n	XCTD depth [m]	Filename
86	133-01	24/09/15 12:29	84° 58.82 N	157° 11.32 E	2511	15062648	1085	XCTD-008609102015
87	135-02	25/09/15 06:39	83° 30.02 N	154° 56.01 E	2779	15062422	1085	XCTD-008709102015
88	136-01	25/09/15 07:54	83° 20.46 N	154° 48.68 E	2786	15062432	1085	XCTD-008809102015
89	137-01	25/09/15 10:00	83° 02.62 N	154° 14.02 E	2800	15062431	1085	XCTD-008909102015
90	138-01	25/09/15 13:39	82° 42.11 N	151° 57.09 E	2793	15062430	1085	XCTD-009009102015
91	139-01	25/09/15 15:41	82° 23.35 N	150° 33.08 E	2798	15062425	1085	XCTD-009109102015
92	140-01	25/09/15 18:51	82° 01.55 N	148° 25.69 E	2665	15062423	1085	XCTD-009209102015
93	141-01	25/09/15 21:18	81° 43.23 N	147° 00.30 E	2556	15062429	1085	XCTD-009309102015
94	142-01	25/09/15 23:17	81° 22.41 N	145° 53.29 E	2313	15062428	1085	XCTD-009409102015
95	143-01	26/09/15 01:22	80° 59.60 N	144° 35.64 E	1871	15062426	1085	XCTD-009509102015
96	148-01	06/10/15 22:17	74° 36.35 N	023° 57.92 E	211	15062424	200	XCTD-000210062015
97	150-01	07/10/15 05:12	74° 10.26 N	023° 43.81 E	414	15062427	396	XCTD-009610072015
98	151-01	07/10/15 06:16	74° 00.89 N	023° 36.49 E	455	15062669	433	XCTD-009710072015
99	152-01	07/10/15 07:17	73° 51.97 N	023° 28.98 E	469	15062670	453	XCTD-009810072015
100	154-01	07/10/15 18:04	73° 35.63 N	023° 18.42 E	450	15062671	434	XCTD-000310072015
101	155-01	07/10/15 18:45	73° 29.57 N	023° 14.02 E	443	15062676	428	XCTD-000410072015
102	156-01	07/10/15 19:31	73° 22.86 N	023° 08.97 E	431	15062673	415	XCTD-000510072015
103	158-01	07/10/15 23:25	73° 08.58 N	023° 01.44 E	410	15062677	395	XCTD-000610072015
104	159-01	08/10/15 00:13	73° 01.15 N	022° 57.93 E	413	15062674	400	XCTD-000710072015
105	160-01	08/10/15 01:11	72° 52.46 N	022° 53.74 E	402	15062680	391	XCTD-000810072015
106	162-01	08/10/15 11:27	72° 37.34 N	022° 46.49 E	382	15062679	372	XCTD-000910072015
107	163-01	08/10/15 12:38	72° 27.84 N	022° 41.49 E	337	15062672	325	XCTD-001010072015
108	164-01	08/10/15 13:43	72° 19.13 N	022° 36.29 E	320	15062675	310	XCTD-001110072015
109	166-01	08/10/15 17:00	71° 59.58 N	022° 24.44 E	369	15062690	357	XCTD-001210072015
110	167-01	08/10/15 18:07	71° 50.35 N	022° 18.80 E	373	15062678	360	XCTD-001310072015

No	Station	Date Time [UTC]	Latitude	Longitude	Water depth [m]	XCTD s/n	XCTD depth [m]	Filename
111	168-01	08/10/15 19:11	71° 41.48 N	022° 13.65 E	371	15062691	361	XCTD-001410072015
112	170-01	09/10/15 01:02	71° 21.62 N	021° 52.01 E	319	15062692	309	XCTD-001510072015
113	171-01	09/10/15 01:51	71° 15.03 N	021° 39.29 E	297	15062686	290	XCTD-001610072015
114	172-01	09/10/15 02:44	71° 07.69 N	021° 26.42 E	228	15062688	219	XCTD-001710072015

Tab. 3.5: Details of mooring deployments

Mooring	Latitude Longitude	Water Depth [m]	Instrument Type	Serial Number	Instrument Depth
Nansen	85°17.51 N 60° 0.87 W	3870 m	ASL IPS5 RAS-500 SBE 37 ODO ET861G ADCP SBE 37 ODO Sono Vault Sediment trap ADCP Seaguard SBE 37 SBE 37 Sediment trap SBE 37 Seaguard	51182 13380-02 13037 896 22388 13012 1060 2004371 22389 563 12481 12479 2004372 12477 522	30 47 47 176 176 178 187 209 216 722 2168 3168 3723 3725 3730
Karasik	87°0.97 N 59°15.52 E	4711 m	ASL IPS5 SBE 37 ODO ET861G ADCP SBE 37 ODO Sediment tap ADCP RCM7 SBE 37 ODO SBE 37 ODO Sediment trap SBE 37 ODO RSM8	51184 13491 835 23456 13490 2009404 23549 8050 13489 13488 2012411 13487 9391	65 72 126 228 230 259 266 773 3259 3609 4564 4569 4571

Tab. 3.6: Details of glider and Argo float deployments and recoveries

WMO-Nr.	Ser.No	Date	Time [UTC]	Position		Depth [m]	Comments
ARGO profiler							
4901426	OIN14DARL20	2015/10/04	17:40	74°0.163'N	6°20.500'E	2225,7	deployment
Gliders							
68459	558	2015/10/05	7:00	75°33.43'N	2°39.72'E	3716	recovery
6800955	127	2015/10/05	10:28	75°23.43'N	1°08.59'E	3749	recovery

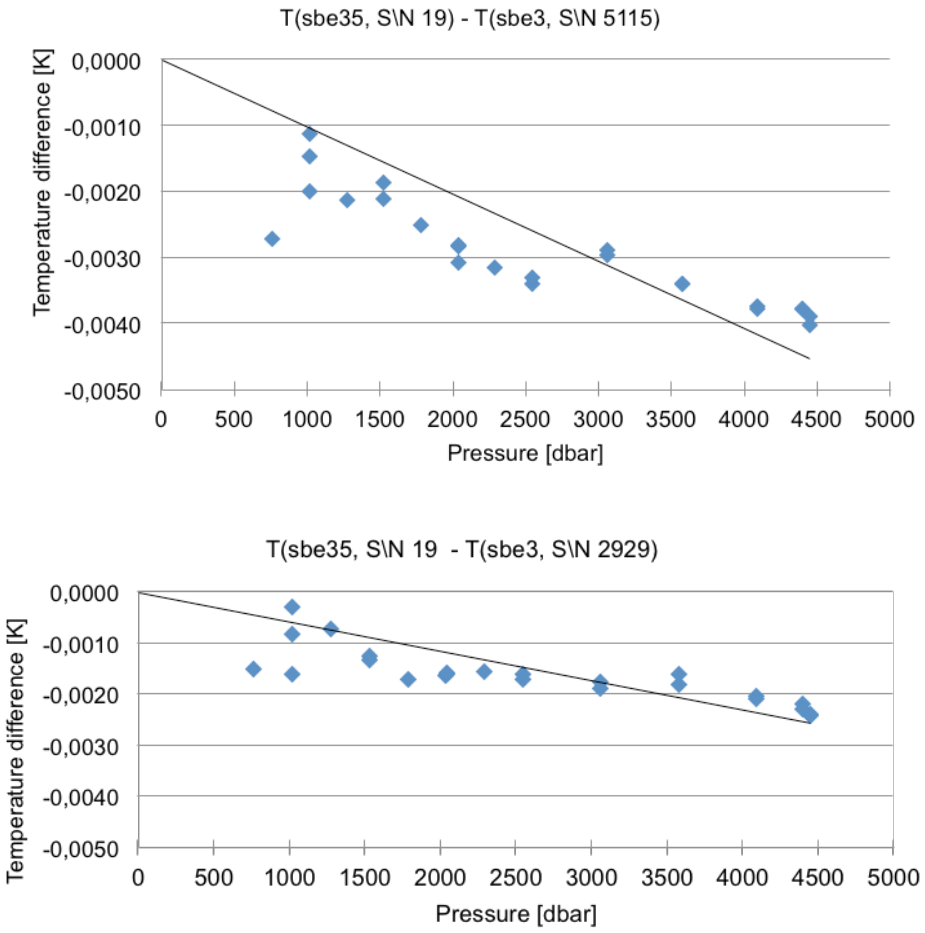

Fig. 3.2: Pressure dependence of a CTD temperature sensor SBE35 identified by comparison with SBE3 thermometers at station 117-2.

Upper panel: T(sbe35, S\N 19) - T(sbe3, S\N 5115) vs. pressure

Lower panel: T(sbe35, S\N 19) - T(sbe3, S\N 2929) vs. pressure

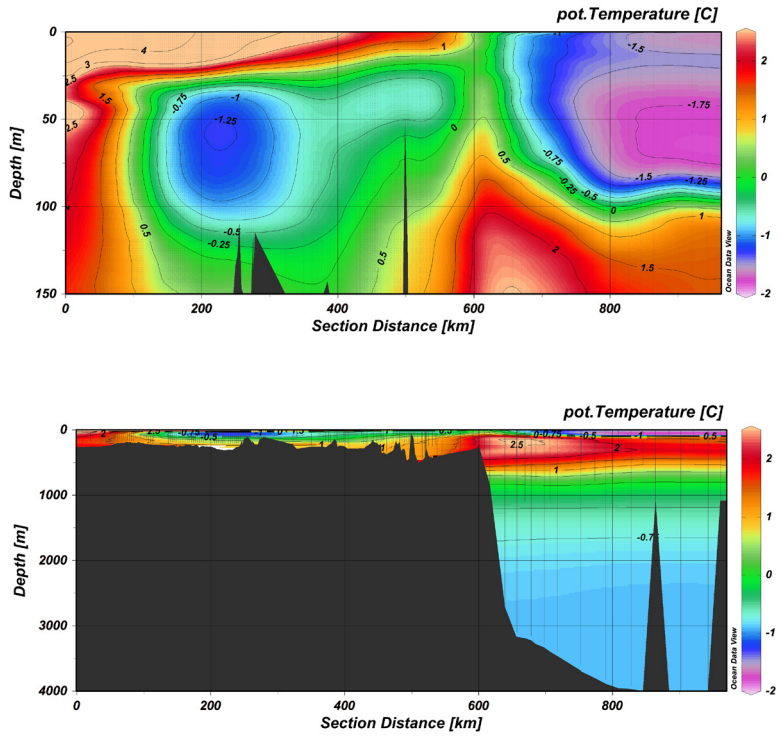

Fig. 3.3: Potential temperature, referenced to 0 dbar, from CTD, XCTD, UWCTD and UCCTD casts along 30°E (section 1, see Fig. 3.1). Locations of CTD casts are denoted by thin black lines. Both the full section and an enlarged near-surface part are shown. Contours denote temperature in °C.

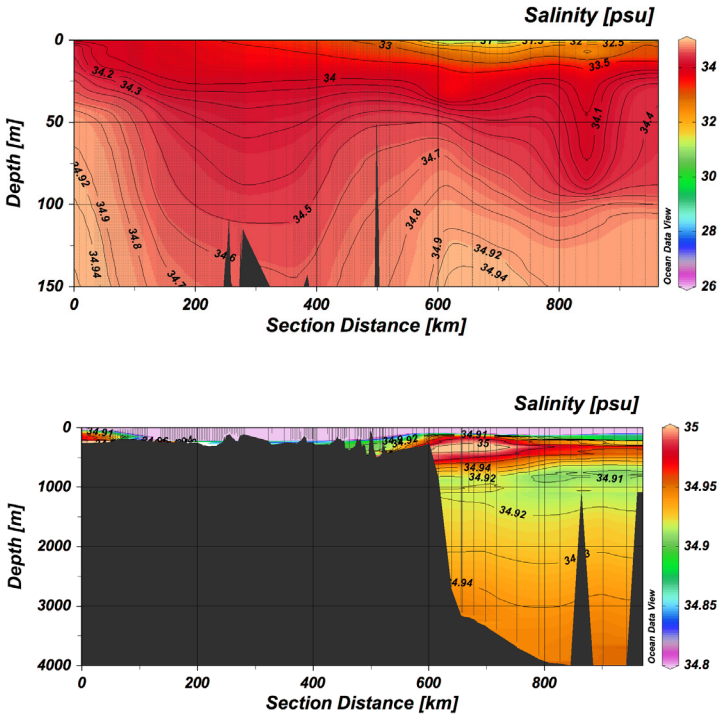

Fig. 3.4: Salinity along the section 1. Contours denote practical salinity on the PSS78 scale

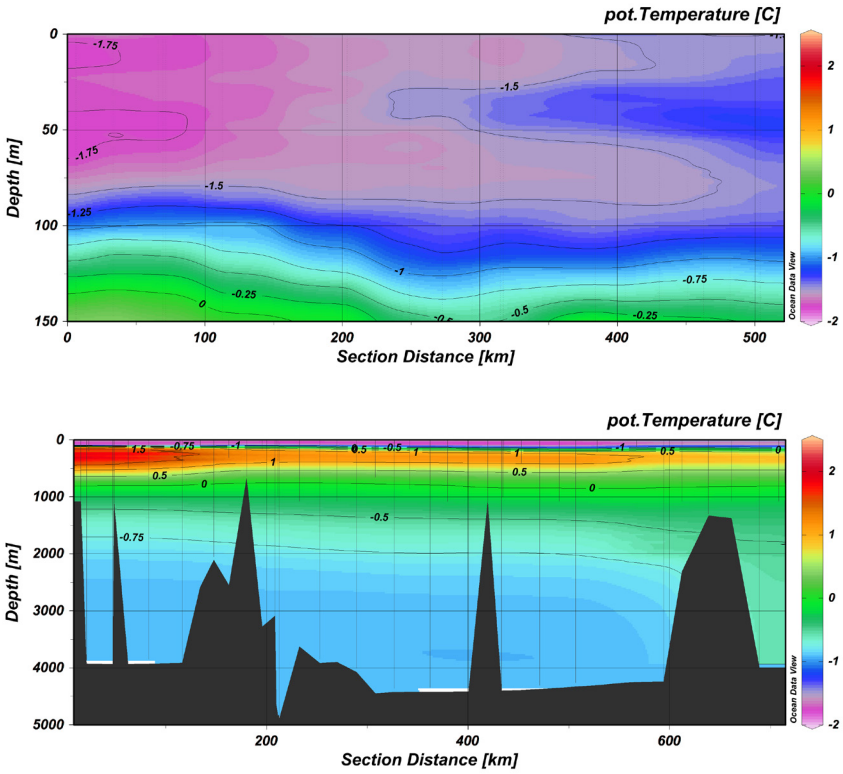

Fig. 3.5: Potential temperature, referenced to 0 dbar, from CTD, XCTD and UCCTD casts along 60°E/120°W (section 2, see Fig. 3.1). Locations of CTD casts are denoted by thin black lines. Both the full section and an enlarged near-surface part are shown. Contours denote temperature in °C.

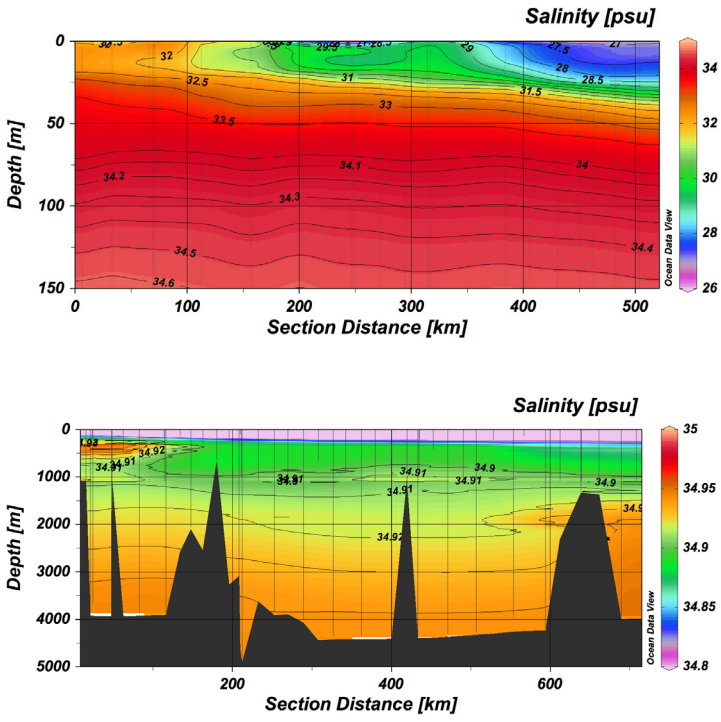

Fig. 3.6: Salinity along the section 2. Contours denote practical salinity on the PSS78 scale

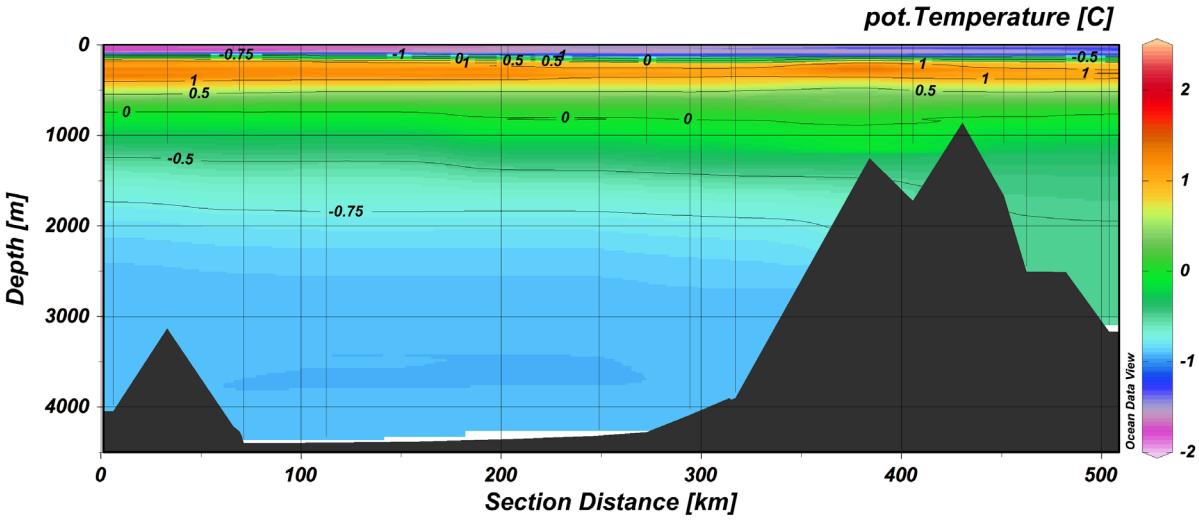

Fig. 3.7: Potential temperature, referenced to 0 dbar, from CTD, XCTD and UCCTD casts along section 5 (see Fig. 3.1). Locations of CTD casts are denoted by thin black lines. Both the full section and an enlarged near-surface part are shown. Contours denote temperature in °C.

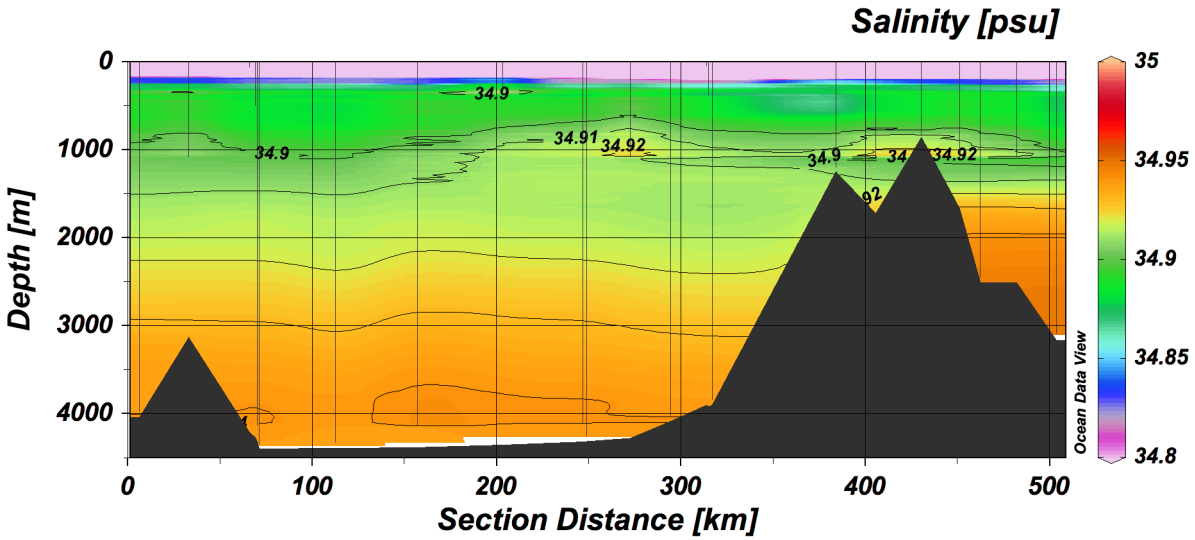

Fig. 3.8: Salinity along the section 5. Contours denote practical salinity on the PSS78 scale

References

Joyce TM (1989) On the in situ calibration' of shipboard ADCP. J. Atm. Oceanic Technol., 6, 169–17

4. SEA ICE PHYSICS

Stefan Hendricks[1], Robert Ricker[1], Larysa Istomina[2], Justin Beckers[3], Hazel Hartman Jenkins[1]

[1]AWI
[2]IUP
[3]UAlb

Grant No. AWI_PS94_00

Introduction

Recent evaluations of trends in Arctic sea ice extent observed by passive microwave satellite missions shows a downward trend of -3.8% per decade of total yearly averaged sea ice cover, whereat multi-year ice coverage is effected the most (-11.5 % per decade). While these are yearly averaged values, the spread in the seasonal cycle is most pronounced during the summer minimum, where the three lowest observed ice extents occurred between 2007 and 2012. The reduction of summer sea ice cover and its shift to a dominant seasonal ice type has implications on the energy balance of the Arctic Ocean through the ice-albedo feedback, increased absorption of solar radiation and the ice function as a habitat.

Except passive microwave estimations of sea-ice concentration and a satellite retrieval algorithms of melt pond concentrations, most observations of the mass balance during summer and the following freeze-up period rely on airborne, ship-borne and *in-situ* observations. The main objective of the sea ice physics group was therefore to extend the time series of essential climates variables (ECV), such as sea ice thickness, which was taken from *Polarstern* during the summer and the early freeze-up season of 2015. Besides the continuation of the sea-ice thickness time series, one objective was to use technical advances of ice thickness sensors to measure the spatial variability of sea-ice porosity and its influence of sea-ice volume estimation. This is motivated by the earlier anecdotal findings of significant ice porosity, which might lead to a bias in ice volume estimation by means of sea-ice thickness measurements alone.

4.1 Airborne sea ice surveys

Objectives

The summer minimum extent of sea ice is mainly controlled by its thickness distribution at the start of the melting season. The increasing loss of ice volume in the recent decade is manifested in a series of record lows of summer ice extent, but its magnitude is poorly quantified due to a lack of ice thickness information derived from remote sensing data. Satellite data on ice thickness exists mostly from the spring or late autumn period, when the ice surface is cold and altimeters can be used to estimate its height above the water surface. The ice thickness distribution during the melting season can only be measured during ship cruises, preferably with airborne surveys to minimize ship route selection bias. Sea ice thickness data derived from electromagnetic induction (EMI) data measured during *Polarstern* cruises in the Transpolar Drift exist from 1991 on, with additional airborne electromagnetic (AEM) data since 2001. The objective of airborne survey during TransArc-2 is to continue this time series, with additional documentation of the ice surface parameters.

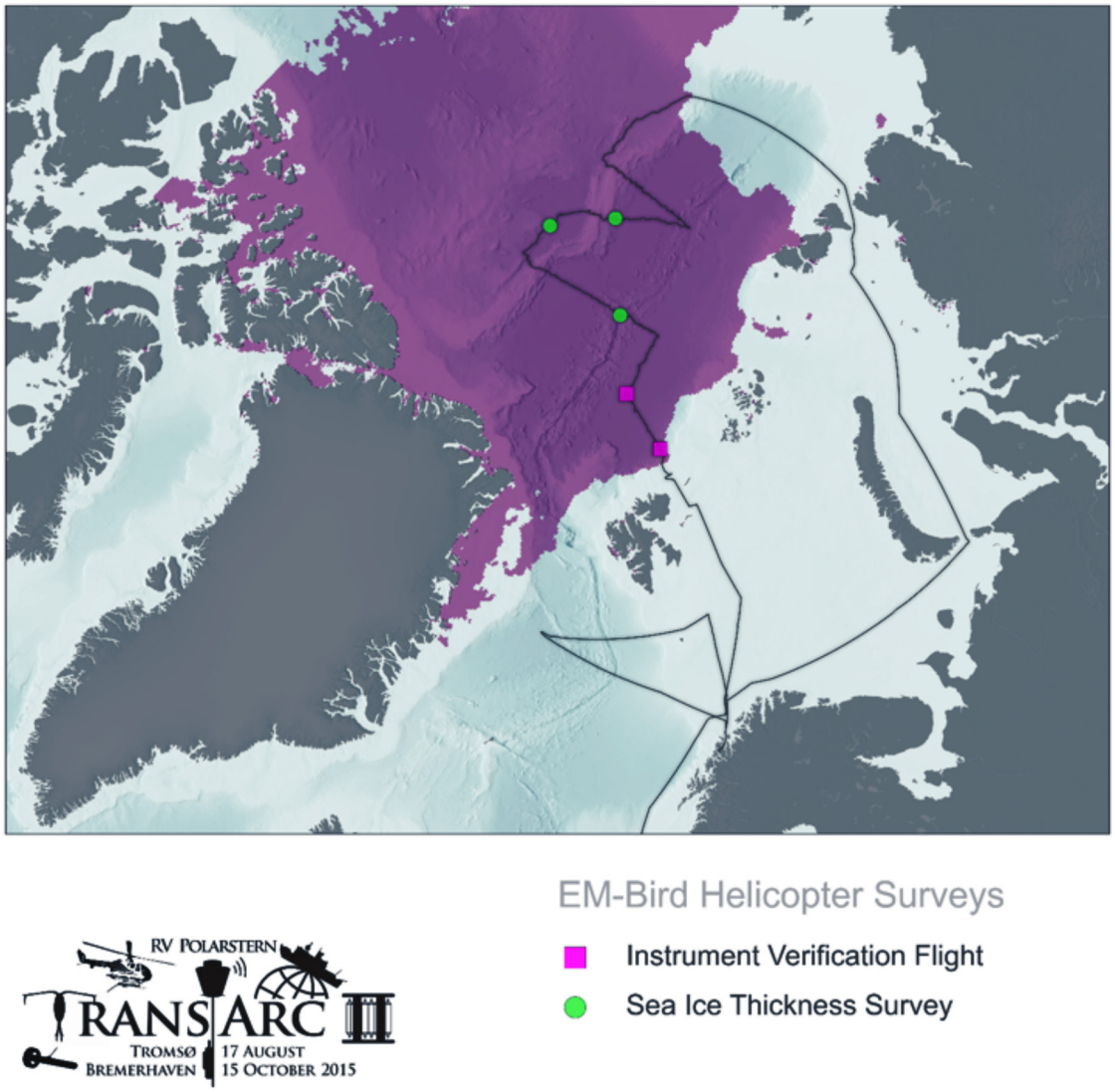

Fig. 4.1: Location of all EM-Bird helicopter surveys

Tab. 4.1: List of airborne EM (AEM) sea ice thickness and aerial imagery survey flights

Station	Gear	Longi-tude	Lati-tude	Comment	Start Date	Start Time	End Date	End Time
PS94/HANT-1	AEM	30.931	81.868	ID: maisie_20150822_01 Instrument Verification Flight	22.08.2015	11:52	22.08.2015	12:44
PS94/HANT-3	AEM	30.610	84.486	ID: 20150827_01 Instrument Verification Flight	27.08.2015	11:57	27.08.2015	12:22
PS94/HANT-16	AEM	58.844	87.019	ID: 20150902_01	02.09.2015	07:08	02.09.2015	09:12
PS94/HANT-21	AEM	-171.793	87.885	ID: 20150913_01	13.09.2015	12:13	13.09.2015	14:19
PS94/HANT-23	AEM	135.618	86.648	ID: 20150916_01	16.09.2015	10:45	16.09.2015	11:49

Work at sea

We used an airborne electromagnetic (AEM) induction sensor (MAiSIE: Multi Sensor Airborne Sea Ice Explorer, Norwegian Geotechnical Institute) to measure sea ice thickness by helicopter surveys. The AEM sensor was towed on a 20m-long cable at an altitude between 10 and 15 m above the ice surface. The method utilizes the difference of electrical conductivity between sea ice and sea water to estimate the thickness of sea ice, including the snow layer if present. MAiSIE was equipped with a nadir-looking Canon EOS 5D MkII digital camera. The nadir images are used as a documentation of sea ice surface conditions and for the assessment of melt pond fractions. The internal timestamp of the camera was synchronized with the GPS timestamp of the AEM sensor, so that sensor attitude and altitude information can be used to geo-reference each image.

Preliminary results

Throughout the entire cruise, flight operations were significantly hampered by unfavorable weather conditions with persistent low clouds, fog and snow showers. Therefore, only 5 flights with the EM-Bird were accomplished (Fig. 4.1 and Table 4.1). The first two flights did not result in scientific data, but were necessary to assess sensor noise at altitudes higher than 300 feet and to verify the instrument readiness after a failure of an EM transmitter amplifier in-flight after the first take-off. Of the three other flights, two had to be aborted due to deteriorating weather conditions.

A preliminary quality control was done on-board, but the post-processing and data product generation will be done after the cruise.

Due to the sparseness of the AEM data collection, additional mummy chair stations with ground-based EM sensors were implemented to partially fill the gap of ice thickness information (see following section).

Data management

The sea ice thickness data will be released following final processing in the PANGAEA database and other international databases like the Sea Ice Thickness Climate Data Record (Sea Ice CDR). Aerial images will be archived at the AWI long-term data storage system.

4.2 Sea Ice thickness and porosity

Objectives

Similar to the AEM measurements, on-ice sea ice thickness surveys using electromagnetic inductions sensors are a continuation of measurements from former cruises ranging back to the early 1990s. At each ice station the ice floe is surveyed with one or more EM sensors to receive thickness characteristics and distribution of individual floes. In addition, coincident snow depth measurements are necessary to assess the snow depth distribution and obtain sea ice thickness, since the ground-based EM sensors only measure the sum of snow and ice thickness.

Under summer conditions sea ice is both highly porous and permeable; however, measurements of sea ice porosity and their influence on EM sensors and on the total ice volume are spatially and temporally limited. In addition to collecting data on ice porosity with sea ice cores, we aim to retrieve ice porosity by geophysical inversion of the same ground-based electromagnetic induction (EM) sensors that are used for the ice thickness surveys. Furthermore, over the past decade several new ground-based (EM) sensors have been developed and utilized over

sea ice in the Arctic and Antarctic. Therefore we also test and compare four different sensors (Geophex GEM2-484, Geophex GEM2-512, GSSI EMP-400, GeoSensors SIS, Table 4.2) with respect to sea ice thickness measurements.

The primary objectives are therefore to extent existing long-term time series of the essential climate variable (ECV) sea ice thickness and to use technological advances to better assess the uncertainty of the time series and to obtain new parameters. The tasks for this objective can be broken down as following:

1. Obtain high resolution ice thickness and snow depth data of individual floes (*Sea Ice Thickness Surveys*)
2. Compare electromagnetic induction (EM) measurements of sea ice from three different sensors with varying frequencies and transmitter/receiver coil spacing's (*EM Inter-comparison*)
3. Assess retrieval of sea ice porosity by geophysical inversion of the EM sensor data using sea ice porosity measurements from ice core as validation (*Sea Ice Porosity*)
4. Collect measurements of conductivity and temperature of the water below the ice and in melt ponds as they influence the EM sensor response (*Under-Ice CTD*)

Table 4.2: List of used ground EM devices during PS94 and sensor setups.

EM device	Frequencies Setup [Hz]	Coil spacing [m]
Geophex GEM2-484	1530, 5310, 18330, 63030, 93090	1.67
Geophex GEM2-512	5010, 9030, 15990	1.67
GSSI EMP400	5000, 9000, 16000	1.219
GeoSensor Sea Ice Sounder (SIS)	9000	1.0/2.0/4.0

Work at sea

The on-ice work at sea was performed at:

- 7 full-length ice stations of more than 8 hours duration
- 1 short-duration helicopter-based ice station with two landings
- 6 short-duration stations accessed by mummy-chair.

The scientific programme at each of the full-length stations varied somewhat due to fog and darkness but generally began with a floe-survey of total thickness using one or more of the EM sensors along with a Snow Hydro MagnaProbe measurements of snow depth. The floe-survey was followed by the calibration of the EM sensors, drilling of EM sensor calibration site and the acquisition of two sea ice cores for temperature and porosity at the calibration site. One or two shallow CTD casts were made at the EM calibration site using the Ruskin RBR Concerto CTD from York University. The depth of each cast varied with the water currents but always extended deeper than 40 m.

A 50 m EM sensor inter-comparison and validation line was established so as to include level and deformed ice. Measurements of the EM response were made at each meter of the line with all of the available EM sensors. Then at each meter, holes were drilled and measurements of snow depth, ice thickness and freeboard were taken. Furthermore, the thickness of the

refrozen melt pond ice and the depth of melt ponds were also measured. Additional CTD casts and porosity cores were occasionally acquired along the validation line along with occasional measurements of melt pond water conductivity.

At mummy-chair stations a reduced programme of EM measurements of sea ice + snow thickness (total thickness) using the GEM2-484 sensor and MagnaProbe measurements of snow depth was conducted. In addition, one to five drill-hole measurements of ice thickness were made for calibration/validation of the GEM2-484. Additionally, at several mummy-chair based stations, buoys were deployed (for a full description see chapter 5). At the helicopter-based stations the measurements were reduced to EM measurements of sea ice + snow thickness (total thickness) using the GEM2-484 sensor and several calibration drill-hole measurements of ice thickness.

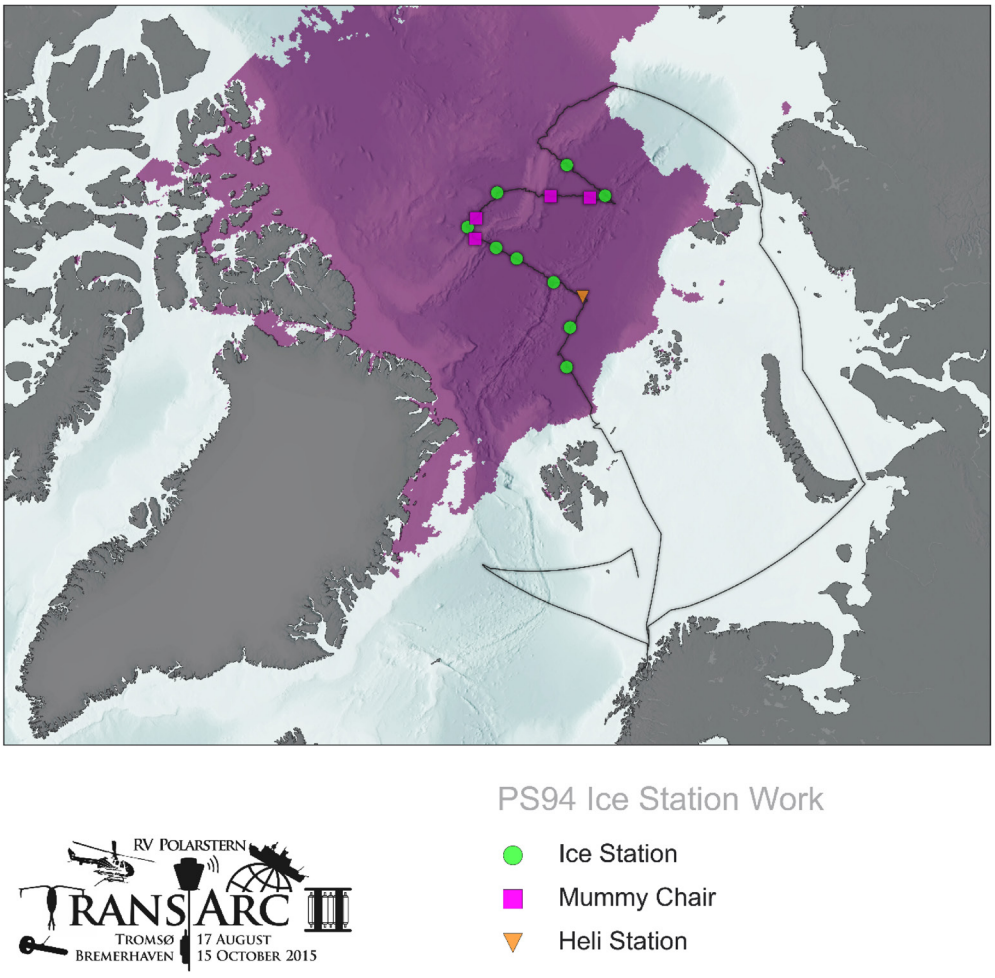

Fig. 4.2: Location of all sea ice work on ice, mummy chair and helicopter stations

Sea Ice Thickness Surveys

We used the ground-based electromagnetic devices to measure sea ice plus snow thickness. The method is based on the contrast of electrical conductivity between ocean water and sea ice (including snow). GEM-2-484 surveys were made during all stations, other sensors depending on availability of station time. The device was pulled over the snow cover, mounted in a plastic

sled. The sampling rate was 10 Hz. Surveys with the other EM devices have been carried out occasionally. For calibration purpose a wooden ladder was used to allow a stepwise increase of the distance to the conductive layer.

The snow depth during GEM-2 surveys was measured with a MagnaProbe and approximately 2 m point spacing. The device measures the snow depth and records it on a data logger for later down-loading to a computer. The method is based on a disk, which slides on a pole. The height of the disk above the pole end indicates the snow depth and is electronically recorded. We started magna probe measurements after substantial snow accumulation where an average snow layer of >10 cm has been observed (station ICE-3). During the GEM-2 surveys the person who operated the MagnaProbe usually walked about 3-4 m in front or behind the GEM-2 sled.

Table 4.3 gives an overview the types of measurements (survey, cal, drilling, drift) at each station. The MagnaProbe snow depth profiles are summarized in Table 4.3.

EM Inter-comparison

EM sensor inter-comparison consisted of:

- EM measurements at each meter of a 50 m long profile established so as to include representative ice types: level ice, melt ponds and a ridge. The physical properties of the EM sensors are described under the Thickness and Snow Depth Survey's section above.
- Additional sea ice thickness surveys of the floes. In addition to the Geophex GEM2-484 sensor used for sea ice thickness surveys, additional EM sensors, such as the GeoSensors SIS and the GSSI EMP-400 were occasionally towed along the same profile or just over the same floe in order to compare the measurements point-to-point or by their statistical distributions.
- EM sensor thermal drift measurements after being initialized from ambient air temperature and after initialization at near room temperature. Each sensor was placed in a fixed location, separate from the other sensors by > 15m and set to collect data while other tasks were completed.

Sea Ice Porosity

Ice core work-at-sea involved the acquisition of cores at the calibration site of the EM sensor. A 9 cm diameter core was acquired using a Kovacs Ice Drilling Equipment Inc. Mark II ice corer. At each site the temperature core was acquired first and temperature was measured with a Thermo 110 at 0.1 m intervals from top to bottom. Care was taken to ensure the core was not in full sun and that measurements of temperature were captured quickly. The porosity core was acquired next and was placed immediately into sealed bags. One temperature core was sectioned and processed as an example porosity core to develop the processing methodology. The method requires accurate estimates of ice volume and ice mass and the latter measurement cannot be performed on a ship. Ice porosity measurements will be completed in AWI in Bremerhaven.

Under-Ice CTD

CTD under-ice work included:

- One or more CTD casts at the EM calibration/sea ice porosity core acquisition site with the Ruskin RBR Concerto CTD. Each first cast was triggered by a conductivity threshold of 0.1mS/cm and recorded at 6Hz for both directions of travel through the column.
- Additional CTD casts at features of interest/as time allowed.

Preliminary results

Sea Ice Thickness Surveys

A quicklook product of the sea ice thickness and snow depth surveys has been created of the individual floes. Corresponding maps have been made available for site selection of other measurements directly after the surveys. The final revision of the EM data will require an extensive quality control and postprocessing using results from the calibration procedures on the ice stations. Fig. 4.3 shows an example map of a survey using the GEM-2-484 during station ICE-6 on November 09, 2015. We used the imaginary part (Quadrature) of the 5,310 Hz signal for the conversion into thickness. A projection algorithm using DSHIP information of the position of the Trimble 1 GPS antenna and the heading was applied to create a local reference frame using a cartesian coordinate system and eliminate the effect of the drift and rotation of the ice floe.

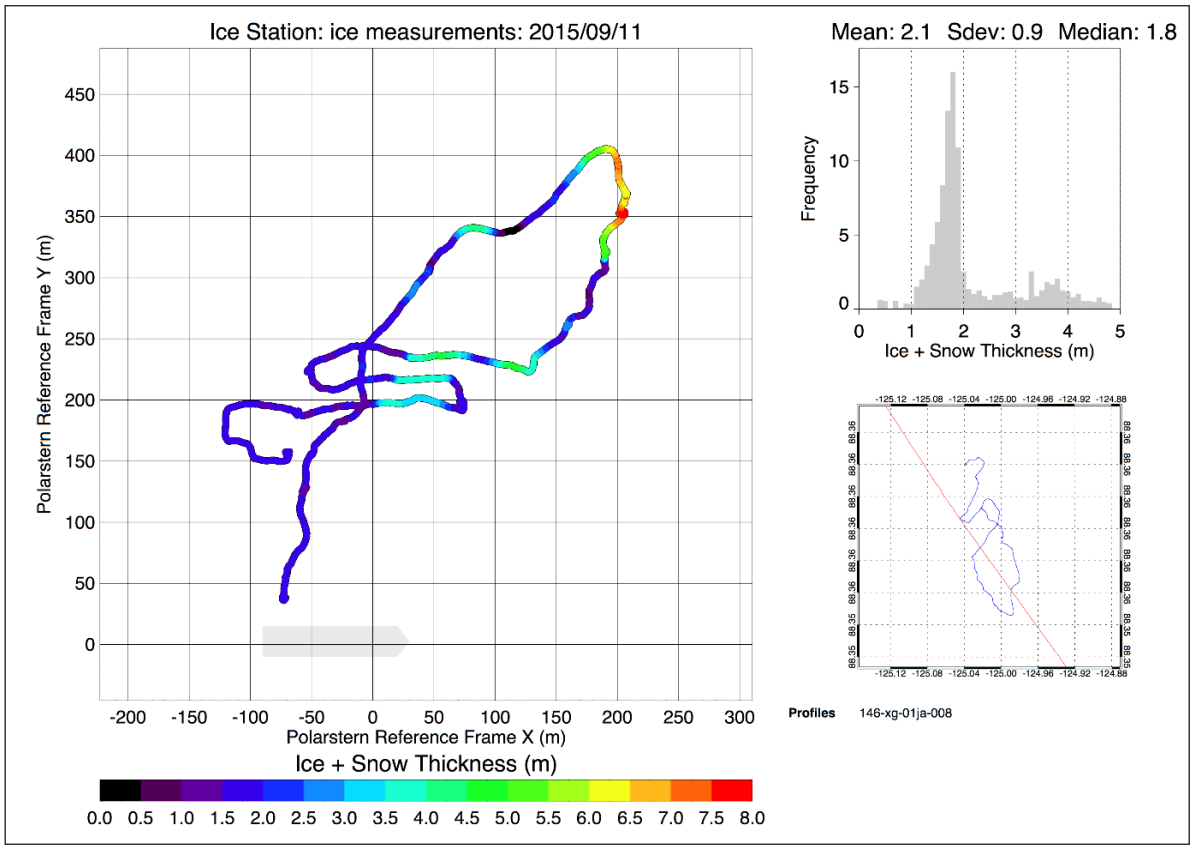

Fig. 4.3: Example ice plus snow thickness map (left panel) from gem2-484 on 09.11.2015 after drift correction (lower right panel). Measurement locations are given in a reference frame relative to the ship position (grey box). The upper right panel shows the corresponding histogram.

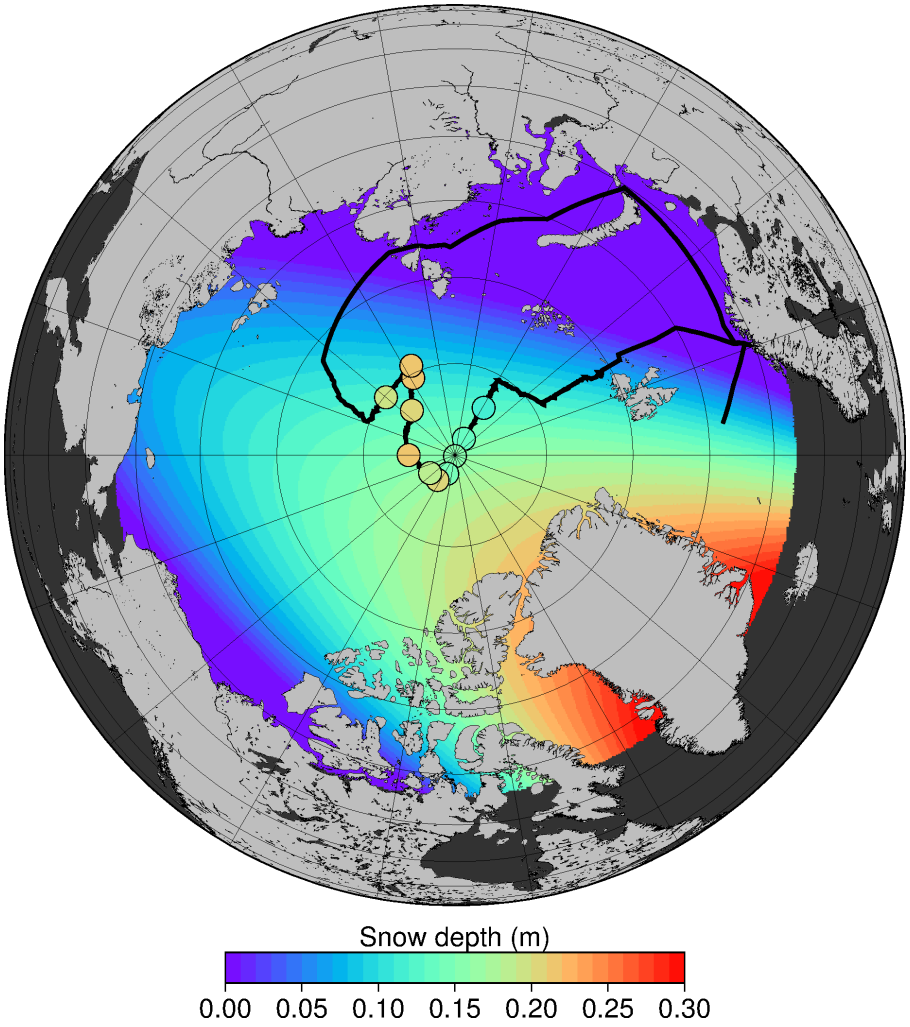

Fig. 4.4: Mean MagnaProbe-measured snow depth for each station. The background shows the climatologic snow depth for September, derived from the climatology by Warren et al. (1999).

In the example of Fig. 4.3, the histogram reveals a primary modal thickness of 1.8 m. Heavily deformed, thick ice has been found at (200 m, 350 m).

The MagnaProbe snow depth data do not need further processing and are ready for archiving. Fig. 4.4 shows averaged snow depth of each ice station along the cruise track. All measurements were carried out in September. Therefore, the gridded average September snow depth derived from the Warren climatology is shown in the background. While the first 4 stations coincide with the climatology, the latter stations show consistently higher snow depth. A composite of all total thickness observations from all surveys is in Fig. 4.5. The most frequent ice+snow thickness is 1.4 m, which is marginally thicker than in previous years considering the large modal snow depth of 0.15 m.

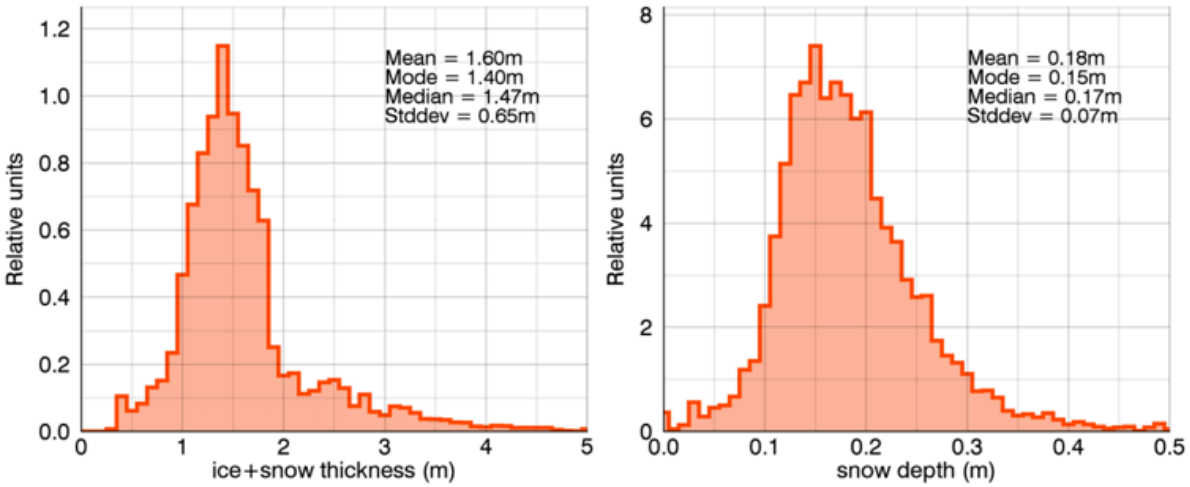

Fig. 4.5: Histograms of ice plus snow thickness (left panel) and snow depth (right panel) taking into account surveys at all stations.

EM Inter-comparison: Thermal Drift: Hot-Cold Drift & Cold-Drift

Two thermal drift experiments were conducted to examine the thermal response of the four EM sensors. Fig. 4,6 and Fig. 4.7 below present the EM response of the various EM sensors during the cold drift experiment. The EM signal amplitude was computed from the in-phase and quadrature response and then normalized. In Fig. 4.6 the 5 kHz response of the EMP, GEM2-484 and GEM2-512 are shown along with a histogram. During the cold drift, EM sensors were well equilibrated with the outdoor air temperature and set to record in a fixed location apart from each other and other sources of interference. The GEM2-484 and GEM2-512 were low-pass filtered as they record data at 10Hz while the EMP records at 1Hz. The histogram for each sensor has been aligned using the modal value to provide an indication of the distribution of the thermal noise. Interestingly, the GEM2-484 shows decreasing amplitude over time while the amplitude measured by the GEM2-512 increases over time and the EMP-400 measured a non-linear change in amplitude. Equivalent data exists from the same cold-drift experiment but for the 9 kHz response of the GEM2-512, the EMP-400 and the SIS sensor. For the SIS sensor, the horizontal-co-planar (HCP, or horizontal receiver and transmitter) and horizontal cross-planar (HXP, or Horizontal Transmitter, Vertical Receiver) response of all coils (1 m, 2 m, and 4 m) have been measured.

During the hot drift experiment the EM sensors were taken from heated (~20ºC) storage and setup on the ice in fixed locations separated from each other and other possible sources of interference and set to record as the sensors cooled to ambient air temperature. While standard operating procedure is to allow the sensors to cool to ambient air temperature, this experiment provides an indication of the thermal drift rates of the different sensors and their sensitivity to such changes.

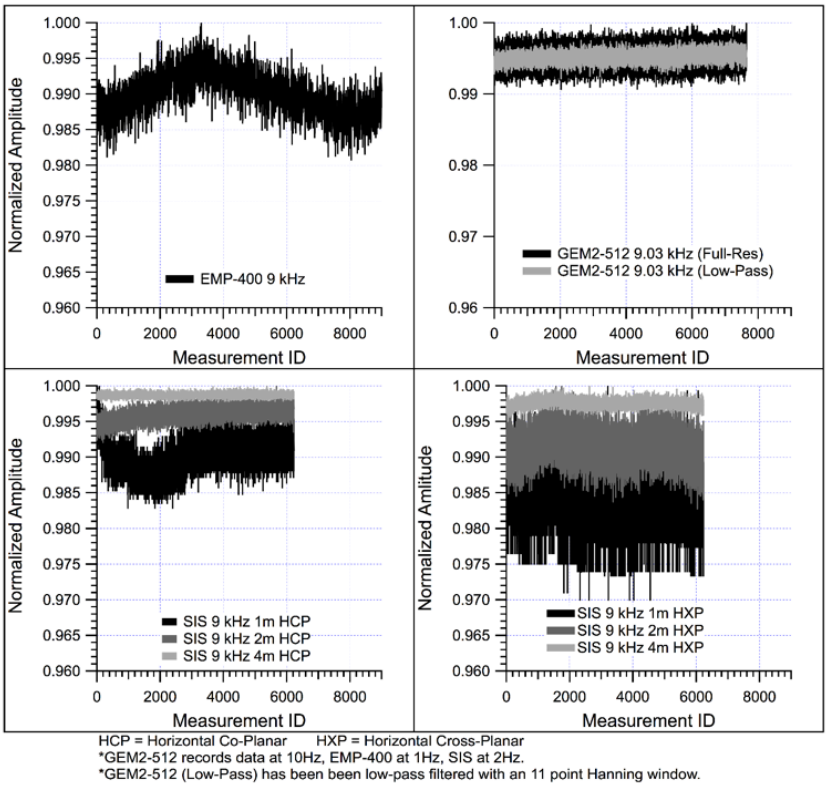

Fig.4.6: Cold drift experiment of several EM-sensors: Any signal change is due to changing sensor characteristics, not due to changes of the physical environment. Exemplary data channels from three sensors: (top left) GSSI EMP-400, (top right) Geophex GEM-2, (bottom) GeoSensors SIS.

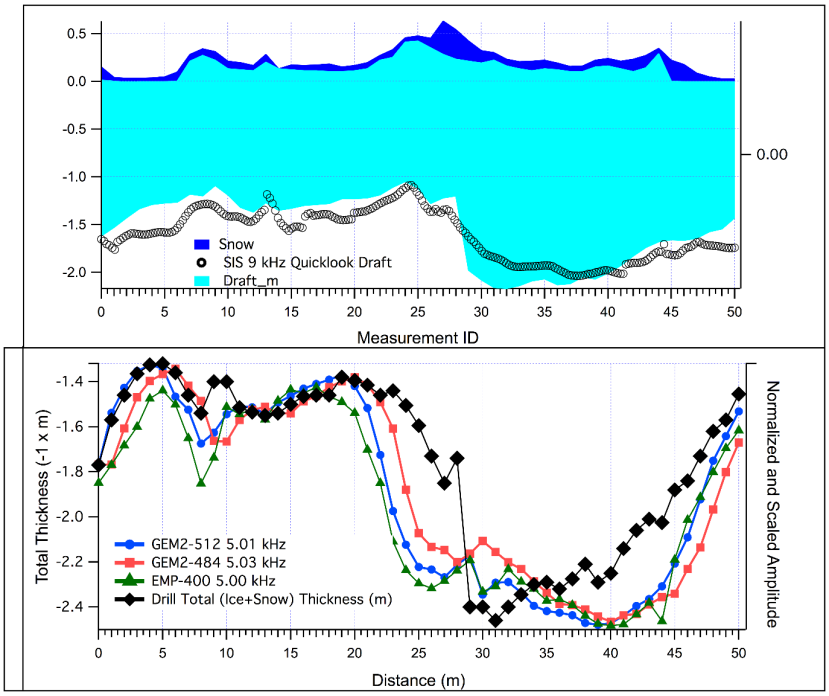

Fig. 4.7: Inter-comparison of different EM ice thickness sensors along a profile with known thickness. (top panel) Ice thickness (turquoise) and snow depth (dark blue) at drillhole locations. and GeoSensor SIS Quicklook ice thickness (bottom panel) normalized EM channels of other EM sensors (GEM2-512, GEM2-484, EMP-400; right axis) with total ice thickness from drill hole measurements (black line with diamond markers; left axis).

EM Inter-comparison: Drill-Line Inter-comparison

Fig. 4.7 provides an example of the drill-line inter-comparison but also shows the normalized EM amplitude response along with the total (snow + ice) thickness measured along the line. In addition to the thickness comparisons, the EM sensors will data will be utilized for geophysical inversions of parameters such as ice porosity, ice conductivity and water conductivity.

Sea Ice Porosity

A total of 7 temperature and 14 porosity cores were acquired. Porosity was also measured on the temperature cores (see Table 4.3 for a list of all cores). Differences between temperature-core porosity and porosity-core porosity may be due to the increased time for drainage of the temperature cores during the temperature measurements. Fig. 4.8 provides an example of the ice core salinity and the corresponding density (a proxy for porosity) profile for the temperature core acquired on September 11, 2015 (20150911A1/A2). Ice core density was measured both by mass and volume of solid ice and by the liquid and solid volumes. Mass measurements are highly inaccurate on-board a moving ship; however, measurements of liquid volume remain accurate.

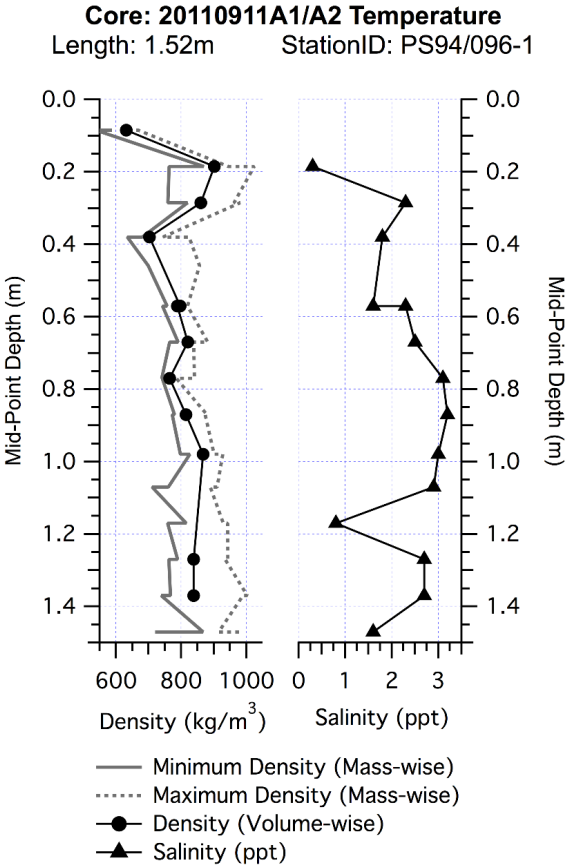

Fig. 4.8: Example of sea-ice density profile (measured mass-wise and volume-wise) and bulk salinity of melted core sections

Under-Ice CTD

A total of 14 CTD casts were made at 6 of the full-length ice stations (Table 4.3) with one additional cast performed with the RBR CTD attached to the main CTD-Large rosette of the physical oceanography team for calibration. The raw data provided has not been corrected or adjusted in any way. The CTD recorded at 6Hz and the raw data files include data collected during the downfall and upwards retrieval (Fig. 4.9). Multiple casts at a site were split into separate files afterwards by examining the depth profile.

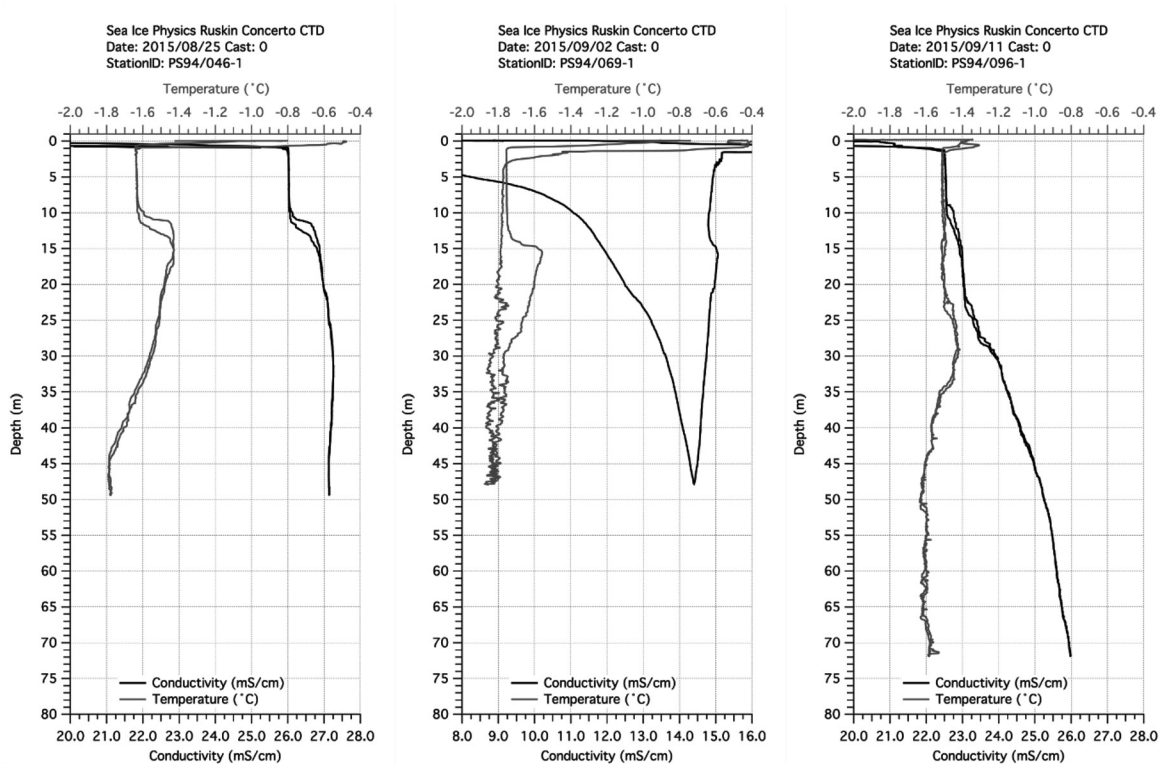

Fig. 4.9: CTD casts taken at stations PS94/046-1, PS95/069-1, and PS94/096-1

Data management

Finalized ice thickness data from the EM sensors and snow depth data will be made available in PANGAEA within 3 years. All data will be provided in both delimited ASCII files and in a self-describing compact format such as HDF5 or NETCDF. Ice core porosity will be processed at AWI. EM data will be processed at York University, the University of Alberta, and at AWI.

4.3 Optical properties of sea ice

Objectives

The characteristic feature of the sea ice in summer is the presence of melt ponds, which affect albedo, mass balance and heat balance of the ice. 96% of total annual heat input through sea ice occurs from May to September when the melt ponds are present. The increased amount of energy passing through the sea ice affects also eco-systems and geochemical processes in and beneath the sea ice. Due to large role the melt ponds play in the amount of energy both transmitted through and reflected from the sea ice, it is important to study the optical properties of the ponds in detail, which is the objective of the optical work during this cruise. This work complements studies from the expeditions PS78 (ARK-XXVI/3; TransArc, 2011) and PS80 (ARK-XXVII/3; IceArc, 2012).

For the satellite retrievals of sea ice properties, an atmospheric correction is necessary, which includes the well-known Rayleigh scattering correction and a correction for atmospheric aerosols. Their distribution is non-uniform both horizontally and vertically in the atmospheric column, and their amount and distribution in the Arctic are not well known. Therefore *in-situ* aerosol optical depth (AOD) measurements are of extreme importance and they have also been performed during the cruise.

Work at sea

The optical measurements consisted of

- Manual under-ice measurements of irradiance and radiance under selected melt ponds during 8 ice stations (Fig. 4.2). These measurements were performed with two Ramses spectral radiometers (320-950 nm, Trios GmbH, Rastede, Germany), the first with a cosine receiver and the second with a narrow angle (field of view 7°) receiver fixed on a foldable arm (L-arm).
- Surface measurements of solar irradiance with Ramses spectral radiometers above the sea ice for each measurement in (1).
- Surface albedo (incident and reflected irradiance) measurements using a FieldspecPro II (350-2500 nm, Analytic Spectral Devices, Boulder, USA) on L-arm cites, selected representative melt pond and sea ice surfaces during the ice stations.
- A radiation station was deployed during the last ice station.

Furthermore, a total of 5 ice cores were retrieved from selected L-arm sites for texture analysis (Table 4.3). As a contribution to the extremely sparse dataset of AOD in the high Arctic, a series of underway AOD measurements have been performed with a hand-held sunphotometer Microtops II (Table 4.4).

Tab. 4.4: List of all underway aerosol optical depth measurements taken by a mobile sun photometer (Mikrotops)

Label	DateTime	DateTime	Latitude	Longitude
PS94/AOT1	08/17/2015 13:10:12	08/17/2015 13:11:24	69.698	19.074
PS94/AOT2	08/19/2015 07:32:32	08/19/2015 07:34:19	76.911	30.142
PS94/AOT3	08/19/2015 10:13:22	08/19/2015 10:14:55	77.337	30.404

Label	DateTime	DateTime	Latitude	Longitude
PS94/AOT4	08/21/2015 11:41:38	08/21/2015 11:42:52	81.129	29.093
PS94/AOT5	08/21/2015 13:00:31	08/21/2015 13:01:12	81.285	29.174
PS94/AOT6	08/21/2015 15:46:19	08/21/2015 15:46:59	81.449	30.201
PS94/AOT7	08/22/2015 10:39:01	08/22/2015 10:40:32	81.860	30.821
PS94/AOT8	08/22/2015 13:01:05	08/22/2015 13:03:38	81.858	30.866
PS94/AOT9	08/24/2015 15:31:05	08/24/2015 15:31:59	82.912	30.933
PS94/AOT10	08/29/2015 14:11:49	08/29/2015 14:12:37	85.277	60.040
PS94/AOT11	09/13/2015 07:46:56	09/13/2015 07:48:01	88.034	-162.511

Data management

All optical data will be published, including related sea-ice properties in PANGAEA in the format of Nicolaus and Katlein (2012) and Istomina et al. (2013).

4.4 Routine sea ice observations

Objectives

The longest ranging datasets of physical parameters of sea ice originate from visual observations during ship cruises, however standards for ice observations vary between different research vessels. As a recommendation by the Climate in the Cryosphere (CliC) Committee, a standardized ice observation protocol for Arctic sea ice was established.

Work at sea

Hourly sea ice observations were carried out by observers on the bridge of the *Polarstern*. Observers were trained to follow the ASSIST protocol (Arctic Shipborne Sea Ice Standardization Tool) at the beginning of the cruise, and the observations were checked during the cruise, so that consistent errors could be corrected. Observations were not taken repeatedly while one station, as the ship drifted alongside the same area of ice. Some observations were taken during the ship's night by researchers on the night watches, but daytime coverage was more extensive. Photos were taken manually at the same time as the observations, looking portwards, forewards, and starboardwards.

During the cruise more than 280 visual observations were made. Each entry consists of ice concentration, ice types and thickness and surface properties for each ice type. Position, heading, and basic meteorological parameters were noted, and the ice conditions such as total ice concentration were additionally documented with three photos. The images captured cover a wide range of ice conditions and types, from freshly-forming sheet ice to thick multiyear ice. These images have already been used to train observers onboard, and may be used for teaching and as a check against other data collected on the cruise.

Data management

ASSIST ice observations are archived and distributed by the International Arctic Research Center (IARC) of the University of Alaska, Fairbanks. A summary table including all observations will be archived in PANGAEA after quality controL

4.5 Sea Ice remote sensing data products

Objective

Sea ice remote sensing data can be used to support decision making for cruise track planning, ice navigation and assessing ice conditions (e.g. for selection of larger ice floes in the marginal ice zone) ahead of the time of arrivaL While optical and infrared maps with medium resolution, as well as sea ice concentration data are available at the weather office of *Polarstern*, medium to high resolution radar imagery of sea ice are not yet routinely available for research in the high latitudes. One obstacle are the rather large data sizes in areas where bandwidth for data transmission is limited, another is the need to minimize the delay between data acquisition to delivery to the ship to mere hours.

Continuing the first trial at the *Polarstern* cruise PS92, radar imagery of the European Earth Observation Mission Sentinel-1A was sent to the sea ice physics group onboard.

Work at sea

Sentinel 1A radar backscatter data provided by Drift & Noise Polar Services was send to an ftp server at two area sizes and resolutions (100 km @ 40 meter ground resolution) and (500 km @ 150 km ground resolution). A scene was automatically generated, if one or several following radar images provided data within the area that was centered on the real-time position of *Polarstern*. The data files were available as ftp download and highly compressed quicklooks at a coarse resolution (2 km) were emailed for evaluation of the usefulness of each scene by an onboard operator before manually downloading the larger files via ftp. The larger scenes were received as geotiffs with a 16bit grayscale depth with a file size between 2 and 6 Mb. The raw geotiffs as well as postprocessed maps with location of stations were copied to a public server location and made available to the bridge with a live overlay of the current ships position. The order of Sentinel 1A radar data was stopped as soon as *Polarstern* left the sea ice.

In total, 155 quickview scenes with a cumulated file size of 2.93 Mb were sent to *Polarstern*. Especially near the North Pole many of the quickview scenes showed insufficient coverage of Sentinel 1A data and the higher resolution counterpart were not downloaded by the operator. Instead, only 15 wide area (500 km @ 150 m resolution) with a total file size of 112 Mb and 18 close up areas (100 km @ 40 m resolution) with a total file size of 89 Mb were downloaded via ftp between August 22 and September 24 2015.

The location of the quickview, wide and close-up scenes are visualized in Fig. 4.10. Further post processing of selected scenes included merging with sea ice concentration data from the AMSR2 sensor of the Japanese Space Agency (JAXA). An example is given in Fig. 4.11.

Data management

Sentinel 1A data is available at the Sentinel Data Portal of the European Copernicus Earth Observation Program at full resolution.

References

Istomina L, Nicolaus M, Perovich D (2013) Spectral albedo of sea ice and melt ponds measured during *POLARSTERN* cruise ARK XXII/3 (IceArc) in 2012, doi:10.1594/ PANGAEA.815111, Pangaea.

Nicolaus M, Katlein C (2012) Solar radiation over and under sea ice during the *Polarstern* cruise ARK-XXVI/3 (TransArc) in summer 2011, doi:10.1594/PANGAEA.786717, Pangaea.

Warren S, Rigor I, Untersteiner N, Radionov VF, Bryazgin NN, Aleksandrov YI, Colony R (1999) Snow depth on Arctic sea ice, J. CliM, 12, 1814–1829.

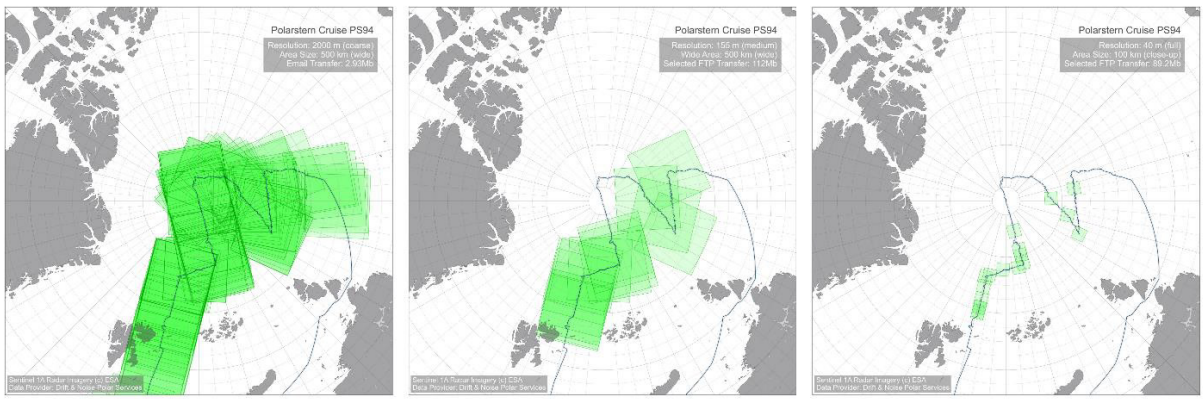

Fig. 4.10: Location of Sentinel-1A radar image subsets available to ice navigation and scientific site selection: (left) coarse resolution email subsets, (middle) medium resolution wide area scenes manually downloaded via ftp, (right) high resolution close-ups manually downloaded via ftp.

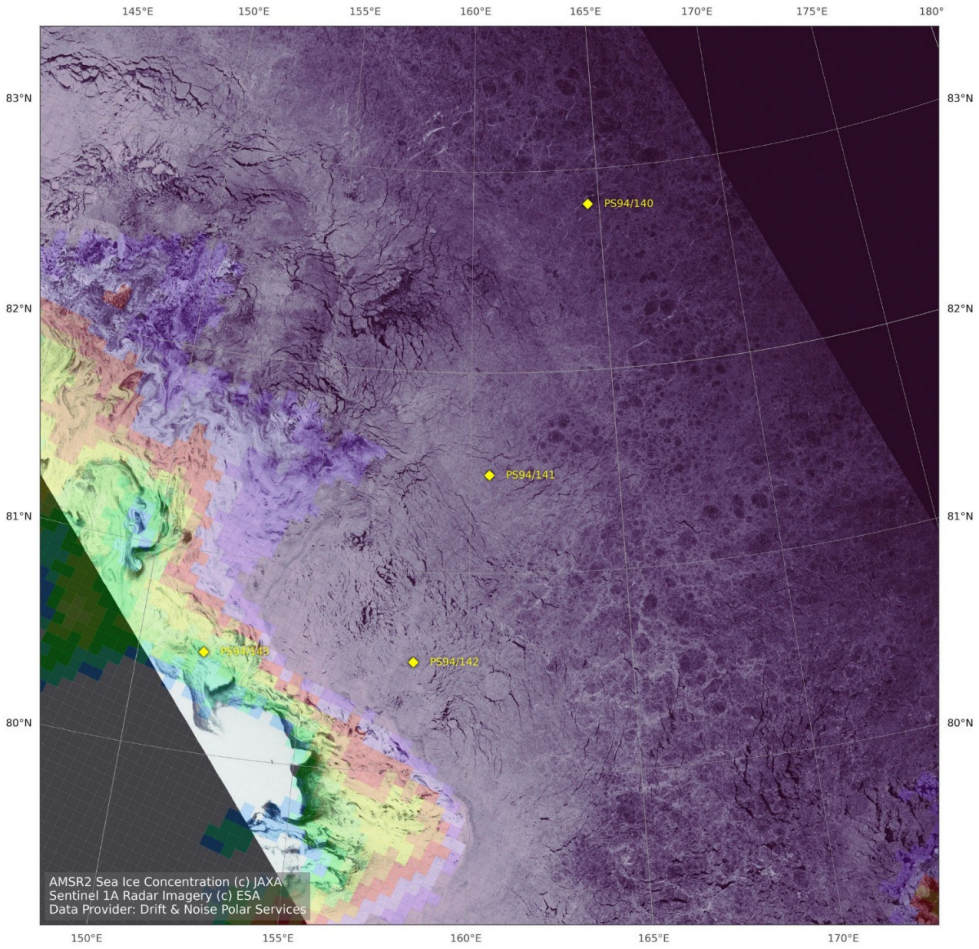

Fig. 4.11: Composite of Sentinel 1A radar image (ESA) and AMSR2 sea ice concentration data (JAXA) overlaid with planned stations in the Laptev Sea

Tab. 4.3: List of electromagnetic induction sea ice thickness profiles during stations: ICE - regular ice station, HELI - Helicopter station, MUMMY - mummy-chair station at starboard side of *Polarstern*. Measurements are separated into: survey - floe survey, cal - calibration with the wooden ladder, drilline - measurements along 50m drilline, drift - drift evaluation at a fixed position on the floe.

Station	Name	date	longitude	latitude	Gear	type	file label	comment
PS94/0046-1	ICE-1	25.08.2015	30.33931	83.71406	GEM2-484	survey	gem2-484_20150825_Survey	survey gps file damaged
						cal	gem2-484_20150825_Calib	
					GEM2-512	cal	gem2-512_20150825_Calib	
					SIS	survey	SISSRV_20150825	
						cal	SISCAL_20150825	
PS94/0054-1	ICE-2	28.08.2015	42.55930	85.08853	GEM2-484	survey	gem2-484_20150828_Survey	
						cal	gem2-484_20150828_Calib	
						drilline	gem2-484_20150828_Drill_001 gem2-484_20150828_Drill_002	
					GEM2-512	survey	gem2-512_20150828_Survey	
						cal	gem2-512_20150828_Calib	
						drilline	gem2-512_20150828_Drill_001 gem2-512_20150828_Drill_002	
					SIS	cal	SISCAL_HEIGHTADJ_20150825	
					EMP400	survey	EMPSRV_20150828	

Station	Name	date	longitude	latitude	Gear	type	file label	comment
						cal	EMPCAL_20150828	
						drilline	EMPDRL_20150828	
PS94/0059-1	HELI-1	30.08.2015	60.36009	85.51776	GEM2-484	survey	125-xg-03ja-013 126-xg-03ja-02e 127-xg-03ja-00a 128-xg-01ja-008	two floes sampled
PS94/0069-1	ICE-3	02.09.2015	58.70657	86.99722	GEM2-484	survey	129-xg-01ja-010	
						cal	130-xg-01ja-128	
						drilline	131-xg-01ja-008 132-xg-01ja-098	
					GEM2-512	cal	134-xr-01ja-087	gps file broken
						drilline	133-xr-01ja-198	gps file broken
					SIS	drilline	SISDRL_20150902	
					EMP400	drilline	EMPDRL_20150902	
PS94/0081-1	ICE-4	05.09.2015	61.09556	88.99035	GEM2-484	survey	gem2-484_20150905_Survey_001 gem2-484_20150905_Survey_002	
						cal	139-xg-04ja-320	
						drilline	140-xg-05ja-0d4	
					GEM2-512	drilline	141-xg-05ja-05f	
					SIS	survey	SISSRV_20150905	
						drilline	SISDRL_20150905	
					EMP400	survey	EMPSRV_20150905	
						cal	EMPCAL_20150905	
						drilline	EMPDRL_20150905	

Station	Name	date	longitude	latitude	Gear	type	file label	comment
PS94/0087-1	ICE-N	07.09.2015	-90.00661	89.95442	GEM2-484	survey	142-xr-01ja-1e0	North Pole ice station, gps file broken
PS94/0093-1	MUMMY-1	09.09.2015	-112.71165	88.91040	GEM2-484	survey	143-xg-01ja-010	
PS94/0096-1	ICE-5	11.09.2015	-125.01961	88.35697	GEM2-484	survey	145-xg-01ja-008 146-xg-01ja-008	
						cal	147-xg-01ja-099	
						drilline	148-xg-01ja-2fd 149-xg-01ja-0a2	
					SIS	survey	SISSRV_20150911	
						cal	SISCAL_20150911	
						drilline	SISDRL_20150911	
PS94/0098-1	MUMMY-2	12.09.2015	-144.25290	88.33872	GEM2-484	survey	150-xg-01ja-010	
PS94/0101-1	ICE-6	13.09.2015	179.89545	87.49598	GEM2-484	survey	151-xg-02ja-055	
						cal	152-xg-02ja-29a	
						drilline	153-xg-03ja-07b	no drilling, conductivity measurements of underlying slush
					GEM2-512	cal	155-xg-03ja-024	
						drilline	154-xg-03ja-024	no drilling, conductivity measurements of underlying slush
					SIS	survey	SISSRV_20150913	
						cal	SISCAL_20150913	
						drilline	SISDRL_20150913	no drilling, conductivity measurements of underlying slush
					EMP400	cal	EMPCAL_20150914	

Station	Name	date	longitude	latitude	Gear	type	file label	comment
						drilline	EMPDRL_20150914	no drilling, conductivity measurements of underlying slush
PS94/0107-2	MUMMY-3	16.09.2015	133.88808	86.62752	GEM2-484	survey	157-xg-05ja-0f8	
PS94/0112-1	MUMMY-4	17.09.2015	118.41286	85.21521	GEM2-484	survey	158-xg-01ja-010	
						cal	159-xg-01ja-158	
PS94/0117-1	ICE-7	18.09.2015	115.98337	84.56133	GEM2-484	survey	160-xg-02ja-138 161-xg-02ja-1fb	
						cal	162-xg-02ja-32c	
						drilline	165-xg-01ja-020	
						drift	43-xg-31mr-038	
					GEM2-512	cal	163-xg-01ja-008	
						drilline	166-xg-01ja-010	
						drift	164-xg-01ja-0b8	
					SIS	cal	SISCAL_20150918	
						drilline	SISDRL_20150918	
						drift	SISDFT_20150918	
					EMP400	survey	EMPSRV_20150918	
						cal	EMPCAL_ CAL1_20150918 EMPCAL_ CAL2_20150918 EMPCAL1_ CAL1_20150918	
						drilline	EMPDRL_ DRL1_20150918 EMPDRL_ DRL2_20150918	

Station	Name	date	longitude	latitude	Gear	type	file label	comment
						drift	EMPDFT_20150918	
PS94/0125-1	ICE-8	22.09.2015	139.97401	85.08702	GEM2-484	survey	168-xg-01ja-028	
						drift	44-xg-04ap-02b	
					GEM2-512	drift	169-xg-02ja-006	
					SIS	drift	SISDFT_20150922	
					EMP400	drift	EMPDFT_20150922	

5. INSTALLATION OF AUTONOMOUS, ICE-TETHERED PLATFORMS

Mario Hoppmann[1], Benjamin Rabe[1], Sergey Pisarev[2], Nicolas Villacieros[3], Jean-Philippe Savy[3], Marcel Nicolaus[1] (not on board), Christine Provost[3] (not on board)

[1] AWI
[2] SIO
[3] LOCEAN

Grant No. AWI_PS94_00

Objectives

An important tool to increase observational data in the still sparsely sampled Arctic Ocean has become more and more feasible during the last decade: autonomous, ice-tethered measurement platforms, which are able to capture data year-round, and, by their drift, extend the area of manned expeditions.

During PS94, a suite of autonomous instruments have been installed on ice floes to provide measurements of physical, biological and biogeochemical parameters in the upper ocean and sea ice, as well as of near-surface atmospheric conditions.

Sea-ice based buoys and profilers are deployed during ice stations and by helicopter several kilometers off the *Polarstern* cruise track. Types of sea ice buoys include GPS drifters for the study of ice dynamics, snow-depth and ice-mass-balance buoys for monitoring ice growth and snow accumulation throughout the following winter, radiation stations for energy budget estimations, and ice-tethered profilers to monitor upper ocean properties.

The main focus of buoy deployments lies on regions as far into the eastern marginal seas of the Arctic Ocean as possible, which are areas where observations by autonomous systems are typically sparse and the expected lifetime of the instruments is highest.

The buoy deployments support long-term monitoring programmes such as the International Arctic Buoy Programme, and are further coordinated within the FRAM infrastructure programme and the French Ice Atmosphere Ocean Observing System (IAOOS) project.

The network of ice-tethered platforms is expected to play a crucial role in understanding the linkages between the atmosphere, sea ice and upper ocean in the high Arctic. It will further allow us to improve our process understanding and to derive reliable models of the physical and biogeochemical states of the future Arctic Ocean.

Work at sea

Platforms were deployed during ice stations or during helicopter landings (Fig. 5.1).

Nine types of platforms were deployed, investigating the properties of the upper ocean, the sea ice and its snow cover, and the atmosphere.

1. Surface Velocity Profilers (SVPs), manufactured by Metocean Data Systems Limited, Canada, report GPS position, air temperature and barometric pressure at hourly intervals.

2. Sea-ice mass balance buoys (IMB), manufactured by SAMS Research Services Ltd, report GPS position as well as temperature (rise) values from a thermistor chain through air, snow, sea ice and ocean. The chain is equipped with 240 thermistors at a spacing of 0.02 m. Resistor elements mounted near the thermistors may be heated, and by a determination of the temperature rise after a certain interval, different media may be distinguished by their different thermal conductivity. The different parameters are transmitted via iridium at varying intervals.

3. Snow height beacons (SB), manufactured by Metocean Canada, report GPS position, air and surface temperatures, barometric pressure, as well as 4 snow depths at a spacing of ~1 m, at hourly intervals.

4. A polar area weather station (PAWS) manufactured by Metocean Canada, reports GPS position, air and surface temperature, barometric pressure, relative humidity as well as wind velocity and direction in 3-hour intervals.

5. A spectral radiation station (SRS), consisting of three RAMSES spectral irradiance sensors manufactured by TriOS Optical Sensors, records incoming, reflected and transmitted irradiance at 2-hour intervals and transmitsthe data daily.

6. The Bio-ITP system (Fig. 5.2), manufactured by Woods Hole Oceanographic Institution (WHOI, USA) measures temperature/salinity/depth/oxygen/fluorescence/ PAR profiles with 1 Hz (nominally 0.25 m) vertical resolution between 5 and 760 m, at 36-hour intervals. The McLane profiler is equipped with a CTD unit (Seabird Electronics, Inc. model 41CP), a Wetlabs Eco-Triplet fluorometer and a photosynthetically active radiation sensor (QCP2300, Biospherical Instruments) on a wire tether, using an inductive modem to communicate the data to a surface unit.

7. IAOOS platforms, developed by France-based LOCEAN and LATMOS, are mainly composed of a profiling CTD unit which is additionally equipped to measure dissolved oxygen. The profilers are comparable to the ARGO float system, except that they are tethered to a cable along which they can repeatedly profile vertically from the surface down to 800 m depth. The data is transmitted to the surface unit using an inductive modem technique. The atmospheric observations are provided by a microlidar and an optical depth radiometer. Finally, air, snow, sea-ice and seawater temperatures are monitored by a SAMS IMB mounted on the surface unit.

8. The BAS IMB is another variation of a thermistor-string based sea-ice mass balance buoy, provided by the British Antarctic Survey (BAS). The units report GPS position as well as temperature (rise) values from a thermistor chain through air, snow, sea ice and ocean. The units are also equipped with a sideways-looking camera.

9. The SATICE is equipped with a high-rate, high-precision GPS receiver reporting in sub-hourly, sub-decimeter precision in three dimensions. It further features standard meteorological sensors, an ultrasonic snow pinger for snow depth retrieval, a digital camera, a sea level sensor and a conductivity cell. The unit deployed during PS94 is part of a network of five units deployed over a time span of 5 years.

All observing systems report their data through the iridium satellite network at regular intervals. The buoy deployments are summarized in Table 1. In total, 8 SVPs, 6 SAMS IMBs, 8 SBs, 1 PAWS, 1 SRS, 2 BAS IMBs, 1 SATICE, 1 Bio-ITP and 4 IAOOS were deployed.

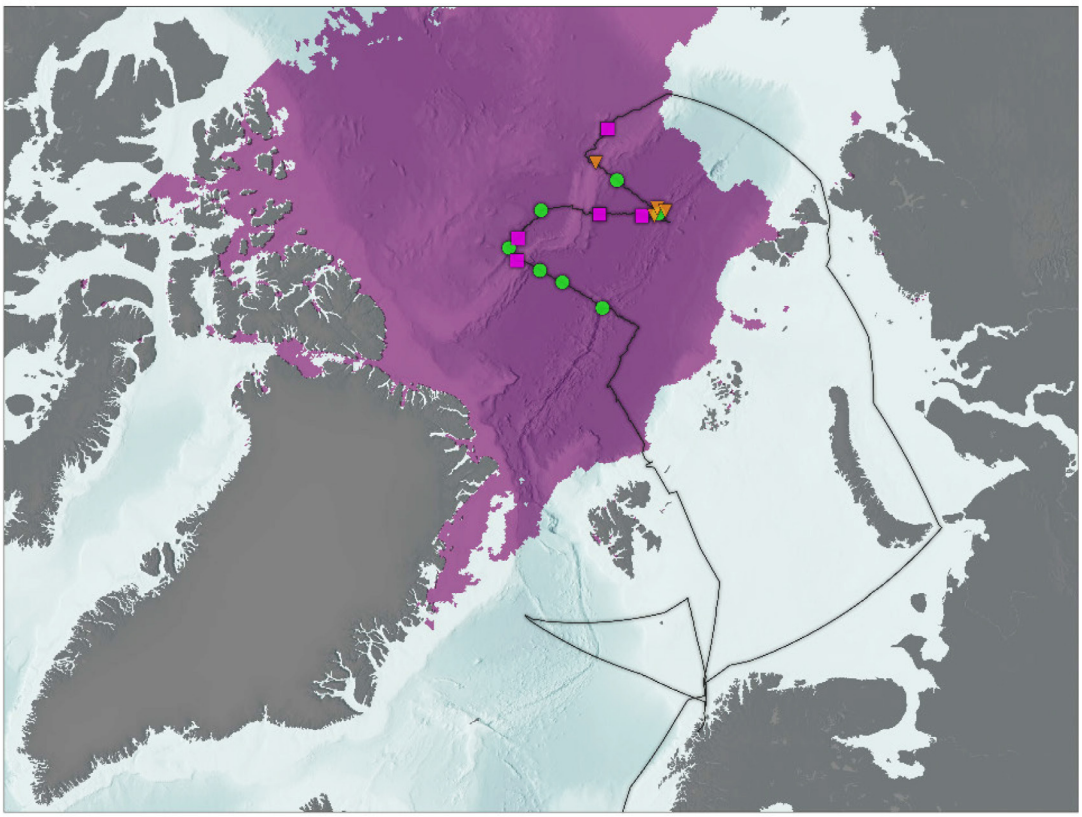

Fig 5.1: buoy deployments during ice stations (green), by mummychair (pink) and by helicopter (orange) along the cruise track (solid line). The shaded area indicates the September 2015 mean sea ice extent.

Fig. 5.2: Deployment of Bio-ITP

Preliminary results

Fig. 5.3 shows the drift track of all SVPs, SAMS IMBs and SBs as of 11 October 2015.

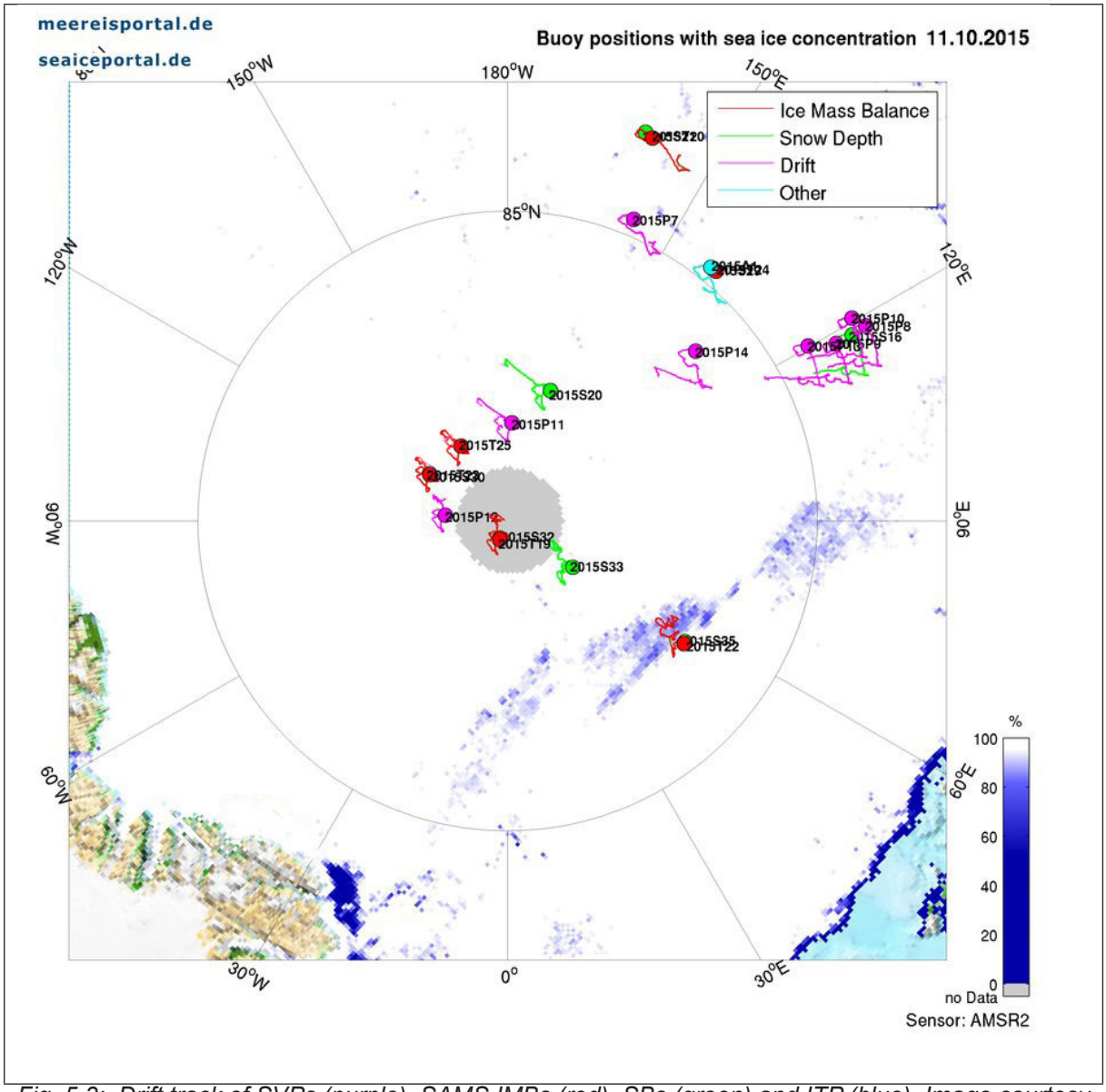

Fig. 5.3: Drift track of SVPs (purple), SAMS IMBs (red), SBs (green) and ITP (blue). Image courtesy of www.meereisportal.de (11.10.2015).

Data management

SVP, SAMS IMB, SB and PAWS data are available in near real time on www.meereisportal.de. The positions and meteorological data of the SVPs and snow height beacons are automatically uploaded to the database of the International Arctic Buoy Program (IABP), which is publically accessible. These buoys also contribute to the Global Telecommunication System (GTS). Data of all buoys will be archived in the online databases PANGAEA and Coriolis within one year after a buoy ceases transmitting. The ITP data can be downloaded from the WHOI ITP web site (www.whoi.edu/itp). All buoy data will be available through the FRAM data portal at a later time.

Tab. 5.1: List of deployed platforms with deployment data. Abbreviations: SVP: Surface velocity profiler; IMB: Ice mass balance buoy; SB: snow height beacon; SRS: spectral radiation station; PAWS: polar area weather station; ITP: ice-tethered profiler; IAOOS: Ice Atmosphere Ocean Observing System.

Buoy Type	IMEI	Name	Date	Time [UTC]	Longitude	Latitude	Station
SVP	300234062888920	2015P12	02.09.2015	16:15:00	88° 54.58 N	112° 45.34 W	093-01
SVP	300234062887930	2015P14	16.09.2015	13:30:00	86° 37.78 N	133° 52.57 E	107-02
SVP	300234062888930	2015P13	17.09.2015	13:30:00	85° 12.89 N	118° 23.70 E	112-02
SVP	300234062884920	2015P11	13.09.2015	11:00:00	88° 05.37 N	167° 08.14 W	Heli
SVP	300234061188690	2015P9	19.09.2015	05:16:00	84° 45.79 N	115° 45.12 E	Heli
SVP	300234061186310	2015P10	19.09.2015	05:33:00	84° 30.52 N	118° 21.14 E	Heli
SVP	300234061774560	2015P8	19.09.2015	05:50:00	84° 15.94 N	115° 45.12 E	Heli
SVP	300234061776560	2015P7	24.09.2015	04:00:00	84° 58.414 N	153° 10.287 E	Heli
SAMS IMB	300234061266810	AWI7_1 / 2015T22	02.09.2015	16:15:00	87° 00.41 N	58° 39.77 E	069-01
SAMS IMB	300234061264830	AWI6_1 / 2015T19	08.09.2015	00:00:00	88° 21.79 N	125° 10.06 W	Northpole
SAMS IMB	300234062427080	AWI7_2 / 2015T23	11.09.2015	23:30:00	88° 21.79 N	125° 10.06 W	096-01
SAMS IMB	300234061263820	AWI7_4 / 2015T25	12.09.2015	12:00:00	88° 20.31 N	144° 18.90 W	098-01
SAMS IMB	300234062429080	AWI7_3 / 2015T24	22.09.2015	06:00:00	85° 5.00 N	139° 57.56 E	125-01
SAMS IMB	300234061261790	AWI6_2 / 2015T20	25.09.2015	07:00:00	83° 30.07' N	154° 56.58' E	135-01
BAS IMB	300025010842220	IMB005	11.09.2015	18:00:00	88° 20,85'N	124° 40'W	096-01
BAS IMB	300025010848700	IMB006	14.09.2015	04:00:00	87° 30'N	179° 50'E	101-01
SB	300234062785480	2015S35	02.09.2015	16:15:00	87° 00.41 N	58° 39.77 E	069-01
SB	300234062784540	2015S33	06.09.2015	16:30:00	88° 59.14 N	60° 57.98 E	081-01
SB	300234062782480	2015S32	08.09.2015	00:00:00	90 N	0 E	North-pole
SB	300234062789420	2015S30	11.09.2015	23:30:00	88° 21.79 N	125° 10.06 W	096-01
SB	300234062328760	2015S20	14.09.2015	12:00:00	87° 29.73 N	179° 53.72 E	101-01
SB	300234062428050	2015S16	19.09.2015	08:00:00	84° 33.78 N	115° 59.81 E	117-01
SB	300234062788470	2015S29	22.09.2015	06:00:00	85° 5.00 N	139° 57.56 E	125-01
SB	300234062423070	2015S21	25.09.2015	06:00:00	83° 30.07 N	154° 56.58 E	135-01
SRS			23.09.2015	01:00:00	85° 5.00 N	139° 57.56 E	125-01
PAWS	300234062784500	2015A1	23.09.2015	01:00:00	85° 5.00 N	139° 57.56 E	125-01
SATICE		SATICE07	06.09.2015	16:00:00	88° 59.55'N	61° 10.09'E	081-01
ITP		ITP93	23.09.2015	01:00:00	85° 5.00 N	139° 57.56 E	125-01
IAOOS	300025010340400	IAOOS10	05.09.2015	22:30:00	88° 59.55'N	61° 10.09'E	081-01
IAOOS	300025010340050	IAOOS11	11.09.2015	15:50:00	88° 20,85'N	124° 40'W	096-01
IAOOS	300025010347770	IAOOS14	14.09.2015	02:44:00	87° 30'N	179° 50'E	101-01
IAOOS	300025010342860	IAOOS15	18.09.2015	23:57:00	84° 32.55'N	115° 57.65'E	117-01

6. GEOTRACES

Michiel Rutgers van der Loeff[1], Micha Rijkenberg[2],
and the GEOTRACES scientific party (the corresponding names of the participating party are listed under the respective articles)

[1]AWI
[2]NIOZ

Grant No. AWI_PS94_00

Objectives

GEOTRACES (www.geotraces.org) is an international programmeme that aims to determine global ocean distributions of selected trace elements and isotopes, including their concentration, chemical speciation and physical form, and to evaluate the sources, sinks and internal cycling of these species. This knowledge is needed to characterize more completely the physical, chemical and biological processes regulating their distributions so that the response of these cycles to global climate change can be predicted, and their impact on the carbon cycle and climate understood (Henderson et al., 2007).

Warming of Arctic terrestrial areas caused increased river discharge, which, combined with net loss of the Greenland ice-cap and melting of sea ice, resulted in a freshening of surface waters and increased stratification. These climate-induced changes are expected to change the biogeochemical cycling and therefore the distribution of many Trace Elements and Isotopes (TEI's).

Work at sea

As part of a pan-Arctic GEOTRACES effort in coordination with Canadian and US initiated research cruises in 2015, we have carried out a sampling programme of TEIs (Table 6.1) including all tracers considered as key TEIs by Henderson et al. (2007).
In total we have carried out 30 GEOTRACES stations (Table 6.2). At 28 stations we sampled with the Ultra Clean CTD where we collected ancillary parameters with the normal Rosette (Table 6.2). At two stations we used only the normal Rosette. At 21 Large Stations (included in the GEOTRACES stations), large volume samples were collected for natural and artificial radionuclides and for rare earth elements and Nd isotope composition. At 10 Super Stations (a subset of the Large Stations) we additionally deployed *in situ* pumps to sample TEI in the particulate phase and to sample Radium isotopes. Three Basin Stations (Sta 50 in the Nansen Basin, 81 in the Amundsen Basin and 101 in the Makarov Basin) were sampled additionally for Cd and Pb and triple oxygen isotopes.

Intercalibration and intercomparison are an essential part of the GEOTRACES programme. For this purpose a cross over station had been agreed between the expeditions of RV *Polarstern* and USCG *Healy* at 87.5°N, 180°E in the Makarov Basin. This station was sampled by our cruise (Sta 101) just about 10 days after it had been sampled by USCG *Healy* (their station 20). This joint sampling with short delay will serve as intercomparison between the two teams for all parameters analysed. Additional samples were collected for intercalibration programmes to be distributed among GEOTRACES partners, especially with colleagues on the US and Canadian ships (details below). Our tracks crossed once more at the North Pole. This station (PS94-87, Healy Sta 19) was not scheduled as a cross over station and was not sampled for

all GEOTRACES parameters on *Polarstern*, but the cast with the Ultra Clean CTD (PS94-87/1) will provide an additional opportunity for intercomparison of hydrographic and trace metal data among the two ships, in this case even synoptic, i.e. without time delay. The mutual visits to each other's laboratories was used for an extensive exchange of experience.

Preliminary/expected results

Our sections across the Barents shelf, Nansen Basin, Amundsen Basin into the Makarov Basin (Station 1-101) will provide continuous TEI profiles from the northern tip of Norway (Nordkap) to the cross over station in the Makarov Basin. In combination with the results of the synoptic US and Canadian studies we expect to provide maps of the distribution of TEIs in the Arctic including a full section from the Barents Sea to the Bering Strait. Comparison with previous data may allow us to determine whether distributions have changed, which could be indicative of changes in water mass circulation, primary productivity, or particle fluxes. The second section across the Lomonosov Ridge (Stations 115-134) will provide a second section of the Transpolar Drift. This section can be extended by combination with Healy station 21.

The final section across Bear Island Trough (Sta 147-173) characterizes the TEI distribution in the Gateway between Norway of Svalbard. In combination with the hydrographical data (chapter 3) and with the mooring array with current meters at 20°E (operated by the Institute of Marine Research, Norway) it will be possible to calculate TEI fluxes through this major inflow pathway of Atlantic water to the Arctic Ocean.

Data management

Data from a crossover station with the US cruise and other intercalibration results from duplicate sampling will be submitted to the GEOTRACES Standards and Intercalibration Committee for evaluation and approval. All data and metadata will be submitted to the international GEOTRACES data management office (BODC, www.bodc.ac.uk/geotraces) under the data management scheme agreed upon in the GEOTRACES programme available at http://www.geotraces.org. Most data and metadata will also be submitted to the PANGAEA data base. First data will be presented at the AGU Ocean Sciences meeting 2016, we expect to include a large amount of data in the second GEOTRACES Intermediate Data Product, due 2017. This will be made available through the website www.egeotraces.org where the data of the 2007-2009 IPY (International Polar Year) expeditions can also be found.

References

Henderson GM, Anderson RF et al. (2007) GEOTRACES - An international study of the global marine biogeochemical cycles of trace elements and their isotopes. Chem Erde-Geochem, 67, 85-131.

Tab. 6.1: GEOTRACES and ancillary parameters sampled during PS94

GEOTRACES parameters	Name	Institute
Trace metals	Micha Rijkenberg	NIOZ
Particulate trace metals	Aridane G. Gonzalez	IUEM
Fe Ligands	Loes Gerringa, Hans Slagter	NIOZ
mercury	Lars-Eric Heimbürger	MIO Marseille
Fe isotopes	Michael Staubwasser	Uni Köln
REE, Nd isotopes	Ronja Paffrath	Uni Oldenburg
$^{230}Th/^{231}Pa$	Ole Valk Sandra Gdaniec	AWI, Swedish Museum of Natural History

^{234}Th, ^{210}Pb/^{210}Po	Viena Puigcorbe	UAB, Barcelona
Radium isotopes, ^{228}Th	Michiel Rutgers van der Loeff	AWI
Artificial radionuclides ^{129}I, ^{236}U	Núria Casacuberta	ETH, Zurich
Ancillary parameters		
Nutrients	Jan van Ooijen	NIOZ
CO_2 and oxygen	Adam Ulfsbo	Uni Gothenburg
	Elisabeth Jones	NIOZ/UK
pCO_2, NO_3, pH sensors	Daniel Scholz	AWI
^{18}O	Dorothea Bauch	GEOMAR
Dissolved organic matter	Heather Reader	DTU-Aqua

Parameters collected for other groups	**Name**	**Contact person TransArc II**
N and O isotopes in nitrate	Raja Ganeshram	Michiel vd Loeff
Cd, Pb, Cr isotopes	Wafa Abouchami and Stephen Galer	Micha Rijkenberg
Triple oxygen isotopes	Boaz Luz	Michiel vd Loeff
Si isotopes	Claudia Ehlert	Ronja Paffrath
CFC	Bill Smethie	Michiel vd Loeff
dissolved Ti	Peter Croot	Micha Rijkenberg
Pu-isotopes	Tim Kenna	Nuria Casacuberta
Not-GEOTRACES samples		
humic substances	Luis Laglera	Hans Slagter
rubisco protein	Monica Orellana	Micha Rijkenberg
bPSi,POC/N, Chl a, Seston	Eva-Maria Noethig	Nicole Hildebrandt
HPLC (pigments)	Ilka Peeken	Nicole Hildebrandt
Heme	Maria Nielsdottir	Daniel Scholz

Tab. 6.2: GEOTRACES Stations with Rosette types and cast numbers

Station	Station type	Ultra Clean cast	Rosette cast	Rosette type	ISP cast	Basin
PS94/0002	GT		1 (REE)	S		
PS94/0004	Super	2 + 6	3+5	S	4	
PS94/0018	Large		1+3+5	S		
PS94/0032	Super	4	5+7+9	S	8	
PS94/0040	Large	2	1+3	L		
PS94/0050	Super	3	1+4+6+8	S	5	X
PS94/0054	GT	3				
PS94/0058	Large	7	1+3	L		
PS94/0064	GT	2				
PS94/0069	Large	2	4+5	L		

Station	Station type	Ultra Clean cast	Rosette cast	Rosette type	ISP cast	Basin
PS94/0070	Large	4	1	L		
PS94/0081	Super	4 + 10	2+5+7	L	9	X
PS94/0087	GT	1				
PS94/0091	GT	2				
PS94/0096	Super	4	2+6	L	5	X
PS94/0099	GT	1+3				
PS94/0101	Super	4 + 8	2+5+7+9	L	6	
PS94/0117	Super	3	2+4+6	L	7	
PS94/0119	GT	1				
PS94/0121	GT	2				
PS94/0125	Super	3	2+5	L	8	
PS94/0130	GT	2				
PS94/0134	Large	2	1 (deep only)	L		
PS94/0147	GT	2				
PS94/0149	Large	2	1+4	S		
PS94/0153	Super	2	1+4	S	6	
PS94/0157	GT	2				
PS94/0161	Super	2	1+4	S	5	
PS94/0169	Large	3	1+4	S		
PS94/0173	Large	2	1	S		

6.1 Nutrients

Jan van Ooijen NIOZ

Objective

The nutrients phosphate (Murphy & Riley, 1962), silicate (Strickland & Parsons, 1968), nitrite and nitrate (Grasshoff et al., 1983) will be measured at all GEOTRACES stations to determine its distribution in the Eurasian sector of the Arctic Ocean. The nutrients are important parameters allowing other parameters to be related to biological activity such as primary production and remineralization. Nutrients function also as tracers of water masses.

Work at sea

Equipment and Methods

Nutrients were analysed in an air-conditioned lab container with a, Technicon TRAACS 800, continuous flow auto analyser. During this cruise I measured about 2,300 samples. Samples originate from CTD 1800, Ice floes and related some 300, Surface Waters 50, and lab experiments 150 approx. CTD samples were measured unfiltered whereas the ice related and experiment samples were 0.2 µm filtered prior to analysis. Measurements were made simultaneously on four channels: phosphate, silicate, nitrate and nitrite together, and nitrite separately. All measurements were calibrated with standards diluted in low nutrient seawater (LNSW), and LNSW was used as wash-water between the samples. For the Ice related samples having different salinities, all samples were diluted with LNSW or demineralised water (18.2 M Ohm) to a salinity of approx. 12 or 26. This allows the samples to be analysed all within the same calibration salinity.

The colorimetric methods used

Phosphate

Ortho-phosphate is measured by formation of a blue reduced Molybdophosphate-complex at pH 0.9-1.1 (Murphy and Riley, 1962). Potassium Antimonyltartrate used as the catalyst and ascorbic acid as a reducing agent. The absorbency is measured at 880 nm.

Silicate

Measured as a blue reduced Silicomolybdenium-complex at 800 nm (Strickland and Parsons, 1972). Ascorbic acid is used as reducing agent and oxalic acid is used to prevent interference of phosphate.

Nitrite

Diazotation of nitrite with sulfanylamide and N-(1-naphtyl)-ethylene diammonium dichloride to form a pink dye measured at 550 nm (Grasshof, 1983).

Nitrate and Nitrite

Nitrate is first reduced in a copperized cadmium-coil using imidazole as buffer and is then measured as nitrite at 550 nm (Grasshof, 1983).

Sample handling

The samples were collected in 100 ml high-density polyethylene sample bottles, taken directly and unfiltered from the CTD-rosette bottles. The samples were kept cool and dark stored in a refrigerator and analysed typically within 16 hours as a maximum. Analyses were carried out using high-density polyethylene "pony-vials" with a volume of 6 ml as sample cups. For duplicate analysis purposes in-between runs, the deepest sample at every CTD-station was capped in a pony-vial to be measured for a second time in the next run. To avoid evaporation during the runs, all vials including the calibration standards used were sealed with "parafilm" under tension, so that the sharpened sampler-needle easily penetrated through leaving a small hole in the film.

Calibration and Standards

Nutrient primary stock standards were prepared at the laboratory at NIOZ by weighing and solute them in demineralised water. All standards are kept in a so called 100 % humidity box at lab temperature to prevent evaporation.

The calibration standards were prepared daily by diluting the separate stock standards, using three electronic pipettes, into four volumetric 100 ml PP flasks (pre-calibrated at the lab) filled with low nutrient sea water LNSW. The background values of the LNSW were measured on board and added to the calibration values to get the absolute nutrient values.

Cocktail standard

This standard acts as a lab reference and its use is described under "quality control". It is made in the lab containing a mixture of phosphate, silicate and nitrate in demineralised water containing 40 mg Hg_2Cl_2 per litre as a preservative. Every time it was used it was diluted 250 times with the same pipette, and the same volumetric flask.

Quality Control

Our standards have already be proven by inter calibration exercises like ICES and Quasimeme, and last years the RMNS exercise organised from Dr. Michio Aoyama Meteorological Research Institute (MRI), Japan, to be within the best obtainable limits to the mean of the better laboratories. To gain some accuracy the Cocktail standard is monitored now since 2008, showing in-between runs reproducibility better than 1.0 % , but typically 0.8% of its average value.

	Average value	S.D.	N
PO_4	0.901 µM	0.006 µM	70
SiO_2	13.94 µM	0.06 µM	70
NO_3	13.66 µM	0.05 µM	70

The advantage of a cocktail standard is like using a reference standard with three nutrients mixed in one bulk, giving each run a good overview of the machine's output. It also gives you a tool to normalise data from run to run for oceanographic purpose from station to station to produce transect plots.

Others have reported the use of a real reference sample supplied from deep water (2,000 m) but this reference sample is not stable over a period longer than three weeks.

For the semi-final data no corrections (within 0.015 µM) were made based on normalising on the average cocktail standard value. Final data will be ready 2 months after the cruise.

Statistics
Mean Detection Limits: calculated as 2.82 x S.D. of nine 2 % (from the full range) spiked samples (EPA norm).

	µM/l	Used ranges µM/l:	Applied level:
PO_4	0.003	1.75	0.04 µM
SiO_2	0.03	24.8	0.50 µM
NO_3+NO_2	0.04	26.0	0.52 µM
NO_2	0.008	1.00	0.02 µM

*Precision in single run***:** 12 sample bottles were measured for this test.

	Average	Stdev
PO_4	0.902	0.002
SiO_2	13.77	0.06
NO_3+NO_2	13.67	0.02
NO_2	0.028	0.002

Accuracy
To gain accuracy this cruise reference material for nutrients were measured parallel to the deep CTD sections containing stable values for PO_4, SiO_2 and NO_3 and NO_2.
Reference Material for Nutrients in Seawater (RMNS) produced by KANSO lot BU and lot BT was used.

Expected results

During this cruise 2,300 samples were measured. The CTD's provided 1,800 samples, the ice work some 300 samples, 50 samples of surface waters and there were 150 samples originating from on board laboratorium samples. The nutrients are important parameters allowing other parameters to be related to biological activity such as primary production and remineralization. Nutrients can also be used as tracers of water masses. Silicate can be used as a tracer of hydrothermal plumes.

Data management

See introduction of chapter 6 for details on GEOTRACES data management. All nutrients data are available among all cruise participants. Jan C. van Ooijen (Royal NIOZ) should become co-author on any articles that comprise nutrient data. If only very few nutrient data

are used, and/or that the nutrient data is not really pivotal for the scientific interpretation, mentioning in Acknowledgments will be adequate. For additional information, please contact Micha Rijkenberg (email: Micha.Rijkenberg@nioz.nl) or Jan van Ooijen (Jan.van.Ooijen@nioz.nl), Royal Netherlands Institute for Sea Research, P.O. Box 59, 1790 AB Den Burg, The Netherlands, Telephone 31 222 369465

References

Murphy J, Riley JP (1962) A modified single solution method for the determination of phosphate in natural waters. Analytica Chim. Acta, 27, 31-36.

Strickland JDG, Parsons TR (1968) A practical handbook of seawater analysis, first edition, Fisheries Research Board of Canada, Bulletin no, 167, 65.

Grasshoff K, Ehrhard M, Kremling K (1983) Methods of seawater analysis, 2nd ed. Verlag Chemie GmbH, Weinheim.

6.1.1 Stable N & O isotopes of nitrate

R.S. Ganeshram (not on board) UE

Objectives

To collect water samples for combined O and N stable isotopes of nitrate and where possible to collect suspended particles for C and N stable isotopes on glass fibre filters (collaboration with Ilka Peeken and Eva-Maria Noethig).

Work at sea

Water samples were collected with the ultraclean CTD with an online Acropak filter into 125ml sample bottles in duplicates after rinsing 3 times with seawater leaving a headspace. The collected samples were stored frozen at -20°C. Samples were collected at all 40 stations at alternative depths starting with the near surface bottle.

Expected results

The broad scientific aim is to understand what controls N balance in the Arctic and the Arctic through flow. Arctic through flow into the North Atlantic is depleted in N relative to P. This has significant influence on (1) preformed N contents and N:P ratios of North Atlantic Deep water and the excess P also drives N-fixation in the Atlantic. By using stable N and O isotopes of nitrate, nutrient and water mass information I wish to evaluate whether N balance of the Arctic is controlled by (1) Relative proportions of Atlantic and Pacific water masses entering the Arctic; or (2) due to terrestrial nutrients sources to the Arctic: or (3) nutrient recycling processes within the Arctic Ocean. We will use isotope data along with nutrients and water mass information in our interpretations.

Data management

See introduction of chapter 6 for details on GEOTRACES data management.

6.1.2 Biogeochemical cycling of silicon – stable isotopes

Ronja Paffrath ICBM
C. Ehlert, K. Pahnke (not on board)

Objectives

In most oceanic regions, the silicon isotope composition ($\delta^{30}Si$) of water masses varies as a function of input from land, diatom primary production in surface waters and diatom silica dissolution at greater depth, together with physical water mass circulation and mixing.

Therefore, the oceanic $\delta^{30}Si$ distribution bears information on the dominant pathways and processes by which silicon is cycled within the ocean (e.g. de Souza et al., 2012a). However, often the interpretation is difficult because the $\delta^{30}Si$ always represents a mixed signal of the numerous pathways and processes. The Arctic Ocean is a unique system to study the silicon cycle, because here the diatom primary productivity and silicic acid utilization in the water column is very low and quasi restricted to a short season in the year. Therefore, seawater $\delta^{30}Si$ signatures in the Arctic will mainly represent the input of terrestrial dissolved and particulate silicon via rivers, which both have a lighter $\delta^{30}Si$ signature than the surrounding seawater, and subsequent dissolution of the particles and physical water mass mixing. With our applied methods we will be able to analyse separately and therefore distinguish the silicon isotope composition of the lithogenic (terrestrial derived) particles from the *in-situ* produced diatom biogenic silica. Both particle types should have distinctly different silicon isotope compositions (higher $\delta^{30}Si$ for biogenic particles and low $\delta^{30}Si$ for lithogenic particles, respectively). This allows us to study the terrestrial input and its influence on the seawater $\delta^{30}Si$ composition without or very little influence from biological fractionation, thus improving our understanding of the biogeochemistry of silicon in the ocean. We will then further compare the results with data from the Canadian and US GEOTRACES cruises (M. Brzezinski, D. Varela, pers. communication), the Atlantic (de Souza et al., 2012a), the Pacific (e.g., De Souza et al., 2012b; Grasse et al., 2013) and in particular the Southern Ocean (e.g. Varela et al., 2004, Fripiat et al., 2007) to evaluate and contrast the processes affecting silicon biogeochemistry. We will investigate the effects of enhanced river input and extended shelf areas in the Arctic *versus* no river discharge and restricted shelf extent in the Southern Ocean as well as the different circulation regimes, upwelling (Southern Ocean, Equatorial Pacific) *versus* no upwelling (Arctic), and the different particle compositions of opal-rich (Southern Ocean, Equatorial Pacific) *versus* opal-poor (Arctic).

Although production and subsequent burial of diatom silica is very low in the Arctic, the combination of a short growth season before and during the time of the cruise and the sampling of suspended particles together with sediment samples will provide unique information about the transfer of the surface water utilization signal, possibly with a very strong fractionation by sea ice diatoms, through the water column to the deep ocean and will therefore provide important general information on the applicability of diatom $\delta^{30}Si$ as a paleo proxy in the global ocean.

Currently, the silicon cycle in the Arctic region is not yet influenced by anthropogenic disturbances. However, this will likely change in the future. A future temperature increase and an associated decrease in permafrost may cause an increase in depth of the weathering active soil layer, land plant biomass, atmospheric precipitation, and river discharge, which may also increase the river silicon flux and stimulate future diatom growth in the Arctic and therefore influence the global silicon as well as carbon cycle (Tréguer and De La Rocha, 2013). With this project we will provide a baseline study on the present day silicon isotope distribution in the Arctic Ocean for future evaluation of the impact of climate change on the silicon cycle. This project will contribute the first $\delta^{30}Si$ data from the central and eastern Arctic Ocean. Our results will provide information about the main input sources of dissolved silicon via the major Siberian rivers by investigating the dissolved as well as particulate (suspended particles) $\delta^{30}Si$ signatures along the wide eastern Arctic shelf regions and the Arctic basin.

Work at sea

The work at sea was conducted by Ronja Paffrath and included mainly seawater sampling for dissolved silicon isotopes at 20 stations (up to 16 depths per station) from the conventional (not trace metal clean) rosette and additional surface water samples taken with the ships intake system upon leaving each station (see section 5.12 for map). The sample volume required

per analysis is 1-2 L from the rosette (1 L at depth, 2 L in the lower-concentrated upper water column) and 5 L from the ships intake (for the highly depleted surface waters). Seawater will be filtered through AcroPak filter cartridges (0.8/0.45 µm pore size, Supor® pleated membrane) directly from the Niskin bottles (same sampling as for Nd isotopes and REEs). Afterwards no further onboard treatment is necessary and samples will be stored in plastic boxes for the transport to the home laboratory in Oldenburg.

Suspended particles were sampled at 10 stations with up to 12 depths using *in-situ* pumps, surface sediments from the multicorer or boxcorer were collected at 10 stations for the determination of sedimentary biogenic and lithogenic silicon isotope composition. Dirty ice was collected at 2 stations using plastic tools. These samples are shared among a larger group (see section 5.11) in order to analyse a range of parameters on a homogenized sample. The dirty ice will be melted under clean conditions and the particles will be collected by filtration over the same filter type used for suspended particles.

Expected results

The results will provide unique information about silicon biogeochemical cycling under the conditions of high terrestrial input, extensive shelf area and low diatom productivity not found in other ocean regions. We will study the input of the terrigenous sources to the Arctic and mixing with Atlantic and Pacific seawater, trace the transformation processes (formation and remineralization) of particulate silicon in the water column and the transfer to the underlying sediments.

Data management

See introduction of chapter 6 for details on GEOTRACES data management.

References

De Souza GF, Reynolds BC, Rickli J, Frank M, Saito MA, Gerringa LJA, Bourdon B (2012a) Southern Ocean control of silicon stable isotope distribution in the deep Atlantic Ocean. Global Biogeochemical Cycles, 26(GB2035). doi:10.1029/2011GB004141.

De Souza GF, Reynolds BC, Johnson GC, Bullister JL, Bourdon B (2012b) Silicon stable isotope distribution traces Southern Ocean export of Si to the eastern South Pacific Thermocline Biogeosciences, 9, 4199–4213. doi:10.5194/bg-9-4199-2012.

Fripiat F, Cardinal D, Tison JL, Worby A, André L (2007) Diatom-induced silicon isotopic fractionation in Antarctic sea ice Journal of Geophysical Research, 112(G02001). doi:10.1029/2006JG000244.

Grasse P, Ehlert C, Frank M (2013) The influence of water mass mixing on the dissolved Si isotope composition in the Eastern Equatorial Pacific. Earth and Planetary Science Letters, 380, 60–71. doi:10.1016/Jepsl.2013.07.033.

Tréguer PJ, De La Rocha CL (2013) The world ocean silica cycle. Annual Review of Marine Science, 5, 477–501. doi:10.1146/annurev-marine-121211-172346.

Varela DE, Pride CJ, Brzezinski M (2004) Biological fractionation of silicon isotopes in Southern Ocean surface waters. Global Biogeochemical Cycles, 18(GB1047). doi:10.1029/2003GB002140.

6.2 CO_2 System and dissolved oxygen

Elizabeth Jones[1], Adam Ulfsbo[2], [1]NIOZ
L.G. Anderson[2], H.J.W. de Baar[1] (not on board) [2]UGOT

Objectives

The overarching objective of this study is to further improve our understanding of the carbon system in the rapidly changing Arctic Ocean, with an emphasis on the spatial and temporal variability of carbon dioxide (CO_2) fluxes and net community production (NCP) using novel high-resolution methods in the surface mixed layer within the central basins. More specifically, we aim at improving our understanding of the feedbacks by physical and biogeochemical processes on the Arctic Ocean carbon system within the surface mixed layer. This also includes carbon transformation on the large shelf areas and the exchange with the deep central basins, as well as likely changes in the effect by export of marine produced organic matter to the deep central Arctic Ocean when the sea-ice coverage is absent during the productive summer season. In addition, apart from hydrography, a thorough knowledge of the carbon system is essential for the understanding of the distribution of trace elements in the ocean in terms of their cycling, sources and sinks, supporting the on board GEOTRACES programme.

In addition to the four core marine carbonate system parameters: dissolved inorganic carbon (DIC), total alkalinity (TA), pH, and the partial pressure of CO_2 (pCO_2), the participants on board were responsible for underway measurements of dissolved O_2/Ar (Section 6.2.1) and discrete samples for dissolved oxygen (Section 6.2.2.).

Work at sea

Seawater samples were taken from the Niskin bottles mounted to the CTD rosette at depths throughout the water column, but with a bias towards the upper water column. Ice cores were collected at 8 ice stations and 2 deployments of the Mummy Chair from the ship. Cores were typically sectioned with a stainless saw from the bottom upwards on site or in the –20°C container onboard. Core sections were transferred to the laboratory in plastic containers and immediately placed in individual 1 L PVF Tedlar bags and sealed with plastic clips. Excess air was removed with a Nalgene hand pump via Tedlar bag valve and sections were allowed to melt in the dark at laboratory temperature. Upon melting, usually within 20-24 hours, the bulk ice melt was carefully transferred to 250 ml borosilicate glass bottles using Tygon tubing. Samples for under ice water were collected at some stations when possible using either a plastic bottle and titanium weight on a line or a peristaltic pump.

DIC and TA were determined on all seawater and ice core melt samples. Both DIC and TA are measured in parallel with a VINDTA 3C instrument (MARIANDA, Kiel). The accuracy is set by internationally recognized and widely used certified reference material (CRM), batch 144, obtained from Prof. A. Dickson at Scripps Institute of Oceanography (USA). DIC is the sum of all dissolved inorganic carbon species and is determined by a precise coulometric method (Dickson et al., 2007). For every coulometric cell that was used in the coulometer, at least two CRMs were measured in duplicate at the beginning and the end of the analyses, where differences in the measurements infer the precision of the instrument. The TA measurements were made by potentiometric titration with a strong acid (HCl) as a titrant. The acid consumption up to the second endpoint is equivalent to the titration/total alkalinity. The system uses a highly precise Metrohm Titrino for adding acid, a pH electrode and a reference electrode. The measurement temperature for both DIC and alkalinity was 25°C. Analyses were usually carried out immediately after sampling from the CTD and upon complete melt of the ice core sections. In a very few cases, samples had to be stored prior to analysis and where fixed with mercuric chloride solution and were stored in the dark. A total of 57 stations and 10 ice cores were

sampled for DIC and TA (Table 6.2.1), totalling about 1,100 samples. The precision for DIC and TA was determined from the in-bottle CRM duplicate analyses to be better than 2 µmol/kg. The accuracy was checked against frequent analysis of CRMs.

A total of 54 stations were sampled for seawater pH (Table 6.2.1) using borosilicate bottles (250 mL), having tight plastic screw caps, and were rinsed with at least one bottle volume and filled to the rim. All samples were thermostated to 25°C at least 30 min prior to analysis directly after sampling. Seawater pH was determined spectrophotometrically (Clayton and Byrne, 1993) using the sulfonephthalein indicator m-Cresol Purple (mCP). Purified mCP (Liu et al., 2011) was purchased from the laboratory of Robert H. Byrne, University of South Florida, USA. The indicator solution (0.2 mM) was prepared by dissolving pre-weighed mCP indicator in 0.5 L filtered seawater (0.20 µm) of about salinity 34. The indicator was adjusted to a pH in the same range as the samples, approximately ± 0.2 pH units, by adding a small volume of concentrated HCl or NaOH. Before running a set of samples, the pH of the indicator was measured using a 0.02 cm cuvette. The measurements were performed on board within hours of sampling. The shipboard setup is based on the absorption ratios of the indicator at wavelengths 434 nm, 578 nm, and 730 nm (background correction) using a 1-cm flow cuvette and a diode array spectrophotometer (Agilent 8453). Each run consists of the three main steps; i) rinsing of tubing and cuvette with sample (15 mL) ii) sample blank (25 mL) and iii) sample run (20 mL) including indicator (0.5 mL). The sample is pumped and mixed using a Kloehn V6 syringe pump (Norgren) with a zero-dead volume syringe. Sample temperature is measured directly after the cuvette. The magnitude of the perturbation of seawater pH caused by the addition of indicator solution is calculated and corrected for using the method described in Chierici et al. (1999). The instrument setup is controlled by a PC running a LabView program (Fransson et al., 2013). The pH values are corrected to 25°C on the total scale. The overall precision from duplicate sample analysis was better than ±0.001 pH units. The accuracy is mainly set by the accuracy of the physico-chemical characterizations of the indicator with respect to temperature dependence and the determination of the equilibrium constants of the indicator, as well as the purity of the indicator (Liu et al., 2011). The accuracy was checked against Certified Reference Material for total alkalinity and total dissolved inorganic carbon, indicating that it should be well below 0.01 pH units.

Surface water partial pressure of CO_2 (pCO_2) was determined along the ships track from the ship's underway seawater supply (Fig. 5.2.1). Sea surface pCO_2 is obtained with a General Oceanics (GO850) system with an infra-red analyser (LiCOR 7000), both for seawater using an water-air equilibrator and for the atmosphere, the air being pumped from the crow's nest.

Preliminary/expected results

Across the Arctic Ocean, the vertical profiles of DIC and alkalinity typically showed a high consistency. Very low values for DIC and alkalinity occurred near the sea ice edge and within other areas of recent sea ice melt, consistent with reduced salinity. A minimum in pCO_2 of about 100 µatm also occurred in this region. As alkalinity is thought to be conservative, the gradient within the deep water column was expected to be very low. This could be confirmed and revealed the high precision achieved with the analyses. The values of DIC and alkalinity in ice core melts showed variation within the ice profile and between different ice stations, with very low values compared to seawater samples.

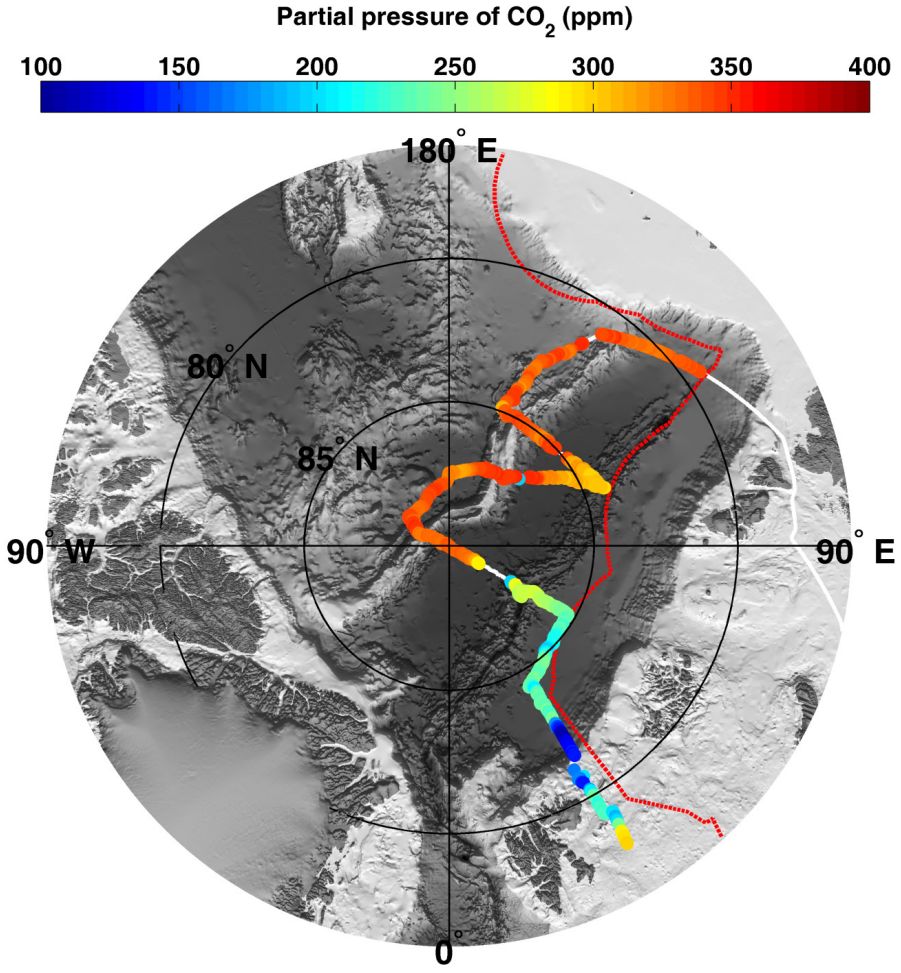

Fig. 6.2.1. Sea surface partial pressure of CO_2 (ppm) along the PS94 cruise track (white line). The red dashed line indicates the Russian Exclusive Economic Zone.

6.2.1 Net community production using O_2/Ar ratios in surface waters

Elizabeth Jones[1], Adam Ulfsbo[2]

[1]NIOZ
[2]UGOT

Objectives

The objective of this project is to estimate net community productivity in the Arctic Ocean using dissolved O_2/Ar measurements (Ulfsbo et al., 2014), investigate the physical and biological controls on oxygen saturation variability in the upper Arctic Ocean (Eveleth et al., 2014), and constrain the biogeochemical controls on carbon fluxes. Oxygen in the mixed layer is influenced by biology, and by physical processes such as bubble injection, temperature and pressure changes. Because argon (Ar) has similar solubility properties as oxygen, the oxygen derived from physical processes can be estimated from the argon concentration relative to its saturation ([Ar]sat). The oxygen derived from biology is equal to the total oxygen minus the oxygen derived from physical processes.

Work at sea

Biological oxygen supersaturation was measured continuously by Equilibrator Inlet Mass Spectrometry (EIMS, Fig. 6.2.2) provided by Nicolas Cassar, Duke University, USA, a method

previously described (Cassar et al., 2009). Briefly, seawater from the ship's underway system was pumped through a gas equilibrator, the headspace of which was connected to a quadrupole mass spectrometer for continuous elemental O_2/Ar ratio measurements. The ion current ratio was calibrated by periodically sampling ambient air. From the O_2/Ar supersaturation, a gas exchange rate, and the oxygen concentration at saturation, the net biological oxygen flux across the ocean surface will be estimated. The oxygen optode (Aanderaa 4835) will be calibrated post-cruise against discrete Winkler samples from the ship's underway intake line.

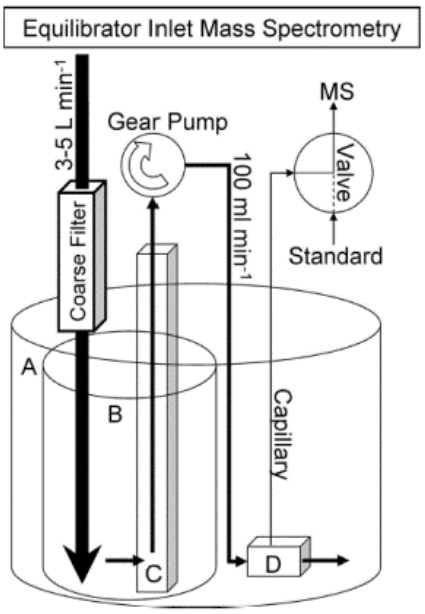

Fig. 5.2.2. Setup of the Equilibrator Inlet Mass Spectrometry. The large seawater reservoir (A) sits in a sink. After going through an inline coarse filter (500 µm pore size), seawater flows into the inner reservoir (B) at a rate of 3-5 L min-1 (large arrow). Most of the water running into B overflows into A, which is used as a water bath thermostated to the temperature of ambient seawater. A small fraction (100 mL min-1) of the high flow rate is pulled with a gear pump through a filter sleeve (C), with 100 and 5 µm pore size on the outside and inside, respectively.

From the gear pump, the seawater flows through the equilibrator (D). The equilibrator sits in reservoir A to keep its temperature identical to that of the incoming seawater. A capillary, attached to the headspace of the equilibrator, leads to a multiport Valco valve. This valve alternates between admitting gas from the equilibrator and ambient air to the quadrupole mass spectrometer. An optode (not shown) in container B measures total oxygen saturation. Also not shown is a water flow meter located downstream of the equilibrator and thermocouples monitoring temperatures through the system (from Cassar et al., 2009).

Preliminary/expected results

Our preliminary observations suggest net autotrophic conditions in the deep basins with large biological activity in the marginal sea ice.

6.2.2 Dissolved oxygen

Elizabeth Jones[1], A. Ulfsbo[2]

[1]NIOZ
[2]UGOT

Dissolved oxygen in seawater was determined by direct spectrophotometry of total iodine at 456 nm (Pai et al., 1993). The method is based on the classical Winkler method with respect

to sampling and pickling reagents up to the point of titration with thiosulfate, according to the following redox-reactions:

$$2\ Mn^{2+} + 2\ OH^- \rightarrow 2\ Mn(OH)_2$$
$$2\ Mn(OH)_2 + O_2 \rightarrow 2\ MnO(OH)_2$$
$$2\ MnO(OH)_2 + 8\ H^+ + 6\ I^- \rightarrow 2\ Mn^{2+} + 2\ I_3^- + 6\ H_2O$$

First an excess of dissolved manganese and a strong base with an excess of iodide ions are added to the seawater sample, the Mn2+ is oxidized by the dissolved oxygen in the water to higher oxidation states and precipitates as MnO(OH)2 to the bottom of the sample bottle. After a few hours, an excess of strong acid is added to the sample, to reduce the manganese back to the Mn2+ form. With the reduction of manganese the iodide ions become oxidized to iodine in the form of I3- ions, which has an intense yellow color, and was spectrophotometrically analysed using a flow-through cuvette (1 cm) and a peristaltic pump.

Work at sea

Samples for dissolved oxygen were collected from the specified Niskin bottle on the CTD rosette (Table 6.2.1). Samples for sensor calibration were generally taken below 400 m depth. Samples were stored under water in the dark until analysis within one week of sampling. Standards for the calibration curve were prepared before each set of sample analyses using seawater from the ship‘s surface intake line. Pickling reagents and sulphuric acid were added in reverse order A pre-prepared potassium iodate standard solution (KIO3, 70.16 mM) was added in a step-wise manner (0, 200, 300, 400, 500, 650, 750 µL). The calibration curve was fitted to a quadratic polynomial function since the spectrophotometer in use had a slightly non-linear response as determined pre-cruise. A total of 32 stations were sampled for dissolved oxygen. The precision was determined to be on the order of 0.30 µmol/L from duplicate sample analysis. The accuracy was determined as 0.89 µmol/L (0.4 %) by multiple sample analysis of a large batch of air-equilibrated deepwater (2,500 m).

Preliminary/expected results

The dissolved oxygen will be used for post-cruise calibration of the oxygen sensors mounted on the small (AWI) and large (NIOZ) CTD-rosettes.

Data management

The DIC, TA, pH, and pCO_2 data will undergo processing after the cruise. The final data will be submitted to data centers, as has been done with all data of previous cruises with *Polarstern*. The usual data center for carbon research is the Carbon Dioxide Information and Analysis Center (CDIAC; Boulder, USA).

See introduction of chapter 6 for details on GEOTRACES data management.

References

Cassar N, Barnett BA, Bender ML, Kaiser J, Hamme RC, Tilbrook B (2009) Continuous High-Frequency Dissolved O2/Ar Measurements by Equilibrator Inlet Mass Spectrometry. Analytical Chemistry, 81, 1855-1864, doi: 10.1021/ac802300u.

Chierici M, Fransson A, Anderson LG (1999) Influence of m-cresol purple indicator additions on the pH of seawater samples: correction factors evaluated from a chemical speciation model. Marine Chemistry, 65(3-4), 281–290, doi:10.1016/S0304-4203(99)00020-1.

Clayton TD, Byrne RH (1993) Spectrophotometric seawater pH measurements: total hydrogen ion concentration scale calibration of m-cresol purple and at-sea results. Deep Sea Research Part I, 40(10), 2115–2129, doi:10.1016/0967-0637(93)90048-8.

Dickson AG, Sabine CL, Christian JR (2007) Guide to best practices for ocean CO_2 measurements. PICES Special Publication, 173 pp., North Pacific Marine Science Organization (PICES), Sidney, British Columbia

Eveleth R, Timmermans ML, Cassar N (2014) Physical and biological controls on oxygen saturation variability in the upper Arctic Ocean. J GeophyS ReS Oceans, 119, 7420–7432, doi:10.1002/2014JC009816.

Fransson A, Engelbrektsson J, Chierici M (2013) Development and Optimization of a Labview program for spectrophotometric pH measurements of seawater. pHspec ver 2.5, University of GothenburG.

Liu X, Patsavas MC, Byrne RH (2011) Purification and Characterization of meta-Cresol Purple for Spectrophotometric Seawater pH Measurements. Environmental Science & Technology, 45(11), 4862–4868, doi:10.1021/es200665D.

Pai SC, Gong GC, Liu KK (1993) Determination of dissolved oxygen in seawater by direct spectrophotometry of total iodine. Marine Chemistry, 41, 343-351.

Ulfsbo A, Cassar N, Korhonen M, van Heuven S, Hoppema M, Kattner G, Anderson LG (2014) Late summer net community production in the central Arctic Ocean using multiple approaches. Global Biogeochemical Cycles, 28, doi:10.1002/2014GB004833.

Tab. 6.2.2.1: Stations and parameters sampled for DIC, TA, pH, and O2

Year	Month	Day	Station	Cast	DIC, TA	pH	O2	Deployment	Ice core
2015	8	22	4	1	x	x	x	CTD	
2015	8	21	18	3	x	x	x	CTD	
2015	8	23	32	2	x	x	x	CTD	
2015	8	23	34	1			x	CTD	
2015	8	24	40	1	x	x	x	CTD	
2015	8	24	40	3	x	x	x	CTD	
2015	8	29	46	4	x	x	x	CTD	x
2015	8	26	50	1	x	x	x	CTD	
2015	8	26	50	4	x	x	x	CTD	
2015	8	27	50	6	x	x		CTD	
2015	8	28	54	2	x	x	x	CTD	x
2015	8	29	58	1	x	x	x	CTD	
2015	8	30	58	3	x	x	x	CTD	
2015	8	30	58	5	x	x		CTD	
2015	8	30	59	1			x	CTD	
2015	9	1	62	1	x	x	x	CTD	
2015	9	1	66	1	x	x		CTD	
2015	9	2	68	1	x	x	x	CTD	
2015	9	2	69	4	x	x	x	CTD	x

Year	Month	Day	Station	Cast	DIC, TA	pH	O2	Deployment	Ice core
2015	9	2	69	5	x	x		CTD	
2015	9	3	70	1	x	x	x	CTD	
2015	9	4	75	1			x	CTD	
2015	9	4	76	1	x	x	x	CTD	
2015	9	5	80	1			x	CTD	
2015	9	6	81	2	x	x	x	CTD	x
2015	9	6	81	5	x	x	x	CTD	
2015	9	6	81	7	x	x		CTD	
2015	9	7	85	1	x	x	x	CTD	
2015	10	5	87	1	x			UCC	
2015	10	3	89	1	x	x	x	CTD	
2015	9	9	91	1	x	x		CTD	
2015	9	10	94	1			x	CTD	
2015	9	11	96	2	x	x		CTD	x
2015	9	12	96	7	x	x		CTD	
2015	10	2	99	2	x	x		CTD	
2015	9	15	101	2	x	x	x	CTD	x
2015	9	14	101	5	x	x	x	CTD	
2015	9	14	101	7	x	x		CTD	
2015	9	14	101	9	x	x		CTD	
2015	9		107					mummy chair	x
2015	9		112					mummy chair	x
2015	9	19	117	2	x	x	x	CTD	x
2015	9	19	117	4	x	x		CTD	
2015	9	19	117	7	x	x		CTD	
2015	9	20	118	1	x	x		CTD	
2015	9	20	119	1	x			UCC	
2015	9	21	121	1	x	x	x	CTD	
2015	9	23	123	1	x	x	x	CTD	
2015	9	22	125	2	x	x	x	CTD	x
2015	9	22	125	5	x	x		CTD	
2015	9	22	125	7	x	x		CTD	
2015	9	23	128	1	x	x		CTD	
2015	10	2	130	1	x	x		CTD	
2015	9	24	132	1	x	x	x	CTD	
2015	9	24	134	1	x	x		CTD	
2015	9	26	134	3	x			UCC	
2015	10	7	147	1	x	x		CTD	
2015	10	7	149	1	x	x		CTD	
2015	10	7	153	1	x	x		CTD	
2015	10	7	157	1	x	x		CTD	

Year	Month	Day	Station	Cast	DIC, TA	pH	O2	Deployment	Ice core
2015	10	8	161	1	x	x		CTD	
2015	10	8	165	1	x	x		CTD	
2015	10	9	169	1	x	x		CTD	
2015	10	9	173	1	x	x		CTD	

6.2.3 Triple Oxygen isotopes of dissolved O_2

Dorothea Bauch[1] [1]GEOMAR
Boaz Luz[2] (not on board) [2]HUJ

Objectives

The objective of this study is tracing sources of photosynthetic O_2 to the depth of the Arctic Ocean. This will give us new insights on mechanisms involved in formation of dense deep waters in the Arctic, in particular, and more generally, in the world ocean.

Work at sea

A total of 96 water samples of about 200 mL were taken for triple oxygen isotopes of dissolved O_2 from the CTD-rosette. For this water was sucked by a bubble-free procedure into preevacuated glas flasks. A deep station was sampled in each of the visited deep basins in parallel to all Geotraces proxies as well as the accompanying parameters $\delta^{13}C_{DIC}$ and $\delta^{18}O$. About 24 samples were taken in the Nansen, Amundsen and Makarov basins (stations 50, 81 and 101, respectively). In addition the upper 500 m was sampled in the western part of the Makarov basin and a shallow station was sampled on the Bear-Island section within the inflow of Atlantic Waters into the Barents Sea (station 169).

Preliminary/expected results

As soon as the samples arrive in Jerusalem, we will follow established procedures for seawater removal, gas extraction and purification of O_2. Then we will start mass spectrometric measurements. The latter will take time due to the extreme high precisión. I expect to have results by the end of April 2016. As explained above, we will use the results for tracing sources of photosynthetic O_2 to the Deep Arctic Ocean.

Data management

See introduction of chapter 6 for details on GEOTRACES data management.

6.3 Clean sampling of trace metals using an all titanium ultraclean ctd and sampler system

Sven Ober[1], Micha Rijkenberg[1], Loes Gerringa[1], Jan van Ooijen[1], Hans Slagter[1], Lars-Eric Heimbürger[2], Aridane Gonzales[3], Michael Staubwasser[4], H.de Baar (not on board)

[1]NIOZ
[2]UB
[3]IUEM
[4]UNIK

Objectives

During this cruise we sampled 28 full depth stations for a suite of bio-essential trace elements Mn, Fe, Co, Ni, Cu, Zn, Cd and the mostly anthropogenic (pollutant and/or potentially toxic) trace metals Hg and Pb. Samples were taken in an ultraclean way using the titanium ultraclean

CTD and sampler system as developed and build at the Royal NIOZ (de Baar et al., 2008; Rijkenberg et al., in press).

Work at sea

During this expedition a so called 'Ultra Clean CTD' was used. This 'Ultra Clean CTD' is a CTD equipped with 24 polypropylene watersamplers each with a volume of 24 liters. The samplers are closed using a butterfly-type closing mechanism powered using seawater hydraulics (Rijkenberg et al. in press). During the first meters of the downcast the samplers open automatically and a spring-loaded accumulator is filled with water. This process stops at 30 meter depth. During the upcast the bottles are closed via a hydraulic multiplexer using the pressurised water in the accumulator. This water sampling system is developed and manufactured by Royal NIOZ. The frame is made of titanium and lowered by a cable made of Dyneema (diameter: 11 mm). This cable however had no electrical conductors so powering and communication with the CTD is not possible through this cable. To overcome this problem a SBE17 (S\N 17-0374) in a titanium housing was installed. This instrument has a chargeable NiMH-battery for powering all the electronics in the frame, memory for storing the data and a programmemable Auto Firing Module which fires bottles at desired depths. The underwater-unit was a SBE9+ (S\N 790). Only a thermometer SBE3+ (S\N 032118), a conductivity-sensor SBE4 (S\N 043035) and an underwater-pump SBE5 (S\N 050882) were installed due to the limited power capacity of the battery. All pressure housings were made of titanium.

The UCC has a rectangular frame made of titanium, has wheels and can be parked in a clean-air container (de Baar et al., 2008). The container provides an ultraclean environment for sub-sampling. Just prior to a cast it can be pushed out of the container on a dedicated pallet. This pallet can be moved over deck to the CTD launching spot by using a long forklift. After the cast this procedure is reversed.

The software package 'SeatermAF-V2' contains all the functions needed for programming and testing of the SBE17. It also provides a function for downloading of the CTD-data after a cast. The CTD-data can be processed in the usual way using the package 'SBEDataprocessing '.

During the start-up phase we had to overcome a wide variety of problems, but after that everything worked fine. An overview of the problems can be found in UCC-station-list in de column 'Remarks' of Table 6.3.1.

Tab. 6.3.1: The UCC station list

Sta.	Cast	Scans averaged	Remarks
4	2	n/a	OK, all bottles closed, but data appeared to be unreadable.
4	6	n/a	Failed (Diagnosis: 'Faulty memory-blocks').
			Former cast had the same problem, but this became only clear after this cast.
8	2	n/a	First 3 bottles closed, no water-sampling was done,
			reason initially unclear, but this became clear after the next cast.
30	1	n/a	Failed, due to bad Multivalve-cable. Exchanged by spare.
32	4	1	OK, downloading data took 9 hours at highest speed!, back to default-value 24
40	2	n/a	Multivalve-main-chip appeared to have corroded contacts
50	3	24	OK

Sta.	Cast	Scans averaged	Remarks
54	3	24	OK, Bottles 22, 23 and 24 open due to a leaking main-tube of the hydraulics.
58	7	24	OK
64	2	24	OK
69	2	24	OK
70	4	24	OK
76	2	n/a	Failed, due to a memory-problem of SBE17 (not recognized) and
			a minor problem with Multivalve (recognized and solved)
81	1	n/a	Failed, due to a memory-problem of SBE17. This problem co-incided with
			the problems of the Multivalve during the former cast.
81	4	n/a	OK, surface-cast for M. Staubwasser. He didn't want the CTD data, so no data.
81	10	24	OK
87	1	24	OK, Northpole !
91	2	24	OK
96	4	24	OK
99	1	24	OK
99	3	24	OK
101	4	24	OK
101	8	24	OK
117	3	24	OK
119	1	4	OK
121	2	4	OK
125	4	24	OK
130	2	24	OK
134	2	24	OK
147	2	4	OK
149	2	4	OK
153	2	4	OK
157	2	4	OK
161	2	4	OK
169	3	4	OK
173	2	4	OK

Preliminary/expected results

Fig. 6.3.1 shows the stations that were successfully sampled with the ultraclean CTD sampler system. A total of 28 stations were sampled with success resulting in the availability of roughly 16,200 Liters of trace metal clean seawater available for sampling for different parameters.

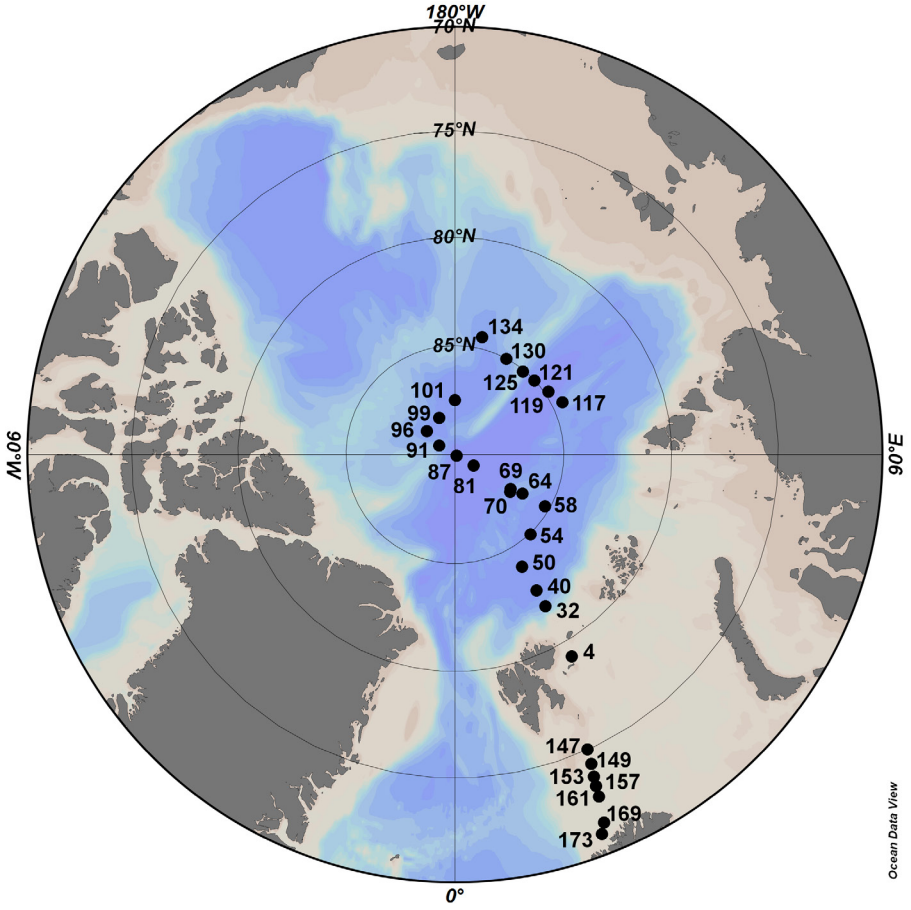

Fig. 6.3.1:Station map of successful UCC casts

Data management

See introduction of chapter 6 for details on GEOTRACES data management.

References

de Baar HJW, Timmermans KR, Laan P, De Porto HH, Ober S, Blom JJ, Bakker MC, Schilling J, Sarthou G, Smit MG, Klunder M (2008) Titan: A new facility for ultraclean sampling of trace elements and isotopes in the deep oceans in the international Geotraces program. Mar. Chem., 111, 4-21.

Rijkenberg MJA, de Baar HJW, Bakker K, Gerringa LJA, Keijzer E, Laan M, Laan P, Middag R, Ober S, van Ooijen J, Ossebaar S, van Weerlee EM, Smit MG (2015) “PRISTINE”, a new high volume sampler for ultraclean sampling of trace metals and isotopes. Mar. Chem., in press.

6.4 Dissolved Fe, Mn, Zn, Ni, Cu, Cd, Pb

Micha Rijkenberg NIOZ

Objectives

The Arctic Ocean is rapidly changing due to recent global warming (IPCC report 2013). Arctic sea ice declines and exists now mostly of first-year sea ice (Haas et al., 2008; Stroeve et al., 2011; Maslanik et al., 2011) enabling future economic activities. Warming of Arctic terrestrial areas caused increased river discharge which, combined with net loss of the Greenland ice-cap and melting of sea ice, resulted in a freshening of surface waters and increased stratification. We need to understand how climate induced changes will change the biogeochemical cycling and therefore the still unknown distribution of many bio-essential and pollutant trace metals in the Arctic to understand the consequences for the Arctic marine ecosystems. As the Arctic Ocean is part of the thermohaline circulation changes in the Arctic will also affect the distribution of trace metals in the global oceans (Gerringa et al., 2015). We are now able to precisely analyze a suite of bio-essential trace metal elements Mn, Fe, Co, Ni, Cu, Zn, Cd and the mostly anthropogenic potentially toxic trace metals Pb and at high concentrations Cu and Zn. This allows us to compare library samples from the central Arctic expedition in 2007 (Klunder et al., 2012a, 2012b; Middag et al., 2011; Thuróczy et al., 2011) with samples of Canadian, US and European research cruises in 2015 as well as an expedition to Fram Strait (2016) aimed to quantify the exchange of trace metals between the Arctic and Atlantic Oceans. The data collected in this project as part of the pan-Arctic GEOTRACES effort will also provide a first-ever baseline of the pollutant-type metals useful to assess the impact of future commercial activities in the Arctic.

Work at sea

At 28 stations, a total of 559 samples for the measurement of dissolved trace metals (250 ml, 0.2 µm filtered) and about 280 samples for the measurement of total dissolvable trace metals (unfiltered and acidified for a period of at least 6 months) were taken from the ultraclean CTD sampler system (de Baar et al., 2008; Rijkenberg et al., in press). The samples of dissolved trace metals were filtered using the 0.2 µm Sartobran 300 cartridges of Sartorius. The dissolved and total dissolvable trace metal samples were acidified with 2ml/L 12M Baseline grade Seastar HCl (final pH of 1.8). At NIOZ, the trace metals will be extracted from the seawater samples using a seafast system (Lagerström et al., 2013) and measured by a Thermo Element-II single collector HR-ICP-MS.

A total of 559 samples were measured on board for their dissolved iron (DFe) concentration by automated Flow Injection Analysis (FIA) after a modified method of De Jong et al., 1998. Filtered (0.2 µm) and acidified (pH 1.8, 2ml/L 12M Baseline grade Seastar HCl) seawater was concentrated on a column containing aminodiacetid acid (IDA).This material binds only transition metals and not the interfering salts. After washing the column with ultrapure water, the column is eluted with diluted hydrochloric acid. After mixing with luminol, peroxide and ammonium, the oxidation of luminol with peroxide is catalysed by iron and a blue light is produced and detected with a photon counter. The amount of iron is calculated using a standard calibration line, where a known amount of iron is added to low iron containing seawater. Using this calibration line a number of counts per nM iron is obtained. Samples were analysed in triplicate and average DFe concentrations and standard deviation are given.

Concentrations of DFe measured during the PS94 cruise ranged from 20 pM in the surface of the Nansen basin up to 12.5 nM in a nepheloid layer near Svalbard along our Bear Island transect.

The standard deviation varied between 0% and 37% (the latter being exceptional), but was on average 2.9% and generally < 5% in samples with DFe concentrations higher than 0.1 nM. The average system blank was determined at 0.017 nM ± 0.02 nM and was defined as a sample loaded for 5 seconds and measured daily. The average limit of detection was determined at 0.06 nM and was defined as 3*standard deviation of the mean blank as measured daily. The consistency of the FIA system over the course of the day was verified using a drift standard. Drift has been observed and seemed to be variable from day to day. All data will be corrected for this daily drift. Certified SAFe and GEOTRACES standards (Johnson et al., 2007) for the long term consistency and absolute accuracy was measured on a regular basis.

Preliminary/expected results

As an example of the data collected we present here the depth profile of DFe as measured at the North Pole, Fig. 5.4.1. The higher surface concentrations of DFe were found in the transpolar drift.

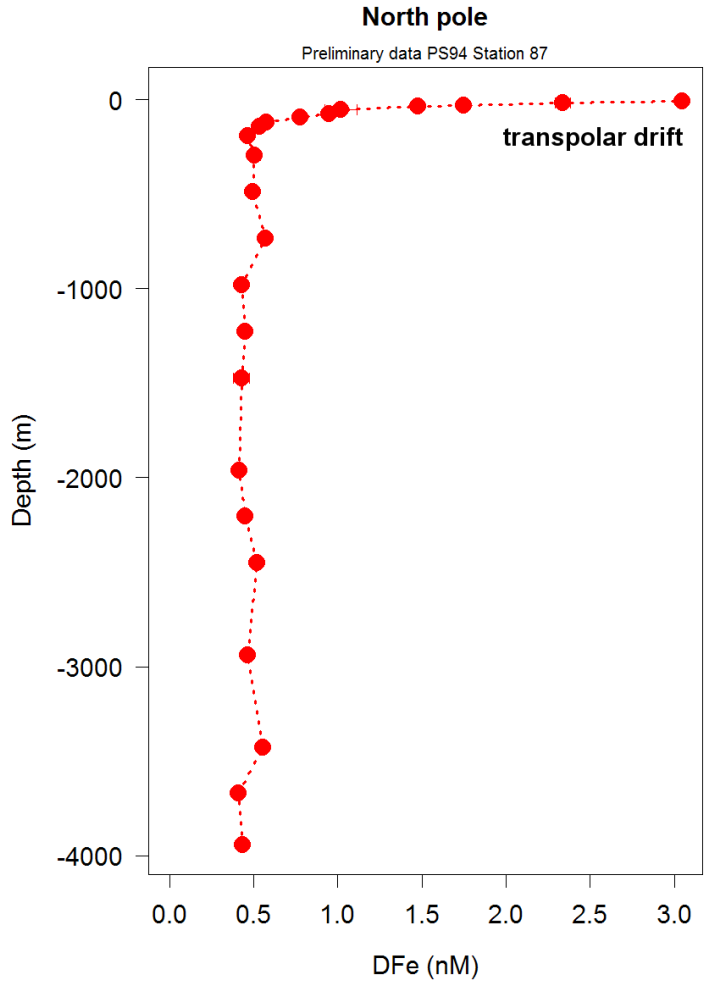

Fig. 5.4.1: Depth profile of DFe at the North Pole

Data management

See introduction of chapter 6 for details on GEOTRACES data management.

References

de Baar HJW, Timmermans KR, Laan P, De Porto HH, Ober S, Blom JJ, Bakker MC, Schilling J, Sarthou G, Smit MG, Klunder M (2008) Titan: A new facility for ultraclean sampling of

trace elements and isotopes in the deep oceans in the international Geotraces program. Mar. Chem., 111, 4-21.

Gerringa LJA, Rijkenberg, MJA, Schoemann V, Laan P, de Baar HJW (2015) Organic speciation of dissolved iron in the West Atlantic Ocean. Mar. Chem., in press.

Haas C, Pfaffling A, Hendricks S, Rabenstein L, Etienne J-L, Rigor I (2008) Reduced ice thickness in Arctic Transpolar Drift favors rapid ice retreat. Geophys. Res. Lett., 35, L17501.

IPCC, Climate Change 2013: The physical Science Basis, Summary for Policymakers. Working group I: Contribution to the fifth assessment report of the intergovernmental panel on climate change, 2013, 27.

Johnson KS, Boyle E, Bruland K, Measures C, Moffett J, Aquilarislas A, Barbeau K, Cai Y, Chase Z, Cullen J, Doi T, Elrod V, Fitzwater S, Gordon M, King A, Laan P, Laglera-Baquer L, Landing W, Lohan M, Mendez J, Milne A, Obata H, Ossiander L, Plant J, Sarthou G, Sedwick P, Smith GJ, Sohst B, Tanner S, van den Berg S, Wu J (2007) Developing Standards for Dissolved Iron in Seawater. Eos, Transactions Am. Geoph. Union, 88, 131-132.

de Jong JTM, den Das J, Bathmann U, Stoll MHC, Kattner G, Nolting RF, de Baar HJW (1998) Dissolved iron at subnanomolar levels in the Southern Ocean as determined by ship-board analysis. Anal. Chim. Acta, 377, 113-124.

Klunder MB, Bauch D, Laan P, de Baar HJW, van Heuven S, Ober S (2012a) Dissolved iron in the Arctic shelf seas and surface waters of the central Arctic Ocean: Impact of Arctic river water and ice-melt. J. Geophys. Res., 117, C01027.

Klunder MB, Laan P, Middag R, de Baar HJW, Bakker K (2012b) Dissolved iron in the Arctic Ocean: Important role of hydrothermal sources, shelf input and scavenging removal. J. Geophys. Res., 117, C04014.

Lagerström ME, Field MP, Séguret M, Fischer L, Hann S, Sherrell RM (2013) Automated on-line flow-injection ICP-MS determination of trace metals (Mn, Fe, Co, Ni, Cu and Zn) in open ocean seawater: Application to the GEOTRACES program. Mar. Chem., 155, 71-80.

Maslanik J, Stroeve J, Fowler C, Emery W (2011) Distribution and trends in Arctic sea ice age through spring 2011. Geophys. Res. Lett., 38, L13502.

Middag R, de Baar HJW, Laan P, Klunder MB (2011) Fluvial and hydrothermal input of manganese into the Arctic Ocean. Geochim. Cosmochim. Acta, 75, 2393-2408.

Rijkenberg MJA, de Baar HJW, Bakker K, Gerringa LJA, Keijzer E, Laan M, Laan P, Middag R, Ober S, van Ooijen J, Ossebaar S, van Weerlee EM, Smit MG (2015) “PRISTINE”, a new high volume sampler for ultraclean sampling of trace metals and isotopes. Mar. Chem. in press.

Stroeve J, Serreze M, Holland M, Kay J, Malanik J, Barrett A (2011) The Arctic’s rapidly shrinking sea ice cover: a research synthesis. Climatic Change, 110, 1005-1027.

Thuróczy C-E, Gerringa LJA, Klunder MP, Laan P, Le Guitton M, de Baar HJW (2011) Distinct trends in the speciation of iron between the shelf seas and the deep basins of the Arctic Ocean. J. Geophys. Res., 116, C10009.

6.5 Organic speciation of Fe

Hans Slagter, Loes Gerringa, Micha Rijkenberg NIOZ

Outline

Iron is a biologically essential element which is limiting primary production in many ocean areas (de Baar et al., 1990; Martin et al., 1990) and dissolves poorly in seawater. Iron's inorganic solubility in seawater of pH 8.1 is between 0.1 and 0.2 nM (Millero et al., 1998) and concentrations found above this are recognized to be bound to dissolved organic ligands (Gledhill and van den Berg, 1994; Liu and Millero, 2002). Many different substances are recognized to bind Iron, making up a pool of ligands. However, the relative contributions and interactions at play in this ligand pool are still poorly characterized. Work on the characterization of this ligand pool is ongoing, employing different techniques to identify its constituents (Gledhill and Buck, 2012). Examples are different approaches to Competing Ligand Exchange – Adsorptive Stripping Voltammetry (CLE-AdCSV) (Rue and Bruland, 1995; Croot and Johansson, 2000; van den Berg, 2006), characterization using mass-spectrometric methods (McCormack et al., 2003; Mawji et al., 2011; Velasquez et al., 2011) and detection and characterization of specific functional groups using chemical assays (Macrellis et al., 2001).

Possible contributions to the ligand pool are made by biological processes, e.g. bacteria producing siderophores (Haygood et al., 1993) and phytoplankton producing exudates such as polysaccharides (Hassler et al., 2011). Marine viruses lyse both marine bacteria and phytoplankton, releasing cell content and contributing to the dissolved and particulate matter pools (Brussaard et al., 2008), also releasing ligands as part of these processes (Poorvin et al., 2011). Humic substances (HS) are part of the dissolved organic matter (DOM) in seawater with a terrestrial and/or riverine origin and are important contributors to the ligand pool in estuarine areas (Laglera and van den Berg, 2009). Not much is currently known about the composition of the ligand pool in the Arctic Ocean. As the Arctic Ocean is a mediterranean sea with major terrestrial inputs, the relative contribution to the ligand pool of riverine input is expected to be large. The only thorough measurement of organic ligands in the Arctic Ocean has been performed during the International Polar Year 2007 by Thuroczy et al., (2011). This study inventoried organic ligands with full depth profiles in the Nansen, Amundsen and Makarov basins. A major interest to us on the PS94 TransArcII expedition is the crossing of the transpolar drift (TPD), which transports riverine water from the Siberian shelf areas and thus the major Arctic rivers within the halocline across the arctic basins. The TPD eventually transports these waters into the Norwegian Greenland seas through Fram strait (Gordienko and Laktionov, 1969; Rudels, 2009; Rutgers van der Loeff et al., 2012) and thus transports these riverine fractions eventually into the northern North Atlantic. The TPD's drift trajectory changes with the Arctic Oscillation (AO) index, shifting further northward towards the Beaufort gyre in AO- conditions, and can be traced in a number of ways. Stable oxygen isotope analysis ($\delta^{18}O$) indicates the influence of meteoric waters that consists mainly of terrestrial runoff introduced into the surface waters and transported in the TPD (Bauch et al., 2011). Rutgers van der Loeff et al., (2012) were able to infer transfer times of shelf waters through ^{228}Th and ^{228}Ra signatures of about 1 to 3 years. Finally the TPD may also be identified by the presence of terrestrially sourced coloured- or chromophoric DOM (CDOM). CDOM has its origin in the breakdown of biological material, with terrestrial and marine sources being major contributors (Nelson and Siegel, 2012). In the open ocean the signal from marine sources dominates the CDOM pool, however in the TPD in which the CDOM pool has a strong terrestrial origin, the terrestrial signal dominates (Stedmon et al., 2011; Granskog et al., 2012). CDOM is a heterogeneous mix of organic material, some characterization of which is possible by the measurement of its absorptive properties (Mopper and Schultz, 1993; Stedmon and Markager, 2001), as well as through detailed measurement of its fluorescent subset (FDOM) (Stedmon and Markager,

2005). Humic substances are represented in the CDOM pool as 'gelbstoff', with a distinct fluorescence signal (Coble et al., 1990; Mopper and Schultz, 1993). This fluorescence signal is also easily measured using an *in-situ* fluorometer mounted on a CTD rosette frame.

Objectives

Crossing into the TPD and its higher terrestrial runoff component, we hope to elucidate different contributors to the ligand pool by a combination of techniques. Electrochemical measurements were performed to ascertain total iron ligand concentrations and binding strengths. Humic substances will also be measured electrochemically using fulvic acid as a standard. Furthermore, absorbance and fluorescence spectra will be measured as an indicator of terrestrial water and humic substances. Given the documented influence of biological activity on the organic ligand pool, we wish to decouple the contribution of humic substances to the iron binding ligand pool from more local biological production of iron binding ligands. Therefore, samples were collected for flowcytometric enumeration of phytoplankton, bacteria and viruses in the home lab.

Work at sea

Stations sampled
All samples were taken from the Ultra Clean sampling system (UCC). Fe Ligands samples were measured on board electrochemically, CDOM samples were measured on board spectrophotometrically. Samples will be analysed by flow cytometry in the home lab, and samples to measure humics were taken for Dr. Luis Laglera (UIB).

Tab. 6.5.1: Overview of stations and samples for analysis of organic speciation of Fe

Station	Cast	# bottles	Properties to be measured
4	2	8	Fe Ligands, CDOM, flow cytometry, humics
32	2	14	Fe Ligands, CDOM, flow cytometry, humics
40	2	3	Fe Ligands
50	2	13	Fe Ligands, CDOM, flow cytometry
64	2	10	Fe Ligands, CDOM, flow cytometry
69	2	14	Fe Ligands, CDOM, flow cytometry, humics
70	4	2	Fe Ligands
81	10	14	Fe Ligands, CDOM, flow cytometry, humics
87	1	14	Fe Ligands, CDOM, flow cytometry, humics
91	2	8	Fe Ligands, CDOM, flow cytometry, humics
96	4	13	Fe Ligands, CDOM, flow cytometry, humics
99	3	14	Fe Ligands, CDOM, flow cytometry, humics
101	4	13	Fe Ligands, CDOM, flow cytometry
117	3	14	Fe Ligands, CDOM, flow cytometry, humics
119	1	8	Fe Ligands, CDOM, flow cytometry
121	2	8	Fe Ligands, CDOM, flow cytometry, humics
125	3	14	Fe Ligands, CDOM, flow cytometry, humics
130	2	8	Fe Ligands, CDOM, flow cytometry, humics
134	2	12	Fe Ligands, CDOM, flow cytometry, humics

Iron binding dissolved organic ligands

The concentration and binding strengths of organic iron binding ligands is measured using CLE-AdSV. A known ligand is added to a natural sample, which is allowed to equilibrate with increasing iron additions in discrete subsamples, constituting a titration with iron. The added ligand (AL) is in competition for iron with the natural ligands in the sample. As it is added in surplus, the natural ligands will be saturated with iron in the higher additions of the titration, whereas the AL will continue to take up iron. After equilibration the subsamples are measured from low to high additions with a voltammetric scan. The current peak recorded is equivalent to the concentration of the iron - AL complex.

0.02 M AL stock solutions were made using *2-(2-Thiazolylazo)-p-cresol* (TAC) after Croot and Johansson (2000). AL are dissolved in 2 times quartz distilled (2QD) methanol. A borate-ammonia buffer was used to maintain pH in treated samples during voltammetric scans. The buffer was adjusted to keep the pH at 8.05 in a titration subsample consisting of seawater, buffer and Fe standard addition. Buffers were prepared at the home lab, where they were cleaned of trace metal contaminations using equilibration with MnO_2 particles after van den Berg and Kramer (1979).

The voltammetric setup consists of a Metrohm 663 VA stand, control hardware (Metrohm Autolab II and IME 663) and a consumer laptop PC running Metrohm Autolab's Nova 1.9 as well as GPES 4.9. The VA stand is equipped with a Teflon measuring cell containing a Hg drop multimode electrode (Metrohm); a reference electrode (double-junction, Ag/AgCl, 3 M KCl, Metrohm), an auxiliary electrode (glassy carbon, Metrohm) and a Teflon stirrer. The system was connected to an N_2 line for purging and Hg drop formation pressure. Laminar flow cabinets were used to maintain trace metal clean conditions for sample manipulations (Interflow) and sample preparation (AirClean systems).

TAC was added to a final concentration of 10 µM. The dropsize of the mercury drop on the 663 VA stand was set to 1 (smallest). The samples were purged for 180 seconds. Deposition lasted for 140 seconds at -0.4 V. The sample was left to rest for 5 seconds followed by a differential pulse scan from -0.4 to -0.9 V, step size 0.002 V. In order to adjust for vibrations equipment was first moved to a less affected location (from trockenlabor I to the chemielabor further forward in the ship). Subsequently the scan rate of the measurement protocol was increased to further minimize the effect of vibration to a point where a sufficiently low concentration of the Fe-TAC complex could be discerned. Final scan rate was 39 mV s^{-1}, from an interval of 0.05 s, with a modulation of 0.004 s.

Scan current peaks were manually measured using Nova software. The dissolved Fe concentration, as measured on board by dr. Micha Rijkenberg using Flow Injection Analysis (FIA), is added to the Fe additions and data is parsed into an R script (Micha Rijkenberg) for non-linear regression to the Langmuir isotherm (Gerringa et al., 2014) yielding natural ligand concentrations and binding strengths.

Humic substances

Humic substances were measured from their complexation with iron through cathodic stripping voltammetry (CSV) in the presence of an oxidizer. In this method an oxidizer increases the current signal of the dissociating iron-humic complex at the electrode, making the signal discernible from the system's baseline (Laglera et al., 2007). Samples were buffered by the same borate buffer solution used in CLE-AdSV above and humic substances were saturated with iron by adding 30 nM from a 3 µM acidified dilution of an ISP standard (Fluka). Potassium bromate was used as an oxidizer to enhance the reduction peak of the complexed iron, added in a concentration of 0.013 M. A fulvic acid standard (Suwannee River Fulvic Acid Standard I,

International Humic Substances Society (IHSS), St. Paul, USA) was used to verify and quantify the presence of humic substances by a series standard additions to every sample in a range of 0.1 to 0.4 mg/L. The *in-situ* CDOM fluorometer on the CTD rosette frame (dr. Haardt), casts of which generally preceded UCC casts, was employed to target a sample at the depth of the CDOM maximum. A humic acid standard (Suwannee River Humic Acid Standard II, IHSS) was also used as a calibration reference for this fluorometer by dr. Heather Reader.

Spectrophotometry

Chromophoric dissolved organic matter (CDOM) was analysed spectrophotometrically after Mopper and Schultz (1993). Depths were specifically chosen in parallel to ligand and humic measurements from UCC samples in coordination with dr. Heather Reader's CDOM and DOC sampling from the normal CTD rosette sampler, also taking CDOM fluorescence from the rosette fluorometer into account.

Absorbance spectra were recorded between 200 and 1,000 nm, and fluorescent emission spectra were recorded between 360 and 540 nm at an excitation wavelength of 250 nm. Samples were measured in a quartz cell with a path length of 1cm (Suprasil®, Hellma Analytics) using a SpectraMax M2 mutimode spectrophotometer (Molecular Devices). Daily measurements of a 0.2 mg · L^{-1} quinine sulphate standard dissolved in MQ were made as an equivalent reference for the expression of CDOM fluorescence measurements.

Preliminary results

A start was made with the analysis of data on board, and offered here is the preliminary data for total iron binding ligand concentration (LT) and its ratio to dissolved iron as measured in the ligand sample bottles (dFe.FeL) for the full depth station on the North Pole (station 87, Figs. 6.5.1a and 6.5.1b). High concentrations of dFe and LT are observed, clearly showing the influence of the TPD in the upper 150 m. The ratio of LT over dFe, the amount of excess ligands available for iron to bind to, decreases to <1 at the very surface. This means that an excess Fe over the ligands exists. An excess of Fe over the solubility product (between 0.1 and 0.2 nM) is unlikely as this should precipitate (Millero et al., 1998). The excess iron may also be present in colloidal form, or bound irreversible to unknown complexes. Another possibility is that TAC underestimates the concentration of LT in the presence of humic substances (Laglera et al., 2011). This possibility will be further explored in the home lab using a different AL (Abualhaija and van den Berg, 2014).

CDOM fluorescence measurements (Fig. 6.5.1c) at this station, here preliminarily expressed in arbitrary units (a.u.), also show the same surface increase indicative of the TPD. An unexpected high value for LT is observed at 2,000 m (Fig 6.5.1a). While this can be due to the preliminary character of this data, an increase at this depth is replicated in CDOM fluorescence (Fig. 6.5.1c).

Measurement of humic substances clearly shows a presence of humic substances as a defined peak at and around the CDOM max, whereas deep samples do not (not illustrated). This further solidifies our belief that this station is well within the TPD, where the influence of terrestrial water is greatest.

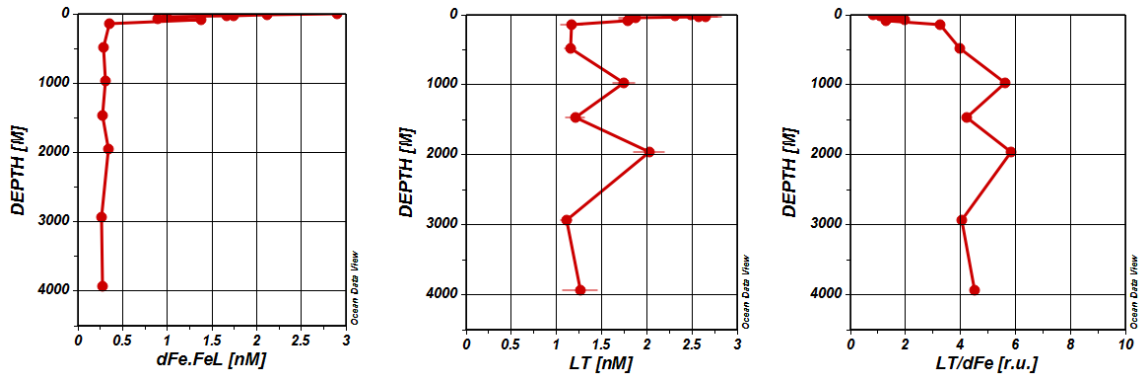

a.

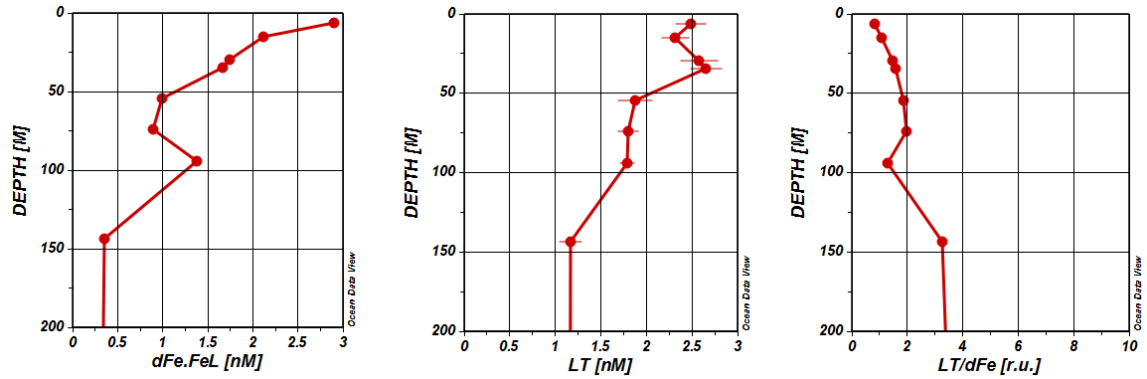

b.

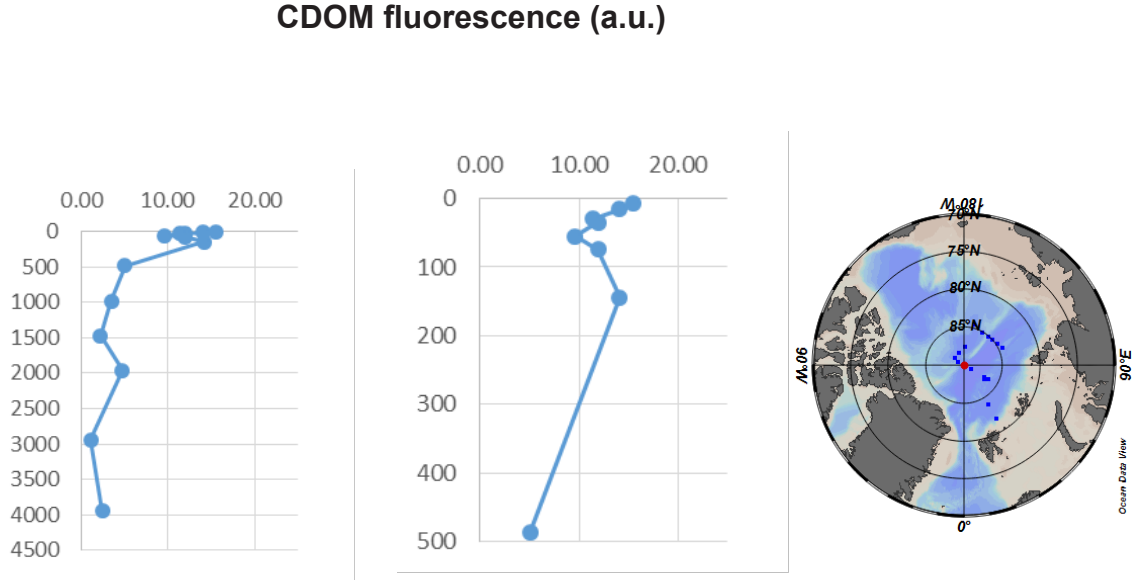

c.

Fig. 6.5.1: Dissolved iron measured from ligand sample bottles (dFe.FeL), total ligand concentration (LT) and the ratio of LT and dFe for the entire depth profile (a) and for the upper 200 m (b). CDOM fluorescence for the entire depth profile and the upper 500 m (c).

Acknowledgements
We are most grateful to Captain Schwarze and the crew of *Polarstern*. We are especially thankful to the firm and gentle leadership of chief scientist Ursula Schauer. We are also indebted to Aridane Gonzalez, Lars-Eric Heimbürger and Michael Staubwasser for their efforts as part of the UCC sampling team, as well as Sven Ober for operation and maintenance of the UCC system.

Data management

See introduction of chapter 6 for details on GEOTRACES data management.

References

Mahmoud M Abualhaija, Constant MG van den Berg (2014) Chemical speciation of iron in seawater using catalytic cathodic stripping voltammetry with ligand competition against salicylaldoxime. Marine Chemistry, 164, 60–74.

De Baar HJW, Buma AGJ, Nolting RF, Cadee GC, Jacques G, Tréguer PJ (1990) On iron limitation of the Southern Ocean: experimental observations in the Weddell and Scotia Seas. Mar. Ecol. Progress Ser., 65, 105-122.

Bauch D, Rutgers van der Loeff M, Andersen N, Torres-Valdes S, Bakker K, and Abrahamsen EP (2011) Origin of freshwater and polynya water in the Arctic Ocean halocline in summer 2007. Progress in Oceanography, 482-495, doi:10.1016/j.pocean.2011.1007.1017.

Brussaard CPD, Wilhelm SW, Thingstad F, Winbauer MG, Bratbak G, Heldal M, Kimmance SA, Middelboe M, Nagasaki K, Paul JH, Schroeder DC, Suttle CA, Vaqué D, Wommack KE (2008) Global-scale processes with a nanoscale drive: the role of marine viruses. The ISME Journal, 0, 1-4, doi: 10.1038/is-mej.2008.31.

Coble PG, Green S, Blough NV, Gagosian RB (1999) Characterization of dissolved organic matter in the Black Sea by fluorescence spectroscopy. Nature 348, 432-435.

Croot PL, Johansson M (2000) Determination of Iron Speciation by Cathodic Stripping Voltammetry in Seawater Using the Competing Ligand 2-(2-Thiazolylazo)-p-cresol (TAC). Electroanalysis, 12 (8), 565-576.

Gledhill M, van den Berg CMG (1994) Determination of complexation of iron (III) with natural organic complexing ligands in seawater using cathodic stripping voltammetry. Marine Chemistry, 47, 41-54.

Gledhill M, Buck KN (2012) The organic complexation of iron in the marine environment: a review. Frontiers in microbiology, 3, 69(1-17).

Gordienko PA, Laktionov AF (1969) Circulation and physics of the Arctic Basin Waters, Annals of the International Geophysical Year. Oceanography, 94-112.

Granskog MA, Stedmon CA, Dodd PA, Amon RMW, Pavlov AK, de Steur L, Hansen E (2012) Chracteristics of colored dissolved organic matter (CDOM) in the Arctic outflow in the Fram Strait: Assessing the changes and fate of terrigenous CDOM in the Arctic Ocean. Journal of Geophysical Research 117, C12021, 1-13, doi: 10.1029/2012JC008075.

Haygood MG, Holt PD, Butler A (1993) Aerobactin production by a planktonic marine *Vibrio* sp.. Limnol, Oceanogr., 38, 1091-1097.

Hassler CS, Schoemann V, Nichols CM, Butler ECV, Boyd PW (2011) Saccharides enhance iron bioavailability to Southern Ocean phytoplankton. PNAS, doi: 10.1073/ pnas.1010963108.

Laglera LM, van den Berg CMG (2009) Evidence for geochemical control of iron by humic substances in seawater, Limnol. Oceanogr., 54, 610-619.

Laglera LM, Battaglia G, van den Berg CMG (2011) Effect of humic substances on the iron speciation in natural waters by CLE/CSV. Marine Chemistry, 127, 134-143.

Liu X, Millero FJ 2002 The solubility of iron in seawater, Marine Chemistry 77, 43-54.

Macrellis HM, Trick CG, Rue EL, Smith G, Bruland KW (2001) Collection and detection of natural iron-binding ligands from seawater. Marine Chemistry, 76, 175-187.

Martin JH, Fitzwater SE, Gordon RM (1990) Iron deficiency limits phytoplankton growth in Antarctic waters. Glob. Biogeochem. Cyc., 4, 5-12.

Mawji E, Gledhill M, Milton JA, Zubkov MV, Thompson A, Wolff GA, Achterberg EP (2011) Production of siderophore type chelates in Atlantic Ocean waters enriched with different carbon and nitrogen sources. Marine Chemistry, 124, 90-99.

McCormack P, Worsfold PJ, Gledhill M (2003) Separation and Detection of siderophores produced by marine bacterioplankton using High-Performance Liquid Chromatography with Electrospray Ionization Mass Spectrometry. Analytical Chemistry, 75, 2647-2652.

Millero FJ (1998) Solubility of Fe(III) in seawater. Earth and Planetary Science Letters, 154, 323-329.

Mopper K, Schultz CA (1993) Fluorescence as a possible tool for studying the nature and water column ditribution of DOC components, Marine Chemistry, 41, 229-238.

Nelson NB, Siegel DA 2012 The Global Distribution and Dynamic of Chromophoric Dissolved Organic Matter. Annu. Rev. Marine. Sci., 2013.5, 447-476.

Poorvin L, Sander SG, Velasquez I, Ibisanmi E, LeCleir GR, Wilhelm SW (2011) A comparison of Fe bioavailability and binding of a cathecholate siderophore with virus-mediated lysates from the marine bacterium Vibrio alginolyticus PWH3a. Journal of Experimental Marine Biology and Ecology, 399, 43-47.

Rudels B (2009) Ocean Current: Arctic Ocean Circulation. Encyclopedia of Ocean Sciences, 2nd ed., 211-225.

Rue EL, Bruland, KW (1995) Complexation of iron(III) by natural organic ligands in the Central North Pacific as determined by a new competitive ligand equilibration / adsorptive cathodic stripping voltammetric method. Marine Chemistry, 50, 117-138.

Rutgers van der Loeff M, Cai P, Stimac I, Bauch D, Hanfland C, Roeske T, Moran SB (2012) Shelf-basin exchange times of Arctic surface waters estimated from $^{228}Th/^{228}Ra$ disequilibrium. Journal of Geophysical Research, 117, C03027, 1-24.

Stedmon CA, Markager S (2001) The optics of chromophoric dissolved organic matter (CDOM) in the Greenland Sea: An algorithm for differentiation between marine and terrestrially derived organic matter. Limnol. Oceanogr, 46, 2087-2093.

Stedmon CA, Markager S (2005) Resolving the variability in dissolved organic matter fluorescence in a temperate estuary and its catchment using PARAFAC analysis. Limnol, Oceanogr., 50, 686-697.

Stedmon CA, Amon RMW, Rinehart AJ, Walker SA (2011) The supply and characteristics of colored dissolved organic matter (CDOM) in the Arctic Ocean: Pan Arctic trends and differences. Marine Chemistry, 124, 108-118.

van den Berg CMG (2006) Chemical Speciation of Iron in Seawater by Cathodic Stripping Voltammetry with Dihydroxynaphthalene. Analytical Chemistry, 78, 156-163.

Velasquez I, Nunn BL, Ibisanmi E, Goodlett DR, Hunter KA, Sander SG (2011) Detection of hydroxamate siderophores in coastal and Sub-Antarctic waters off the South Eastern Coast of New Zealand. Marine Chemistry, 126, 97-107.

6.6 Organic speciation of copper

Aridane G. Gonzales IUEM
G. Sarthou[1] (not on board)
L.G. Anderson[2], H.J.W. de Baar[1] (not on board)

Objective

The community structure of phytoplankton in the open ocean can only be understood with enough information on the distribution and speciation of trace metals (Sunda, 1994, 2012). In the case of copper (Cu), its study in natural waters is essential because it is a required element for the respiratory proteins and oxidases (Baron et al., 1995), but Cu is also toxic according to the free copper concentration and not the total Cu levels (Anderson and Morel, 1978; Sunda and Lewis, 1978).

Cu can be supplied to surface seawater by different pathways such as atmospheric deposition, resuspension material from sediments, diffusion, upwelling and hydrothermal vents. In addition, the exact magnitudes of these sources are not exactly known. In this sense, we have also to consider the anthropogenic sources of Cu to the ocean via aerosol depositions (Jordi et al., 2012) or anti-fouling paint for marine ships (Karlsson et al., 2010). The understanding of Cu chemistry is also relevant because thermodynamically Cu(II) is favored in seawater, where more than 90% is organically complexed with ligands mostly produced biologically (Coale and Bruland, 1988; Croot et al., 2000; Moffett et al., 1990; van den Berg, 1984, 1987). These ligands have been commonly ranked according to their conditional stability constants, as strong ligands (L1) with a conditional stability constant of about 1012.5 and weaker ligands (L2) from 1010-12.5. The concentration of copper ligands in the Arctic can come from the river inputs, both Canadian and Russian. In addition, the Transpolar Drift can transport high level of dissolved organic matter through the Arctic Ocean that is directly affecting to the Cu organic speciation.

In this work, we examine both distribution and speciation of dissolved copper along 6 transects across the Arctic Ocean (North Pole included). This work is conducted in the framework of the GEOTRACES programme (www.geotraces.org).

Work at sea

The samples were always collected in the ultra clean CTD system from NIOZ, filtered over a 0.2 µm filter size using N_2 overpressure. In addition, ice-rafted sediment samples were collected in two different locations, which will be used to measure the concentration of copper ligands. Ice-cores and seawater in the ice-stations were also collect to determine the copper ligand capacity and the diffusion of ligands to the surface seawater from the ice cover.

Expected results

The samples will be analyzed in a clean laboratory facilities in Brest (LEMAR-IUEM). Dissolved Cu concentrations and the dissolved Cu titrations will be carried out by using the voltammetric method of Campos and van den Berg (1994) using the artificial ligand Salicylaldoxime (SA). For each station we collected 12 samples from the water column and several replicates. The data collected during the analysis will be treated by a non-linear optimization of a Langmuir isotherm (Guerringa et al., 1995). Copper speciation will be performed via competitive ligand exchange/cathodic stripping voltammetry (CLE-CSV) measurements in a µAutolab connected to a Metrohm VA 663 voltammeter used in the static mercury drop electrode mode. Each sample is divided in 10 mL aliquots in 25 mL Teflon bottles, buffered with 200 µL of 1 M solution (final concentration 0.01 M) of 4-(2-hydroxyethyl)-1-piperazinepropanesulfonic acid (EPPS). After, Cu is added with a range of different concentrations from 0-90 nM. After one hour SA

is added to a final concentration of 1-2 µM (the detection window will be selected before analysis) and keeping at least 6 h of equilibrium time (Campos and van den Berg, 1994). The method is deposition and initial potential of −0.15 V, deposition time of 60 s, modulation time of 0.01 s, interval time of 0.1 s, final potential of −0.9 V, modulation amplitude of 50 mV, and scan speed of 20 mV/s (Campos and van den Berg, 1994). To determine ligand concentration and conditional stability constant data from Cu titrations, the fraction of Cu present as the Cu(SA)2 complex at each point on the titration curve must be known. Therefore, the system must be calibrated accurately so that [Cu(SA)2] can be calculated from the peak current signal generated by the cathodic scan.

Data management

See introduction of chapter 6 for details on GEOTRACES data management.

References

Anderson DM, Morel FMM (1978) Copper sensitivity of Gonyaulaxtamarensis. Limnol. Oceanogr., 23, 283–295

Baron M, Arellano JB, Gorge JL (1995) Copper and photosystem-II — a controversial relationship. Physiol. Plant., 94 (1), 174–180.

Campos MLAM, van den Berg CMG (1994) Determination of copper complexation in sea water by cathodic stripping voltammetry and ligand competition with salicylaldoxime. Anal. Chim. Acta., 284, 481–496.

Coale KH, Bruland KW (1990) Spatial and temporal variability in copper complexation in the North Pacific. Deep-Sea Res. A Oceanogr. Res. Pap., 37 (2), 317–336.

Croot PL, Moffett JW, Brand L (2000) Production of extracellular Cu complexing ligands by eucaryotic phytoplankton in response to Cu stress. Limnol. Oceanogr., 45, 619–627.

Gerringa LJA, Herman PMJ, Poortvliet TCW (1995) Comparison of the linear van den Berg/Ruzic transformation and a non-linear fit of the Langmuir isotherm applied to Cu speciation data in the estuarine environment. Mar. Chem., 48, 131–142.

Jordi A, Basterretxea G, Tovar-Sánchez A, Alastuey A, Querol X (2012) Copper aerosols inhibit phytoplankton growth in the Mediterranean Sea. Proc. Natl. Acad. Sci., 109 (52), 21246–21249.

Karlsson J, Ytreberg E, Eklund B (2010) Toxicity of anti-fouling paints for use on ships and leisure boats to non-target organisms representing three trophic levels. Environ. Pollut., 158 (3), 681–687.

Moffett JW, Zika RG, Brand LE (1990) Distribution and potential sources and sinks of copper chelators in the Sargasso Sea. Deep-Sea Res., 37, 27–36.

Sunda WG (1994) Trace metal/phytoplankton interactions in the sea. In: Bidoglio, G, Stumm, W (Eds.), Chemistry of Aquatic Systems: Local and Global Perspectives. Kluwer Academic, Dordrecht, pp. 213–247.

Sunda WG, Lewis JAM (1978) Effect of complexation by natural organic ligands on the toxicity of copper to a unicellular alga, *Monochrysislutheri*. Limnol. Oceanogr., 23, 870–876.

Sunda W (2012) Feedback interactions between trace metal nutrients and phytoplankton in the ocean. Front. Microbiol., 3.

van den Berg CMG (1984) Determination of the complexing capacity and conditional stability constants of complexes of Cu(II) with natural organic ligands in seawater by cathodic stripping voltammetry of copper–catechol complex ions. Mar. Chem., 15, 1–18.

van den Berg CMG, Merks AGA, Duursma EK (1987) Organic complexation and its control of dissolved concentrations of copper and zinc in the Scheldt Estuary. Estuar. Coast. Shelf Sci., 24 (6), 785–797.

6.7 Mercury

Lars Eric Heimbürger UB

Objectives

Mercury levels in Arctic biota are among the highest in aquatic ecosystems and impact the health of Arctic wildlife and human populations (AMAP 2011). The idea has taken hold that the Arctic is a global mercury sink and that its main entry route is via the atmosphere (AMAP 2011). A recent three-dimensional GEOS-Chem model run by Fisher et al., (2013) puts both ideas into question and argues that the Arctic Ocean is net source and boreal rivers to be the major input (Sonke and Heimbürger 2012). Their findings shift current paradigms of the Arctic mercury research that has focused for the past 20 years on atmospheric phenomena and cycling (e.g. atmospheric mercury depletion events). It has been shown for the Arctic (Beattie et al., 2014) and for Antarctica (Cossa et al., 2011) that sea ice, in particular brine formation is a major player in polar Hg budgets. Yet, the Arctic Ocean itself remains undersampled. No central Arctic Ocean mercury profiles have been published thus far. This is why the following key questions remain to be answered:

- Is the Arctic Ocean a global sink or a source for mercury?
- What is the cause for the high mercury concentrations in Arctic marine biota: anthropogenic Hg emissions or is that a “normal natural” phenomenon?
- What is the impact of boreal rivers: how much of the dissolved and particulate mercury is transported to the central Arctic Ocean?
- How much of the rapidly deposited mercury during atmospheric mercury depletion events is re-emitted to the atmosphere and which portion of it is bioavailable (bioamplified along the marine food chain)?
- What is the overall impact of warming climate to the Arctic Mercury cycle? Will warming climate shift Hg’s biogeochemical cycle and the functioning of the Arctic ecosystems in a way that we should expect even higher methylmercury levels in marine biota? Our few preliminary results from the 2011 *Polarstern* Arctic cruise show that:
- Methylmercury concentrations in the Arctic Ocean are highest in the marginal sea ice zone and just below the halocline (~200 m-depth)
- Methylmercury concentrations are among the highest observed (together with the Mediterranean Sea (Heimbürger et al., 2010) and the Southern Ocean (Cossa et al., 2011)) in the Global Ocean
- Total mercury concentrations of the Central Arctic Ocean are suggest anthropogenic enrichments (Lamborg et al., 2014)

Work at sea

Seawater

- We sampled for mercury speciation in seawater at the 28 GEOTRACES UCC stations.
- Unfiltered total mercury (tHg) was determined on board on 572 samples (typically 24 depths resolution, with the exception of the shallow stations) following a method that we had developed for the 2011 TransArc cruise, and validated (Heimbürger et al., 2015).

Unfiltered total methylmercury was sampled at all stations (typically 12 depths) following also a method that we had developed for the 2011 TransArc cruise, and validated (Heimbürger et al., 2015). The acidification (HCl double-distilled, 0.4 % v:v) rapidly converted dimethylmercury into monomethylmercury. We will therefore measure total methylmercury as the sum of both. On selected stations we purged off dimethylmercury prior to acidification to determine, later on, monomethylmercury alone. At selected stations we attempted to sample for mercury stable isotopes. At this point we can communicate on the used method.

Zooplankton

The Zooplankton group provided samples from 12 stations. The samples consist in the pooled material from the multinet sampling. All samples were sieved to remove excess water and frozen (-20°C). The samples will be freeze-dried and analyzed via CVAAS for total particulate mercury (USEPA, 2007), and if the quantity allows for particulate total methylmercury as well as mercury stable isotopic signatures.

Sediment

The benthos group provided 12 sediment cores, 9 were subsampled from the large diameter multi-corer barrels into smaller ones (d = 9 cm), and 3 were sliced on board into approximately 5 mm subsamples and stored in individual PE plastic bags. All samples were frozen (-20°C). The samples will be freeze-dried and analyzed via CVAAS for total particulate mercury (USEPA, 2007), and if the quantity allows for particulate total methylmercury as well as mercury stable isotopic signatures.

Suspended particles

Eva-Maria Noethig's group (Imke Peterson, Franz Schröter) sampled for suspended particles via filtration of about 10L seawater from the Niskin bottles from the classic CTD. They provided a total of 44 GFF filters (47 mm) of various depths, mostly within the upper 200 m. The samples will be analyzed via CVAAS for total particulate mercury (USEPA, 2007), and if the quantity allows for particulate total methylmercury.

Viena Puigcorbe sampled for suspended particles via in situ pumps (McLane LV08). She provided a total of 17 QMA filters (142 mm) sampled at 50 and 100 m-depth (see section 5.13). The samples will be analyzed via CVAAS for total particulate mercury (USEPA, 2007). The large filtered volume should allow measuring mercury stable isotope signatures as well.

Sea-ice

The sea ice biogeochemistry group provided ice cores for all ice stations. The cores were sliced on the ice into approximately 10 cm sections, melted on board and transferred into individual sample bottles for later determination of tHg and MeHg.

Expected results

Our results, and those of our Canadian and American counterparts, will largely contribute to the understanding of mercury in the arctic, and we may say that the Arctic Ocean is not undersampled anymore. The shipboard tHg indicate consistent surface enrichments, which is contrary to the global ocean.

Methylmercury in seawater will be measured early 2016.

Data management

See introduction of chapter 6 for details on GEOTRACES data management.

References

Heimbürger LE, Sonke JE, Cossa D, Point D, Lagane C, Laffont L, Galfond BT, Nicolaus M, Rabe B, van der Loeff MR (2015) Shallow methylmercury production in the marginal sea ice zone of the central Arctic Ocean. Sci. Rep. 5.USEPA (2007). Method, 7473.

6.8 Fe Isotopic composition

Michael Staubwasser UNIK

Objectives

The objectives are: 1) To sample depth profiles across the Transpolar drift and the Siberian shelf to analyze the Fe isotope composition of dissolved Fe and particulate Fe and map the Fe isotope distribution in the Arctic Sea. 2) To trace a potential Fe-isotopic signature in the water column from sedimentary diagenetic Fe reflux and/or resuspension from shelf sediments. 3) To study the impact of isotopic exchange between dissolved Fe and particle surface-bound Fe on marine particles in order to clarify to what extend the isotopic composition of dissolved Fe can be considered conservative – which is a requirement for using Fe isotopes as a source tracer.

Work at sea

Seawater samples were filtered (0.22 µm) partly within the routine N_2-pressured sampling procedure used in the NIOZ Clean Container (2 L samples, see section 5.3), partly in a flow cabinet (4L) with a peristaltic pump. On-board measurements of filtered seawater performed by M. J.A. Rijkenberg yielded comparable results for both methods. Seawater samples were acidified (HCl, pH 2) and stored for on-shore mass spectrometry analysis. From the peristaltic pump filtration the filter discs were also stored. Four transects (1a, 2, 4, 6) were sampled during the cruise. Except for Transect 4 the entire water column was sampled at up to 12 depths. Additionally, a small number of samples from under-ice water, and from molten ice cores were taken for complementary analysis. Transect 2 comprises two sites from the Gakkel Ridge, a slow-spreadingvolcanic ridge, where during the cruise two hydrothermal plumes could be identified by there temperature anomalies in the CTD profiles. In addition an isotope exchange experiment was conducted with three 20 L samples of surface layer water from the Transpolar Drift. A ^{58}Fe enriched spike (98 % purity) was added. Samples were filtered (0.22 µm) and ultra-filtered (10 kDa) after 3 days and 3 weeks, respectively. A final set of samples will be filtered on-shore three weeks after the cruise. A large volume sample was also taken from bottom water with resuspended material – according to transmissivity sensor data – on the Barents Sea shelf for a similar experiment to be undertaken on-shore.

Expected results

I expect to find a distinct isotopic signature for at least two of the three largest sources of Fe to the Arctic Seas, i.e. Fe from hydrothermal sources and Fe transported from the Arctic Russian rivers into the Transpolar Drift (Klunder et al., 2012a, 2012b). The third source – resuspension along the continental slope – cannot be addressed due to the withheld permission to sample the Laptev Sea shelf and slope within the Russian economic zone. I expect to detect an isotopic

signature from the Gakkel Ridge plumes comparable to observations on the Atlantic Ocean mid-ocean ridge, where a hydrothermal plume could be identified by its distinct negative $\delta^{56}Fe$ signature compared to deep water in the rest of the ocean (Conway & John, 2014). Fe in the Transpolar Drift derived from Arctic rivers is likely to show a more complex isotopic signature. Given the large concentration in the range of an order of magnitude higher than expected from thermodynamic equilibrium of inorganic species (see section 5.5), the principal source must be colloidal Fe discharged from the rivers. Organically bound colloidal Fe in Artic Rivers has a negative $\delta^{56}Fe$ signature, whereas hydroxide-bound Fe has a positive $\delta^{56}Fe$ signature (Ingri et al. 2006). It is possible that the latter may proportionally increase in abundance if redox cycling occurs on the shelf. In this case, the isotopic signature will likely be altered due to the preferential removal of light isotopes during oxidative precipitation of sedimentary Fe in the water column (Staubwasser et al., 2013). Because open ocean $\delta^{56}Fe$ profiles obtained so far indicate that dissolved Fe has a higher $\delta^{56}Fe$ value than any of the major sources (Conway & John, 2014), it is likely that dissolved and suspended Fe undergo isotopic exchange. The purpose of the Fe-spike enriched exchange experiment is to determine the equilibrium fractionation factor (if applicable) between dissolved, colloidal and particulate Fe.

Data management

See chapter 5 for details on data management.

References

Conway TM, John SG (2014) Quantification of dissolved iron sources to the North Atlantic Ocean. Nature, 511, 212-215.

Ingri J et al. (2006) Iron Isotope Fractionation in River Colloidal Matter. Earth Plan. Sci. Lett., 245 792-798.

Klunder MB et al. (2012a) Dissolved iron in the Arctic shelf seas and surface waters of the central Arctic Ocean: Impact of Arctic river water and ice-melt. J. Geophys. Res., 117, C01027, doi:10.1029/2011JC00713.

Klunder et al. (2012b) Dissolved iron in the Arctic Ocean: Important role of hydrothermal sources, shelf input and scavenging removal. J. Geophys. Res., 117, C04014, doi:10.1029/2011JC007135.

Staubwasser M et al. (2013) Isotope fractionation between dissolved and suspended particulate Fe in the oxic and anoxic water column of the Baltic Sea Biogeosciences, 10, 233–245.

6.9 Cd, Cr, and Pb isotopes

S. Galer (not on board) MPIM

Objectives

A Multi-Trace Metal Isotope Study of the Arctic Ocean - Cycling and isotope fractionation of Cd, Cr and Pb in the Arctic Ocean

Recent studies have documented that the Cd isotopic composition of seawater exhibits mass-dependent isotope fractionation, thought to be due to uptake of Cd by phytoplankton (Ripperger et al., 2007; Abouchami et al., 2011, 2014; Gault-Ringold et al., 2012; Yang et al., 2012; Xue et al., 2013; Conway and John, 2015). Our Cd isotope data from the Southern Ocean, Northwest Atlantic and Southwest Atlantic have shown that Cd isotopic variations in cadmium-depleted surface waters track changes in biological productivity while deeper waters show relatively uniform isotopic compositions, although Cd concentrations increase along the great conveyor (Abouchami et al., 2011, 2014; Xie et al., 2013; Janssen et al., 2014). By contrast, the few Cd isotope data available for the Arctic Ocean show limited isotopic fractionation in the surface layer compared to deeper waters, despite being cadmium depleted (Ripperger et al., 2007).

Our objective is to investigate, in detail, the stable Cd isotope fractionation in the Arctic Ocean by acquiring concentration and isotope data at high resolution along the cruise track and in the water column. Surface waters and several depth profiles at key stations allow us to assess the degree of isotope variability associated with contributions from various sources ─ river runoff, precipitation, evaporation, sea ice and exchanges with the North Pacific and Atlantic Basins ─ to the Arctic Ocean's freshwater budget.

Chromium (Cr), in contrast to Cd, is a redox sensitive element - with two oxidation states Cr(VI) and Cr(III) - whose isotopic fractionation has up until now mainly been used to trace the oxygenation levels of the past oceans (Frei et al., 2009). In oxic seawater, Cr(VI) is highly soluble while Cr(III) is particle reactive and forms insoluble (oxy-)hydroxide compounds. Chromium concentration data are abundant and are at nanomolar levels in seawater (1-7 nM), but Cr isotope data are restricted to a single profile (5 samples) in the Argentine Basin and show isotopically "heavier" chromium than average continental crust (Bonnand et al., 2013). Our aim is to obtain the first measurements of the Cr isotopic composition of Arctic seawater and establish a mass balance of the Cr budget for sources to the Arctic Ocean.

Lead isotope measurements will be performed to document the distribution and cycling of Pb in the water column, identify anthropogenic (shallow) and natural (deep) sources of Pb in the Arctic Ocean Basin, and assess ventilation rates and mixing in the surface gyres. Important goals are to investigate the extent of downward penetration of anthropogenic lead in the thermocline, particle reactive behaviour in the shelf regions, and evaluate the influence of hydrothermal lead inputs in the deeper Arctic Ocean near to the Gakkel Ridge.

Work at sea

Five full vertical profiles were taken, distributed along the cruise track, at Stations 4, 50, 81 and 101, covering most of the Arctic Basin, and Station 161 on the continental shelf between Norway and Spitzbergen. In addition, a surface transect was sampled between Stations 117-134 in the eastern Artic sector. Each profile consists of 8 to 11 depths, collected on board using the Ultraclean Titan frame (de Baar et al., 2008) by our NIOZ colleagues. Seawater volumes varied between 20 L for surface waters, 4 L for intermediate depth and 1 L for deep waters. The

samples were filtered into double-bagged, polyethylene bottles and canisters (acid cleaned in Mainz prior to the cruise) and acidified to pH of 2 using ultra-clean Seastar HCl (low level Cd blank). The returned samples will be analysed in the clean-room laboratories of the Max Planck Institute for Chemistry in Mainz (Germany) by thermal ionization mass spectrometry (TIMS) using proven double-spike technology already established for Pb, Cd and Cr isotopes.

Expected results

The isotope and concentration data, combined with historical data, may shed light on the effect of the increase of the Arctic Ocean's freshwater content over the past few decades, predominantly in the west, on the trace metal budget of the Arctic Ocean.

Data management

See introduction of chapter 6 for details on GEOTRACES data management.

References

Abouchami W, Galer SJG., de Baar HJW, Alderkamp AC, Middag R, Laan P, Feldmann H, Andreae MO (2011) Modulation of the Southern Ocean cadmium isotope signature by ocean circulation and primary productivity. Earth Planet. Sci. Lett., 305, 83-91.

Abouchami W, Galer SJG, de Baar HJW, Middag R, Vance D, Zhao Y, Klunder M, Mezger K, Feldmann H, Andreae MO (2014) Biogeochemical cycling of cadmium isotopes in the Southern Ocean along the Zero Meridian. Geochim. Cosmochim. Acta, 127, 348–367.

Bonnand et al. (2013) The chromium isotopic composition of seawater and marine carbonates. Earth Planet. Sci. Lett. 382, 10-20.

Conway TM ,John SG (2015) Biogeochemical cycling of cadmium isotopes along a high-resolution section through the North Atlantic Ocean. Geochim. Cosmochim. Acta, 148, 269-283.

De Baar HJ et al. (2008) Titan: A new facility for ultraclean sampling of trace elements and isotopes in the deep oceans in the international Geotraces program. Mar. Chem., 11, 4-21.

Frei R, Gaucher C, Poulton SW, Canfield DE (2009) Fluctuations in Precambrian atmospheric oxygenation recorded by chromium isotopes. Nature, 461, 250–253.

Galer SJG, Abouchami W, Xie RC, Janssen DJ, Rickenberg M, Gerringa L, Cullen JT, de Baar HJW (2014) Global oceanic cadmium isotope distribution. Goldschmidt Conference, Sacramento.

Gault-Ringold M, Adu T, Stirling CH, Frew RD, Hunter KA (2012) Anomalous biogeochemical behavior of cadmium in subantarctic surface waters: mechanistic constraints from cadmium isotopes. Earth Planet. Sci. Lett., 341–344, 94–103.

Janssen DJ et al. (2014) Undocumented water column sink for cadmium in open ocean oxygen-deficient zones. Proceedings of the National Academy of Sciences, 11, 6888-6893.

Janssen DJ, Cullen JT, Abouchami W, Galer SJG, de Baar HJW (2014) Cadmium Isotopes along the Line-P transect in the Northeast Subarctic Pacific. Goldschmidt Conference, Sacramento.

Ripperger S, Rehkämper M, Porcelli D, Halliday AN (2007) Cadmium isotope fractionation in seawater – a signature of biological activity. Earth Planet. Sci. Lett., 261, 670–684.

Xue Z, Rehkämper M, Horner TJ, Abouchami W, Middag R, van de Flierdt T, de Baar HJW (2013) Cadmium isotope fractionation in the Southern Ocean. Earth Planet. Sci. Lett., 382, 161–172.

Xie RC, Galer SJG, Abouchami W, Rijkenberg M, de Jong J (2014) Cadmium isotope distribution along the western boundary of the South Atlantic. Ocean Sciences Meeting, Honolulu.

Yang SC, Lee DC, Ho TY (2012) The isotopic composition of cadmium in the water column of the South China Sea. Geochim. Cosmochim. Acta, 98, 66–77.

6.10 Particulate trace metals

Aridane G. Gonzalez IUEM
H. Planquette (not on board)

Objective

The main sources of particulate trace metal to the ocean are the atmospheric deposition (Jickells et al., 2005; Sarthou et al., 2003; Mahowald et al., 2009), rivers (Lam etal., 2006; 2012), hydrothermal (Tagliabue et al., 2010), sediments (Kalnejais et al., 2007), ice and sea-ice (Raiswell et al., 2008).

The distribution of particulate trace metals in the Arctic Ocean will help to understand the sources and the scavenging process (Venchiarutti and Rutgers Van Der Loeff, 2011), the mixing process in the deep ocean (Charette et al., 2007) and the transport from the shelf (Lacan et al., 2012). On the other hand, chemical speciation of particulate trace metals will help to understand the bioavailability of these particles to the phytoplankton community.

The goal in this cruise is to study the vertical and spatial distribution of particulate trace metals along the Arctic Ocean, quantify the lateral transport of particulate trace metals from the Russian rivers by the Transpolar Drift. The Artic Ocean is one of the most sensible oceans to the thermohaline circulation and physico-chemical properties.In this work, we will examine both vertical and spatial distribution of particulate trace metals along 6 transects across the Arctic Ocean (North Pole included). This work is conducted in the GEOTRACES programme (www.geotraces.org) during the expedition PS94 on the German icebreaker *Polarstern* began 17th August (Tromso) to 15th October 2015 (Bremenhaven).

Work at sea

Particulate trace metal were collected in the ultra clean CTD system from NIOZ, filtered over a 0.45 µm filter size using N_2 overpressure until an optimal volume between 6-10 L during at least 5 hours.

On the other hand, ice-cores and surface seawater in the ice-stations were collected to determine the concentration of particulate trace metals. In addition, ice-rafted sediment samples were collected in two different locations, which will be used to measure the concentration of metals both in particles (sediments) and solution (after filtering).

Expected results

These samples will be analyzedin a clean laboratory facilities in Brest (LEMAR-IUEM). The concentration of metals will be carried out by using an Elemental Scientific Sector-Field Inductively Coupled Plasma Mass Spectrometry (SF-ICP-MS) with a detection limit of: Al = 0.496 nM; P = 2.55 nM; Mn= 0.014 nM; Fe = 0.063 nM; Co = 0.003 nM; Cu = 0.089 nM; Zn = 0.051 nM, Cd = 0.002 nM and Ba = 0.006 nM; Planquette and Sherrell, 2012).

Data management

See introduction of chapter 6 for details on GEOTRACES data management.

References

Charette MA, Gonneea ME, Morris P, Statham PJ, Fones GR, Planquette H, Salter I, NaveiraGarabato, A (2007) Radium isotopes as tracers of iron sources fueling a Southern Ocean phytoplankton bloom. Deep-Sea Research II, 54, 1989-1998.

Jickells T et al. (2005) Global Iron Connections Between Desert Dust, Ocean Biogeochemistry, and Climate. Science, 308, 67-71.

Kalnejais LH, Martin WR, Signall RP, Bothner MH (2007) Role of sediment resuspension in the remobilisation of particulate-phase metals from coastal sediment. Environmental Science Technology ,41, 2282–2288.

Lacan F, Tachikawa K, Jeandel C (2012) Neodymium isotopic composition of the oceans: a compilation of seawater data. Chemical Geology, 300-301, 177-184, 10.1016/j.chemgeo.2012.01.019.

Lam PJ, Ohnemus DC and Marcus MA (2012) The speciation of marine particulate iron adjacent to active and passive continental margins. Geochimica et Cosmochimica Acta, 80, 108-124.

Lam PJ, Bishop JKB, Henning CC, Marcus MA, Waychunas GA, Fung IY (2006) Wintertime phytoplankton bloom in the subarctic Pacific supported by continental margin iron. Global Biogeochemical Cycles 20(1), GB1006.

Mahowald N et al. (2009) Atmospheric Iron deposition: Global distribution, variability and human perturbations. Annual Reviews of Marine Sciences, 1, 245-278.

Planquette H, and Sherrell RM (2012) Sampling suspended particles from rosette-mounted bottles for determination of trace elements: methodology and comparison with in situ pumping. Limnology and Oceanography: Methods, 10, 367-388.

Raiswell R, Benning LG, Tranter M and Tulaczyk S (2008) Bioavailable iron in the Southern Ocean: the significance of the iceberg conveyor belt. Geochemical Transactions, 9, 7.

Sarthou G, Baker AR, Kramer J, Laan P, Laës A, Ussher S, Achterberg EP, de Baar HJW, Timmermans KR, Blain S (2003) Influence of atmospheric inputs on the iron distribution in the subtropical North-East Atlantic Ocean. Marine Chemistry, 104,186-202.

Tagliabue A, Bopp L, Dutay JC, Bowie AR, Chever F, Jean-Baptiste P, Bucciarelli E, Lannuzel D, Remenyi T, Sarthou G, Aumont A, Gehlen M, Jeandel C (2010) Hydrothermal contribution to the oceanic dissolved iron inventory. Nature Geoscience, 3, 252-256.

Venchiarutti C, and Rutgers van der Loeff M (2011) Scavenging of ^{231}Pa and thorium isotopes based on dissolved and size-fractionated particulate distributions at Drake Passage (ANTXXIV-3). Deep-Sea Research II, 58, 2767-2784.

6.11 Ice-rafted sediments

Aridane G. Gonzalez[1], Lars-Eric Heimbürger[2], Sandra Gdaniec[3], Ronja Paffrath[4], Heather E. Reader[5]

[1]IUEM,
[2]UB/MIO,
[3]SMNH,
[4]ICBM,
[5]DTU

Objective

The Arctic Ocean presents exceptional conditions to study and characterize the continental inputs and extended shelf. The entrainment of shelf sediments into sea ice during its formation on the Siberian shelf is a unique mechanism for the transport of terrigenous and shelf sourced material to the deep basins. The goal of the sampling effort was to collect samples to measure a variety of parameters summarised in the table below to characterize the flux and reactivity of elements from the shelf to the basins, and better understand the importance of this transport mechanism.

Work at sea

The ice-rafted sediment group took samples in two different locations with a plastic beaker from the deck. The samples were stored in plastic bags at -20°C.

Expected results

These samples will be treated and melted in the clean laboratory facilities of LEMAR (Brest) in order to satisfy the necessity of each scientist. The different parameters targeted by the ice-rafted sediment team are summarized in the table below.

Scientist	Parameter
Aridane G. Gonzalez (IUEM)	Particulate trace metals and Organic Speciation of Copper
Micha Rijkenberg (NIOZ)	Dissolved trace metals
Heather E. Reader (DTU)	Organic Matter Characterization and Dissolved Organic Carbon
Loes Guerringa and Hans Slagter (NIOZ)	Fe binding Organic Ligands and Dissolved Humic Substances
Michael Staubwasser (University of Koeln)	Reactive Fe species and Fe isotopes
Lars-Eric Hamburger (MIO)	Mercury
Sandra Gdaniec and Per Andersson (SMNH)	Pa/Th
RonjaPaffrath and Katharina Pahnke (ICBM)	Nd and Sr isotopes, Rare Earth Elements
*Walter Geibertand Gesine Mollenhauer (AWI)	232Th and 14C
*RonjaPaffrath and Claudia Ehlert (ICBM)	Si isotopes

*These parameters will be analyzed in the case we have enough sample volume.

6.12 Neodymium isotopes, rare earth element concentrations and long-lived natural radionuclides

Michiel Rutgers van der Loeff[1], Ole Valk[1], Ronja Paffrath[2], Sandra Gdaniec[3]
M. Roy-Barman[4], K. Pahnke[2], P. Andersson [3] (not on board)

[1]AWI,
[2]ICBM,
[3]SMNH,
[4]LSCE

Objectives

The unique conditions in the Arctic of input, removal, and exchange processes in relation to particle composition, particle fluxes, and circulation are acting on trace element and isotope distributions in the Arctic Ocean. These distributions are sensitive to the environmental changes already taking place in the Arctic. We propose that the processes in this region can be ideally addressed by a combined study of Nd isotopes ($^{143}Nd/^{144}Nd$, εNd), rare earth elements (REE), Th isotopes and ^{231}Pa, and that the results will add important insights into trace element and isotope biogeochemistry in the Arctic. Moreover, the simultaneous analysis of the other GEOTRACES key parameters on the same cruise and on all cruises of our international partners (US, Canada) will provide a solid basis for the evaluation and modelling of biogeochemical processes in the Arctic.

Our study will test the following overriding hypothesis: The exceptional conditions in the Arctic Ocean of high continental inputs and extended shelf areas, contrasting with low particle fluxes and low opal production in the deep basins uniquely affect the distribution and budgets of εNd, REE, Th isotopes, and ^{231}Pa. A detailed study of these tracers will help to understand their behaviour in the Arctic Ocean, with relevance for the processes controlling these and other trace element and isotope distributions globally.

Specific objectives of the proposed work to test this hypothesis include:

- Investigation of the effect of particles on the distribution of εNd, REEs, Th isotopes, and ^{231}Pa (and by extension, on other TEIs) in the water column with a particular focus on particle composition (opal-rich vs. opal-poor), particle fluxes, and terrigenous input.
- Investigation of exchange processes at the margins with exceptionally large shelf areas (εNd for margin-seawater exchange, Th and Pa isotopes for boundary scavenging) and provenance of particles supplied to the Arctic by rivers and ice.
- Determination of whether changes in the circulation of the Beaufort Gyre have led to further changes in the distribution of dissolved ^{230}Th, ^{231}Pa, REE, and Nd isotopes in comparison to the situation in 1991-2001.
- Investigation of the REE and Nd isotopic composition of the contributions of Siberian rivers and Pacific water to the Arctic.
- Determination of the influence of hydrothermal activity at Gakkel Ridge on seawater

In more detail, we want to exploit the unique boundary conditions in the Arctic and their strong contrast to those in other ocean basins, particularly those in the Southern Ocean, to improve our understanding of biogeochemical processes in the ocean in general and the Arctic in particular and to develop a common interpretation of these tracers. We particularly hope to see to what extent the large continental inputs in the Arctic (river, shelf, dirty ice) affect εNd and REE in the water column and how the low opal content in the Arctic compared to the large range in opal concentrations in the Southern Ocean influences the vertical REE distribution and contributes to a less efficient separation between ^{231}Pa and ^{230}Th in the Arctic. Terrigenous

particles are transported to the central Arctic both in suspension in river water and ice rafted in “dirty ice”. The combined analysis of Nd and Sr isotopes ($^{87}Sr/^{86}Sr$) on terrigenous river and dirty ice particles will provide insight into the provenance of particles as well as particle-seawater interactions and lateral transport of particles. In turn, this will afford insight into the potential impact of future changes on these distributions. We will further investigate the relative contributions of Pacific and Atlantic waters in the Arctic using their distinct εNd signatures, and investigate whether the recently reported circulation changes and freshwater input to the Arctic over the past decade (Karcher et al., 2012) have also impacted the trace element and isotope distributions in the Arctic since the first studies were carried out (samples collected in 2000-2001: ^{230}Th, ^{231}Pa by Bacon et al. (1989), Scholten et al. (1995), Edmonds et al. (2004), and ourselves (unpublished results), obtained n the years 1983, 1991, 1994, 2007: εNd and REE from (Andersson et al., 2008; Porcelli et al., 2009; Zimmermann et al., 2009).

The study of REE, Nd and Th isotopes and ^{231}Pa in the water column and particles in the Arctic (this cruise, and US and Canadian cruises) will provide a baseline of their distributions for the evaluation of expected future changes in this rapidly changing environment.

Work at sea

Water samples were taken at 20 stations (up to 16 depths per station) for dissolved Th and Pa isotopes and 21 stations for dissolved REE and Nd isotopes (Fig. 6.12.1). The water samples were filtered directly from the Niskin bottles (Fig. 6.12.2) using Acropak500 cartridges (0.8/0.45µm pore size, Supor® pleated membrane). Five to 20 L were sampled for determination of dissolved trace element isotopes (Th, Pa, Nd) and 100 ml of seawater was sampled for REE concentrations. All samples were acidified to pH ~2 using concentrated ultra clean hydrochloric or nitric acid (1ml acid per 1 liter of seawater). Samples for Nd isotopes were acidified to pH ~3.5 and REEs were pre-concentrated onboard using C18 cartridges (Waters Inc.) filled with a complexing agent.

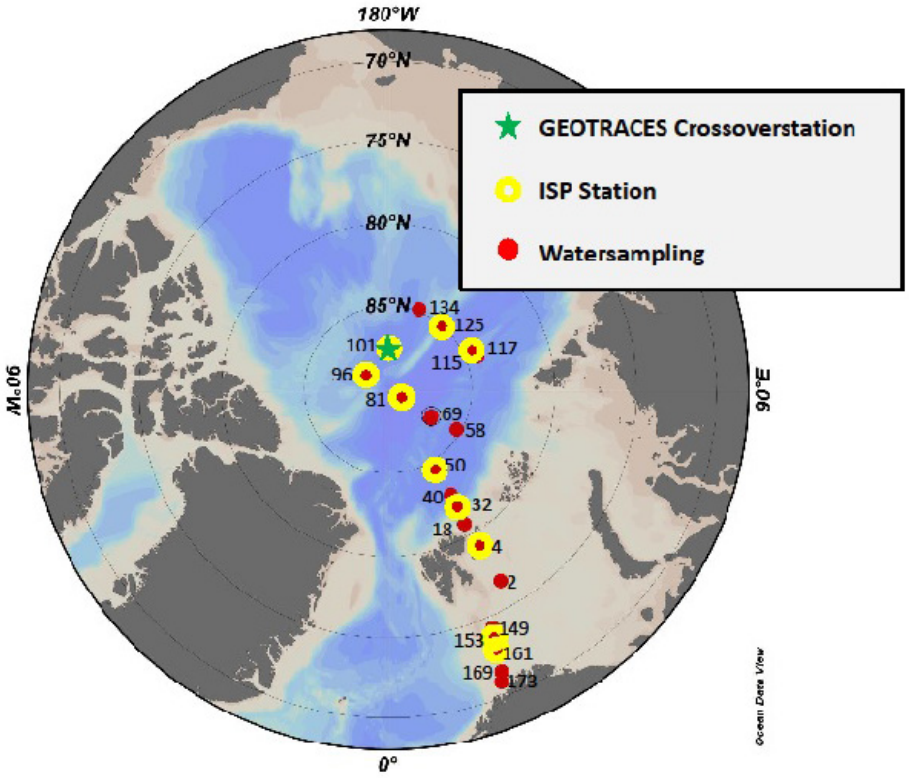

Fig. 6.12.1:Station map

Fig. 6.12.2: Sampling of seawater for REE, Si and Th, Pa, Nd isotopes

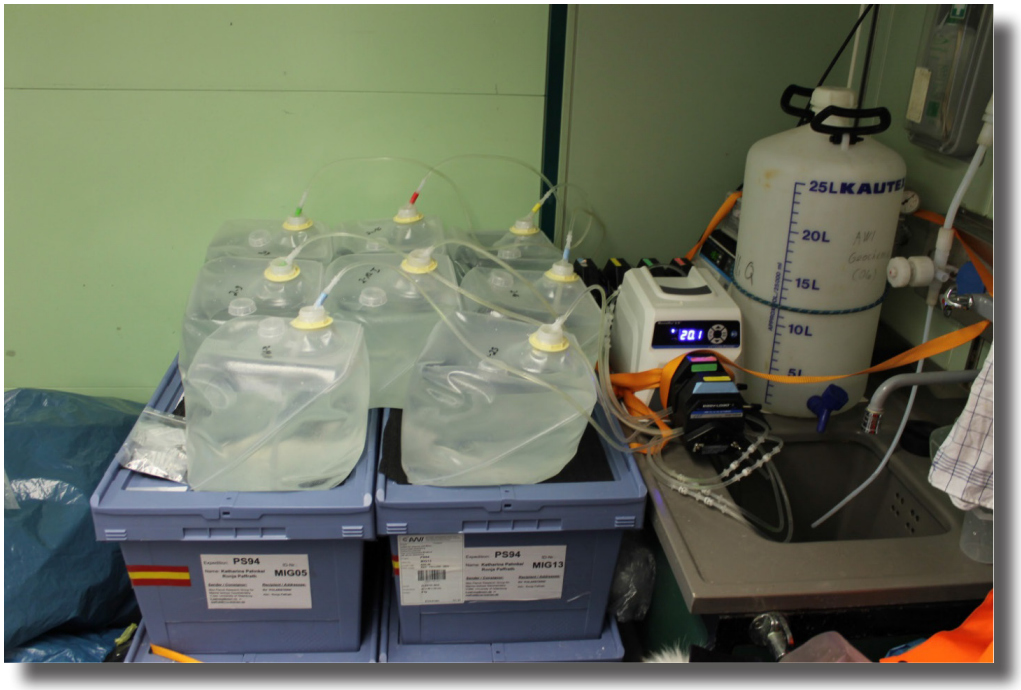

Fig. 6.12.3: Preconcentration of Nd isotopes using C18 cartridges

The study of Pa and Th is shared between the Bremerhaven (AWI) and Stockholm (SMNH) labs, with AWI concentrating on the deep basins and SMNH on the exchange with the shelves. Water samples for Pa and Th were divided accordingly between Ole Valk and Sandra Gdaniec. Three intercalibration stations in the central Arctic were sampled, where both water and particles were collected for Ole Valk and Sandra Gdaniec. One of these stations was the "crossover station" where our American colleagues sampled water and particles for REE, Nd isotopes and Pa/Th as well. The results from these intercalibration samples will be submitted to the GEOTRACES Standards and Intercalibration Committee for evaluation and approval.

Suspended particles were sampled at 10 stations at up to 12 depths per station using *in-situ* pumps (Mc-Lane and Challenger). The filters (Supor®-0.8µm) were pre-cleaned with 1N HCl and 18 Ω MQ water. Sampled filters were cut onboard (Fig. 6.12.3) under a laminar flow hood with HEPA filter and stored in plastic sample bags. ^{230}Th, ^{232}Th, ^{231}Pa, REE, trace and major elements, and biogenic Si, will be analyzed at our home labs. ^{234}Th was analyzed onboard by beta counting (see section 6.13).

Fig. 6.12.4: Dirty ice seen from the working deck

Twice the ship stopped when abundant "dirty ice" was observed from the bridge. Five to seven liters of dirty ice were collected at these 2 stations using plastic tools. These samples are shared among a larger group (see section 6.11) in order to analyse a range of parameters on a homogenized sample. The dirty ice will be melted under clean conditions and the particles will be collected by filtration over the same filter type used for suspended particles. Surface sediments (1-2 g dry weight) were collected using either MUC or box corer at 10 stations for Nd isotopes, ^{231}Pa/^{230}Th and REE analyses on the lithogenic and authigenic phases.

Expected results

The results will provide an unprecedented spatial and vertical resolution of dissolved and particulate REE concentrations, Nd and Th isotopes, and ^{231}Pa distributions in the Central

Arctic. The results are expected to provide insight into the terrigenous sources to the Arctic, their impact on the dissolved trace element and isotope distributions, and the influence of rivers and Pacific and Atlantic waters on these distributions. Additionally, we expect to be able to evaluate the results with respect to data collected on previous expeditions (1991-2001). Ice conditions did not allow us to proceed as far south into the Alpha Ridge/Canada Basin as in 2007 or 2011. It is therefore questionable whether we can confirm the trend of decreasing ^{230}Th activities observed 2007.

Data management

Data from a crossover station with the US cruise and other intercalibration results from duplicate sampling will be submitted to the GEOTRACES Standards and Intercalibration Committee for evaluation and approval. All data and metadata will be submitted to the international GEOTRACES data management office (GDAC at BODC, www.bodc.ac.uk/geotraces) under the data management scheme agreed upon in the GEOTRACES programme available at http://www.geotraces.org. Most data and metadata will also be submitted to the PANGAEA database.

References

Andersson PS, Porcelli D, Frank M, Björk G, Dahlqvist R, Gustafsson Ö (2008) Neodymiumisotopes in seawater from the Barents Sea and Fram Strait Arctic-Atlantic gateways. Geochim. Cosmochim. Acta, 72, 2854-2867.

Bacon MP, Huh CA, Moore RM (1989) Vertical profiles of some natural radionuclides over the Alpha Ridge, Arctic Ocean. Earth Planet. Sci Lett., 95, 15-22.

Edmonds HN, Moran SB, Cheng H, Edwards RL (2004) ^{230}Th and ^{231}Pa in the Arctic Ocean: implications for particle fluxes and basin-scale Th/Pa fractionation. Earth Planet. Sci Lett., 227,155-167.

Henderson GM, Anderson RF et al. (2007) GEOTRACES - An international study of the global marine biogeochemical cycles of trace elements and their isotopes. Chem. Erde-Geochem., 67: 85-131.

Karcher M, Smith JN, Kauker F, Gerdes R, Smethie WM (2012) Recent changes in Arctic Ocean circulation revealed by iodine-129 observations and modeling. J. Geophys. Res., 117, C08007.

Porcelli D, Andersson PS, Baskaran M, Frank M, Björk G, Semiletov I (2009) The distribution of neodymium isotopes in Arctic Ocean basins. Geochim. Cosmochim. Acta, 73, 2645-2659.

Scholten JC, Rutgers van der Loeff M, 1995 Distribution of ^{230}Th and ^{231}Pa in the water column in relation to the ventilation of the deep Arctic basins. Deep Sea Res, II 42, 1519-1531.

Zimmermann B, Porcelli D, Frank M, Andersson PS, Baskaran M, Lee D, Halliday AN (2009) Hafnium isotopes in Arctic Ocean water. Geochim. Cosmochim. Acta, 73, 3118-3233.

6.13 Natural radionuclides – short lived

Viena Puigcorbé[1], Nnuria Casacuberta[2], Michiel Rutgers van der Loeff[3]
P. Masqué[1] (not on board)

[1]UAB,
[2]LIP,
[3]AWI

Objectives

^{234}Th and ^{210}Po as tracers of export production of POC

Part of the carbon dioxide fixed in photosynthesis is transferred to the interior of the ocean, mainly by gravitational settling of particulate organic carbon (POC). Quantifying this export is essential for determining the efficiency of the biological carbon pump, which is a key component of the marine and global carbon cycle. Besides carbon, the vertical drawdown of particles connects the ocean surface with the deep waters, affecting the distribution of nutrients and biominerals and it represents an important food source for pelagic but also for benthic organisms (Smith et al., 2008), making the study of the particle cycling of broad interest for a variety of research fields.

The natural pairs of radionuclides ^{234}Th/^{238}U and ^{210}Po/^{210}Pb have been frequently used to provide information on particle export and export production (Benitez-Nelson and Moore, 2006; Buesseler et al., 1992; Verdeny et al., 2009). In a closed system, a radioactive isotope should be in secular equilibrium with its progeny. In the oceanic water column, a deficit of the decay product with respect to the concentration of the parent is found when its particle affinity is larger, due to removal by uptake by particles. Disequilibria among the activities of these tracer pairs indicate exportation to deeper waters, and it can be used to derive the flux of particles that are removed from the surface layer on time scales of weeks (half life of ^{234}Th = 24 days) to months (half life of ^{210}Po = 138 days), becoming a powerful tool for tracing export events occurring on similar time scales such as phytoplankton blooms.

Our objective is to quantify the POC export flux by measuring the depletion of these radionuclides with respect to their parents in the upper water column. Differences in ice coverage conditions at the sampled stations will be examined in order to better assess the influence of ice thickness and the timing of the ice melting on particle export. In order to convert the radionuclide fluxes to a POC export fluxes, POC/^{234}Th and POC/^{210}Po ratios will be determined in sinking particles (e.g. Buesseler et al., 2006).

Work at sea

Water samples

Total ^{234}Th was measured at 14 stations (Fig. 1) from 4 L of seawater collected at 12-21 discrete depths over the upper 400-500 m. Samples were treated following the MnO_2 co-precipitation method (Benitez-Nelson et al., 2001; Pike et al., 2005) and counted onboard using a gas flow proportional low-level RISO beta counter (counting statistics <5 %). Uranium-238 activity, due to its conservative behaviour in seawater, is typically derived from salinity (Owens et al., 2011). However, additional seawater samples were collected to analyze ^{236}U (see section 6.15) from which ^{238}U concentrations are obtained as a byproduct, allowing us to confirm the U-salinity relationship.

Lead-210 and ^{210}Po samples were collected in 10 L cubitainers at 4 stations (Fig.6.13.1). Samples will be processed according to the Co-APDC chelate co-precipitation technique, adapted from Boyle and Edmond (1975). During the cruise only the precipitation and filtration steps were carried out. The rest of the radiochemical procedure will be done at the home laboratory, as well as the measurements by alpha spectrometry (Rigaud et al., 2013).

Particulate samples

Size-fractionation of particulate samples (large (>53 µm) and small (1-53 µm)) for analyses of ^{234}Th, ^{210}Po, ^{210}Pb, POC and PON were collected by sequential filtration using *in-situ* filtration pumps (ISP) at 10 stations (Fig. 6.13.11). Two pumps were deployed at 50 and 100 m at 10 stations (see section 5.12). Pumps filtered on average 400 L during 2.5 h. Large particles were retained using a 53 µm mesh screen and removed from the screen by rinsing it with 0.2 µm filtered seawater. Small particles were collected on a pre-combusted QMA filter. Three subsamples of 25 mm in diameter were taken to measure ^{234}Th, ^{210}Po, ^{210}Pb, POC and PON. Six additional subsamples (12 mm diameter) will be used to analyze multiple trace metals (see section 6.3 and 6.10) and the rest of the filter will be dedicated to the analysis of mercury (Hg) and Hg isotopes (see section 6.7).

Additionally, 6-10 L water samples were collected from the CTD-rosette at each station where ^{234}Th profiles were sampled (Fig. 6.13.1). Samples were collected over the upper 300 m at 6-9 depths and filtered through pre-combusted QMA filter to obtain additional POC/^{234}Th data, which will also be compared to the results obtained from the *in-situ* filtration pumps.

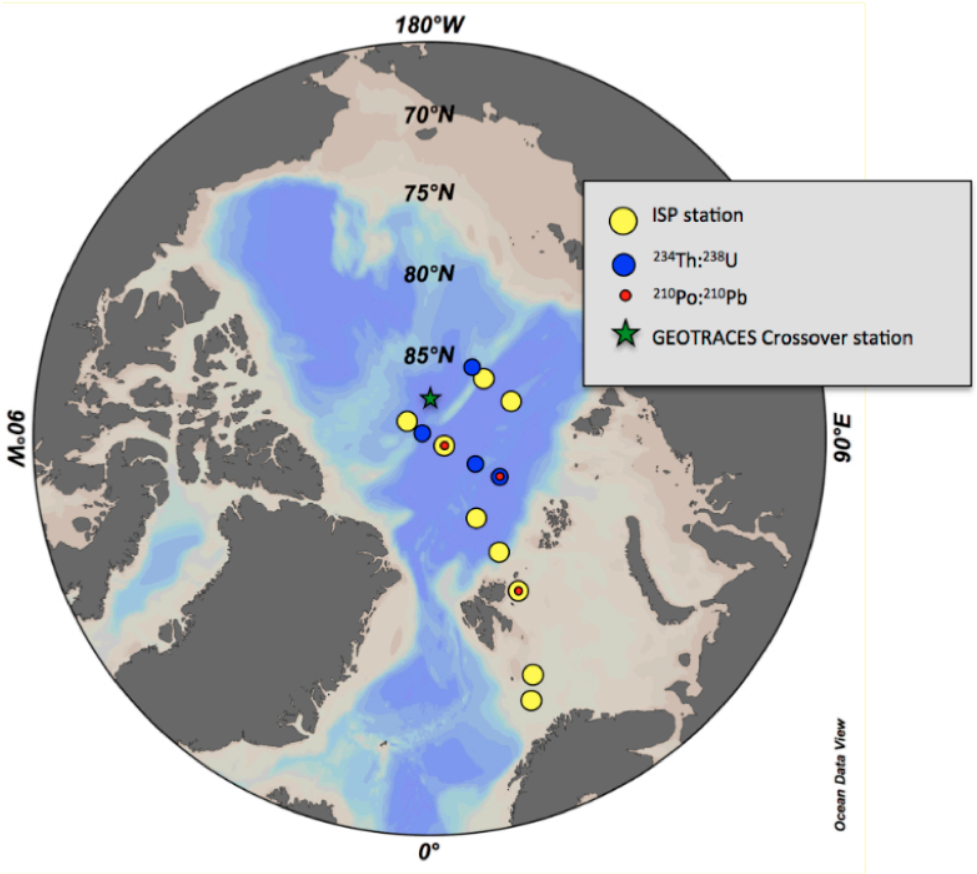

Fig. 6.13.1: Station location for the different parameters analyzed. ISP station correspond to stations where ^{234}Th:^{238}U profiles where obtained, together with particulate samples collected using ISP. At GEOTRACES crossover station (green star) all the parameters were sampled.

Particulate ^{234}Th activities were also measured on a 25 mm ø subsample of the 142 mm Supor® filters dedicated to the analysis of particulate ^{230}Th/^{231}Pa, Nd isotopes, Rare Earth Elements (REE), together with trace and major elements and biogenic Si (see Chapter 6.12).

Samples were collected at 10 stations (4, 32, 50, 81, 96, 101, 117, 125, 153 and 161) along the entire water column using ISP. The 25 mm subsamples of the main filters were dried at 50 ºC overnight and counted on board.

Preliminary results

Results obtained from these samples are expected to provide insights into particle export in the central Arctic. This area is known to have low export production (Cai et al., 2010; Lalande et al., 2014) but the increasing and accelerating melt of the sea ice cover might alter the phytoplankton community and increase primary productivity (Arrigo et al., 2008; Frey et al., 2014), therefore affecting POC export and other elements' biogeochemical budgets (Boetius et al., 2013).

In general, low and shallow ^{234}Th deficits were measured from seawater samples; therefore we expect to obtain low export fluxes, in agreement with previous studies carried out in the Central Arctic Ocean. However, differences can be observed between stations, with marked decreases in ^{234}Th activities at stations near the shelf and those that might be influenced by the Transpolar Drift. We will investigate the causes of those differences considering factors such as primary productivity, ice coverage, water masses, etc., in order to better describe the particle fluxes in this region.

Preliminary particulate ^{234}Th concentrations measured in the Supor® filters along the entire water column are presented in Fig. 6.13.2, where higher concentrations can be seen at the shelf and near the bottom of the slope, as well as in the surface waters that might be affected by the Transpolar Drift.

Data management

See introduction of chapter 6 for details on GEOTRACES data management.

References

Arrigo KR, van Dijken G, Pabi S (2008) Impact of a shrinking Arctic ice cover on marine primary production. Geophys. Res. Lett., 35, L19603.

Benitez-Nelson C, Buesseler KO, Rutgers van der Loeff M, Andrews J, Ball L, Crossin G, Charette MA (2001) Testing a new small-volume technique for determining ^{234}Th in seawater. J. Radioanal. Nucl. Chem., 248, 795–799.

Benitez-Nelson CR, Moore WS (2006) Future applications of ^{234}Th in aquatic ecosystems. Mar. Chem., 100, 163–165.

Boetius A, Albrecht S, Bakker K, Bienhold C, Felden J, Fernández-Méndez M, Hendricks S, Katlein C, Lalande C, Krumpen F (2013) Export of algal biomass from the melting Arctic sea ice. Science, 339, 1430–1432.

Boyle EA, Edmond JM (1975) Determination of trace metals in aqueous solution by APDC chelate co-precipitation. Anal. Methods Oceanogr., 44.

Buesseler KO, Bacon MP, Kirk Cochran J, Livingston HD (1992) Carbon and nitrogen export during the JGOFS North Atlantic Bloom Experiment estimated from ^{234}Th:^{238}U disequilibria. Deep Sea Res Part A Oceanographic Res. Pap., 39, 1115–1137.

Buesseler KO, Benitez-Nelson CR, Moran SB, Burd A, Charette M, Cochra JK, Coppola L, Fisher NS, Fowler SW, Gardner WD (2006) An assessment of particulate organic carbon to thorium-234 ratios in the ocean and their impact on the application of ^{234}Th as a POC flux proxy. Mar. Chem., 100, 213–233.

Cai P, Rutgers van der Loeff M, Stimac I, Nöthig EM, Lepore K, Moran SB (2010) Low export flux of particulate organic carbon in the central Arctic Ocean as revealed by ^{234}Th:^{238}U disequilibrium. J. Geophys. Res, 115, C10037.

Frey KE, Comiso JC, Cooper LW, Gradinger RR, Grebmeier JM, Saitoh SI, Tremblay JÉ (2014) Arctic Ocean Primary Productivity [in Arctic Report Card 2014], Arctic Report Card, 2014.

Lalande C, Nöthig EM, Somavilla R, Bauerfeind E, Shevchenko V, Okolodkov Y (2014) Variability in under-ice export fluxes of biogenic matter in the Arctic Ocean. Global. Biogeochem. Cycles, 2013GB004735.

Owens SA, Buesseler KO, Sims KWW (2011) Re-evaluating the ^{238}U-salinity relationship in seawater: Implications for the ^{238}U-^{234}Th disequilibrium method. Mar. Chem.r 127, 31–39.

Pike SM, Buesseler KO, Andrews J, Savoye N (2005) Quantification of Th-234 recovery in small volume seawater samples by inductively coupled plasma-mass spectrometry. J. Radioanal. Nucl. Chem., 263, 355–360.

Rigaud S, Puigcorbé V, Cámara-Mor P, Casacuberta N, Roca-Martí M, Garcia-Orellana J, Benitez-Nelson CR, Masqué P, Church T (2013) A methods assessment and recommendations for improving calculations and reducing uncertainties in the determination of ^{210}Po and ^{210}Pb activities in seawater Limnol. Ocean. Methods, 11, 561–571.

Smith CR, Leo FC De, Bernardino AF, Sweetman AK, Arbizu PM (2008) Abyssal food limitation, ecosystem structure and climate change. Trends Ecol. Evol., 23, 518–528.

Verdeny E, Masqué P, Garcia-Orellana J, Hanfland C, Kirk Cochran J, Stewart GM (2009) POC export from ocean surface waters by means of ^{234}Th/^{238}U and ^{210}Po/^{210}Pb disequilibria: A review of the use of two radiotracer pairs. Deep Sea Res. Part II Top. Stud. Oceanogr., 56, 1502–1518.

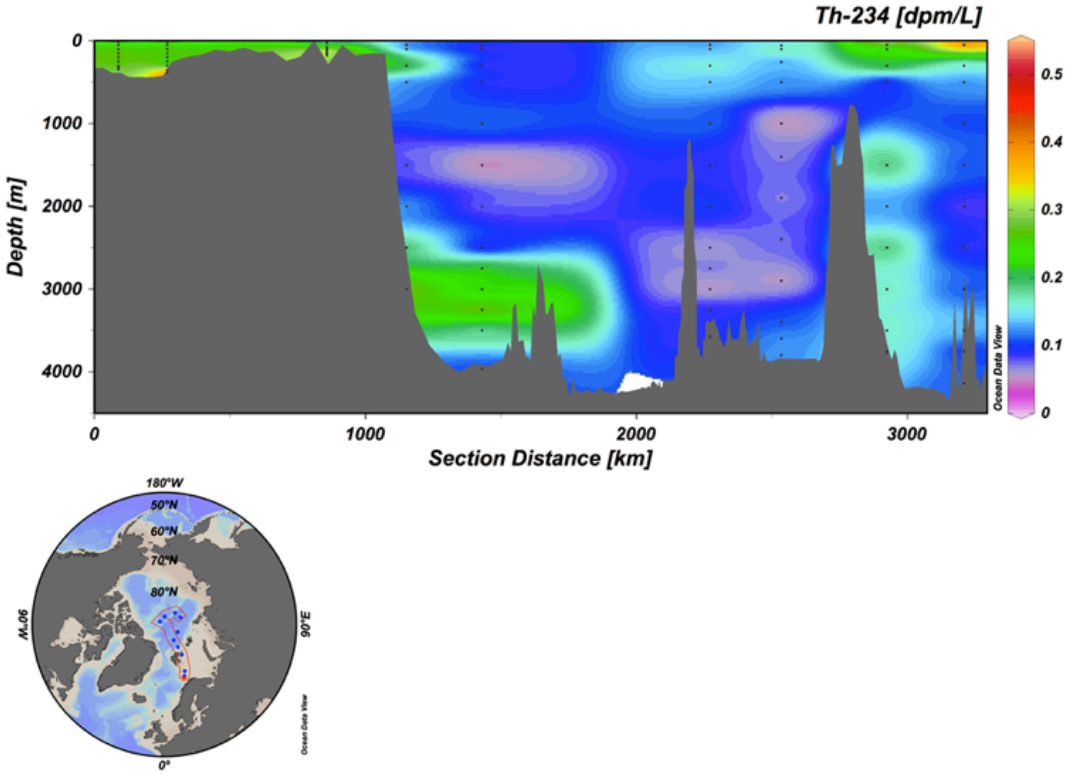

Fig. 6.13.2: (Top) Section plot of ^{234}Th particulate concentrations measured at 10 stations (see text and Fig. 6.13.1 for further information) along the entire water column. (Bottom) Map of station's locations.

6.14 Radium isotopes

Michiel Rutgers van der Loeff AWI

Objectives

Four natural isotopes of radium (the radium quartet) occur in the ocean. ^{228}Ra (half life 5.8y) is a known tracer for shelf waters. It is strongly enriched in the Arctic shelves and in the Transpolar Drift waters that originate in the Siberian shelves (Rutgers van der Loeff et al., 1995). ^{223}Ra and ^{224}Ra are short lived (11.4 and 3.7 d half life, respectively). They can trace near-shore processes (Kadko et al., 2005) but can also be used as indirect tracer of the distribution of their parent nuclides, ^{228}Th (Rutgers van der Loeff et al., 2012) and ^{227}Ac (Geibert et al., 2008). The fourth isotope, ^{226}Ra (half life 1600yr), is stable on the time scale of mixing of the Arctic Ocean and can be used as yield tracer for the analysis of other isotopes. Since Pacific and Atlantic source waters have distinct ^{226}Ra activities, the isotope can serves as tracer for the origin of water masses. In previous expeditions we have studied the distribution of the radium quartet in surface waters, we now want to include measurements of depth profiles of these isotopes in the water column for the study of exchange rates between shelf/slope and open ocean.

Work at sea

Water column profiles

At all 10 deployments of the *in-situ* pumps (ISP, see section 6.12), we mounted 75-mm MnO_2-coated acrylic cartridges (Henderson et al., 2013) in the pumps at 4 to 8 depths to collect dissolved radium and thorium isotopes by adsorption on the MnO_2. At the three basin stations (54, 81, 101) we made $BaSO_4$ precipitates of weighed 20-L aliquots for subsequent analysis of ^{226}Ra with gamma spectrometry. Additional 1-L samples were collected here for mass spectrometric analysis of ^{226}Ra.

Surface water

Throughout the cruise, surface water samples were collected from the ship's seawater intake. During PS94 this intake was connected to the centrifugal pump with inlet close to the moon pool (Klaus Pumpe) at 11m depth and was sampled close to this inlet to avoid possible ingrowth of ^{224}Ra from ^{228}Th adsrobed to the walls of the tubings. Seawater was prefiltered by passing over an uncoated cartridge and then passed over a MnO_2- absorber for the collection of Radium. As MnO_2 absorber we used either two columns filled with loose MnO_2 fiber in series, or two MnO_2-cartridges identical to the ones used in the *in-situ* pumps. The absorption efficiency of the cartridges (90± 7 %, even in the ISP with flow rates up to around 3 L/min) was clearly superior to that of the fiber columns (83±7 % at flow rates not exceeding 1 L/min) and during the last part of the cruise the cartridge method was used exclusively.

The activities of ^{223}Ra and ^{224}Ra were determined by alpha scintillation counting of the radon emanation in a delayed coincidence counting system (RaDeCC; Moore and Arnold, 1996). ^{228}Th was determined through a new generation of its daughter ^{224}Ra by a second RaDeCC count after 20-30 days. This second count was completed on board for samples up to Sta 120 (Fig. 6.14.1) and will be continued in the home laboratory for the samples collected on the last (Bjørn Øya) transect. The ^{228}Ra/^{226}Ra ratio will be determined later in the home laboratory using gamma spectrometry.

Preliminary and expected results

^{224}Ra and ^{228}Th distributions in the water column must be largely supported by parent ^{228}Ra and display the sources in surface water (especially from the shelf in the Trans Polar Drift) and at the seafloor. The actual distribution of ^{228}Ra awaits further analysis at AWI.

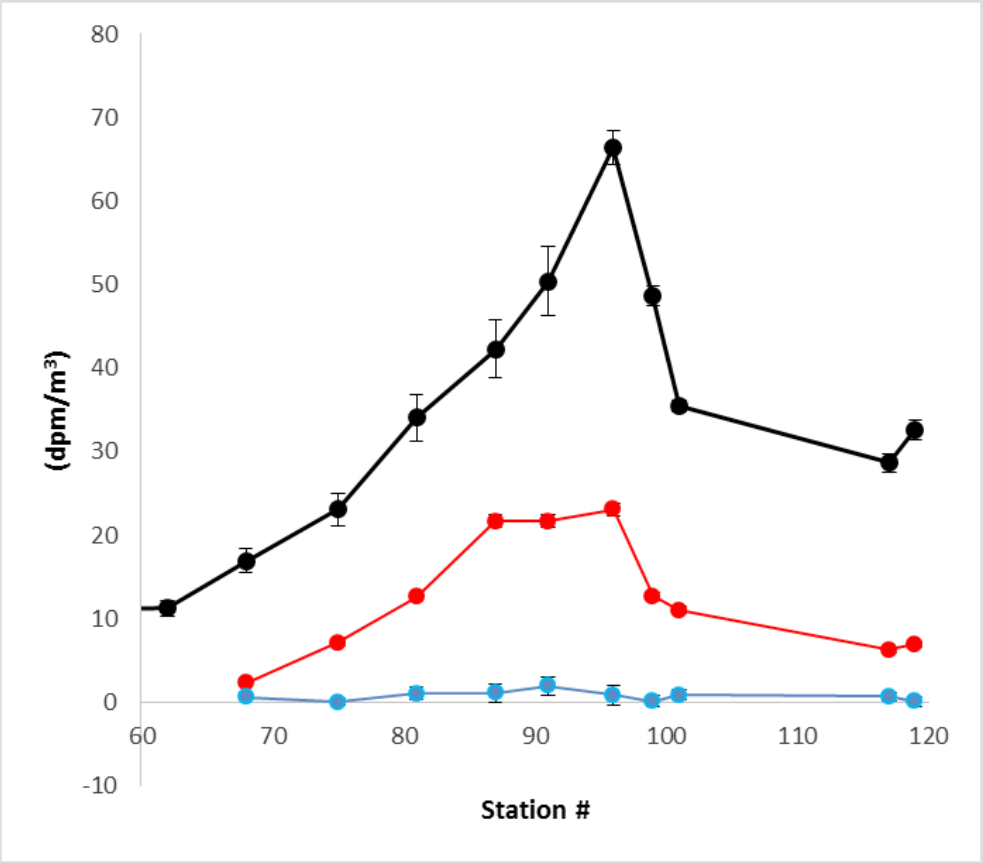

Fig. 6.14.1: Black, dissolved and blue, particulate ^{224}Ra in surface waters at time of sampling. Red, particulate 228Th as determined from the activity of daughter ^{224}Ra after four weeks of ingrowth.

Ingrowth of ^{224}Ra into the particulate material collected from the surface water with uncoated filters (Fig. 6.14.1) showed that ^{228}Th, not ^{224}Ra was present in the particulate phase, with a clear maximum at station 87-96, likely related to the Trans Polar Drift. Once the concentrations of parent ^{228}Ra are available we will investigate whether there is a depletion of ^{228}Th with respect to ^{228}Ra in the surface layer, which could then be interpreted as a measure of export production on a longer timescale (half-life ^{228}Th 1.9 year) than is provided by the study of ^{234}Th (24 days) and ^{210}Po (138 days) (see section 6.13) and contribute to resolve the discrepancy between the extremely low export production measured 2007 with ^{234}Th by Cai et al. (2010) and the observation 2012 of fresh sedimentation at the seafloor of the deep basins by Boetius et al. (2013).

From the distribution of radium isotopes we hope to derive exchange rates of the shelf and slope with the open ocean at various depths. These exchange rates are needed in models describing the distribution of other tracers like ^{230}Th and ^{231}Pa. A long recount of the deep radium samples will be used to quantify ^{227}Ac. After correction for activity supported by ^{231}Pa (see section 6.12), we will investigate whether the excess-^{227}Ac activity can be used to derive vertical mixing rates in the deep water.

Data management

See introduction of chapter 6 for details on GEOTRACES data management.

References

Boetius A, Albrecht S, Bakker K, Bienhold C, Felden J, Fernández-Méndez M, Hendricks S, Katlein C, Lalande C, Krumpen T, Nicolaus M, Peeken I, Rabe B, Rogacheva A, Rybakova E, Somavilla R, Wenzhöfer F, Party RPA-SS (2013) Export of Algal Biomass from the Melting Arctic Sea Ice. Science, 339, 1430-1432.

Cai P, Rutgers van der Loeff MM, Stimac I, Nöthig EM, Lepore K, Moran SB (2010) Low export flux of particulate organic carbon in the central Arctic Ocean as revealed by ^{234}Th:^{238}U disequilibrium. Journal of Geophysical Research - Oceans, 115, C10037.

Geibert W, Charette M, Kim G, Moore WS, Street J, Young M, Paytan A (2008) The release of dissolved actinium to the ocean: A global comparison of different end-members. Marine Chemistry, 109, 409.

Henderson PB, Morris PJ, Moore WS, Charette MA (2013) Methodological advances for measuring low-level radium isotopes in seawater. Journal of Radioanalytical and Nuclear Chemistry, 296, 357-362.

Kadko D, Muench R, (2005) Evaluation of shelf-basin interaction in the western Arctic by use of short-lived radium isotopes: The importance of mesoscale processes. Deep Sea Research Part II: Topical Studies in Oceanography, 52, 3227.

Moore WS, Arnold R (1996) Measurement of ^{223}Ra and ^{224}Ra in coastal waters using a delayed coincidence counter. J. Geophys. Res., 101, 1321-1329.

Rutgers van der Loeff MM, Key RM, Scholten JC, Bauch D, Michel A (1995) ^{228}Ra as a tracer for shelf water in the Arctic Ocean. Deep-Sea Res. II, 42, 1533-1553.

Rutgers van der Loeff MM, Cai P, Stimac I, Bauch D, Hanfland C, Roeske T, Bradley Moran S (2012) Shelf-basin exchange times of Arctic surface waters estimated from ^{228}Th/^{228}Ra disequilibrium. Journal of Geophysical Research - Oceans, 117, C03024, doi:03010.01029/02011JC007478.

6.15 Artificial radionuclides as tracers of water masses

Nuria Casacuberta[1], Viena Puigcorbé[2], Michiel Rutgers van der Loeff[3]

[1]LIP,
[2]UAB,
[3]AWI,

Objectives

Artificial radionuclides have been widely used as oceanic tracers to study watermass circulation. Radioactive tracers (^{99}Tc, ^{90}Sr, ^{137}Cs and ^{129}I) dispersed from European nuclear fuel reprocessing plants located at Sellafield (formerly Windscale) in the UK and La Hague in France (Kershaw & Baxter, 1995) have proved particularly powerful to that aim. The discharged radioactive waste in coastal waters of northwest Europe has been used to track the water movement through the North Sea (Kershaw & Baxter, 1995), the Norwegian Coastal Current (Alfimov, Aldahan et al., 2004), the Arctic Ocean (Smith, Ellis et al., 1999, Smith, McLaughlin et al., 2011, Karcher, Smith et al., 2012) and the Nordic Seas (Alfimov, Aldahan et al., 2004). The atmospheric weapon tests performed in the 1950's and 1960's have been another source of artificial radionuclides to the marine environment (Povinec, Aarkrog et al., 2005). Other than ^{137}Cs, ^{90}Sr, ^{99}Tc, ^{129}I, etc., in recent years, several studies have measured the anthropogenic occurrence of ^{236}U ($T_{1/2}$=23 My) in the ocean and pointed out its potential to become a new oceanographic tracer (Steier, Bichler et al., 2008, Christl, Lachner et al., 2012, Sakaguchi, Kadokura et al., 2012, Eigl, Srncik et al., 2013). Its conservative behavior in seawater and the fact that has it not yet reached steady state in the oceans, together with new developments in Accelerator Mass Spectrometry, proved that the ^{236}U/^{238}U atomic ratio can be used as a marker of water masses, particularly in the Arctic and Atlantic Oceans (Casacuberta, Christl et al., 2014). Atom ratios between different artificial radionuclides can be used to identify the sources of radionuclides in the (Kershaw and Baxter, 1995) marine environment (i.e. ^{240}Pu/^{239}Pu and ^{90}Sr/^{137}Cs) and track the water masses circulation (i.e. ^{129}I/^{137}Cs). For example, ^{129}I/^{137}Cs tracer measurements are used in simple mixing/advection models to estimate transit times from the North Sea to the Arctic Ocean. Similarly, and due to the different input functions of ^{129}I and ^{236}U from European reprocessing plants, the ^{129}I/^{236}U could become a potential tool in tagging the water masses in the North Atlantic and Arctic Oceans (Christl et al., 2012). The objective of our work during the PS94 cruise is to obtain a comprehensive dataset of artificial radionuclides in the Arctic Ocean to: i) constrain the sources of artificial radionuclides to the Arctic Ocean (i.e. global fallout, reprocessing plants, rivers); ii) use the ^{236}U/^{238}U atom ratio and ^{129}I/^{236}U to identify water masses in the Arctic Ocean; iii) use the ^{129}I/^{137}Cs and ^{129}I/^{236}U to constrain the transit times of waters from the North Sea to the Arctic Ocean; and iv) use them as tracers of the water circulation in the Arctic Ocean.

Work at sea

A total number of 360 seawater samples (131 for ^{236}U and ^{129}I and 98 for Pu-isotopes) were taken for artificial radionuclide analysis during the PS94 cruise. Full depth profiles of different volumes were collected at 17 stations during the cruise track, covering the three main deep Arctic Basins: Nansen, Amundsen and Makarov Basins, as well as a transect in the Barents Sea. All samples were collected from a 24 bottles rosette coupled to a three Conductivity Temperature Depth (CTD) system.

For the analysis of ^{129}I, a subsample of 200 – 500 mL was taken and processed on board, following the method by Michel et al. (2012). Briefly, Woodward iodine was added to the pre-calibrated sample and all iodine species were oxidized with $Ca(ClO)_2$ to iodate and subsequently reduced with NH_3OHCl and $NaHSO_3$ to iodide. After 45 minutes, pH was raised to 5-6 and

Iodine was extracted with a BioRad ® 1x8 anion exchange resin. Iodine was finally eluted with concentrated potassium nitrate solution (2.25 M) and precipitated as AgI. Precipitates were kept in filters for its final AMS measurement at ETH AMS Tandy (Zürich).

For the analysis of ^{236}U, 3 to 10 L samples were pre-processed on board. Samples were acidified and spiked with 3 pg of ^{233}U immediately after its collection. After 24 hours equilibration, uranium isotopes were pre-concentrated with Fe(OH)3 and kept in 250 mL bottles for its subsequent chemical analysis and measurement at ETH Zürich.

5 L samples were taken for Pu-isotopes analysis for Timothy Kenna (LDEO). Samples were stored in plastic cubitainers for its further delivery to US and its final analysis.

Other than seawater samples, a total of 5 ice stations were sampled during the cruise PS94 of RV *Polarstern* in the central Arctic in September 2015. Sea ice cores were retrieved using a standard 9 cm Kovacs ice corer, placed in plastic tubes and brought to the -20°C freezer/ cold lab. Cores were sectioned with a band saw either at discernible stratigraphic boundaries possibly related to different ice types or ice origin, or in the absence of such features to yield sufficient amounts for ^{129}I and ^{236}U analysis. Core sections were melted in cleaned plastic drums at room temperature and processed in the chemistry lab within 2 days.

Expected results

Distribution of artificial radionuclides in the Arctic Ocean will be used as tracers of water circulation in the Arctic Ocean. The ^{129}I/^{236}U atom ratio will be used in combination to ^{236}U/^{238}U ratio with the aim to: i) constrain the sources of artificial radionuclides to the Arctic Ocean (i.e. global fallout, reprocessing plants, rivers); ii) identify water masses in the Arctic Ocean; iii) constrain the transit times of waters from the North Sea to the Arctic Ocean.

Pu-isotopes will be used as tracers for understanding sources, pathways, dynamics and the fate of pollutants and particles in the Arctic Ocean. Due to the well-defined spatial and temporal inputs of Pu, the long half-lives of ^{240}Pu and ^{239}Pu and its unique chemical properties, Pu can be used as tracer for various physical and biogeochemical ocean processes, including circulation, sedimentation and biological productivity, and hence a means of assessing the impacts of global climate change.

Data management

See introduction of chapter 6 for details on GEOTRACES data management.

References

Alfimov V, Aldahan A, Possnert G, Kekli A, Meili M (2004) Concentrations of ^{129}I along a transect from the North Atlantic to the Baltic Sea. Nuclear Instruments and Methods in Physics Research Section B: Beam Interactions with Materials and Atoms, 223–224(0), 446-450.

Alfimov V, Aldahan A, Possnert G, Winsor P (2004) Anthropogenic iodine-129 in seawater along a transect from the Norwegian coastal current to the North Pole. Marine Pollution Bulletin, 49(11–12), 1097-1104.

Casacuberta N, Christl M, Lachner J, van der Loeff MR, Masque P, Synal HA (2014) A first transect of U-236 in the North Atlantic Ocean. Geochimica et Cosmochimica Acta, 133, 34-46.

Christl M, Lachner J, Vockenhuber C, Lechtenfeld O, Stimac I, Rutgers van der Loeff M, Synal HA (2012) A depth profile of uranium-236 in the Atlantic Ocean. Geochimica et Cosmochimica Acta, 77(0), 98-107.

Eigl R, Srncik M, Steier P, Wallner G (2013) $^{236}U/^{238}U$ and $^{240}Pu/^{239}Pu$ isotopic ratios in small (2 L) sea and river water samples. Journal of Environmental Radioactivity, 116(0), 54-58.

Karcher M, Smith JN, Kauker F, Gerdes R, Smethie WM (2012) Recent changes in Arctic Ocean circulation revealed by iodine-129 observations and modeling. Journal of Geophysical Research, Oceans 117(C8), C08007.

Kershaw P, Baxter A (1995) The transfer of reprocessing wastes from north-west Europe to the Arctic. Deep Sea Research Part II: Topical Studies in Oceanography, 42(6), 1413-1448.

Povinec PP, Aarkrog A, Buesseler KO, Delfanti R, Hirose K, Hong GH, Ito T, Livingston HD, Nies H, Noshkin VE, Shima S, Togawa O (2005) ^{90}Sr, ^{137}Cs and $^{239,240}Pu$ concentration surface water time series in the Pacific and Indian Oceans – WOMARS results. Journal of Environmental Radioactivity, 81(1), 63-87.

Sakaguchi A, Kadokura A, Steier P, Takahashi Y, Shizuma K, Hoshi M, Nakakuki T, Yamamoto M (2012) Uranium-236 as a new oceanic tracer: A first depth profile in the Japan Sea and comparison with caesium-137. Earth and Planetary Science Letters, 333–334(0), 165-170.

Smith JN, Ellis KM, Boyd T (1999) Circulation features in the central Arctic Ocean revealed by nuclear fuel reprocessing tracers from Scientific Ice Expeditions 1995 and 1996. Journal of Geophysical Research Oceans, 104(C12), 29663-29677.

Smith JN, McLaughlin FA, Smethie WM, Moran SB, Lepore K (2011) Iodine-129, 137Cs, and CFC-11 tracer transit time distributions in the Arctic Ocean. Journal of Geophysical Research Oceans 116(C4), C04024.

Steier P, Bichler M, Fifield KL, Golser R, Kutschera W, Priller A, Quinto E, Richter S, Srncik M, Terrasi P, Wacker L, Wallner A, Wallner G, Wilcken KM, Wild EM (2008) Natural and anthropogenic ^{236}U in environmental samples. Nuclear Instruments and Methods in Physics Research Section B: Beam Interactions with Materials and Atoms, 266(10), 2246-2250.

7. PLANKTON ECOLOGY AND BIOGEOCHEMISTRY IN A CHANGING ARCTIC OCEAN (PEBCAO)

Nicole Hildebrandt[1], Vanessa S. Köhler[1], Ksenia N. Kosobokova[2], Imke Petersen[1], Juliane Riedel[1], Franz Schröter[1]
not on board: Katja Metfies[1], Barbara Niehoff[1], Eva-Maria Nöthig[1]

[1]AWI
[2]IORAS

Grant No. AWI_PS94_00

Objectives

The Arctic Ocean is strongly affected by climate change, e.g. increasing temperatures and shrinking sea ice, which in turn will have large impact on the pelagic ecosystem with consequences for the carbon cycle and sequestering. Long-term investigations of biogeochemical plankton parameters as well community composition analyses for all plankton size classes, from pico- to large zooplankton, are thus required to understand and predict future ecosystem functioning. Shifts in species composition are expected: For example, at the base of the food web smallest algae may become more important. At higher trophic levels, zooplankton organisms then have to cope with changes in food supply and, thus, have to adjust their species-specific patterns in population dynamics, depth distribution, and feeding biology. In addition to increasing temperatures and shrinking sea ice, recent changes in the circulation (shift of the boundary between Atlantic and Pacific water masses) may also alter the pelagic system. Also, the increasing advection of relatively warm Atlantic water masses inhabited by boreal species could favour the distribution of Atlantic communities, which could finally replace the Arctic fauna.

Since the nineties, ecological investigations of phyto- and zooplankton biomass, species composition, productivity, sedimentation and biochemical parameters (i.e. chlorophyll *a*, particulate organic carbon & nitrogen, carbonate and biogenic silica) have been carried out in the central Arctic Ocean with *Polarstern* (8 cruises between 1993 and 2014). Plankton biomass and carbon flux during summer close to and beneath the sea ice do not yet appear to have increased, however, marginal ice zones have moved closer to the pole. Thus, former ice covered regions are ice-free for longer time and allow a different summer population to develop. In addition, earlier investigations in the Eurasian Basin demonstrated that the composition and distribution of protists and the pelagic fauna in the Arctic Ocean are strongly affected at regional and even basin scales by Atlantic water from the Fram Strait and from the Barents Sea. The ecological niches, e.g. preferences and tolerances, of advected zooplankton species then determine their success in inhabiting the Arctic basins.

Molecular biological investigations on biodiversity, HPLC and flow cytometry reveal strong gradients of biomass and from diatoms to picoplankton-dominated communities from the Atlantic to the Pacific sector. Specific hypotheses we intend to test are:

1. Less sea ice in summer will promote higher production followed by higher sedimentation in regions that have been totally ice covered before.

2. Shifts in species compositions on different trophic levels will change trophic interactions and change fluxes and export of organic matter.

3. Changes like the inflow of warmer Atlantic water masses may also alter the pelagic system and export fluxes.

In 2015, specific aims of the zooplankton studies were focused on

1. relating composition, abundance, biomass and spatial distribution of zooplankton communities across the basins and ridges to water circulation patterns and primary productivity and protist composition,

2. understanding the trophodynamic relationships among zooplankton species within the Arctic pelagic communities by continued biochemical analyses (i.e. carbon and nitrogen content, stable isotope ratios),

3. building the DNA sequence library needed for molecular approaches to assess community structure and identifying regional and basin-scale population patterns within the Arctic using molecular markers.

The results gained during this cruise will be compared to earlier cruises to improve projections of future status or change.

Work at sea

Phytoplankton and protist community

Water samples were taken for analysing unicellular plankton organisms distribution and biomass and for biogeochemical measurements (pigments, POC/N PbSi) from Niskin bottles attached to a CTD/rosette sampling system from 5-7 depths at 25 stations (Table 7.1, Fig. 7.1). Aliquots of seawater were filtered for later analysis of particulate organic carbon and nitrogen (POC/PON), particulate biogenic silica (PbSi), HPLC pigments, fractionated (>10 µm; 3 µm; 0.4 µm) and unfractionated chlorophyll *a* concentration (chl *a*), and molecular genetic analyses. Ten additional stations were exclusively sampled for chl *a* (Table 7.1, Fig. 7,1). Water was generally sampled at depths of 2 m, 10 m, 20 m, 30 m, 50 m, 100 m and 200 m, however, sampling depths in the upper 50 metres were adjusted to match the depth of the chl *a* maximum whenever present. Samples for molecular analyses were collected at three depths in the upper 50 m of the water column, including the chl *a* maximum. Water samples for chl *a* concentration and HPLC pigment analyses were taken within the upper 100 m and immediately filtered with Whatman GF/F glass microfibre filters. POC/PON and PbSi were generally sampled down to 200 m depth. On stations where moorings with attached sediment traps were deployed (see section “Export fluxes”), 12 samples in the entire water column were sampled for these parameters. POC/PON was filtered on pre-combusted GF/F filters. Cellulose acetate filters were used to filter for later PbSi analyses. Filters were frozen at -20 °C (chl *a*, POC/PON, PbSi, seston) and -80 °C (HPLC) to be processed in the home laboratory. Additionally, 200 ml of seawater were sampled at 5 depth layers within the upper 50 m and preserved with hexamethylentetramine-buffered formaldehyde for later identification and enumeration of larger (> 3 µm) phyto- and protozooplankton cells under the microscope at the home laboratory.

For molecular analyses of protist community composition and determination of fractionated chl *a* concentrations, water samples were sequentially filtered onto Millipore polycarbonate filters with a pore-size of 10 µm, 3 µm and 0.4 µm. In parallel, filters were collected for analyses of ambient bacterial communities according to the same filtration procedure, except that the 0.4 µm filter was exchanged by an 0.2 µm filter. Subsequent to filtration, filters were stored at -20 °C until further analyses in the laboratory.

After leaving the sea ice - on the way to the Russian EEZ - five underway chl *a* samples were taken in duplicates using the ship's seawater pump. The filtration procedure and sample storage were performed as stated above.

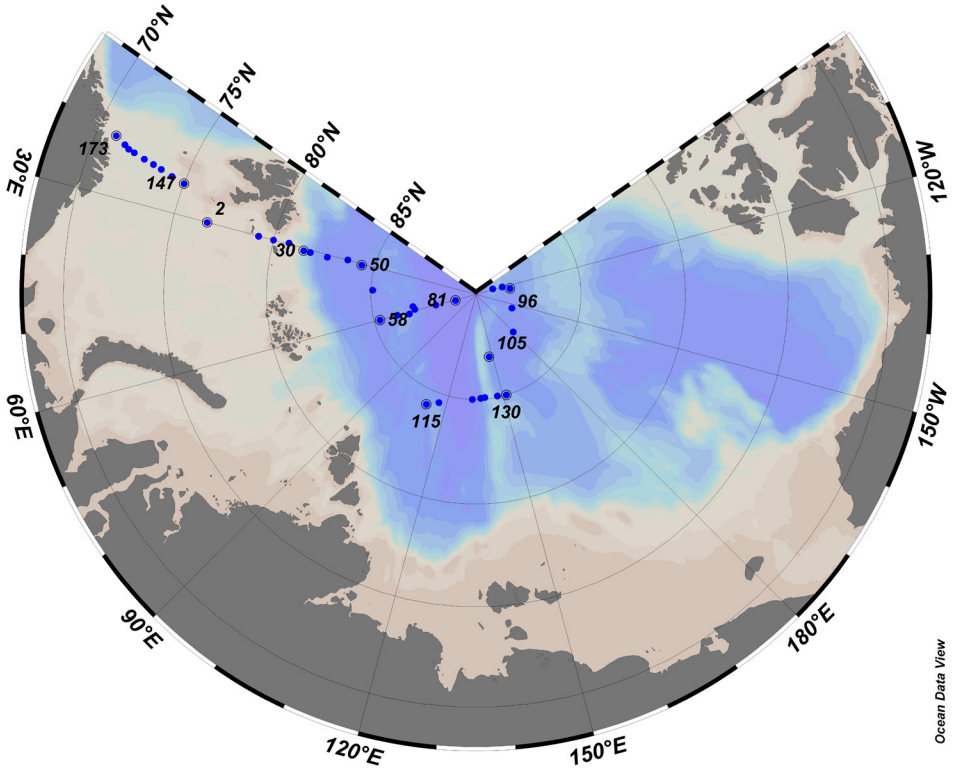

Fig. 7.1: Locations of stations sampled by the PEBCAO group

An Apstein net (mesh size 20 µm) was deployed at nine ice stations to a depth of 10 m. Aliquots of the catches were scanned on board to obtain a quick overview of the species composition of unicellular microplankton using a Zeiss Axiovert 40 C microscope. Photos were taken with a Zeiss AxioCam MRc camera and processed with the respective software.

Export Fluxes

In order to investigate the vertical particle flux over a one-year period, sediment traps (K.U.M.) were deployed on two moorings in the Nansen Basin (PS94/058) and at the Gakkel Ridge (PS94/069) close to the Karasik Peak (see chapter 3). At both mooring sites, one sediment trap was mounted at 200 - 300 m below the sea surface and another one was placed ~150 m above the sea floor. This work is part of the AWI FRAM project. The mooring in the Nansen Basin will be exchanged in 2016, and then deployed for another two years. In addition to the other parameters, at these locations 12 water samples were taken with the Niskin bottles for the determination of seston (total particulate matter). They were filtered on pre-combusted and pre-weighed Whatman GF/F filters which were stored frozen at -20 °C.

Zooplankton sampling

For the investigation of large-scale distribution and species composition, zooplankton was collected by a multiple closing net (Type MAXI, 0.5 m^2 mouth opening, Hydrobios, Kiel; Fig. 7.2). The multinet was equipped with nine nets (150 µm mesh size) and provided stratified sampling of the entire water column from the bottom to the surface.

Sampling was carried out in the Arctic Ocean and in the southern Barents Sea. In the Arctic Ocean, we sampled a total of 15 stations (Table 7.1, Fig. 7.1) on two transects (Fig. 3.1, transect 1+2 and 4) with the sampling intervals bottom-3000-2000-1000-500-200-100-50-25-0 m. The majority of stations were taken in the deep region (seven of them deeper than 3,000 m, plus two deeper than 4,000 m). Three stations were taken at the Gakkel and Lomonosov ridges, one in the slope region, and two in the shelf region (depths <400 m). Our sampling protocol followed standard procedures as applied during previous *Polarstern* cruises to the deep Arctic basins (1993-2012). The comparison of data obtained during PS94 with these historical data will then be used for assessing changes in the Arctic pelagic biota related to ongoing climate change and the entire data set can also be considered a starting point for the first zooplankton time series in the history of the investigation of the Arctic.

Fig. 7.2: Multinet Type Maxi with additional net bag for non-quantitative, depth-integrated zooplankton sampling.

In the southern Barents Sea, along the 24°E meridian, five stations were taken between 75° and 73°N (Table 7.1, Fig. 7.1). The entire water column was sampled at the following depth intervals: bottom-350-300-250-200-150-100-50-25-0 m. The zooplankton samples were preserved in 4 % hexamethylentetramine-buffered formaldehyde for later processing.

To investigate the small-scale distribution of zooplankton species in the upper 1,000 m of the water column, the LOKI system (Lightframe On-sight Key species Investigation; Fig. 7.3a) was successfully deployed on 11 stations along the transect from the northern Barents Sea shelf to the Makarov Basin (Table 7.1). The LOKI was equipped with a high-resolution digital camera and sensors measuring temperature, depth, salinity, oxygen, and fluorescence as a proxy for algal abundance. The distribution patterns of the zooplankton organisms can thus directly be related to the hydrography. Combining both approaches (MN and LOKI) allows us to analyze and better understand changes in the zooplankton communities under changing environmental conditions.

In total, approx. 166,000 pictures of zooplankton organisms were taken with the LOKI. These pictures (an example is shown in Fig. 7.3b) will be analysed at the AWI, and species distribution will be related to the environmental parameters and compared with the multinet data.

Live animals for molecular genetics and stable C and N isotope analyses were collected by a 60 cm diameter net (300 µm mesh-size) attached to the outside of the multinet (Fig. 7.2) and from an Apstein net (see section “Phytoplankton and protist community”). Representatives of target species to be used for molecular genetic analyses were removed from live samples, preserved with 96 % ethanol and stored at 0 °C for later determination of their COI sequences plus some additional mitochondrial or nuclear target regions. For the three dominant copepod species – *Calanus hyperboreus*, *C. glacialis*, and *C. finmarchicus* – samples were prepared to explore population genetics at a high spatial resolution. The relatively low availability of most other species will restrict our analysis to a simple comparison of the Eurasian to the Amerasian basin populations.

Animals for stable C and N isotope analyses were also sorted out from live samples and stored at -20 °C for later analyses.

The remainders of the non-quantitative catches were given to Lars-Eric Heimbürger (GEOTRACES group) for analyzing the Hg content of the Arctic zooplankton at MIO. Subsamples of *Thysanoessa* sp. (Euphausiacea) were given to Ellen Damm (AWI) for analysing DMS.

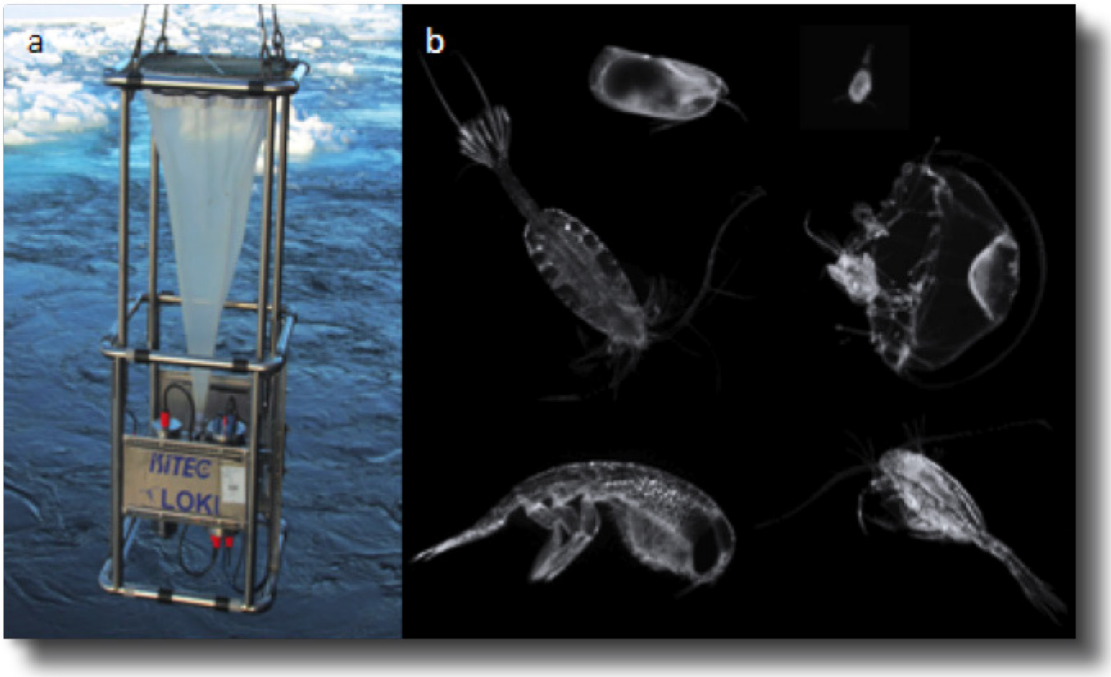

Fig. 7.3: The LOKI system during deployment (a) and a compilation of photographs taken by LOKI, in clockwise direction: Boroecia sp. (ostracod), Oncaea sp. (cyclopoid copepod), Botrynema ellinorae (jelly fish), Metridia longa (calanoid copepod), Themisto libellula (hyperiid amphipod) and Paraeuchaeta sp. (calanoid copepod).

Tab. 7.1: Biogeochemical and biological parameters

Station	HPLC	Chla	DNA/ $Chla_f$	bPSi	POC/ PON	Seston	Micros-copy	Multi-net	LOKI	Bongo net
PS94/002	x	x	x	x	x		x			
PS94/004	x	x	x	x	x		x			
PS94/010								x	x	
PS94/018	x	x	x	x	x		x	x		
PS94/030								x	x	
PS94/032	x	x	x	x	x		x	x	x	
PS94/040	x	x	x	x	x		x	x	x	
PS94/046	x	x	x	x	x		x			

Station	HPLC	Chla	DNA/ $Chla_f$	bPSi	POC/ PON	Seston	Micros-copy	Multi-net	LOKI	Bongo net
PS94/050	x	x		x	x			x	x	
PS94/054	x	x	x	x	x		x			
PS94/058	x	x	x	x	x	x	x	x	x	
PS94/062	x	x	x	x	x		x			
PS94/066	x	x		x	x			x	x	
PS94/069	x	x	x	x	x	x	x			
PS94/070								x	x	
PS94/076	x	x	x	x	x		x			
PS94/081	x	x	x	x	x		x	x	x	
PS94/091	x	x	x	x	x		x	x	x	
PS94/094		x	x				x			
PS94/096	x	x	x	x	x		x	x	x	
PS94/099	x	x	x	x	x		x			
PS94/101	x	x	x	x	x		x			
PS94/105	x	x	x	x	x		x			
PS94/115	x	x	x	x	x		x			
PS94/117	x	x	x	x	x		x	x		
PS94/121	x	x	x	x	x		x			
PS94/123	x	x	x	x	x		x			
PS94/125	x	x	x	x	x		x	x		
PS94/128		x	x				x			
PS94/130	x	x	x	x	x		x	x		
PS94/147		x	x					x		
PS94/149		x	x					x		
PS94/153		x						x		x
PS94/157		x	x					x		
PS94/161		x	x					x		
PS94/165			x							
PS94/167		x								
PS94/169		x								
PS94/173		x								

Chla: chlorophyll *a*; $Chla_f$: fractionated chlorophyll *a*; bPSi: biogenic particulate silica; HPLC: pigment analysis; POC/PON: particulate organic carbon & nitrogen.

Preliminary/expected results

Phytoplankton community

All filters will be analysed in the AWI home laboratory. The survey of important microplankton organisms revealed that most commonly copepod nauplii belonging to the zooplankton together with large diatoms, ciliates and dinoflagellates (protozoa) were found in the 20 µm Apstein net samples of Arctic surface waters (Fig. 7.4).

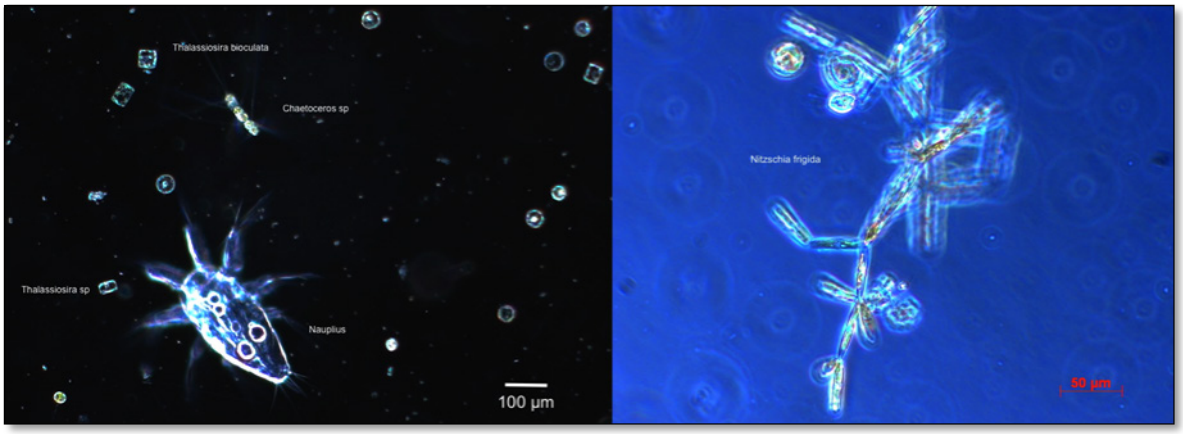

Fig. 7.4: Composition of net plankton > 20 µm in the upper 10 m surface waters in the Nansen Basin (left) and under the close sea ice in the Amundsen Basin (right) taken by F. Schröter, I. Petersen and J. Riedel.

Protist community

Analyses of all samples will take place subsequent to the cruise in the laboratory.

Zooplankton

LOKI pictures revealed that the mesozooplankton community in the upper 1,000 m of the water column was clearly dominated by copepods (Calanoida and Cyclopoida). Chaetognaths, ostracods, hydrozoan medusa, ctenophores and amphipods occurred regularly but in relatively low numbers. In the non-quantitative zooplankton samples used for molecular genetics and stable isotope analyses, a total of 102 planktonic metazoan and 3 protozoan (Radiolaria) species were identified. This yield represents >50 % of the zooplankton species known from the Arctic basins, with only the rarest species still remaining unsampled.

For stable isotope analyses 29 species of most common herbivorous, omnivorous and carnivorous copepods (ca. 20 species), ostracods (1 species), chaetognaths (2 species), amphipods (4 species), pteropods (1 species), and decapods (1 species) were collected to assess relative ratios of grazers versus omnivores and predators. These collections include 244 samples from 6 stations (1-3 replicates for each species at each station) in the Eurasian Basin and above the Lomonosov Ridge.

Quantitative multinet samples as well as LOKI pictures will be analyzed for species abundance and depth distribution at the AWI. The molecular genetic samples collected for DNA barcoding will be analyzed in cooperation with IORAS at facilities of the White Sea Biological Station of the Moscow State University. Stable isotope samples will be analysed at UiT (The Arctic University of Norway) in cooperation with the AWI and IORAS.

Data management

Many of the samples (i.e. pigment analyses, particulate matter in the water column, etc.) will be analysed at AWI within about two years after the cruise. We plan that the full data set will be available at latest about three years after the cruise. Most of species samples and samples which will not be analysed immediately will be stored at the AWI at least for another 10 years. Data will be made available to the public via PANGAEA.

8. ARCTIC IN RAPID TRANSITION (TRACERS, ORGANIC CHEMISTRY, SEA ICE BIOLOGY AND SUSPENDED MATTER)

Dorothea Bauch[1] [1]GEOMAR

Grant No. AWI_PS94_00

Introduction

The ART contributions on PS94 are partly connected to the ART work of PS92 and thus aim to investigate seasonal signals within the Arctic along the Transpolar Drift. The ART programme on PS94 brings together water mass tracer work based on stable oxygen and carbon isotopes ($\delta^{18}O$, $\delta^{13}C_{DIC}$), suspended particulate matter (SPM), dissolved organic matter (DOM, CDOM, FDOM, lignin) and work on sea-ice biology. The work of each group is described accordingly in separate sections.

It has recently been shown that coloured dissolved organic matter (CDOM) plays a key role in the biogeochemistry and radiant heating of the upper layer in the Arctic Ocean (Hill 2008) and enhances the production of carbon monoxide in the ice covered Arctic (Tran et al., 2012). Additional CDOM will directly influence the light regime in the sea ice and the underlying water. Light is one of the key limiting factors for primary production in the ocean, particularly in the Arctic where the export of turbid waters from rivers and coastal regions enhances the delivery of nutrients to micro algal populations, but also impairs photosynthesis by scattering and absorbing sunlight (Retamal et al., 2008).

Therefore it is important to study the pathways of freshwater, suspended particulate matter (SPM), and (CDOM) and the possible response to climate variations in order to understand their impact on the sensitive Arctic ecosystem. In addition, it is important to study these fields with regard to sea-ice biology, as differences in sea-ice biological features were observed in relation to water mass origin: Due to the decrease of the sea-ice thickness, recently new evolving habitats for sea-ice algae were observed in melt ponds (Lee et al., 2011). During the cruise TransArc 2011, particularly in the Atlantic sector of the central Arctic, large aggregates of pelagic derived material accumulating on the bottom of the melt ponds have been found. These apparently new Arctic melt pond ecosystems are likely to have consequences for the carbon budget and thus major implications for the cryo-benthic and cryo-pelagic coupling of the Arctic Ocean. Nitrate was found to limit the algae standing stocks of all habitats (ice, melt ponds und water) in the Pacific sector in contrast to the Atlantic sector (Peeken, 2012).

References

Hill VJ (2008) Impacts of chromophoric dissolved organic material on surface ocean heating in the Chukchi Sea. J Geophys Res-Oceans, 113.

Lee SH, Mcroy CP, Joo HM, Gradinger R, Cui XH, Yun MS, Chung KH, Kang SH, Kang CK, Choy EJ, Son SH, Carmack E, Whitledge TE (2011) Holes in Progressively Thinning Arctic Sea Ice Lead to New Ice Algae Habitat. Oceanography, 24, 302-308.

Peeken I (2012) Sea ice biology. In Schauer, U., ed. The Expedition of the Research Vessel "*Polarstern*" to the Arctic in 2011 (ARK-XXVI/3), Reports on Polar and Marine Research, 649, 101-109.

Retamal L, Bonilla S, Vincent WF (2008) Optical gradients and phytoplankton production in the Mackenzie River and the coastal Beaufort Sea. Polar Biology, 31, 363-379.

Tran S, Bonsang B, Gros V, Peeken I, Sarda-Esteve R, Belvisio S (2012) A survey of carbon monoxide and non-methane hydrocarbons in the Arctic Ocean during summer 2010: assessment of the role of phytoplankton. Biogeosciences Discussion, 9, 4727-4792.

8.1 Water mass signatures ($\delta^{18}O$, $\delta^{13}C_{DIC}$)

Dorothea Bauch[1] [1]GEOMAR

Objectives

The purpose of the analysis of stable oxygen isotope ($\delta^{18}O$) and stable carbon isotopes of the total dissolved inorganic carbon ($\delta^{13}C_{DIC}$) is to provide an assessment of water mass and freshwater composition within the Arctic Ocean and to understand the inter-annual and long-scale variation of these signals. The stable oxygen isotope composition ($\delta^{18}O$) of the water is a conservative tracer and can be used together with hydro-chemical data to distinguish shelf-derived freshwaters (i.e. river water and sea-ice derived melt/brine waters) from Pacific-derived waters and other marine waters. Thus contribution of shelf-derived freshwaters to the halocline, the Atlantic layer and the deep and bottom waters of the Arctic Ocean can be quantified. There are inter-decadal variations in the distribution of the Pacific component in the Arctic Ocean but recently also strong spatial variations were observed in freshwater distributions in the Transpolar Drift in 2007 thus indicating also inter-annual and possibly also seasonal variations. It is not known whether these variations are a permanent feature and whether they are related to the absence of Pacific waters in 2007. The evaluation of freshwater and Pacific water in the Arctic Ocean halocline will thus help to further understand the impact and the potential feedbacks of the Arctic Ocean hydrography on Arctic and global climate change.

Work at sea

Samples for stable oxygen isotope analysis ($\delta^{18}O$) were taken on all CTD-rosette stations in parallel to hydro-chemical sampling and CDOM sampling. Depths levels are concurrent to the GEOTRACES sampling depth. Sampling for $\delta^{13}C_{DIC}$ was performed at selected stations parallel to hydro-chemical sampling and parallel to Multinet casts. Mostly all depth levels over the upper 500 m of the water column were sampled and at a selected station down to the bottom. 50 ml of water was taken for each $\delta^{18}O$ sample. For $\delta^{13}C_{DIC}$ 100 ml samples were drawn by minimizing air-water gas-exchange (without “bubbeling”). Samples were poisoned with 0.2 ml of 0.5-saturated $HgCl_2$.

Samples for $\delta^{18}O$ also include ice cores. Sea-ice samples were provided from the sea-ice biology group from thawed 10 cm section of the salinity core (see section on sea-ice biology and section on ice coring sites, accordingly).

Expected results

No results were obtained at sea. Samples will be analysed on shore by mass-spectrometry. Samples for $\delta^{18}O$ and $\delta^{13}C_{DIC}$ analysis will be transported to Kiel. Analysis will be conducted at the Leibniz Laboratory at Kiel University, Kiel, Germany and at the Stable Isotope Facility at CEOAS at Oregon State University, Oregon, USA within 1 year.

Based on hydrological data and stable oxygen isotope analysis ($\delta^{18}O$) the influence of mainly shelf-derived meteoric waters and modification by sea-ice processes (melting or formation) can be quantified (Bauch et al., 1995).

From previous investigations in the Central Arctic Ocean e.g. in summer 2007 we know that there is spatial and temporal variation of freshwater distribution within the Arctic Ocean halocline on an inter-annual to potentially seasonal timescale (Bauch et al., 2011). With the samples obtained during PS94 we expect to learn more about the inter-annual and long-scale variations of freshwater within the different layers of the Arctic Ocean halocline.

A comparison with results of freshwater assessment based on CDOM will be done and thus we expect to achieve additional information e.g. about the ratio of river and other meteoric waters.

Data management

Data will be stored at the Pangaea data repository and will be made public there within three years.

References

Bauch D, Schlosser P, Fairbanks RF (1995) Freshwater balance and the sources of deep and bottom waters in the Arctic Ocean inferred from the distribution of H218O. Progress in Oceanography, 35, 53-80.

Bauch D, Rutgers van der Loeff M, Andersen N, Torres-Valdes S, Bakker K, Abrahamsen EP (2011) Origin of freshwater and polynya water in the Arctic Ocean halocline in summer 2007. Progress in Oceanography, 482-495, doi:10.1016/j.pocean.2011.1007.1017.

8.2 Dissolved organic matter

Heather Reader[1], Colin Stedmon[1] (not on board), Dennis Hansell[2] (not on board), Rainer Amon[3] (not on board)

[1]DTU-Aqua
[2]RSMAS
[3]TAMU

Objectives

- The main goal of sampling effort was to map the distribution and characteristics of dissolved organic matter (DOM) in the Arctic Ocean. One of the goals is to trace the distribution of terrestrially-sourced DOM, which originates in the Siberian rivers, and its mixing with marine waters in the surface layers of the Arctic Ocean, and compare DOM to other water mass tracers, in particular using the optical properties of DOM (coloured and fluorescent DOM, CDOM and FDOM, respectively). Combining this sampling effort with an on-going monitoring programme in the Fram Strait (see Stedmon et al., 2015), we will evaluate the use of DOM as a new tracer of meteoric water in the Arctic Ocean.
- Further tracing of the influence of the Siberian rivers on the Arctic Ocean ecosystem is achieved by collecting the first detailed vertical profiles of lignin. Lignin is a biomarker that is derived from the tissue of woody plants, and therefore has an exclusively terrestrial source, and can be used as a tracer of river water in marine systems. The sampling of dissolved organic carbon (DOC) will contribute to the concurrent Canadian and US sampling programmes and provide a unique trans-Arctic dataset. Furthermore, the influence of DOM on sea ice algal communities and vice versa was investigated in collaboration with sea ice biology.

Work at sea

Samples were collected for DOC, CDOM and FDOM at all depths concurrent to the GEOTRACES sampling stations, and was coordinated with inorganic nutrients and stable oxygen isotope sampling. Additional samples for DOC, CDOM and FDOM were taken at each CTD-Large station along section 4, focussing on the surface layers (0 – 500 m). Samples for

lignin analysis were collected for 3 stations in each basin (Nansen, Amundsen, and Makarov), as well as one station on section 6, to collect Atlantic water inflow.
CDOM UV-visible absorbance was measured on board using a Perkin-Elmer Lambda-35 spectrophotometer (by agreement with Dr. Piotr Kowalczuk, IOPAN). Excitation-emission matrix fluorescence spectra to characterise FDOM were also measured on board using a Horiba Aqualog fluorescence spectrometer (by agreement with Dr. Astrid Bracher, AWI). DOC samples were frozen for later analysis by Dennis Hansell, RSMAS, Miami, USA. Ligning samples were frozen for later analysis by Rainer Amon, Texas A&M University, Galveston, USA.

Samples from sea ice cores, melt ponds, and under ice water were sampled by the sea ice biology team, and CDOM and FDOM were also measured on board. Sub-samples for DOC from these samples were frozen for later analysis at DTU.

Preliminary/expected results

The DOC measurements will provide a unique basin scale mapping of distributions and contribute to the global sampling effort coordinated by Hansell (Hansell et al., 2009). The DOM and lignin measurements will allow us to develop our understanding of how the quantity and quality of Arctic riverine DOM changes during mixing in shelf seas and transport across the Arctic in the halocline layer. The DOM and lignin datasets will be linked with previously published data from the Siberian rivers (Stedmon et al., 2011; Amon et al., 2012) and with an on-going monitoring programme in the Fram Strait that that focuses on water exiting the Arctic Ocean along the coast of Greenland (Granskog et al., 2012; Stedmon et al., 2015).

Data management

Data from water column DOC measurements will be submitted by Dennis Hansell, RSMAS. Data from lignin measurements will be submitted by Rainer Amon, TAMU. Data from water column CDOM and FDOM will be submitted by Heather Reader, DTU. Data from ice sampling (DOC, CDOM, FDOM) will be submitted first to the sea ice biology group to compile with the rest of their data and then submitted to PANGAEA by the sea ice biology group. All data will be processed and submitted in a timely fashion.

References

Amon RMW et al. (2012) Dissolved organic matter sources in large Arctic rivers. Geochim. Cosmochim. Acta, 94, 217–237, doi:10.1016/j.gca.2012.07.015.

Granskog MA, Stedmon CA, Dodd PA, Amon RMW, Pavlov AK, de Steur L, Hansen E (2012) Characteristics of colored dissolved organic matter (CDOM) in the Arctic outflow in the Fram Strait: Assessing the changes and fate of terrigenous CDOM in the Arctic Ocean. J. Geophys. Res., 117(C12), C12021, doi:10.1029/2012JC008075.

Hansell D, Carlson C, Repeta D, Schlitzer R (2009) Dissolved Organic Matter in the Ocean: A Controversy Stimulates New Insights. Oceanography, 22(4), 202–211, doi:10.5670/oceanog.2009.109.

Stedmon CA, Amon RMW, Rinehart AJ, Walker SA (2011) The supply and characteristics of colored dissolved organic matter (CDOM) in the Arctic Ocean: Pan Arctic trends and differences. Mar. Chem., 124(1-4), 108–118, doi:10.1016/j.marchem.2010.12.007.

Stedmon CA, Granskog M, Dodd P (2015) An approach to estimate the freshwater contribution from glacial melt and precipitation in East Greenland shelf waters using colored dissolved organic matter (CDOM). J. Geophys. Res. Oceans, 120, doi:10.1002/2014JC010501.

8.3 Suspended particulate matter (SPM)

Dorothea Bauch[1] [1]GEOMAR
Carolyn Wegner[1] (not on board)

Objectives

The goal of this study is to improve our understanding of the pathways of suspended particulate matter (SPM) from the Barents shelf to the Nansen Basin which is critical in order to draw the connection between sediment dynamics, optical properties and ecosystem dynamics under a changing climate. Furthermore quantifying the abundance and composition of SPM, and comparing these to sea ice and ocean surface sediment samples is required to understand the significance of large-scale lateral transport, and how this may affect the reconstruction of ice conditions in the geologic past.

Work at sea and at the ice

Sampling for SPM was conducted over the continental shelf break of the Barents Sea at 30°E. For each sample 1l of water was taken from the rosette. Water samples were taken over the whole water column for all stations with up to about 500 m bottom depth. Samples were filtered through pre-weighed HVLP filters by MILLIPORE (0.45 microns), and washed carefully with distilled water after filtering.

Expected results

No results were obtained at sea. To investigate the vertical and horizontal distribution of SPM filter samples will be analysed at GEOMAR. SPM filter data will be used to calibrate the transmissometer recordings from the CTD. In general, losses of light propagating through water can be attributed to two causes: scattering and absorption. By projecting a collimated beam of light through the water and placing a focused receiver at a known distance away, one can quantify these losses. The ratio of light gathered by the transmissometer's receiver to the amount originating at the source is known as the beam transmittance (Tr), which provides an indication of total.

Data management

Data will be stored in the PANGAEA data repository, and will be made publicly available.

8.4 Sea ice biology

Andreas Krell[2], Erika Allhusen[1], Irina Kryukova[3] [1]AWI
Ilka Peeken[1] (not on board) [2]KOWI
[3]SIO

Objectives

Sea ice associated communities play a major role in the cryo-benthic and cryo-pelagic coupling of the Arctic Ocean. The transition from the occurrence of multiyear ice (MYI) to the predominance of first year ice in the investigation area within the past decades and its implications on the sea ice community and associated ecosystem are not well understood.

As a contribution to the German BMBF-project Transdrift, we investigated the sea ice and under-ice algal communities in the Atlantic and the Pacific sector of the Central Arctic to compare these observations with historic data in order to discern long term changes in these habitats. Special emphasis will be placed on recent changes in the melt pond associated communities and their respective role in the Arctic carbon budget.

The impact of DOM and SPM on the optical properties of sea ice will be determined and related to ice algal biomass. The measurement of tracers in the sea ice will help to understand the history of the sampled ice floes. To understand the seeding processes of the sea ice algae, the biodiversity of new ice, particular from the Laptev Sea will be determined and compared to sea ice communities sampled along the transpolar drift in the framework of the Transdrift project.

Work at sea

The sampling of sea ice for biological properties (chapter 9) involved ice-core sections, under-ice water and meltpond water. The depth of the sampling under the ice was determined by CTD profiles and fluorescence probe measurements prior to the water sampling. On site, environmental parameters such as sea ice temperature, snow depth, free board and ice thickness were measured.

Ice core sections were melted in closed plastic barrels filled with 2 L of 0.2 µm filtered sea water at 4°C. Melted samples were subsequently split into 0.5 L aliquots for HPLC, fractionated Chl a and POC filtration. Remaining volumes were pooled into an upper and lower part of the core for analysis of PBSi, fractionated DNA and Utermöhl species enumeration.

Sections of the salinity core were left to melt at 15°C. Salinity was determined with a WTW 315i conductivity probe. The total volume of the melted section was measured and subsequently aliquots for nutrient and ^{18}O stable isotope analysis were taken. Remaining samples were again pooled into upper and lower part of the ice core and samples for cDOM and PABs analysis were taken.

Preliminary results

Average sea ice thickness of the cores was 120 cm and thus in the same range as that of biological FYI cores collected during the Transarc cruise in 2011 during the same season and region. Compared to 2011, when hardly any snow was present, we observed a ubiquitous snow cover on the sea ice. All melt ponds had a refrozen surface of up to 15 cm thickness, which during the second half of the cruise were also covered with snow.

Fig. 8.4.1 shows a typical sea ice salinity and temperature plot revealing an almost isothermal profile of temperatures ranging between -1,3°C and -2,5°C. The salinity profile reveals an

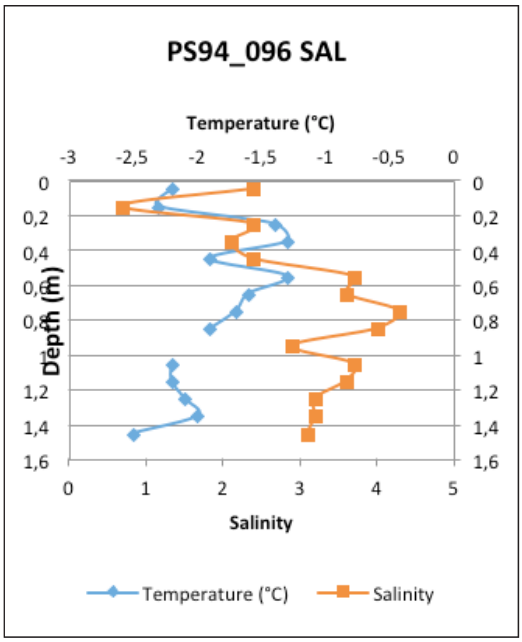

Fig. 8.4.1: Temperature and Salinity profile of an ice core (1.51m total length) taken at station PS94_096

elevated concentration on the surface which reflects brine expulsion after refreezing of the surface melt water, which again is reflected by extremely low salinity immediately below the surface. The remainder of the core shows typical Arctic sea ice salinities corresponding to the temperatures.

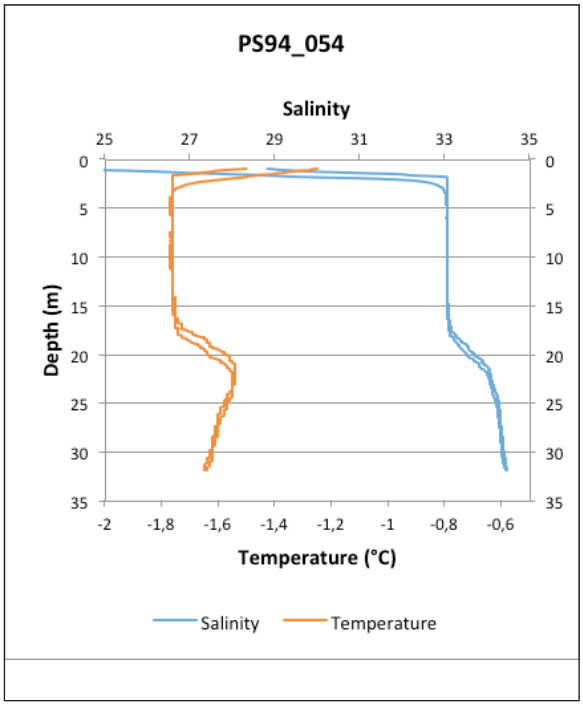

Fig. 8.4.2: Temperature and salinity profile of the upper 30 m of the water column below the ice at station PS94_054

Fig. 8.4.2 shows typical salinity and temperature profiles obtained with the SEA and SUN CTD deployed through an ice core hole. The strong temperature rise and low salinities in the top meter of the water column below sea ice is indicative of recent melting.

Filtered samples will be analysed for POC, HPLC, fractionated Chl a, fractionated DNA, PBSi and PABs and taxonomic species enumeration will be carried out at AWI.

Data management

Data will be stored at the PANGAEA data repository and will be made publicly available there within 2 years after the cruise.

9. BENTHIC BIOGEOCHEMISTRY

Ulrike Hanz[1], Joshua Kiesel[1], Heike Link[1], Karen von Juterzenka[1], Dieter Piepenburg[1,2], Christina Bienhold[3] (last four not on board)

[1] Uni Kiel
[2] AWI
[3] MPI

Grant No. AWI_PS94_00

Objectives

Current environmental changes are very likely to heavily impact the Arctic marine ecosystem, since warming in the northernmost latitudes is considered to be twice or three times the global rate (Wassmann et al., 2011). Nevertheless, research efforts have mostly focused on terrestrial ecosystems, while the marine ecosystem has often been neglected (Wassmann et al., 2011). Thus, in order to evaluate and assess current environmental changes, large-scale and long-term observations are required.

The benthos plays a major role in the marine ecosystem as it degrades and recycles a significant amount of organic matter that enters the seafloor from the euphotic zone (Link et al., 2013a; Link et al., 2013b). Benthic communities are strongly dependent on this carbon supply, which especially counts for deep sea communities (Boetius and Damm 1998). At the seafloor these resources will be either recycled by the local fauna, or stored in the sediment record. Re-mineralized nutrients will be redistributed in the water column and thus, are again available for primary production. However, benthic boundary fluxes are not stable and re-mineralization fluctuates according to season, functional diversity, ice cover, or eventually with changing environmental conditions (Link et al., 2013).

During PS94 we determined patterns of benthic ecosystem functioning by assessing benthic boundary fluxes among different temporal and spatial gradients. This was realized with the help of shipboard microcosm incubations, as well as additional porewater oxygen microprofiles and sediment samples taken for DNA, total organic carbon (TOC), chlorophyll, prokaryotic cell numbers (AODC) and enzymes. Additionally we tried to investigate the impact of benthic biodiversity and abundance on re-mineralization rate, by determining species counts and abundance of the communities we observed. Conclusive, the goal was the quantification of benthic ecosystem functioning under different resource and diversity patterns, while additionally comparing seasonal characteristics (in the Barents Sea), annual differences (central Arctic 2015 *vs* 2011/12 *vs* 1993), different sea-ice cover regimes and varying spatial gradients, namely shelf seas, slopes, mid oceanic ridges and deep sea basins. We thereby hope to assess possible impacts of steadily changing environmental conditions on arctic benthic ecosystems.

Work at sea

Benthic re-mineralization rate and oxygen consumption of benthic organisms was studied using ex-situ sediment core incubations and additional porewater oxygen microprofiles across the Arctic Ocean. Water depths ranged from 377 m in the Barents Sea to 4847 m in the Amundsen Basin. Sediment cores were obtained by deploying a multicorer that extracts 8 sediment cores from the seafloor. At *PS94-66-2, PS94-69-7* and *PS94-105-2* an additional boxcorer was deployed, since benthic topography was likely to cause harm to the more fragile multicorer.

Stations included deep sea basins, the Barents Sea, the Gakkel Ridge, the Lomonosov Ridge and the Karasik Mountain (see Fig. 9.1).

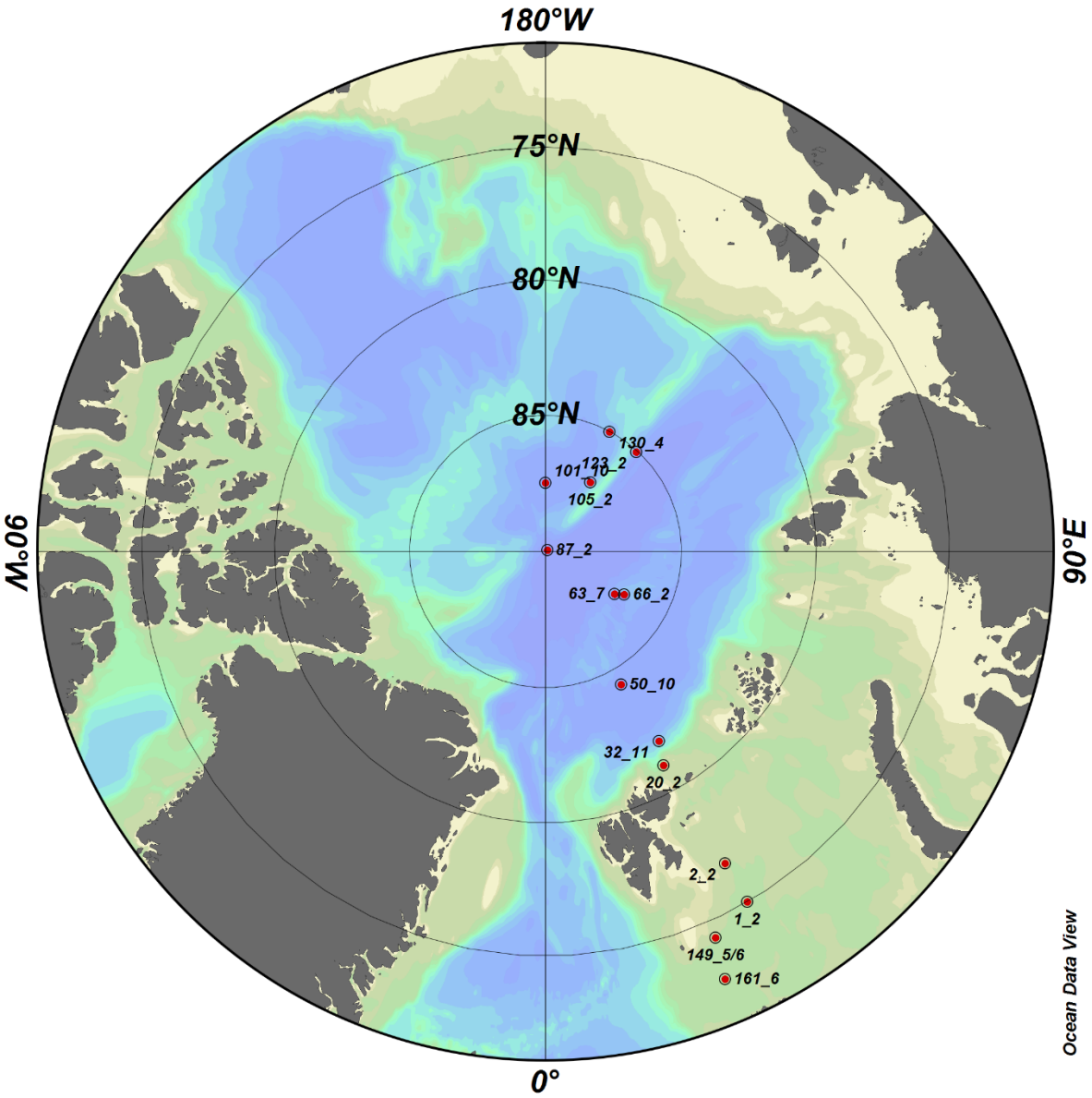

Fig. 9.1: MUC and box corer stations during PS94

Thereby we assessed diverse benthic environments of distinct ocean basins, mid oceanic ridges, continental slopes and shelf seas. This enables us to obtain a more detailed understanding of the arctic benthos among different spatial and temporal gradients, as well as varying sea ice conditions.

Tab.9.1: Station list during PS94

Station	Sampling Device	Date	Latitude	Longitude	Depth [m]	Sea ice coverage [%]	Incubat-ion	O_2 Profile	Micro-bio	Macro-fauna
1-2	MUC	18.08.2015	75°0,055`N	30°0,333`E	378	0	y	y	y	y
2-2	MUC	19.08.2015	76°40,579`N	30°0,213`E	273	0	y	y	y	y

Station	Sampling Device	Date	Latitude	Longitude	Depth [m]	Sea ice coverage [%]	Incubat-ion	O_2 Profile	Micro-bio	Macro-fauna
20-2	MUC	21.08.2015	80°59,762`N	28°58,324`E	377		n	y	y	y
32-10	MUC	22.08.2015	81°51,409`N	30°54,656`E	3164	99	y	y	y	y
50-10	MUC	27.08.2015		29°37,426`E	4000	99	n	y	y	y
66-2	GKG	01.09.2015	86°42,756`N	61°21,732`E	644	100	y	n	y	y
69-7	GKG	02.09.2015	87°1,106`N	58°16,327`E	4847	100	n	n	n	y
87-2	MUC	08.09.2015	89°55,482`N	120°33,864`E	4200	100	y	y	y	y
101-10	MUC	14.09.2015	87°29,807`N	179°54,151`E	3941	90	n	y	y	y
105-2	GKG	16.09.2015	86°58,665`N	146°50,676`E	973,4	90	y	y	y	y
123-2	MUC	22.09.2015	85°03,575`N	137°36,566`E	4048	95	n	y	y	n
130-4	MUC	24.09.2015	85°0,926`N	151°45,503`E	833	100	y	y	y	y
149-5/6	MUC	07.10.2015	74°19,132`N	23°48340`E	292	0	y	y	y	y
161-6	MUC	08.10.2015	72°44,062`N	22°49,248`E	385	0	n	y	y	n

After MUC retrieval, sediment cores were pushed onto a bottom lid and then pushed up with an extruder, so that water phase above the sediment had a width of about 15cm. Afterwards three cores have been directly taken to a temperature controlled water bath of 2°C, where two porewater oxygen microprofiles per core have been obtained. Thereby we will assess oxygen penetration depth and the diffusive oxygen uptake of the respective sediments. Profiles were carried out by using a micromanipulator that has been adjusted to a maximum depth of 6.5cm. Vertical resolution was 100µm and the distance between profiles varied between one- and two cm horizontally. After microprofiles have been successfully finished, sediment samples have been taken with cut and acid cleaned syringes from the respective cores, in order to test for microbiological parameters like AODC, chlorophyll, total organic carbon, enzymes and DNA. Samples have been immediately frozen at -20°C and will be analyzed by Christina Bienhold at the MPI in Bremen. Additionally, one core per station was sampled in order to analyze geochemical tracers like mercury, as it is described in the geotraces section of this cruise report by Lars-Eric Heimbürger.

Three further cores have been brought to a dark, temperature controlled room of 2 to 4°C, where shipboard microcosm incubations have been carried out. We will thereby assess the total sediment oxygen flux by using a non-invasive optical probe (Fibox 3 LCD, PreSens, Regensburg, Germany). Furthermore, nutrient samples of each respective core enable the assessment of re-mineralization rates of nitrate, silicic acid, phosphate and nitrite (Link et al., 2013a).

While working on sediment core incubations, we followed the methodology that has been introduced by Link et al., (2013a). Sediment cores were topped with a stirring motor that homogenized the water column above the sediment. Nutrient samples have been taken with acid cleaned syringes at three times during each incubation. The time of sampling has been synchronized with the rate of benthic oxygen uptake. At the onset of each incubation, sediment cores have been aerated with a bubbling device in order to ensure 100 % oxygen saturation. Then, the first nutrient sample has been taken. When oxygen levels have dropped by 10 %, midway nutrient sampling was conducted while the final sample has been taken when remaining oxygen concentration was at 80 %. This was done in order to prevent suboxic conditions and therefore chemical alterations during final nutrient sampling. After each syringe sample, the taken water has been filtered through Gf/f Whatman filters into 15 ml vials. Vials have been shock frozen at -80°C. After the third and final nutrient sample, syringes have been

taken from the sediments of each core, in order to test for chlorophyll- and phaeopigments, as they are considered indicators of fresh food supply (Link et al., 2013a). Sediment cores have been finally sieved under running seawater with 500 µm mesh size, in order to obtain macrofaunal diversity and abundance. Residues have been preserved in 4 % Formalin and will be analyzed in our home labs.

At stations *66-2* and *105-2* box corer were deployed as bottom topography was suspected to harm the multicorer. Directly after box corer retrieval, 6 subcores for porewater microprofiles and microcosm incubations, as well as syringes for microbiological sampling were pushed gently into the sediment. Afterwards, cores have been carefully topped with bottom water from the rosette, taken at the same station and were treated as described above.

At station *69-7* a boxcorer was deployed for conducting macrofaunal analysis in the vicinity of a hydrothermal vent on the Gakkel Ridge. Hence, a defined amount of sediment has been taken out of the corer and has been sieved over 500 µm, in order to obtain macrofaunal diversity and abundance. Residues have been preserved for later microscopic analysis in 4 % Formalin.

Preliminary results

Besides pore water oxygen microprofiles and benthic oxygen consumption of microcosm incubation sediments, no further results have yet been obtained.

Nevertheless, we expect significant correlations between water depth, sea ice cover and ecosystem functioning in terms of benthic boundary fluxes. This has been indicated before by Boetius and Damm (1998) who wrote that ice cover as well as an increase in water depth strongly reduces abundance and activity of benthic organisms. We additionally hypothesize that sediment oxygen fluxes differ significantly among water depth and the method that has been used. We will therefore compare fluxes derived either from porewater microprofiles (diffusive flux) or from the non-invasive optical probe (total flux), which we have used during the incubations.

Data management

Data archival will be mainly hosted by the information system PANGAEA at the World Data Center for Marine Environmental Sciences (WDC-MARE), which is operated by the Alfred Wegener Institute for Polar and Marine Research, Bremerhaven and the MARUM, Bremen. As soon as data on geotracers, nutrient re-mineralization, oxygen fluxes and microbiological parameter are available, we will submit the respective data to PANGAEA and protect these via a password. Macrofaunal samples are fixed and will be stored at the GEOMAR in Kiel.

References

Boetius A, Damm E (1998) Benthic oxygen uptake, hydrolytic potentials and microbial biomass at the Arctic continental slope. Deep-Sea Research, 45, 239-275.

Link H, Piepenburg D, Archambault P (2013a) Are Hotspots Always Hotspots? The Relationship between Diversity, Resource and Ecosystem Functions in the Arctic. PLoS ONE, 8 9, 1-18.

Link H, Chaillou G, Forest A, Piepenburg D, Archambault P (2013b) Multivariate benthic ecosystem functioning in the Arctic – benthic fluxes explained by environmental paramteres in the southeastern Beaufort Sea. Biogeosciences, 10, 5911-5929.

Wassmann P, Duarte CM, Agustí S, Sejr MK (2011) Footprints of climate change in the Arctic marine ecosystem. Global Change Biology, 17, 1235-1249.

10. METHANE AND DMS IN SEA ICE AND SEA WATER

Ellen Damm[1], Christiane Uhlig[1], Elena Vingradova[2] Gerhard Dieckmann[1]

[1]AWI
[2]SIO

Grant No. AWI_PS94_00

Objectives

Summer sea ice retreat alters water mass formation and convection, which may have profound effect on natural biogeochemical cycles between sea ice and seawater. Especially feedback effects to pathways of climatically relevant trace gases will loom large in the equation of change. Increasing water stratification during sea ice melting is likely to limit nutrient availability in near-surface water, which in turn hampers the enhancement of primary production. A characteristic feature of the Arctic Ocean is the distinct post-bloom nutrient limitation found in the Atlantic-dominated and Pacific-dominated sectors. Nutrient limitation may be also a possible regulator of methane production in surface water. Methanogens form methane via various pathways commonly classified with respect to the type of carbon precursor utilized, e.g. the methylothrophic pathway indicates the intact conversion of a methyl group to methane. The contribution of methylated substrates is potentially large in sea ice, and methylothrophic methanogenis may be a principal pathway from which methane is readily formed by microbial activity. However, the direct evidence of this role of methylated substrates in sea ice is still lacking. In this context the degradation of dimethylsulfoniopropionate (DMSP), an abundant methylated substrate in surface water and sea ice becomes pivotal. DMSP is produced by marine phytoplankton and sea ice algae. Cleavage of DMSP can be carried out by bacteria or by phytoplankton, and leads to formation of DMS (dimethylsulfide) or methanethiol. DMS, an important climate-cooling gas, partly escapes to the atmosphere where it is oxidized to sulphuric acid and methanesulfonic acid. Methanethiol is a key reactive intermediate utilized as sulphur and carbon sources for biosynthesis or energy generation. In anaerobic environments methanethiol act also as precursor for methane production. Our goal is to trace methane cycle between sea ice and sea water, to distinguish the different degradation pathways of DMSP and subsequently to quantify the formation of DMS, methanthiol and methane.

To gain a better understanding on the possible formation of methane from the substrate DMSP we will additionally conduct incubation experiments. Different treatments will be set up by adding DMSP and varying nutrient concentrations to melted sea ice or sea water collected with Niskin bottles. During the experiments DMSP, DMS, methanethiol and methane will be measured on board. Bacterial abundance and community composition (16S) as well as DMSP degradation pathways (degradation genes) will be analysed in the home laboratory. Some of the experiments will be conducted with ^{13}C-labeled DMSP to track the DMSP-derived methyl groups.

Work at sea

Methane, DMS and DMSP were immediately measured on board ship, using gas chromatographs equipped with a flame ionization detector (FID) and a pulsed flame photometric detector (PFPD), respectively. Methane gas samples were stored for analyses of the $\delta^{13}C_{CH4}$ values in the home laboratory.

Water samples for methane analysis have been collected at 50 stations distributed along all hydrographic transects. Samples were taken from Niskin bottles mounted on a rosette

sampler at discrete depths throughout the water column at least up to 200 m and on selected stations up to 500 m water depth. On transect 2 stations 68, 69 and 70 methane concentration was measured up to the bottom. The number of sampling depths varied as a function of the fluorescence signal and the O2- sensor signal.

Water samples for DMS and DMSP analysis have been taken from Niskin bottles at discrete depths up to 100 m. Samples for DMS analysis were carefully alliquoted in glass vials, crimped and measured immediately by gas chromatography equipped with a pulsed flame photometer (PFPD) and a purge and trap system. DMSP measurements have been conducted on the same samples. The vials were opened again and 2 ml sodium hydroxide solution was added. After alkaline cleavage the DMSP was measured with the same procedure as DMS.

Ice cores have been taken on 8 ice stations and at 3 mummy chair stations (see coring site documentation). The complete ice cores were returned to the vessel into the cold (-25°C) container where they were sectioned into 10 cm slides. One half of each slide was used for the measurement of methane concentration and the other one for the analysis of DMS and DMSP concentration. For DMS and DMSP measurement a subsample of 10 cm length and a cross section of 5x5 mm was cut from the middle half slide. This long rectangle was put in a glass vial and immediately crimped with rubber lids in the cold container. When the ice in the vials was melted DMS was measured with a gas chromatograph (Varian 450) equipped with a pulsed flame photometer (PFPD) and a purge and trap system. After DMS analysis the glass vials were opened again to add 2 ml sodium hydroxide solution to the melted ice. Two hours after closing the vials, the DMSP measurement were performed by the same procedure like for DMS. After measurement the exact volumes of the ice samples were determined.

The second half of the slides were putted in a gas tight bag (Kynar bags with polypropylene 2-in 1-valve by Keikaventures) and closed. Subsequent the air was removed by using a vacuum pump. The melted water was filled into 100 ml glass vials where a 20 ml headspace was created after the vials were crimped. The glass vials were shaken for equilibration at least half an hour before retrieving a sample from the headspace with a syringe.

To gain a better understanding on the microbial processes involved in DMSP conversion to DMS and possibly methane, incubation experiments were performed on board. On six different stations (Table 10.1) sea water or sea ice cores were collected. The ice core was crushed to small pieces inside a plastic bag using a hammer. The ice was melted in the under ice water sampled at the same station over night at +5°C. The sea water and melted ice was distributed in the experimental bottles. Incubations were run for up to two weeks at 0°C temperatures in constant light or dark. Control bottles were incubated without any additions in the light. Treatment bottles were spiked with different concentrations of DMSP and a combination of DMSP and NADPH (ß-Nicotinamide Adenine Dinucleotice Phosphate Reduced Form Tetra(Cyclohexylammonium) Salt) hydrogen donor. Experimental bottles were kept closed and gas tight during the course of the experiment. Gas and liquid samples for all parameters shown in Table 10.2 were taken with syringes through a septum in the lid of the bottles, except for the final sampling when the bottle was opened for the liquid sampling. Methane from the headspace as well as DMS and DMSP from the liquid phase were measured directly on board using gas chromatographs equipped with a flame ionization detector (FID) and pulsed flame photometric detector (PFPD), respectively. Samples for the other parameters were fixed and stored at the desired temperatures for later analysis in the home laboratory. Samples for molecular biology were collected onto 0.2 µm Sterivex filtration cartridges filters.

Water from CTDs PS95/105, PS94/117 and PS94/125, will be transported back for further experiments. Additionally, this water was used to prepare enrichment cultures with DMSP, methanol and methylphosphonic acid as substrate. These will be used to isolate strains able to degrade the respective substrates.

Tab. 10.1: Sea ice sampled for microbial incubation experiments

Station	Sample type	comment	Experiment
PS94/34-1	CTD bottles 23+24	5+10m depth	1
PS94/81	sea water + sea ice	under ice water sampled with Kemerer-bottle, bottom 10 cm from 13cm core	2
PS94/101-8	Ultra clean CTD	20m depth	3
PS94/105-1	CTD bottle 22	10m depth	4
PS94/117-6	CTD bottle 11	10m depth	5
PS94/125-7	CTD bottle 7+9	30m depth, cDOM max	6
PS94/125-7	CTD bottle 17	10m depth	7

Tab.10.2: Parameters that were or will be measured on board or in the home laboratory. Except for methane all parameters were determined from the liquid phase.

On board	**Experiment**
Methane (headspace)	1, 2, 4, 5, 6, 7
DMS and DMSP	1, 2, 3
Nutrients (Silikate, Nitrate, Nitrite, Phosphate)	1, 2, 4-7 (only start)
Home laboratory[1]	
Living samples (liquid)	1, 2, 4-7 (only start)
Total counts (bacteria)	1, 2, 4-7 (only start)
Bacterial diversity (Fluorescence-*in-situ*-hybridization, 16S sequencing, denaturing gradient gel electrophoresis)	1, 2, 4-7 (only start)
DMSP conversion genes (qPCR)	1, 2, 4-7 (only start)
Enrichment cultures	4-7 (from start community)

[1]Processing of these samples in the home laboratory are subject to funding and will start in 2017.

Preliminary results

Methane in sea water and sea ice

In the study area, methane concentrations are heterogeneous and correspond to both a clear under-saturation and a clear super-saturation with respect to the atmospheric equilibrium concentration. The equilibrium concentration is calculated as a function of the gas solubility on the basis of the measured temperature and salinity properties and varies between 3.2 to 3.9 nM. Methane super-saturation was detected in surface water at all transects (Fig.10.1). Methane under-saturation was often revealed below the halocline except for transect 1 and 4. At transect 1 enhanced methane concentration was detected in inflowing Atlantic water between 100 and 400 m water depth (Fig.10.2).

In most ice cores (10) methane concentrations varied between 2.1 and 8.5 nM. In one ice core methane concentration was clearly below this range (0.2-1.8 nM) and in one ice core clearly above this range (3.3-55.1nM).

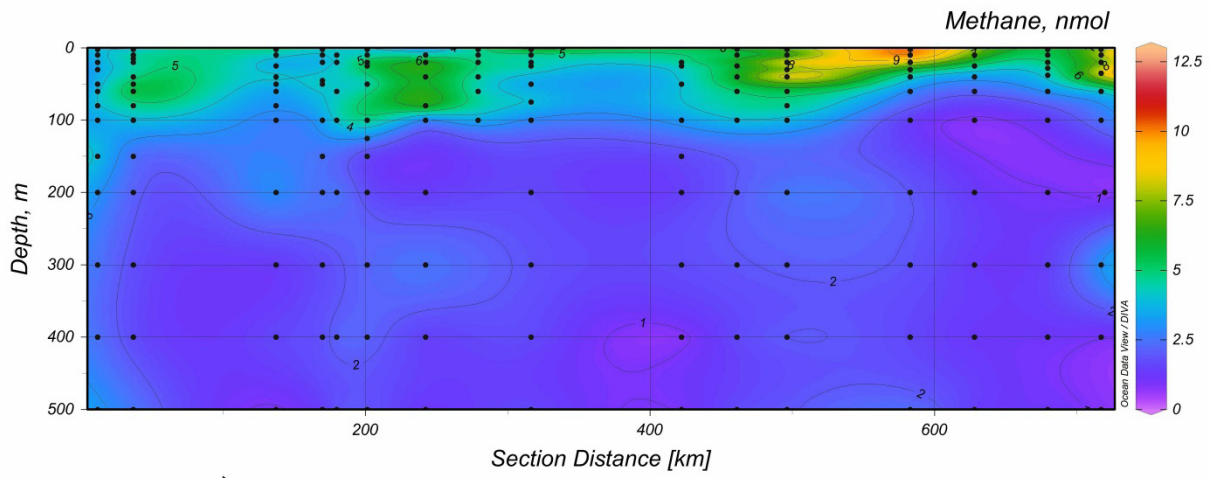

Fig.10. 1: Methane concentration at transect 2

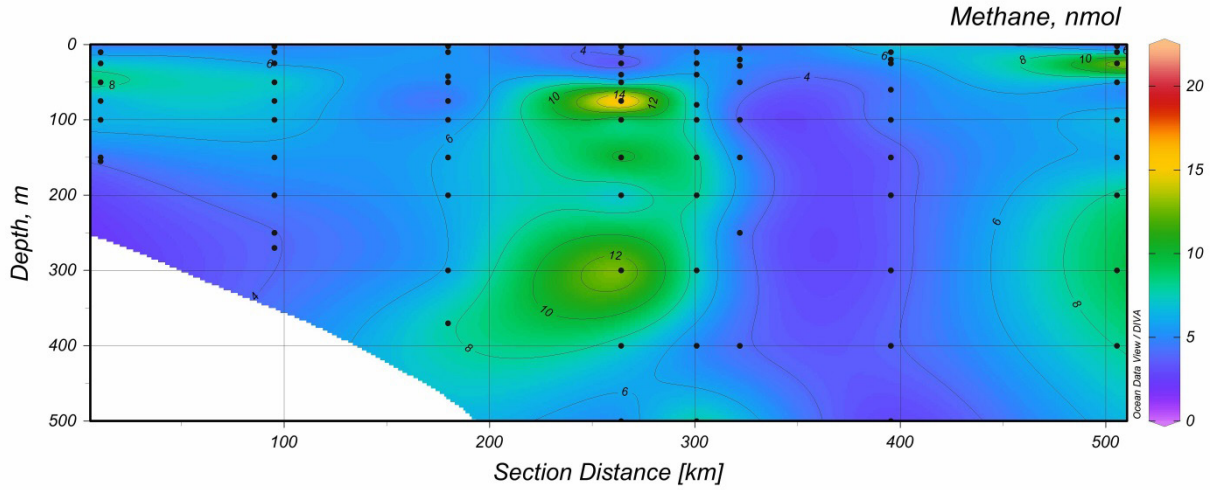

Fig. 10. 2: Methane concentration at transect 1

DMS and DMSP concentrations in sea water and sea ice

DMS and DMSP concentrations are highest on transect 1 and decrease on transects 2 and 3 while both components remain correlated. A mismatch between DMS and DMSP is present at transect 4 which means that DMS concentrations continue to be as low as at transect 3 but DMSP concentrations increase (Fig. 10.3)

Concentrations are significantly higher in ice cores than in seawater.

In general concentrations are highest at the bottom of sea ice and DMS and DMSP are correlated in most ice cores. However, there also exists a mismatch between the two in some ice cores.

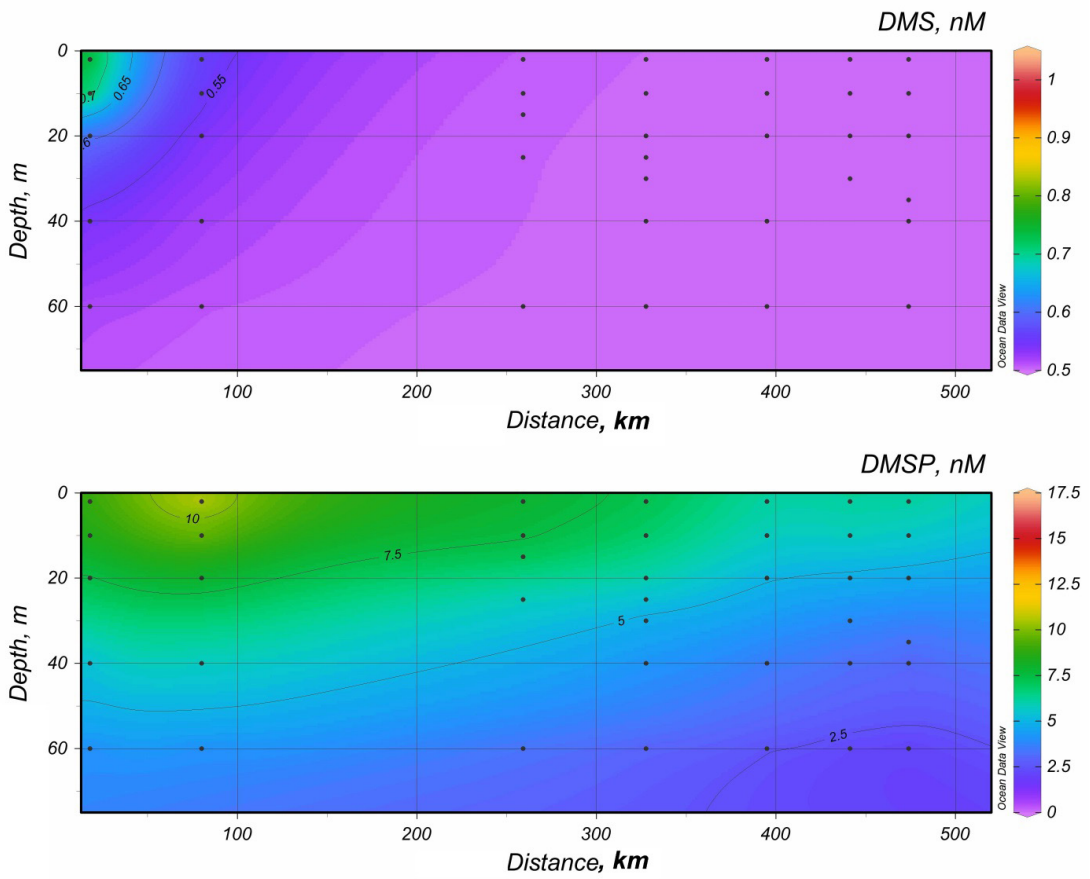

Fig. 10.3 DMS and DMSP concentration at transect 4

Experiments

The experiment with water from station PS81/34 first showed an increase in DMSP levels in the treatments and control which was followed by a decrease. DMSP in the controls was low and DMS was close to the detection limit. Methane formation was not detected. The seawater used for the first experiments was depleted in nutrients.

In the second experiment (sea ice and under ice water PS94/81) we observed DMSP degradation with simultaneous DMS formation in the control as well as DMSP and DMSP-plus-NADPH spiked treatments. Methane concentrations did not differ between controls and treatments. Sea water used for this experiment was depleted in nitrate and had low phosphate levels (0.2 µM).

The third experiment was a contribution to a mercury spike experiment with seawater from 20 m depth from the ultra clean CTD by Lars-Eric Heimbürger. Only DMS and DMSP were measured in this experiment. Due to the short incubation time of only 24h only a very small increase in DMS concentration was observed.

Experiments 4 to 7 were set up in 125 mL crimp-top bottles to only follow methane concentrations. In all experiments methane concentrations were decreasing over time indicating methane oxidation. Clear differences between controls, treatments with addition of DMSP or incubation in the dark were not observed. Few data points indicate slightly higher methane oxidation in DSMP-spiked bottles and in light compared to dark incubations.

Data management

All data collected during the expedition will be stored in the PANGAEA data repository at the AWI within three years after the cruise.

11. SEA ICE FIELD WORK FOR GEOCHEMISTRY AND BIOLOGY

Andreas Krell[1], Erika Allhusen[2], Irina Kryukova[3], Gerhard Dieckmann[2], Christiane Uhlig[2], Elena Vinogradova[3], Ellen Damm[2]

[1]KOWI
[2]AWI
[3]SIO

Grant No. AWI_PS94_00

Sea ice coring and under-ice sampling was carried out in a coherent way for the groups "Production and Cycling of Climate Relevant Trace Gases" (chapter 10) and ART (chapter 8). In addition ice cores and under ice water samples were taken for various other groups and/or parameters. In this chapter the sea ice coring and processing on the ice is documented. Scientific objectives and further processing for individual parameters is described in the respective chapters accordingly.

Work at sea

Ice station summary

11 ice stations were sampled during PS94. 8 were full-length ice stations of more than 6 hours duration and 3 were mummy-chair stations (Table 11.1).

Table 11.1: List of sea ice stations sampled, mc=mummy chair

Station Nr.	Date	Latitude	Longitude
PS94-046	2015.08.25	83.7163	30.3775
PS94-054	2015.08.28	85.086	42.6052
PS94-069	2015.09.02	87.0068	58.6628
PS94-081	2015.09.05	88.9857	60.9663
PS94-096	2015.09.11	88.3607	-125.1147
PS94-098mc	2015.09.12	88.3385	-144.315
PS94-101	2015.09.14	87.5007	179.8043
PS94-107mc	2015.09.16	86.6297	133.8762
PS94-112mc	2015.09.17	85.2148	118.395
PS94-117	2015.09.19	84.4875	115.718
PS94-125	2015.09.22	85.0808	139.9132

Sea ice cores were retrieved using a standard 9 cm Kovacs ice corer, driven by a Makita powerhead. The cores were subsequently processed according to and depending on the requirements for the different parameters to be analyzed (Table 11.2). Some cores were sectioned on-site for bulk ice measurements using a stainless steel butcher's saw. Full-length cores for different parameters were placed in plastic tubing and returned to the ship's cold storage room. CTD depth profiles down to 40 m were conducted through the ice holes and water samples were taken directly under the ice (immediately underneath the ice and at the chlorophyll maximum) using a Kemmerer bottle. Meltponds were sampled where present.

Attempts were made to collect sea-ice brine from sackholes, but failed due to the high porosity of the sea-ice which caused immediate flooding of the sack holes with water from below.

Table 11.2: List of parameters to be analyzed and responsible scientists

Parameter	For scientist	Responsible PI
Methane	Ellen Damm/ Christiane Uhlig	Ellen Damm
DMSP, DMS	Ellen Damm/ Christiane Uhlig	Ellen Damm
Archive	Ellen Damm	Ellen Damm
Texture, temperature	Ilka Peeken	Ilka Peeken
POC, HPLC, Chl a, DNA, PBSi, Taxonomy	Ilka Peeken	Ilka Peeken
Neodym	Georgi Laukert	Ilka Peeken
Salinity, nutrients, PABs	Ilka Peeken	Ilka Peeken
^{18}O	Dorothea Bauch	Dorothea Bauch
Microplastics	Gunnar Gerdts	Ilka Peeken
DIC	Elisabeth Jones	Micha Rijkenberg/ Leif Anderson
Hg, Hg species	Lars-Eric Heimbürger	Ellen Damm
cDOM/DOC	Heather Reader	Ilka Peeken/Dorothea Bauch
^{236}U, ^{129}I	Núria Casacuberta	Michiel vd Loeff
Trace metals	Aridane G. Gonzalez	Micha Rijkenberg
Argon, N_2O	Bruno DeLille	Ellen Damm

Preliminary results

On-site processing

A total of 13 to 15 cores were taken at each coring site of the full-length ice stations. A thorough site description was carried out and entailed ambient air temperature, snow temperature, snow depth, ice conditions and weather conditions. The first core was taken to record temperature at 5 cm intervals by drilling 4 mm holes to the centre of the core and inserting a Testo 720 temperature probe. Cores for biological parameters, salinity, DIC and methane were sawed into 10 cm sections and placed in plastic containers or in the case of methane, in specially sealed plastic bags. All other cores were placed into plastic tubes, sealed with cable ties and taken on board for either storage or in case of DMS for further processing in the freezer lab.

Kemmerer water samplers were deployed through the core holes for water samples for analyses corresponding to the ice core analyses.

At the first 4 stations ice and snow covered meltponds were present in the later course of the cruise no discernible meltponds were found. Sampling of meltponds included the measurement of temperature, salinity, meltpond depth and thickness of the ice cover. Meltpond water was sampled for the same parameters as on the sea ice cores.

On-board processing

For textural analysis 5 mm thick sections were cut from the DMS core in the cold container using a band saw, cleaned and photographed against a black background.

12. OVERVIEW OF PARAMETERS ANALYSED FROM ROSETTE SAMPLES

TransARCII

Participation GEOTRACES

Berth	Name	PI-Transarc	Function	Institute	parameters
1	Michiel Rutgers van der Loeff	Michiel vd Loeff	scientist	AWI	Radium isotopes, 228Th
2	Ole Valk (PhD Michiel vd Loeff)	Michiel vd Loeff	PhD Student	AWI	230Th/231Pa
3	Viena Puigcorbe	Michiel vd Loeff	scientist	Uni Barcelona	234Th
4	Nuria Casacuberta	Michiel vd Loeff	scientist	Uni Barcelona	210Pb/210Po, 129I, 236U
5	Ronja Paffrath (PhD Katharina Pahnke)	Katharina Pahnke	PhD Student	Uni Oldenburg	REE, Nd isotopes
6	Sandra Gdaniec	Michiel vd Loeff	PhD Student	Uni Stockholm	230Th/231Pa
7	Michael Staubwasser	Michael Staubwasser	scientist	Uni Köln	trace metal isotopes
8	Lars-Eric Heimburger	Lars-Eric Heimburger	scientist	Bremen	Hg
9	Adam Ulfsbo	Leif Anderson	scientist	Uni Gothenburg	CO2
10	Micha Rijkenberg	Micha Rijkenberg	scientist	NIOZ	trace metals
11	Loes Gerringa	Micha Rijkenberg	scientist	NIOZ	FeL
12	Hans Slagter	Micha Rijkenberg	PhD Student	NIOZ	FeL
13	Aridane Gonzales	Micha Rijkenberg	France	NIOZ	part trace metals
14	Sven Ober	Micha Rijkenberg	technician	NIOZ	ultraclean CTD
15	Jan van Ooijen	Micha Rijkenberg	technician	NIOZ	nutrients
16	Elisabeth Jones	Micha Rijkenberg/Leif Anders	scientist	NIOZ/UK	CO2 and oxygen (Winkler)
17	Daniel Scholz	Michiel vd Loeff	technician	AWI	sensors

ancillary data					
	Dorothea Bauch	Dorothea Bauch	scientist	GEOMAR	18O

samples will be collected for:				
name		sampling by		parameters
Raja Ganeshram	Michiel vd Loeff	UCC team		N and O isotopes in nitrate
Wafa Abouchami and Stephen Galer	Micha Rijkenberg	UCC team		Cd, Pb, Cr isotopes
Boaz Luz	Michiel vd Loeff	Dorothea Bauch		triple oxygen
Claudia Ehlert	Katharina Pahnke	Ronja Paffrath		Si isotopes
Bill Smethie	Michiel vd Loeff	Oceanography / Geotraces		CFC
Dennis Hansell, Rainer Amon	Ilka Peeken/Colin Stedmon	UCC team or Colin Stedmon		DOC, CDOM, lignin
Peter Croot	Micha Rijkenberg	NIOZ team		dissolved Ti

13. SEMINARS

The following talks were given in the seminar „TransArc II lectures“.

Michael Staubwasser (UNIK):	Isotope composition of dissolved and particulate Fe
Michiel Rutgers van der Loeff (AWI):	Tracers of river and shelf inputs in the Trans-Polar Drift
Dorothea Bauch (GEOMAR):	Freshwater sources in the Arctic Ocean: Stable oxygen isotopes of the water as tracer of Siberian shelf waters
Joshua Kiesel (CAU):	Dynamics and Spatial Variation of Intertidal Seagrass Beds in the Northern Wadden Sea
Loes Gerringa (NIOZ):	Iron in the Ross Sea Polynya
Aridane Gonzalez (IUEM):	The effect of organic exudates on the Fe redox chemistry
Micha Rijkenberg (NIOZ):	Iron in the Arctic Ocean
Franz Schröter (AWI):	Ecuador – Land der Extreme, Teil 1
Ursula Schauer (AWI):	TransArc II – dem arktischen Wandel auf der Spur
Myriel Horn (AWI):	Links between the freshwater budgets of the Arctic Ocean and the subpolar North Atlantic
Nuria Casacuberta (LIP):	U-236 and I-129 in the Arctic Ocean
Stefan Hendricks (AWI):	Die Vermessung von Meereis
Sergey Pisarev (SIO):	Russian seasonal ice camp *Barneo*
Ulrike Hanz (CAU):	Structure of benthic communities from the Kattegat in relation to environmental drivers and historical data
Dorothea Bauch (GEOMAR):	Source waters of the lower halocline
Benjamin Rabe (AWI):	Arctic Ocean circulation – incl. preliminary results from PS94
Robert Ricker (AWI):	Arctic Sea Ice Thickness derived from CryoSat-2
Gerhard Dieckmann (AWI):	Von Plättcheneis zu grünen Eisbergen
Ursula Schauer (AWI)	Using *Polarstern* for observational polar science
Ksenia Kosobokova (SIO):	Wonderworld of Zooplankton
Franz Schroeter (AWI):	Ecuador, Teil 2: Amazonien und Galapagos
Michael Staubwasser (Uni Köln)	Climate change and ancient civilisations
Ellen Damm (AWI)	Sea ice – a blackbox for Arctic methane cycling

Ole Valk (AWI)	230Th and 231Pa, tracer for particle fluxes and deep water circulation in the Arctic Ocean
Nicole Hildebrandt	Zooplankton-Zusammensetzung in der Framstraße im Licht des Klimawandels (+ LOKI-Fotos)
Heather Reader (NTU)	Dynamics of dissolved organic matter
Larysa Istomina (IUB)	All you wanted to know about melt ponds but never dared to ask
Andreas Krell (KOWI)	EU Funding opportunities for early career scientists"
Lars-Eric Heimbürger (UB)	Mercury in the Arctic Ocean Hans Slagter (NIOZ) Catching the players in the iron game of catch"
Ronja Paffrath (ICBM)	Rare Earth Elements in pore water from Spiekeroog Island
Elisabeth Jones (UGro)	Rothera research station: life, science and a little CO_2 chemistry

APPENDIX

A.1 PARTICIPATING INSTITUTIONS

A.2 CRUISE PARTICIPANTS

A.3 SHIP'S CREW

A.4 STATION LIST

A.1 TEILNEHMENDEINSTITUTE/PARTICIPATINGINSTITUTIONS

	Address
AWI	Alfred-Wegener-Institut Helmholtz-Zentrum für Polar- und Meeresforschung Postfach 120161 27515 Bremerhaven, Germany
CAU	Institute for Ecosystem Research of Kiel University Christian-Albrechts-Universität zu Kiel Olshausenstr. 75 24118 Kiel, Germany
DTU	Technical University of Denmark National Institute of Aquatic Resources (AQUA) Kavalergården 6, 2920 Charlottenlund, Denmark
DWD	Deutscher Wetterdienst, Geschäftsbereich Wettervorhersage Seeschifffahrtsberatung Bernhard-Nocht-Straße 76 20359 Hamburg, Germany
FMI	Finnish Meteorological Institute PL 503 00101 Helsinki, Finland
GEOMAR	GEOMAR Helmholtz Centre for Ocean Research Kiel Wischhofstr. 1-3 D-24148 Kiel, Germany
HeliService	HeliService International GmbH Gorch-Fock-Straße 103 26721 Emden, Germany
HUJ	Institute of Earth Sciences The Hebrew University of Jerusalem Jerusalem 91904, Israel
ICBM	Max Planck Research Group for Marine Isotope Geochemistry Institute for Chemistry and Biology of the Marine Environment University of Oldenburg Carl-von-Ossietzky-Straße Oldenburg, Germany

	Address
IUEM	LabexMer – LEMAR, Technopole Brest Iroise Place Nicolas Copernic F - 29280 Plouzane, France
KoWi	Kooperationsstelle EU der Wissenschaftsorganisationen Rue du Trône 98 1050 Bruxelles, Belgium
LDEO	Lamont-Doherty Earth Observatory Department of Geochemistry 61 Rt. 9W Palisades, NY 10964, USA
LIP	Laboratory of Ion Beam Physics ETH-Zürich Otto-Stern-Weg 5 8093 Zürich, Switzerland
LOCEAN	Université Pierre et Marie Curie) Tour 45-46 5E 4 place Jussieu 75005 Paris, France
LSCE	Laboratoire des Sciences du Climat et de l'Environnement Université Paris-Saclay CNRS - LSCE-bât 12 Avenue de la Terrasse 91198 Gif-sur-Yvette cedex, France
MIO	CNRS/Mediterranean Institute of Oceanography Chemin de la Batterie des Lions 13007 MARSEILLE, France
MPI	Max Planck Institute for Marine Microbiology Celsiusstrasse 1 28359 Bremen, Germany
MPIM	Max Planck Institut Mainz Hahn-Meitnerweg 1 55128 Mainz, Germany
NIOZ	Royal Netherlands Institute for Sea Research ‘t Horntje Texel, the Netherlands

	Address
SIO	P.P. Shirshov Institute of Oceanology, Nakhimovskiy prospekt, 36, Moscow, 117997, Russia
SMNH	Swedish Museum of Natural History, Department of Geosciences Frescativägen 40 Stockholm, Sweden
UAB	Universitat Autònoma de Barcelona, Institut de Ciència i Tecnologia Ambientals & Department of Physics 08193-Cerdanyola del Vallès, Spain
UAIB	University of Alberta 1-26 Earth Sciences Building Edmonton, Alberta, T6G 2E3, Canada
UB	University of Bremen, Geochemistry and Hydrogeology, Department of Geosciences, Klagenfurter Straße 28359 Bremen, Germany
UE	School of GeoSciences, University of Edinburgh Sir James Hutton Road Edinburgh, UK, EH9 3FE
UGOT	Department of Chemistry & Molecular Biology, University of Gothenburg, Medicinaregatan 9 c 40530 Göteborg, Sweden
UGR	Centre for Energy and Environmental Sciences, University of Groningen, Nijenborgh 49747 AG Groningen, The Netherlands
UNIK	Institute of Geology and Mineralogy, University of Cologne Greinstraße 4-6 Köln, Germany

A.2 FAHRTTEILNEHMER / CRUISE PARTICIPANTS

Name/ Last name	Vorname/ First name	Institut/ Institute	Beruf/ Profession
Schauer	Ursula	AWI	Chief scientist, Phys. Oceanography
Alhusen	Erika	AWI	Technician, Biogeochemistry
Bauch	Dorothea	GEOMAR	Scientist, Geochemistry
Beckers	Justin	AWI	PhD student, Sea Ice Physics
Casacuberta	Nuria	LIP	Scientist, Geochemistry
Damm	Ellen	AWI	Scientist, Biogeochemistry
Dieckmann	Gerhard	AWI	Scientist, Biogeochemistry
Gdaniec	Sandra	SMNH	PhD Student, Geochemistry
Gerringa	Loes	NIOZ	Scientist, Geochemistry
Gonzalez	Aridane	IUEM	Scientist, Geochemistry
Graupner	Rainer	AWI	Technician, Phys. Oceanography
Hampe	Hendrik	AWI	Student, Phys. Oceanography
Hanz	Ulrike	CAU	Student, Biology
Heim	Thomas	HeliService	Technician
Heimburger	Lars-Eric	UB	Scientist, Geochemistry
Hempelt	Juliane	DWD	Technician, Meteorology
Hendricks	Stefan	AWI	Scientist, Sea Ice Physics
Hildebrandt	Nicole	AWI	Scientist, Biology
Hoppmann	Mario	AWI	Scientist, Phys. Oceanography
Horn	Myriel	AWI	PhD Student, Phys. Oceanography
Istomina	Larysa	AWI	Scientist, Sea Ice Physics
Jager	Harold	HeliService	Pilot
Jenkins	Hazel Hartman	AWI	PhD student, Sea Ice Physics
Jones	Elisabeth	NIOZ	Scientist, Geochemistry
Kiesel	Joshua	CAU	Student, Biology
Köhler	Vanessa	AWI	Student, Biology
Korhonen	Meri	FMI	PhD student, Phys. Oceanography
Kosobokova	Ksenia	SIO	Scientist, Biology
Krell	Andreas	KOWI	Scientist, Biogeochemistry
Kryukova	Idrina	SIO	Scientist, Sedimentology
Miller	Max	DWD	Scientist, Meteorology
Ober	Sven	NIOZ	Technician, Geochemistry
Paffrath	Ronja	ICBM	PhD Student, Geochemistry
Petersen	Imke	AWI	Student, Biology

Name/ Last name	Vorname/ First name	Institut/ Institute	Beruf/ Profession
Pisarev	Sergey	SIO	Scientist, Phys. Oceanography
Puigcorbe	Viena	UAB	Scientist, Geochemistry
Rabe	Benjamin	AWI	Scientist, Phys. Oceanography
Reader	Heather	DTU	Scientist, Biology
Richter	Roland	HeliService	Technician
Ricker	Robert	AWI	Scientist, Sea Ice Physics
Riedel	Juliane	AWI	Student, Biology
Rijkenberg	Micha	NIOZ	Scientist, Geochemistry
Rutgers van der Loeff	Michiel	AWI	Scientist, Geochemistry
Savy	Jean-Philipe	LOCEAN	Scientist, Phys. Oceanography
Scholz	Daniel	AWI	Technician, Biochemistry
Schröter	Franz	AWI	Student, Biology
Slagter	Hans	NIOZ	PhD Student, Geochemistry
Staubwasser	Michael	UNIK	Scientist, Geochemistry
Uhlig	Christiane	AWI	Scientist, Biogeochemistry
Ulfsbo	Adam	UGOT	Scientist, Geochemistry
Valk	Ole	AWI	PhD Student, Geochemistry
Van Ooijen	Jan	NIOZ	Technician, Geochemistry
Villacieros Robineau	Nicolas	LOCEAN	Scientist, Phys. Oceanography
Vaupel	Lars	HeliService	Pilot
Vinogradova	Elena	SIO	Scientist, Biogeochemistry

A.3 SCHIFFSBESATZUNG / SHIP'S CREW

No.	Name	Rank
1	Schwarze, Stefan	Master
2	Pohl, Klaus	Doctor
3	Langhinrichs, Moritz	Chief Mate
4	Hering, !gor	2nd Mate
5	Lauber, Felix	2nd Mate
6	Peine, Lutz G.	2nd Mate
7	Farysch, Bernd	Chief Eng.
8	Grafe, Jens	2nd Eng.
9	Krinfeld, Oleksandr	2nd Eng.
10	Holst, Wolfgang	3rd Eng.
11	Redmer, Jens	E Eng.
12	Fröb, Martin	Chief ELO
13	Christian, Boris	ELO
14	Himmel, Frank	ELO
15	Hüttebräucker, Olaf	ELO
16	Nasis, !lias	ELO
17	Loidl, Reiner	Boatsw.
18	Reise, Lutz	Carpen.
19	Bäcker, Andreas	A.B.
20	Brickmann, Peter	A.B.
21	Brück, Sebastian	A.B.
22	Hagemann, Manfred	A.B.
23	Michaels, Jürgen-Dieter	A.B.
24	Scheel, Sebastian	A.B.
25	Wende, Uwe	A.B.
26	Winkler, Michael	A.B.
27	Preußner, Jörg	Storek.
28	Lamm, Gerd	MM
29	Pinske, Lutz	MM
30	Rhau, Lars-Peler	IVIM
31	Schünemann, Mario	MM
32	Teichert, Uwe	IVIM
33	Redmer, Klaus-Peter	Cook
34	Martens, Michael	Cooksmate
35	Silinski, Frank	Cooksmate
36	Czyborra, Bärbei	Chief Stew
37	Wöckener, Martina	Stwdss/Nur·se
38	Arendt, Rene	2nd Stew.
39	Dibenau,Torsten	2nd Stew.
40	Möller, Wolfgang	2nd Stew.
41	Silinski, Carmen	2nd Stew.
42	Sun, Yong Sheng	2nd Stew.
43	Yu, Kwok Yuen	Laundrym.

A.4 PS94 STATIONSLISTE / STATION LIST

Station	Date	Time	Gear	Action	PositionLat	PositionLon	Water depth [m]
PS94/001-1	18.08.15	20:10:00	CTD/RO	on ground/ max depth	74° 59.94' N	30° 0.27' E	373.0
PS94/001-2	18.08.15	20:46:00	MUC	on ground/ max depth	74° 59.91' N	30° 0.24' E	372.0
PS94/002-1	19.08.15	05:23:00	CTD/RO	on ground/ max depth	76° 40.54' N	30° 0.34' E	265.0
PS94/002-2	19.08.15	05:56:00	MUC	on ground/ max depth	76° 40.58' N	30° 0.23' E	265.0
PS94/003-1	19.08.15	06:34:00	CTD/UW	profile start	76° 45.45' N	30° 2.79' E	261.5
PS94/003-1	19.08.15	06:42:59	CTD/UW	profile end	76° 46.70' N	30° 3.61' E	259.5
PS94/003-2	19.08.15	07:25:00	CTD/UW	profile start	76° 53.51' N	30° 7.79' E	265.7
PS94/003-2	19.08.15	07:34:59	CTD/UW	profile end	76° 54.94' N	30° 8.64' E	259.0
PS94/003-3	19.08.15	07:35:00	CTD/UW	profile start	76° 55.10' N	30° 8.72' E	259.0
PS94/003-3	19.08.15	07:43:59	CTD/UW	profile end	76° 56.38' N	30° 9.48' E	255.7
PS94/003-4	19.08.15	07:44:00	CTD/UW	profile start	76° 56.53' N	30° 9.58' E	256.0
PS94/003-4	19.08.15	07:52:59	CTD/UW	profile end	76° 57.80' N	30° 10.42' E	250.0
PS94/003-5	19.08.15	07:53:00	CTD/UW	profile start	76° 57.97' N	30° 10.54' E	249.7
PS94/003-5	19.08.15	08:02:59	CTD/UW	profile end	76° 59.41' N	30° 11.42' E	248.0
PS94/003-6	19.08.15	08:03:00	CTD/UW	profile start	76° 59.57' N	30° 11.51' E	246.2
PS94/003-6	19.08.15	08:11:59	CTD/UW	profile end	77° 0.85' N	30° 12.22' E	245.5
PS94/003-7	19.08.15	08:12:00	CTD/UW	profile start	77° 1.00' N	30° 12.31' E	247.0
PS94/003-7	19.08.15	08:21:59	CTD/UW	profile end	77° 2.42' N	30° 13.25' E	244.7
PS94/003-8	19.08.15	08:22:00	CTD/UW	profile start	77° 2.58' N	30° 13.35' E	240.0
PS94/003-8	19.08.15	08:30:59	CTD/UW	profile end	77° 3.85' N	30° 14.11' E	235.2
PS94/003-9	19.08.15	08:31:00	CTD/UW	profile start	77° 4.00' N	30° 14.20' E	238.2
PS94/003-9	19.08.15	08:39:59	CTD/UW	profile end	77° 5.27' N	30° 14.99' E	225.0
PS94/003-10	19.08.15	08:40:00	CTD/UW	profile start	77° 5.43' N	30° 15.11' E	224.7
PS94/003-10	19.08.15	08:46:59	CTD/UW	profile end	77° 6.38' N	30° 15.65' E	213.0
PS94/003-11	19.08.15	08:47:00	CTD/UW	profile start	77° 6.54' N	30° 15.74' E	213.2
PS94/003-11	19.08.15	08:55:59	CTD/UW	profile end	77° 7.80' N	30° 16.59' E	208.2
PS94/003-12	19.08.15	08:56:00	CTD/UW	profile start	77° 7.96' N	30° 16.68' E	208.5
PS94/003-13	19.08.15	09:02:00	CTD/UW	profile start	77° 8.91' N	30° 17.26' E	206.0
PS94/003-12	19.08.15	09:02:59	CTD/UW	profile end	77° 8.91' N	30° 17.26' E	206.0
PS94/003-13	19.08.15	09:07:59	CTD/UW	profile end	77° 9.71' N	30° 17.71' E	206.2
PS94/003-14	19.08.15	09:08:00	CTD/UW	profile start	77° 9.86' N	30° 17.80' E	205.0
PS94/003-14	19.08.15	09:13:59	CTD/UW	profile end	77° 10.65' N	30° 18.29' E	205.7
PS94/003-15	19.08.15	09:14:00	CTD/UW	profile start	77° 10.80' N	30° 18.40' E	209.5
PS94/003-16	19.08.15	09:22:00	CTD/UW	profile start	77° 12.06' N	30° 19.17' E	202.0
PS94/003-15	19.08.15	09:22:59	CTD/UW	profile end	77° 12.06' N	30° 19.17' E	202.0

Station	Date	Time	Gear	Action	PositionLat	PositionLon	Water depth [m]
PS94/003-17	19.08.15	09:28:00	CTD/UW	profile start	77° 13.00' N	30° 19.74' E	205.5
PS94/003-16	19.08.15	09:28:59	CTD/UW	profile end	77° 13.00' N	30° 19.74' E	205.5
PS94/003-17	19.08.15	09:34:59	CTD/UW	profile end	77° 13.94' N	30° 20.30' E	189.0
PS94/003-18	19.08.15	09:35:00	CTD/UW	profile start	77° 14.10' N	30° 20.39' E	191.7
PS94/003-18	19.08.15	09:40:59	CTD/UW	profile end	77° 14.88' N	30° 20.99' E	198.5
PS94/003-19	19.08.15	09:41:00	CTD/UW	profile start	77° 15.04' N	30° 21.08' E	199.2
PS94/003-20	19.08.15	09:47:00	CTD/UW	profile start	77° 15.99' N	30° 21.67' E	191.0
PS94/003-19	19.08.15	09:47:59	CTD/UW	profile end	77° 15.99' N	30° 21.67' E	191.0
PS94/003-20	19.08.15	09:53:59	CTD/UW	profile end	77° 16.95' N	30° 22.23' E	183.7
PS94/003-21	19.08.15	09:54:00	CTD/UW	profile start	77° 17.10' N	30° 22.32' E	191.0
PS94/003-22	19.08.15	09:59:00	CTD/UW	profile start	77° 17.89' N	30° 22.84' E	198.2
PS94/003-21	19.08.15	09:59:59	CTD/UW	profile end	77° 17.89' N	30° 22.84' E	198.2
PS94/003-22	19.08.15	10:05:59	CTD/UW	profile end	77° 18.85' N	30° 23.43' E	198.7
PS94/003-23	19.08.15	10:06:00	CTD/UW	profile start	77° 19.01' N	30° 23.55' E	200.5
PS94/003-23	19.08.15	10:12:59	CTD/UW	profile end	77° 19.99' N	30° 24.15' E	198.0
PS94/003-24	19.08.15	10:13:00	CTD/UW	profile start	77° 20.16' N	30° 24.22' E	198.0
PS94/003-25	19.08.15	10:19:00	CTD/UW	profile start	77° 21.13' N	30° 24.78' E	202.0
PS94/003-24	19.08.15	10:19:59	CTD/UW	profile end	77° 21.13' N	30° 24.78' E	202.0
PS94/003-26	19.08.15	10:26:00	CTD/UW	profile start	77° 22.28' N	30° 25.54' E	200.5
PS94/003-25	19.08.15	10:26:59	CTD/UW	profile end	77° 22.28' N	30° 25.54' E	200.5
PS94/003-27	19.08.15	10:32:00	CTD/UW	profile start	77° 23.25' N	30° 26.21' E	197.0
PS94/003-26	19.08.15	10:32:59	CTD/UW	profile end	77° 23.25' N	30° 26.21' E	197.0
PS94/003-28	19.08.15	10:38:00	CTD/UW	profile start	77° 24.21' N	30° 26.75' E	210.5
PS94/003-27	19.08.15	10:38:59	CTD/UW	profile end	77° 24.21' N	30° 26.75' E	210.5
PS94/003-28	19.08.15	10:44:59	CTD/UW	profile end	77° 25.15' N	30° 27.42' E	192.2
PS94/003-29	19.08.15	10:45:00	CTD/UW	profile start	77° 25.31' N	30° 27.52' E	192.2
PS94/003-30	19.08.15	10:51:00	CTD/UW	profile start	77° 26.25' N	30° 28.07' E	206.0
PS94/003-29	19.08.15	10:51:59	CTD/UW	profile end	77° 26.25' N	30° 28.07' E	206.0
PS94/003-30	19.08.15	10:58:59	CTD/UW	profile end	77° 27.33' N	30° 28.74' E	208.7
PS94/003-31	19.08.15	10:59:00	CTD/UW	profile start	77° 27.48' N	30° 28.84' E	210.0
PS94/003-31	19.08.15	11:05:59	CTD/UW	profile end	77° 28.40' N	30° 29.44' E	205.0
PS94/003-32	19.08.15	11:06:00	CTD/UW	profile start	77° 28.55' N	30° 29.56' E	210.2
PS94/003-33	19.08.15	11:13:00	CTD/UW	profile start	77° 29.61' N	30° 30.25' E	217.5
PS94/003-32	19.08.15	11:13:59	CTD/UW	profile end	77° 29.61' N	30° 30.25' E	217.5
PS94/003-33	19.08.15	11:21:59	CTD/UW	profile end	77° 30.82' N	30° 30.99' E	217.2
PS94/003-34	19.08.15	11:22:00	CTD/UW	profile start	77° 30.97' N	30° 31.11' E	217.7
PS94/003-35	19.08.15	11:29:00	CTD/UW	profile start	77° 32.03' N	30° 31.72' E	225.5
PS94/003-34	19.08.15	11:29:59	CTD/UW	profile end	77° 32.03' N	30° 31.72' E	225.5
PS94/003-35	19.08.15	11:36:59	CTD/UW	profile end	77° 33.09' N	30° 32.38' E	225.5
PS94/003-36	19.08.15	11:37:00	CTD/UW	profile start	77° 33.24' N	30° 32.47' E	223.0

Station	Date	Time	Gear	Action	PositionLat	PositionLon	Water depth [m]
PS94/003-36	19.08.15	11:44:59	CTD/UW	profile end	77° 34.30' N	30° 33.16' E	225.5
PS94/003-37	19.08.15	11:45:00	CTD/UW	profile start	77° 34.45' N	30° 33.25' E	226.5
PS94/003-37	19.08.15	11:56:59	CTD/UW	profile end	77° 36.12' N	30° 34.33' E	228.2
PS94/003-38	19.08.15	13:09:00	CTD/UW	profile start	77° 47.26' N	30° 41.53' E	234.0
PS94/003-39	19.08.15	13:21:00	CTD/UW	profile start	77° 49.12' N	30° 42.72' E	247.7
PS94/003-38	19.08.15	13:21:59	CTD/UW	profile end	77° 49.12' N	30° 42.72' E	247.7
PS94/003-40	19.08.15	13:29:00	CTD/UW	profile start	77° 50.37' N	30° 43.61' E	241.5
PS94/003-39	19.08.15	13:29:59	CTD/UW	profile end	77° 50.37' N	30° 43.61' E	241.5
PS94/003-40	19.08.15	13:37:59	CTD/UW	profile end	77° 51.61' N	30° 44.46' E	241.7
PS94/003-41	19.08.15	13:38:00	CTD/UW	profile start	77° 51.77' N	30° 44.55' E	241.0
PS94/003-42	19.08.15	13:46:00	CTD/UW	profile start	77° 53.04' N	30° 45.29' E	234.2
PS94/003-41	19.08.15	13:46:59	CTD/UW	profile end	77° 53.04' N	30° 45.29' E	234.2
PS94/003-43	19.08.15	13:54:00	CTD/UW	profile start	77° 54.29' N	30° 46.10' E	262.5
PS94/003-42	19.08.15	13:54:59	CTD/UW	profile end	77° 54.29' N	30° 46.10' E	262.5
PS94/003-43	19.08.15	14:03:59	CTD/UW	profile end	77° 55.72' N	30° 47.07' E	265.7
PS94/003-44	19.08.15	14:04:00	CTD/UW	profile start	77° 55.88' N	30° 47.16' E	268.0
PS94/003-45	19.08.15	14:14:00	CTD/UW	profile start	77° 57.47' N	30° 48.28' E	242.5
PS94/003-44	19.08.15	14:14:59	CTD/UW	profile end	77° 57.47' N	30° 48.28' E	242.5
PS94/003-46	19.08.15	14:22:00	CTD/UW	profile start	77° 58.74' N	30° 49.04' E	255.5
PS94/003-45	19.08.15	14:22:59	CTD/UW	profile end	77° 58.74' N	30° 49.04' E	255.5
PS94/003-47	19.08.15	14:32:00	CTD/UW	profile start	78° 0.32' N	30° 50.11' E	260.5
PS94/003-46	19.08.15	14:32:59	CTD/UW	profile end	78° 0.32' N	30° 50.11' E	260.5
PS94/003-48	19.08.15	14:41:00	CTD/UW	profile start	78° 1.76' N	30° 51.07' E	248.2
PS94/003-47	19.08.15	14:41:59	CTD/UW	profile end	78° 1.76' N	30° 51.07' E	248.2
PS94/003-49	19.08.15	14:50:00	CTD/UW	profile start	78° 3.18' N	30° 51.99' E	219.2
PS94/003-48	19.08.15	14:50:59	CTD/UW	profile end	78° 3.18' N	30° 51.99' E	219.2
PS94/003-50	19.08.15	14:59:00	CTD/UW	profile start	78° 4.61' N	30° 52.94' E	234.7
PS94/003-49	19.08.15	14:59:59	CTD/UW	profile end	78° 4.61' N	30° 52.94' E	234.7
PS94/003-50	19.08.15	15:06:59	CTD/UW	profile end	78° 5.71' N	30° 53.66' E	231.5
PS94/003-51	19.08.15	15:07:00	CTD/UW	profile start	78° 5.87' N	30° 53.77' E	233.5
PS94/003-52	19.08.15	15:14:00	CTD/UW	profile start	78° 6.96' N	30° 54.57' E	242.2
PS94/003-51	19.08.15	15:14:59	CTD/UW	profile end	78° 6.96' N	30° 54.57' E	242.2
PS94/003-53	19.08.15	15:23:00	CTD/UW	profile start	78° 8.36' N	30° 55.49' E	243.0
PS94/003-52	19.08.15	15:23:59	CTD/UW	profile end	78° 8.36' N	30° 55.49' E	243.0
PS94/003-54	19.08.15	15:31:00	CTD/UW	profile start	78° 9.62' N	30° 56.38' E	231.7
PS94/003-53	19.08.15	15:31:59	CTD/UW	profile end	78° 9.62' N	30° 56.38' E	231.7
PS94/003-55	19.08.15	15:39:00	CTD/UW	profile start	78° 10.88' N	30° 57.13' E	239.7
PS94/003-54	19.08.15	15:39:59	CTD/UW	profile end	78° 10.88' N	30° 57.13' E	239.7
PS94/003-56	19.08.15	15:47:00	CTD/UW	profile start	78° 12.12' N	30° 58.06' E	241.5
PS94/003-55	19.08.15	15:47:59	CTD/UW	profile end	78° 12.12' N	30° 58.06' E	241.5

Station	Date	Time	Gear	Action	PositionLat	PositionLon	Water depth [m]
PS94/003-57	19.08.15	15:55:00	CTD/UW	profile start	78° 13.36' N	30° 58.84' E	272.2
PS94/003-56	19.08.15	15:55:59	CTD/UW	profile end	78° 13.36' N	30° 58.84' E	272.2
PS94/003-57	19.08.15	16:03:59	CTD/UW	profile end	78° 14.60' N	30° 59.69' E	253.7
PS94/003-58	19.08.15	16:04:00	CTD/UW	profile start	78° 14.76' N	30° 59.77' E	255.7
PS94/003-59	19.08.15	16:12:00	CTD/UW	profile start	78° 16.02' N	31° 0.58' E	249.2
PS94/003-58	19.08.15	16:12:59	CTD/UW	profile end	78° 16.02' N	31° 0.58' E	249.2
PS94/003-60	19.08.15	16:21:00	CTD/UW	profile start	78° 17.44' N	31° 1.57' E	260.0
PS94/003-59	19.08.15	16:21:59	CTD/UW	profile end	78° 17.44' N	31° 1.57' E	260.0
PS94/003-61	19.08.15	16:30:00	CTD/UW	profile start	78° 18.86' N	31° 2.62' E	257.7
PS94/003-60	19.08.15	16:30:59	CTD/UW	profile end	78° 18.86' N	31° 2.62' E	257.7
PS94/003-62	19.08.15	16:39:00	CTD/UW	profile start	78° 20.28' N	31° 3.60' E	251.0
PS94/003-61	19.08.15	16:39:59	CTD/UW	profile end	78° 20.28' N	31° 3.60' E	251.0
PS94/003-63	19.08.15	16:48:00	CTD/UW	profile start	78° 21.73' N	31° 4.50' E	258.5
PS94/003-62	19.08.15	16:48:59	CTD/UW	profile end	78° 21.73' N	31° 4.50' E	258.5
PS94/003-64	19.08.15	16:57:00	CTD/UW	profile start	78° 23.15' N	31° 5.54' E	257.2
PS94/003-63	19.08.15	16:57:59	CTD/UW	profile end	78° 23.15' N	31° 5.54' E	257.2
PS94/003-65	19.08.15	17:06:00	CTD/UW	profile start	78° 24.57' N	31° 6.54' E	271.2
PS94/003-64	19.08.15	17:06:59	CTD/UW	profile end	78° 24.57' N	31° 6.54' E	271.2
PS94/003-65	19.08.15	17:15:59	CTD/UW	profile end	78° 26.01' N	31° 7.42' E	278.5
PS94/003-66	19.08.15	17:16:00	CTD/UW	profile start	78° 26.17' N	31° 7.57' E	280.5
PS94/003-66	19.08.15	17:25:59	CTD/UW	profile end	78° 27.58' N	31° 8.58' E	300.5
PS94/003-67	19.08.15	17:26:00	CTD/UW	profile start	78° 27.73' N	31° 8.70' E	300.0
PS94/003-68	19.08.15	17:35:00	CTD/UW	profile start	78° 29.16' N	31° 9.66' E	299.2
PS94/003-67	19.08.15	17:35:59	CTD/UW	profile end	78° 29.16' N	31° 9.66' E	299.2
PS94/003-69	19.08.15	17:45:00	CTD/UW	profile start	78° 30.73' N	31° 10.74' E	306.2
PS94/003-68	19.08.15	17:45:59	CTD/UW	profile end	78° 30.73' N	31° 10.74' E	306.2
PS94/003-70	19.08.15	17:56:00	CTD/UW	profile start	78° 32.46' N	31° 11.96' E	311.7
PS94/003-69	19.08.15	17:56:59	CTD/UW	profile end	78° 32.46' N	31° 11.96' E	311.7
PS94/003-71	19.08.15	18:07:00	CTD/UW	profile start	78° 34.18' N	31° 13.06' E	315.2
PS94/003-70	19.08.15	18:07:59	CTD/UW	profile end	78° 34.18' N	31° 13.06' E	315.2
PS94/003-71	19.08.15	18:18:59	CTD/UW	profile end	78° 35.90' N	31° 14.24' E	307.0
PS94/003-72	19.08.15	18:19:00	CTD/UW	profile start	78° 36.05' N	31° 14.34' E	311.5
PS94/003-72	19.08.15	18:28:59	CTD/UW	profile end	78° 37.44' N	31° 15.35' E	307.7
PS94/003-73	19.08.15	18:29:00	CTD/UW	profile start	78° 37.59' N	31° 15.49' E	305.2
PS94/003-73	19.08.15	18:38:59	CTD/UW	profile end	78° 38.97' N	31° 16.50' E	310.7
PS94/003-74	19.08.15	18:39:00	CTD/UW	profile start	78° 39.12' N	31° 16.60' E	311.0
PS94/003-74	19.08.15	18:49:59	CTD/UW	profile end	78° 40.67' N	31° 17.60' E	289.0
PS94/003-75	19.08.15	18:50:00	CTD/UW	profile start	78° 40.83' N	31° 17.75' E	286.7
PS94/003-75	19.08.15	18:59:59	CTD/UW	profile end	78° 42.22' N	31° 18.77' E	267.5
PS94/003-76	19.08.15	19:00:00	CTD/UW	profile start	78° 42.37' N	31° 18.86' E	269.7

Station	Date	Time	Gear	Action	PositionLat	PositionLon	Water depth [m]
PS94/003-76	19.08.15	19:09:59	CTD/UW	profile end	78° 43.77' N	31° 19.75' E	265.5
PS94/003-77	19.08.15	19:10:00	CTD/UW	profile start	78° 43.92' N	31° 19.88' E	256.7
PS94/003-78	19.08.15	19:19:00	CTD/UW	profile start	78° 45.30' N	31° 20.90' E	242.0
PS94/003-77	19.08.15	19:19:59	CTD/UW	profile end	78° 45.30' N	31° 20.90' E	242.0
PS94/003-78	19.08.15	19:28:59	CTD/UW	profile end	78° 46.69' N	31° 21.82' E	244.2
PS94/003-79	19.08.15	19:29:00	CTD/UW	profile start	78° 46.84' N	31° 21.93' E	238.0
PS94/003-79	19.08.15	19:37:59	CTD/UW	profile end	78° 48.07' N	31° 22.84' E	160.7
PS94/003-80	19.08.15	19:38:00	CTD/UW	profile start	78° 48.23' N	31° 22.92' E	147.7
PS94/003-80	19.08.15	19:46:59	CTD/UW	profile end	78° 49.45' N	31° 23.85' E	134.7
PS94/003-81	19.08.15	19:47:00	CTD/UW	profile start	78° 49.60' N	31° 23.97' E	134.0
PS94/003-81	19.08.15	19:55:59	CTD/UW	profile end	78° 50.81' N	31° 24.76' E	128.5
PS94/003-82	19.08.15	19:56:00	CTD/UW	profile start	78° 50.97' N	31° 24.86' E	124.0
PS94/003-82	19.08.15	20:02:59	CTD/UW	profile end	78° 51.87' N	31° 25.53' E	110.5
PS94/003-83	19.08.15	20:03:00	CTD/UW	profile start	78° 52.02' N	31° 25.64' E	108.0
PS94/003-83	19.08.15	20:12:59	CTD/UW	profile end	78° 53.38' N	31° 26.58' E	147.5
PS94/003-84	19.08.15	20:13:00	CTD/UW	profile start	78° 53.53' N	31° 26.69' E	151.2
PS94/003-84	19.08.15	20:20:59	CTD/UW	profile end	78° 54.58' N	31° 27.50' E	173.7
PS94/003-85	19.08.15	20:21:00	CTD/UW	profile start	78° 54.73' N	31° 27.60' E	177.2
PS94/003-85	19.08.15	20:27:59	CTD/UW	profile end	78° 55.64' N	31° 28.23' E	202.7
PS94/003-86	19.08.15	20:28:00	CTD/UW	profile start	78° 55.79' N	31° 28.33' E	202.0
PS94/003-86	19.08.15	20:34:59	CTD/UW	profile end	78° 56.68' N	31° 29.05' E	202.2
PS94/003-87	19.08.15	20:35:00	CTD/UW	profile start	78° 56.83' N	31° 29.08' E	201.7
PS94/003-87	19.08.15	20:40:59	CTD/UW	profile end	78° 57.59' N	31° 29.65' E	227.0
PS94/003-88	19.08.15	20:41:00	CTD/UW	profile start	78° 57.74' N	31° 29.72' E	228.7
PS94/003-88	19.08.15	20:47:59	CTD/UW	profile end	78° 58.64' N	31° 30.39' E	247.2
PS94/003-89	19.08.15	20:48:00	CTD/UW	profile start	78° 58.78' N	31° 30.52' E	251.0
PS94/003-89	19.08.15	20:56:59	CTD/UW	profile end	78° 59.96' N	31° 31.42' E	241.0
PS94/003-90	19.08.15	21:00:00	CTD/UW	profile start	79° 0.53' N	31° 31.73' E	181.2
PS94/003-90	19.08.15	21:06:59	CTD/UW	profile end	79° 1.40' N	31° 32.44' E	154.7
PS94/003-91	19.08.15	21:07:00	CTD/UW	profile start	79° 1.55' N	31° 32.51' E	160.0
PS94/003-91	19.08.15	21:11:59	CTD/UW	profile end	79° 2.13' N	31° 32.86' E	140.2
PS94/003-92	19.08.15	21:12:00	CTD/UW	profile start	79° 2.28' N	31° 33.00' E	138.0
PS94/003-92	19.08.15	21:16:59	CTD/UW	profile end	79° 2.86' N	31° 33.49' E	147.7
PS94/003-93	19.08.15	21:17:00	CTD/UW	profile start	79° 3.01' N	31° 33.60' E	136.2
PS94/003-93	19.08.15	21:21:59	CTD/UW	profile end	79° 3.60' N	31° 33.97' E	118.0
PS94/003-94	19.08.15	21:22:00	CTD/UW	profile start	79° 3.74' N	31° 34.07' E	119.5
PS94/003-94	19.08.15	21:25:59	CTD/UW	profile end	79° 4.19' N	31° 34.37' E	115.0
PS94/003-95	19.08.15	21:26:00	CTD/UW	profile start	79° 4.34' N	31° 34.47' E	118.7
PS94/003-95	19.08.15	21:36:59	CTD/UW	profile end	79° 5.83' N	31° 35.57' E	118.7
PS94/004-1	20.08.15	00:45:00	CTD/RO	on ground/ max depth	79° 15.07' N	30° 2.87' E	234.0

Station	Date	Time	Gear	Action	PositionLat	PositionLon	Water depth [m]
PS94/004-2	20.08.15	01:23:00	CTD/UC	on ground/ max depth	79° 15.20' N	30° 2.77' E	228.2
PS94/004-3	20.08.15	02:51:00	CTD/RO	on ground/ max depth	79° 14.97' N	30° 2.49' E	230.0
PS94/004-4	20.08.15	03:52:00	ISP	on ground/ max depth	79° 14.97' N	30° 2.17' E	227.2
PS94/004-5	20.08.15	08:26:00	CTD/RO	on ground/ max depth	79° 14.91' N	30° 2.10' E	224.5
PS94/004-6	20.08.15	09:17:00	CTD/UC	on ground/ max depth	79° 14.96' N	30° 1.93' E	226.2
PS94/005-1	20.08.15	10:23:00	CTD/UW	profile start	79° 16.42' N	30° 2.51' E	252.5
PS94/005-1	20.08.15	10:34:59	CTD/UW	profile end	79° 18.07' N	30° 2.72' E	292.7
PS94/005-2	20.08.15	11:16:00	CTD/UW	profile start	79° 24.52' N	30° 0.77' E	332.5
PS94/005-3	20.08.15	11:30:00	CTD/UW	profile start	79° 26.77' N	30° 0.56' E	296.0
PS94/005-2	20.08.15	11:30:59	CTD/UW	profile end	79° 26.77' N	30° 0.56' E	296.0
PS94/005-3	20.08.15	11:46:59	CTD/UW	profile end	79° 29.35' N	29° 59.72' E	273.5
PS94/006-1	20.08.15	12:13:00	CTD/RO	on ground/ max depth	79° 29.98' N	29° 59.99' E	259.0
PS94/007-1	20.08.15	12:58:00	CTD/UW	profile start	79° 34.11' N	30° 0.01' E	263.2
PS94/007-1	20.08.15	13:07:59	CTD/UW	profile end	79° 35.63' N	29° 59.98' E	258.5
PS94/007-2	20.08.15	13:08:00	CTD/UW	profile start	79° 35.80' N	29° 59.95' E	256.5
PS94/007-3	20.08.15	13:20:00	CTD/UW	profile start	79° 37.82' N	29° 59.97' E	262.5
PS94/007-2	20.08.15	13:20:59	CTD/UW	profile end	79° 37.82' N	29° 59.97' E	262.5
PS94/007-3	20.08.15	13:31:59	CTD/UW	profile end	79° 39.69' N	30° 0.07' E	259.7
PS94/007-4	20.08.15	13:32:00	CTD/UW	profile start	79° 39.86' N	30° 0.05' E	256.2
PS94/007-5	20.08.15	13:42:00	CTD/UW	profile start	79° 41.57' N	29° 59.95' E	269.5
PS94/007-4	20.08.15	13:42:59	CTD/UW	profile end	79° 41.57' N	29° 59.95' E	269.5
PS94/007-5	20.08.15	13:55:59	CTD/UW	profile end	79° 43.75' N	29° 59.61' E	235.7
PS94/008-1	20.08.15	14:20:00	CTD/RO	on ground/ max depth	79° 45.04' N	30° 0.37' E	218.7
PS94/008-2	20.08.15	14:42:00	CTD/UC	on ground/ max depth	79° 45.00' N	30° 0.02' E	222.2
PS94/009-1	20.08.15	15:14:00	CTD/UW	profile start	79° 47.45' N	29° 59.97' E	152.0
PS94/009-1	20.08.15	15:22:59	CTD/UW	profile end	79° 48.70' N	29° 59.94' E	143.5
PS94/009-2	20.08.15	15:23:00	CTD/UW	profile start	79° 48.85' N	29° 59.95' E	141.7
PS94/009-2	20.08.15	15:28:59	CTD/UW	profile end	79° 49.64' N	30° 0.06' E	173.5
PS94/009-3	20.08.15	15:29:00	CTD/UW	profile start	79° 49.80' N	30° 0.06' E	210.2
PS94/009-4	20.08.15	15:36:00	CTD/UW	profile start	79° 50.90' N	30° 0.05' E	263.7
PS94/009-3	20.08.15	15:36:59	CTD/UW	profile end	79° 50.90' N	30° 0.05' E	263.7
PS94/009-5	20.08.15	15:46:00	CTD/UW	profile start	79° 52.44' N	30° 0.08' E	243.2
PS94/009-4	20.08.15	15:46:59	CTD/UW	profile end	79° 52.44' N	30° 0.08' E	243.2
PS94/009-6	20.08.15	15:55:00	CTD/UW	profile start	79° 53.81' N	29° 59.94' E	245.2

Station	Date	Time	Gear	Action	PositionLat	PositionLon	Water depth [m]
PS94/009-5	20.08.15	15:55:59	CTD/UW	profile end	79° 53.81' N	29° 59.94' E	245.2
PS94/009-6	20.08.15	16:03:59	CTD/UW	profile end	79° 55.03' N	29° 59.96' E	253.7
PS94/009-7	20.08.15	16:04:00	CTD/UW	profile start	79° 55.19' N	29° 59.98' E	252.2
PS94/009-7	20.08.15	16:12:59	CTD/UW	profile end	79° 56.40' N	29° 60.00' E	250.2
PS94/009-8	20.08.15	16:13:00	CTD/UW	profile start	79° 56.55' N	29° 59.96' E	244.7
PS94/009-9	20.08.15	16:22:00	CTD/UW	profile start	79° 57.92' N	29° 59.94' E	272.5
PS94/009-8	20.08.15	16:22:59	CTD/UW	profile end	79° 57.92' N	29° 59.94' E	272.5
PS94/009-9	20.08.15	16:33:59	CTD/UW	profile end	79° 59.58' N	30° 0.83' E	293.2
PS94/010-1	20.08.15	16:53:00	CTD/RO	on ground/ max depth	79° 59.92' N	29° 59.96' E	292.0
PS94/010-2	20.08.15	17:37:00	MN	on ground/ max depth	79° 59.95' N	29° 59.88' E	294.2
PS94/010-3	20.08.15	18:20:00	LOKI	on ground/ max depth	79° 59.92' N	29° 60.00' E	293.0
PS94/010-3	20.08.15	18:21:00	LOKI	profile start	79° 59.92' N	29° 59.99' E	295.0
PS94/010-3	20.08.15	18:30:00	LOKI	profile end	79° 59.89' N	29° 59.99' E	292.2
PS94/011-1	20.08.15	19:32:00	CTD/UW	profile start	80° 9.01' N	30° 0.03' E	297.5
PS94/011-2	20.08.15	19:37:00	CTD/UW	profile start	80° 9.82' N	29° 59.98' E	284.0
PS94/011-1	20.08.15	19:37:59	CTD/UW	profile end	80° 9.82' N	29° 59.98' E	284.0
PS94/011-2	20.08.15	19:49:59	CTD/UW	profile end	80° 11.77' N	29° 59.96' E	296.7
PS94/011-3	20.08.15	19:50:00	CTD/UW	profile start	80° 11.93' N	29° 60.00' E	298.7
PS94/011-3	20.08.15	20:04:59	CTD/UW	profile end	80° 14.18' N	30° 0.01' E	253.0
PS94/012-1	20.08.15	20:24:00	CTD/RO	on ground/ max depth	80° 15.01' N	29° 59.29' E	248.2
PS94/013-1	20.08.15	20:40:00	CTD/UW	profile start	80° 16.03' N	30° 0.05' E	233.5
PS94/013-2	20.08.15	20:51:00	CTD/UW	profile start	80° 17.86' N	30° 0.06' E	205.2
PS94/013-1	20.08.15	20:51:59	CTD/UW	profile end	80° 17.86' N	30° 0.06' E	205.2
PS94/013-2	20.08.15	20:59:59	CTD/UW	profile end	80° 19.17' N	30° 0.07' E	150.2
PS94/013-3	20.08.15	21:00:00	CTD/UW	profile start	80° 19.34' N	30° 0.05' E	149.7
PS94/013-4	20.08.15	21:06:00	CTD/UW	profile start	80° 20.31' N	29° 59.96' E	193.7
PS94/013-3	20.08.15	21:06:59	CTD/UW	profile end	80° 20.31' N	29° 59.96' E	193.7
PS94/013-4	20.08.15	21:17:59	CTD/UW	profile end	80° 22.13' N	30° 0.02' E	202.0
PS94/013-5	20.08.15	21:18:00	CTD/UW	profile start	80° 22.30' N	29° 60.00' E	198.0
PS94/013-5	20.08.15	21:26:59	CTD/UW	profile end	80° 23.65' N	29° 59.93' E	234.2
PS94/013-6	20.08.15	21:27:00	CTD/UW	profile start	80° 23.81' N	29° 59.92' E	235.5
PS94/013-6	20.08.15	21:36:59	CTD/UW	profile end	80° 25.30' N	30° 0.07' E	219.5
PS94/013-7	20.08.15	21:37:00	CTD/UW	profile start	80° 25.47' N	30° 0.02' E	175.2
PS94/013-7	20.08.15	21:44:59	CTD/UW	profile end	80° 26.64' N	30° 0.04' E	364.2
PS94/013-8	20.08.15	21:45:00	CTD/UW	profile start	80° 26.81' N	30° 0.07' E	338.0
PS94/013-8	20.08.15	21:53:59	CTD/UW	profile end	80° 28.16' N	30° 0.01' E	346.7
PS94/014-1	20.08.15	22:22:00	CTD/RO	on ground/ max depth	80° 29.98' N	29° 59.19' E	378.2

Station	Date	Time	Gear	Action	PositionLat	PositionLon	Water depth [m]
PS94/015-1	20.08.15	22:52:00	CTD/UW	profile start	80° 31.57' N	29° 46.99' E	500.5
PS94/015-2	20.08.15	23:06:00	CTD/UW	profile start	80° 32.94' N	29° 35.46' E	314.0
PS94/015-1	20.08.15	23:06:59	CTD/UW	profile end	80° 32.94' N	29° 35.46' E	314.0
PS94/015-3	20.08.15	23:18:00	CTD/UW	profile start	80° 34.07' N	29° 25.94' E	173.7
PS94/015-2	20.08.15	23:18:59	CTD/UW	profile end	80° 34.07' N	29° 25.94' E	173.7
PS94/015-3	20.08.15	23:25:59	CTD/UW	profile end	80° 34.73' N	29° 20.44' E	228.5
PS94/015-4	20.08.15	23:26:00	CTD/UW	profile start	80° 34.82' N	29° 19.66' E	257.5
PS94/015-5	20.08.15	23:36:00	CTD/UW	profile start	80° 35.75' N	29° 11.76' E	190.7
PS94/015-4	20.08.15	23:36:59	CTD/UW	profile end	80° 35.75' N	29° 11.76' E	190.7
PS94/015-6	20.08.15	23:44:00	CTD/UW	profile start	80° 36.48' N	29° 5.48' E	326.2
PS94/015-5	20.08.15	23:44:59	CTD/UW	profile end	80° 36.48' N	29° 5.48' E	326.2
PS94/015-6	20.08.15	23:53:59	CTD/UW	profile end	80° 37.30' N	28° 58.46' E	291.5
PS94/015-7	20.08.15	23:54:00	CTD/UW	profile start	80° 37.39' N	28° 57.69' E	260.7
PS94/015-8	21.08.15	00:03:00	CTD/UW	profile start	80° 38.24' N	28° 50.79' E	305.2
PS94/015-7	21.08.15	00:03:59	CTD/UW	profile end	80° 38.24' N	28° 50.79' E	305.2
PS94/015-9	21.08.15	00:13:00	CTD/UW	profile start	80° 39.14' N	28° 42.95' E	484.7
PS94/015-8	21.08.15	00:13:59	CTD/UW	profile end	80° 39.14' N	28° 42.95' E	484.7
PS94/015-9	21.08.15	00:26:59	CTD/UW	profile end	80° 40.35' N	28° 32.87' E	444.7
PS94/015-10	21.08.15	00:27:00	CTD/UW	profile start	80° 40.45' N	28° 32.13' E	444.2
PS94/015-10	21.08.15	00:44:59	CTD/UW	profile end	80° 41.88' N	28° 21.71' E	51.2
PS94/016-1	21.08.15	01:26:00	CTD/UW	profile start	80° 45.02' N	28° 28.47' E	80.2
PS94/016-2	21.08.15	01:31:00	CTD/UW	profile start	80° 45.00' N	28° 31.78' E	120.7
PS94/016-1	21.08.15	01:31:59	CTD/UW	profile end	80° 45.00' N	28° 31.78' E	120.7
PS94/016-3	21.08.15	01:35:00	CTD/UW	profile start	80° 44.99' N	28° 34.62' E	190.7
PS94/016-2	21.08.15	01:35:59	CTD/UW	profile end	80° 44.99' N	28° 34.62' E	190.7
PS94/016-3	21.08.15	01:41:59	CTD/UW	profile end	80° 44.98' N	28° 40.56' E	365.2
PS94/016-4	21.08.15	01:50:00	CTD/UW	profile start	80° 45.00' N	28° 49.89' E	492.0
PS94/016-5	21.08.15	01:58:00	CTD/UW	profile start	80° 44.99' N	28° 58.32' E	500.5
PS94/016-4	21.08.15	01:58:59	CTD/UW	profile end	80° 44.99' N	28° 58.32' E	500.5
PS94/016-5	21.08.15	02:18:59	CTD/UW	profile end	80° 45.00' N	29° 19.37' E	484.2
PS94/017-1	21.08.15	02:26:59	XCTD	on ground/ max depth	80° 45.01' N	29° 27.83' E	495.7
PS94/017-2	21.08.15	02:46:59	XCTD	on ground/ max depth	80° 45.01' N	29° 49.11' E	267.0
PS94/017-3	21.08.15	02:55:59	XCTD	on ground/ max depth	80° 45.01' N	29° 58.60' E	257.7
PS94/017-4	21.08.15	03:03:59	XCTD	on ground/ max depth	80° 45.01' N	30° 7.07' E	259.0
PS94/017-5	21.08.15	03:14:59	XCTD	on ground/ max depth	80° 45.27' N	30° 17.34' E	201.7
PS94/017-6	21.08.15	03:30:59	XCTD	on ground/ max depth	80° 45.65' N	30° 4.82' E	248.2

Station	Date	Time	Gear	Action	PositionLat	PositionLon	Water depth [m]
PS94/017-7	21.08.15	03:56:59	XCTD	on ground/ max depth	80° 45.36' N	29° 40.95' E	354.7
PS94/018-1	21.08.15	04:18:00	CTD/RO	on ground/ max depth	80° 45.29' N	29° 40.66' E	367.0
PS94/018-2	21.08.15	05:00:00	LOKI	on ground/ max depth	80° 45.30' N	29° 40.22' E	378.2
PS94/018-2	21.08.15	05:00:02	LOKI	profile start	80° 45.30' N	29° 40.22' E	378.2
PS94/018-2	21.08.15	05:12:01	LOKI	profile end	80° 45.29' N	29° 40.16' E	384.5
PS94/018-3	21.08.15	05:48:00	CTD/RO	on ground/ max depth	80° 45.26' N	29° 39.85' E	393.7
PS94/018-4	21.08.15	06:31:00	MN	on ground/ max depth	80° 45.24' N	29° 39.54' E	403.0
PS94/018-5	21.08.15	07:29:00	CTD/RO	on ground/ max depth	80° 45.23' N	29° 38.85' E	418.5
PS94/019-1	21.08.15	08:01:00	CTD/UW	profile start	80° 47.35' N	29° 33.84' E	423.0
PS94/019-1	21.08.15	08:16:59	CTD/UW	profile end	80° 49.70' N	29° 27.00' E	407.5
PS94/019-2	21.08.15	08:17:00	CTD/UW	profile start	80° 49.86' N	29° 26.69' E	398.5
PS94/019-2	21.08.15	08:34:59	CTD/UW	profile end	80° 52.52' N	29° 20.45' E	431.0
PS94/019-3	21.08.15	08:35:00	CTD/UW	profile start	80° 52.68' N	29° 20.02' E	431.2
PS94/019-3	21.08.15	08:52:59	CTD/UW	profile end	80° 55.34' N	29° 12.47' E	420.5
PS94/020-1	21.08.15	09:00:59	XCTD	on ground/ max depth	80° 56.55' N	29° 8.90' E	409.5
PS94/021-1	21.08.15	09:47:00	CTD/RO	on ground/ max depth	80° 59.72' N	28° 59.45' E	390.0
PS94/021-2	21.08.15	10:22:00	MUC	on ground/ max depth	80° 59.79' N	28° 58.17' E	389.5
PS94/022-1	21.08.15	11:17:59	XCTD	on ground/ max depth	81° 4.66' N	29° 3.16' E	376.0
PS94/023-1	21.08.15	12:02:59	XCTD	on ground/ max depth	81° 10.41' N	29° 7.28' E	352.0
PS94/024-1	21.08.15	12:40:59	XCTD	on ground/ max depth	81° 14.82' N	29° 10.09' E	334.0
PS94/025-1	21.08.15	13:27:00	CTD/RO	on ground/ max depth	81° 18.08' N	29° 13.52' E	327.7
PS94/026-1	21.08.15	14:47:59	XCTD	on ground/ max depth	81° 22.17' N	29° 43.48' E	296.5
PS94/027-1	21.08.15	15:30:59	XCTD	on ground/ max depth	81° 25.80' N	30° 4.58' E	268.0
PS94/028-1	21.08.15	16:14:59	XCTD	on ground/ max depth	81° 29.17' N	30° 26.04' E	646.7
PS94/029-1	21.08.15	18:01:00	MOR	on ground/ max depth	81° 32.65' N	30° 50.83' E	883.5
PS94/030-1	21.08.15	20:02:00	CTD/UC	on ground/ max depth	81° 31.78' N	30° 47.55' E	831.5

Station	Date	Time	Gear	Action	PositionLat	PositionLon	Water depth [m]
PS94/030-2	21.08.15	21:12:00	CTD/RO	on ground/ max depth	81° 31.96' N	30° 46.89' E	841.0
PS94/030-3	21.08.15	22:14:00	MN	on ground/ max depth	81° 32.19' N	30° 48.71' E	852.0
PS94/030-4	21.08.15	23:41:00	LOKI	on ground/ max depth	81° 32.03' N	30° 50.22' E	842.5
PS94/030-4	22.08.15	00:06:00	LOKI	profile end	81° 32.18' N	30° 51.52' E	848.0
PS94/030-4	22.08.15	00:07:01	LOKI	profile start	81° 32.19' N	30° 51.58' E	847.2
PS94/031-1	22.08.15	02:57:00	CTD/RO	on ground/ max depth	81° 41.66' N	30° 55.02' E	2716.2
PS94/032-1	22.08.15	07:49:00	MN	on ground/ max depth	81° 51.71' N	30° 48.83' E	3175.2
PS94/032-3	22.08.15	11:13:00	HN	on ground/ max depth	81° 51.59' N	30° 49.76' E	3172.5
PS94/032-2	22.08.15	11:45:00	CTD/RO	on ground/ max depth	81° 51.58' N	30° 50.32' E	3172.0
PS94/032-4	22.08.15	14:35:00	CTD/UC	on ground/ max depth	81° 51.24' N	30° 53.60' E	3169.0
PS94/032-5	22.08.15	16:06:00	CTD/RO	on ground/ max depth	81° 50.90' N	30° 54.27' E	3166.5
PS94/032-6	22.08.15	17:20:00	LOKI	on ground/ max depth	81° 50.63' N	30° 53.85' E	3165.5
PS94/032-6	22.08.15	17:20:02	LOKI	profile start	81° 50.63' N	30° 53.85' E	3165.5
PS94/032-6	22.08.15	17:52:01	LOKI	profile end	81° 50.50' N	30° 53.55' E	3165.7
PS94/032-7	22.08.15	19:23:00	CTD/RO	on ground/ max depth	81° 50.49' N	30° 51.26' E	3167.5
PS94/032-8	22.08.15	22:06:00	ISP	on ground/ max depth	81° 50.83' N	30° 51.09' E	3168.5
PS94/032-8	23.08.15	03:01:59	ISP	on ground/ max depth	81° 51.38' N	30° 55.03' E	3162.2
PS94/032-9	23.08.15	03:30:00	CTD/RO	on ground/ max depth	81° 51.39' N	30° 54.94' E	3162.7
PS94/032-10	23.08.15	05:12:00	MUC	on ground/ max depth	81° 51.46' N	30° 53.80' E	3166.7
PS94/033-1	23.08.15	07:32:59	XCTD	on ground/ max depth	81° 57.85' N	30° 53.56' E	3194.2
PS94/034-1	23.08.15	09:33:00	CTD/RO	on ground/ max depth	82° 2.47' N	30° 55.54' E	3224.2
PS94/035-1	23.08.15	11:32:00	XCTD	on ground/ max depth	82° 6.56' N	30° 47.78' E	3283.7
PS94/035-1	23.08.15	11:45:00	XCTD	on ground/ max depth	82° 7.69' N	30° 46.83' E	3305.0
PS94/035-1	23.08.15	12:00:59	XCTD	on ground/ max depth	82° 8.10' N	30° 50.77' E	3302.5

Station	Date	Time	Gear	Action	PositionLat	PositionLon	Water depth [m]
PS94/036-1	23.08.15	14:17:00	CTD/L	on ground/ max depth	82° 13.07' N	30° 54.06' E	3326.7
PS94/036-2	23.08.15	16:25:00	CTD/RO	on ground/ max depth	82° 13.33' N	30° 53.46' E	3332.2
PS94/037-1	23.08.15	18:29:59	XCTD	on ground/ max depth	82° 18.52' N	30° 54.68' E	3400.0
PS94/038-1	23.08.15	20:50:00	CTD/L	on ground/ max depth	82° 23.56' N	30° 54.96' E	3464.5
PS94/039-1	23.08.15	23:32:59	XCTD	on ground/ max depth	82° 33.34' N	30° 53.01' E	3605.5
PS94/040-1	24.08.15	02:15:00	CTD/L	on ground/ max depth	82° 42.39' N	30° 55.06' E	3686.2
PS94/040-2	24.08.15	05:25:00	CTD/UC	on ground/ max depth	82° 42.42' N	30° 49.79' E	3695.2
PS94/040-3	24.08.15	07:19:00	CTD/L	on ground/ max depth	82° 42.53' N	30° 47.01' E	3701.0
PS94/040-4	24.08.15	08:26:00	LOKI	profile start	82° 42.64' N	30° 44.17' E	3706.7
PS94/040-4	24.08.15	08:26:01	LOKI	on ground/ max depth	82° 42.64' N	30° 44.17' E	3706.7
PS94/040-4	24.08.15	08:27:00	LOKI	profile end	82° 42.64' N	30° 44.12' E	3706.7
PS94/040-5	24.08.15	11:06:00	MN	on ground/ max depth	82° 43.20' N	30° 37.15' E	3722.5
PS94/041-1	24.08.15	15:25:59	XCTD	on ground/ max depth	82° 54.11' N	30° 55.40' E	3805.7
PS94/042-1	24.08.15	18:55:00	CTD/L	on ground/ max depth	83° 2.66' N	30° 50.46' E	3893.0
PS94/043-1	24.08.15	22:15:59	XCTD	on ground/ max depth	83° 13.28' N	30° 58.43' E	3957.0
PS94/044-1	25.08.15	02:23:00	CTD/L	on ground/ max depth	83° 22.68' N	30° 49.85' E	3969.5
PS94/045-1	25.08.15	05:50:59	XCTD	on ground/ max depth	83° 33.07' N	30° 57.78' E	4031.7
PS94/046-2	25.08.15	10:34:00	HN	on ground/ max depth	83° 42.88' N	30° 20.58' E	4052.5
PS94/046-3	25.08.15	13:13:00	CTD/L	on ground/ max depth	83° 42.29' N	30° 15.14' E	4052.7
PS94/046-4	25.08.15	16:03:00	CTD/RO	on ground/ max depth	83° 41.48' N	30° 5.55' E	4053.7
PS94/046-1	25.08.15	17:33:00	ICE	on ground/ max depth	83° 41.16' N	29° 58.53' E	4054.7
PS94/047-1	25.08.15	21:17:59	XCTD	on ground/ max depth	83° 53.17' N	31° 0.27' E	4013.5
PS94/048-1	26.08.15	00:52:00	CTD/RO	on ground/ max depth	84° 2.29' N	30° 45.52' E	4056.7
PS94/049-1	26.08.15	04:39:59	XCTD	on ground/ max depth	84° 13.11' N	30° 53.88' E	4056.0

Station	Date	Time	Gear	Action	PositionLat	PositionLon	Water depth [m]
PS94/050-1	26.08.15	09:05:00	CTD/RO	on ground/ max depth	84° 23.92' N	30° 42.91' E	4055.7
PS94/050-2	26.08.15	09:26:00	HN	on ground/ max depth	84° 23.90' N	30° 41.69' E	4055.5
PS94/050-3	26.08.15	12:21:00	CTD/UC	on ground/ max depth	84° 23.64' N	30° 32.65' E	4055.7
PS94/050-4	26.08.15	14:41:00	CTD/RO	on ground/ max depth	84° 23.29' N	30° 24.85' E	4055.7
PS94/050-5	26.08.15	17:23:00	ISP	on ground/ max depth	84° 23.02' N	30° 13.80' E	4055.7
PS94/050-6	26.08.15	23:02:00	CTD/RO	on ground/ max depth	84° 23.20' N	29° 55.83' E	4056.2
PS94/050-7	26.08.15	23:58:00	LOKI	on ground/ max depth	84° 23.19' N	29° 54.10' E	4056.5
PS94/050-7	27.08.15	00:28:00	LOKI	profile start	84° 23.18' N	29° 53.15' E	4056.2
PS94/050-7	27.08.15	00:28:01	LOKI	profile end	84° 23.18' N	29° 53.15' E	4056.2
PS94/050-8	27.08.15	00:57:00	CTD/RO	on ground/ max depth	84° 23.15' N	29° 52.19' E	4056.7
PS94/050-9	27.08.15	03:13:00	MN	on ground/ max depth	84° 23.00' N	29° 46.50' E	4056.5
PS94/050-10	27.08.15	07:10:00	MUC	on ground/ max depth	84° 23.08' N	29° 33.70' E	4039.5
PS94/051-1	27.08.15	15:33:59	XCTD	on ground/ max depth	84° 37.07' N	33° 33.47' E	3876.5
PS94/052-1	27.08.15	19:50:59	XCTD	on ground/ max depth	84° 46.96' N	37° 31.00' E	4027.0
PS94/053-1	28.08.15	00:43:59	XCTD	on ground/ max depth	84° 58.57' N	41° 19.37' E	4022.5
PS94/054-1	28.08.15	06:33:00	ICE	on ground/ max depth	85° 5.11' N	42° 37.05' E	4016.2
PS94/054-2	28.08.15	08:28:00	CTD/L	on ground/ max depth	85° 5.47' N	42° 31.97' E	4017.0
PS94/054-3	28.08.15	11:43:00	CTD/UC	on ground/ max depth	85° 5.91' N	42° 26.39' E	4017.2
PS94/054-4	28.08.15	13:40:00	CTD/RO	on ground/ max depth	85° 6.04' N	42° 22.96' E	4018.0
PS94/055-1	28.08.15	21:17:59	XCTD	on ground/ max depth	85° 5.08' N	46° 57.59' E	3943.5
PS94/056-1	29.08.15	01:36:59	XCTD	on ground/ max depth	85° 12.33' N	50° 20.12' E	3986.0
PS94/057-1	29.08.15	07:17:59	XCTD	on ground/ max depth	85° 14.35' N	54° 49.22' E	3963.5
PS94/058-1	29.08.15	15:24:00	CTD/L	on ground/ max depth	85° 16.79' N	60° 2.97' E	3928.0
PS94/058-2	29.08.15	19:28:00	MOR	on ground/ max depth	85° 17.52' N	60° 0.85' E	3928.5

Station	Date	Time	Gear	Action	PositionLat	PositionLon	Water depth [m]
PS94/058-3	29.08.15	20:19:00	CTD/L	on ground/ max depth	85° 17.81' N	59° 56.08' E	3929.2
PS94/058-4	29.08.15	21:29:00	LOKI	on ground/ max depth	85° 18.02' N	59° 56.14' E	3929.5
PS94/058-4	29.08.15	21:59:00	LOKI	profile end	85° 18.03' N	59° 56.16' E	3929.2
PS94/058-4	29.08.15	21:59:01	LOKI	profile start	85° 18.03' N	59° 56.16' E	3929.2
PS94/058-5	29.08.15	22:51:00	CTD/L	on ground/ max depth	85° 18.08' N	59° 56.53' E	3929.2
PS94/058-6	30.08.15	01:05:00	MN	on ground/ max depth	85° 18.10' N	59° 55.26' E	3929.7
PS94/058-7	30.08.15	05:15:00	CTD/UC	on ground/ max depth	85° 18.58' N	59° 49.32' E	3930.5
PS94/059-1	30.08.15	12:03:00	CTD/L	on ground/ max depth	85° 31.01' N	60° 22.15' E	3935.5
PS94/060-1	30.08.15	20:21:59	XCTD	on ground/ max depth	85° 39.05' N	60° 1.56' E	3935.5
PS94/061-1	31.08.15	02:08:00	CTD/L	on ground/ max depth	85° 50.15' N	60° 3.05' E	3929.2
PS94/062-1	31.08.15	17:14:00	CTD/L	on ground/ max depth	86° 8.16' N	59° 51.55' E	3914.2
PS94/062-2	31.08.15	21:25:00	CTD/UC	on ground/ max depth	86° 7.37' N	59° 48.58' E	3914.5
PS94/062-3	31.08.15	23:15:00	CTD/L	on ground/ max depth	86° 6.89' N	59° 48.46' E	3915.2
PS94/063-1	01.09.15	02:55:01	XCTD	on ground/ max depth	86° 17.65' N	59° 25.58' E	2583.0
PS94/063-1	01.09.15	03:04:59	XCTD	on ground/ max depth	86° 17.84' N	59° 34.01' E	2549.7
PS94/064-1	01.09.15	07:13:00	CTD/L	on ground/ max depth	86° 24.99' N	60° 12.41' E	2108.5
PS94/064-2	01.09.15	08:56:00	CTD/UC	on ground/ max depth	86° 24.92' N	60° 9.12' E	2104.2
PS94/065-1	01.09.15	12:10:59	XCTD	on ground/ max depth	86° 33.29' N	61° 21.78' E	2553.7
PS94/066-1	01.09.15	15:26:00	CTD/L	on ground/ max depth	86° 42.75' N	61° 21.65' E	674.0
PS94/066-2	01.09.15	16:30:00	GBG	on ground/ max depth	86° 42.61' N	61° 19.02' E	655.7
PS94/066-3	01.09.15	18:22:00	LOKI	on ground/ max depth	86° 42.72' N	61° 9.58' E	712.5
PS94/066-3	01.09.15	18:23:01	LOKI	profile start	86° 42.72' N	61° 9.55' E	718.0
PS94/066-3	01.09.15	18:44:00	LOKI	profile end	86° 42.68' N	61° 9.09' E	679.2
PS94/066-4	01.09.15	19:22:00	MN	on ground/ max depth	86° 42.60' N	61° 8.49' E	622.0

Station	Date	Time	Gear	Action	PositionLat	PositionLon	Water depth [m]
PS94/067-1	02.09.15	00:06:59	XCTD	on ground/ max depth	86° 51.04' N	60° 1.79' E	3293.7
PS94/068-1	02.09.15	05:11:00	CTD/L	on ground/ max depth	86° 59.81' N	58° 36.90' E	4908.2
PS94/069-1	02.09.15	08:05:00	ICE	on ground/ max depth	87° 0.45' N	58° 39.53' E	4752.0
PS94/069-1	02.09.15	08:16:00	ICE	on ground/ max depth	87° 0.41' N	58° 39.77' E	4753.0
PS94/069-2	02.09.15	10:17:00	CTD/UC	on ground/ max depth	86° 59.89' N	58° 43.84' E	4826.0
PS94/069-3	02.09.15	11:17:00	HN	on ground/ max depth	86° 59.59' N	58° 46.47' E	0.0
PS94/069-4	02.09.15	12:38:00	CTD/L	on ground/ max depth	86° 59.17' N	58° 49.01' E	4838.5
PS94/069-5	02.09.15	14:50:00	CTD/L	on ground/ max depth	86° 58.49' N	58° 50.37' E	4627.5
PS94/069-6	02.09.15	20:22:00	MOR	on ground/ max depth	87° 0.97' N	58° 15.52' E	4669.2
PS94/069-6	02.09.15	20:22:01	MOR	on ground/ max depth	87° 0.97' N	58° 15.52' E	4669.2
PS94/069-7	02.09.15	22:19:00	GKG	on ground/ max depth	86° 59.72' N	58° 10.23' E	4815.2
PS94/070-1	03.09.15	03:55:00	CTD/L	on ground/ max depth	86° 57.19' N	55° 49.57' E	3086.5
PS94/070-2	03.09.15	06:25:00	LOKI	on ground/ max depth	86° 57.17' N	55° 39.17' E	3113.0
PS94/070-2	03.09.15	06:26:00	LOKI	profile start	86° 57.17' N	55° 39.14' E	3114.2
PS94/070-2	03.09.15	06:57:00	LOKI	profile end	86° 57.18' N	55° 37.86' E	3113.7
PS94/070-3	03.09.15	08:40:00	MN	on ground/ max depth	86° 57.25' N	55° 34.19' E	3179.5
PS94/070-4	03.09.15	12:07:00	CTD/UC	on ground/ max depth	86° 57.21' N	55° 26.21' E	3253.7
PS94/070-5	03.09.15	14:29:00	GKG	on ground/ max depth	86° 56.93' N	55° 16.02' E	3652.2
PS94/070-6	03.09.15	16:18:00	GKG	on ground/ max depth	86° 56.80' N	55° 5.46' E	3653.7
PS94/071-1	03.09.15	20:37:59	XCTD	on ground/ max depth	87° 11.25' N	57° 58.77' E	3861.0
PS94/072-1	04.09.15	00:08:00	CTD/L	on ground/ max depth	87° 21.78' N	59° 39.80' E	3917.2
PS94/073-1	04.09.15	03:52:59	XCTD	on ground/ max depth	87° 31.41' N	60° 0.55' E	4180.0
PS94/074-1	04.09.15	07:18:00	CTD/L	on ground/ max depth	87° 41.54' N	59° 59.80' E	4075.7
PS94/075-1	04.09.15	10:41:59	XCTD	on ground/ max depth	87° 51.97' N	60° 15.66' E	4418.5

Station	Date	Time	Gear	Action	PositionLat	PositionLon	Water depth [m]
PS94/076-1	04.09.15	13:56:00	CTD/L	on ground/ max depth	88° 1.75' N	59° 52.76' E	4424.5
PS94/076-2	04.09.15	17:28:00	CTD/UC	on ground/ max depth	88° 1.83' N	59° 33.02' E	4424.0
PS94/076-3	04.09.15	19:32:00	CTD/RO	on ground/ max depth	88° 1.98' N	59° 27.24' E	4424.7
PS94/077-1	04.09.15	21:49:59	XCTD	on ground/ max depth	88° 10.34' N	60° 43.50' E	4422.2
PS94/078-1	05.09.15	01:25:00	CTD/L	on ground/ max depth	88° 21.05' N	59° 47.72' E	4418.5
PS94/079-1	05.09.15	06:29:59	XCTD	on ground/ max depth	88° 30.36' N	60° 50.39' E	4419.7
PS94/080-1	05.09.15	10:53:00	CTD/L	on ground/ max depth	88° 41.63' N	60° 10.71' E	4414.5
PS94/081-1	05.09.15	18:00:00	ICE	on ground/ max depth	88° 59.14' N	60° 57.98' E	4401.2
PS94/081-2	05.09.15	20:04:00	CTD/L	on ground/ max depth	88° 59.37' N	61° 3.80' E	4401.2
PS94/081-3	05.09.15	20:09:00	HN	on ground/ max depth	88° 59.38' N	61° 4.12' E	4401.2
PS94/081-4	05.09.15	23:19:00	CTD/UC	on ground/ max depth	88° 59.70' N	61° 14.76' E	4401.7
PS94/081-5	06.09.15	01:29:00	CTD/L	on ground/ max depth	88° 59.93' N	61° 16.76' E	4400.2
PS94/081-6	06.09.15	02:55:00	LOKI	on ground/ max depth	89° 0.13' N	61° 17.58' E	4400.0
PS94/081-6	06.09.15	02:55:01	LOKI	profile start	89° 0.13' N	61° 17.58' E	4400.0
PS94/081-6	06.09.15	03:28:00	LOKI	profile end	89° 0.22' N	61° 18.19' E	4400.0
PS94/081-7	06.09.15	04:00:00	CTD/L	on ground/ max depth	89° 0.30' N	61° 19.15' E	4399.7
PS94/081-8	06.09.15	06:18:00	MN	on ground/ max depth	89° 0.62' N	61° 26.15' E	4399.5
PS94/081-9	06.09.15	11:14:00	ISP	on ground/ max depth	89° 0.89' N	61° 44.12' E	4399.5
PS94/081-9	06.09.15	16:24:59	ISP	on ground/ max depth	89° 0.69' N	61° 43.50' E	4399.5
PS94/081-10	06.09.15	18:08:00	CTD/UC	on ground/ max depth	89° 0.58' N	61° 46.71' E	4399.5
PS94/082-1	06.09.15	22:11:59	XCTD	on ground/ max depth	89° 9.93' N	59° 56.74' E	4390.5
PS94/083-1	07.09.15	02:18:00	CTD/L	on ground/ max depth	89° 19.71' N	58° 45.16' E	4372.0
PS94/084-1	07.09.15	05:57:59	XCTD	on ground/ max depth	89° 30.16' N	60° 2.44' E	4352.2
PS94/085-1	07.09.15	11:17:00	CTD/L	on ground/ max depth	89° 38.95' N	58° 17.12' E	4329.7

Station	Date	Time	Gear	Action	PositionLat	PositionLon	Water depth [m]
PS94/086-1	07.09.15	16:27:59	XCTD	on ground/ max depth	89° 50.18' N	46° 52.51' E	4306.2
PS94/087-1	08.09.15	04:28:00	CTD/UC	on ground/ max depth	89° 55.81' N	120° 11.69' W	4263.5
PS94/087-2	08.09.15	07:25:00	MUC	on ground/ max depth	89° 54.97' N	121° 45.05' W	4262.2
PS94/088-1	08.09.15	12:07:59	XCTD	on ground/ max depth	89° 48.47' N	113° 16.01' W	4251.0
PS94/089-1	09.09.15	01:26:00	CTD/L	on ground/ max depth	89° 34.00' N	119° 27.46' W	4239.7
PS94/090-1	09.09.15	05:28:59	XCTD	on ground/ max depth	89° 24.14' N	119° 17.06' W	2306.7
PS94/091-1	09.09.15	09:38:00	CTD/L	on ground/ max depth	89° 10.00' N	116° 49.82' W	1342.7
PS94/091-2	09.09.15	11:01:00	CTD/UC	on ground/ max depth	89° 9.80' N	116° 40.79' W	1331.0
PS94/091-3	09.09.15	12:22:00	MN	on ground/ max depth	89° 9.59' N	116° 26.11' W	1323.2
PS94/091-4	09.09.15	14:16:00	LOKI	on ground/ max depth	89° 9.23' N	116° 0.87' W	1317.0
PS94/091-4	09.09.15	14:16:02	LOKI	profile start	89° 9.23' N	116° 0.87' W	1317.0
PS94/091-4	09.09.15	14:48:01	LOKI	profile end	89° 9.13' N	115° 53.76' W	1317.7
PS94/092-1	09.09.15	18:19:59	XCTD	on ground/ max depth	88° 57.17' N	112° 41.18' W	1376.2
PS94/093-1	09.09.15	19:24:00	ICE	on ground/ max depth	88° 54.60' N	112° 55.37' W	1710.2
PS94/093-1	09.09.15	19:41:00	ICE	on ground/ max depth	88° 54.59' N	112° 52.73' W	1691.2
PS94/094-1	10.09.15	09:12:00	CTD/L	on ground/ max depth	88° 42.53' N	118° 54.42' W	3996.0
PS94/095-1	10.09.15	17:14:59	XCTD	on ground/ max depth	88° 32.21' N	121° 2.99' W	3994.5
PS94/096-1	11.09.15	06:10:00	ICE	on ground/ max depth	88° 21.79' N	125° 10.06' W	3614.0
PS94/096-2	11.09.15	07:37:00	CTD/L	on ground/ max depth	88° 21.59' N	125° 5.65' W	3611.5
PS94/096-3	11.09.15	09:09:00	HN	on ground/ max depth	88° 21.38' N	125° 0.82' W	3597.0
PS94/096-4	11.09.15	10:43:00	CTD/UC	on ground/ max depth	88° 21.18' N	124° 55.77' W	3586.7
PS94/096-5	11.09.15	13:51:00	ISP	on ground/ max depth	88° 20.84' N	124° 46.60' W	3583.5
PS94/096-6	11.09.15	20:29:00	MN	on ground/ max depth	88° 20.25' N	124° 31.82' W	3579.2
PS94/096-7	11.09.15	23:02:00	CTD/L	on ground/ max depth	88° 20.29' N	124° 21.76' W	3574.2

Station	Date	Time	Gear	Action	PositionLat	PositionLon	Water depth [m]
PS94/096-8	12.09.15	00:11:00	LOKI	on ground/ max depth	88° 20.30' N	124° 16.36' W	3572.0
PS94/096-8	12.09.15	00:45:00	LOKI	profile start	88° 20.29' N	124° 13.67' W	3570.5
PS94/096-8	12.09.15	00:45:01	LOKI	profile end	88° 20.29' N	124° 13.67' W	3570.5
PS94/097-1	12.09.15	11:47:59	XCTD	on ground/ max depth	88° 19.29' N	143° 43.71' W	3804.0
PS94/098-1	12.09.15	13:22:59	ICE	on ground/ max depth	88° 20.17' N	144° 7.96' W	3806.5
PS94/099-1	12.09.15	20:59:00	CTD/UC	on ground/ max depth	88° 10.89' N	155° 49.49' W	3765.5
PS94/099-2	12.09.15	22:43:00	CTD/L	on ground/ max depth	88° 10.78' N	155° 45.58' W	3761.5
PS94/099-3	13.09.15	01:51:00	CTD/UC	on ground/ max depth	88° 10.96' N	155° 39.60' W	3763.0
PS94/100-1	13.09.15	11:09:01	XCTD	on ground/ max depth	87° 54.40' N	170° 0.11' W	3979.0
PS94/101-1	13.09.15	20:42:00	ICE	on ground/ max depth	87° 29.71' N	179° 54.70' E	3995.5
PS94/101-1	13.09.15	21:05:00	ICE	on ground/ max depth	87° 29.73' N	179° 53.72' E	3995.5
PS94/101-2	13.09.15	22:26:00	CTD/L	on ground/ max depth	87° 29.84' N	179° 50.47' E	3995.7
PS94/101-3	13.09.15	23:31:01	HN	on ground/ max depth	87° 29.96' N	179° 48.61' E	3995.7
PS94/101-4	14.09.15	01:23:00	CTD/UC	on ground/ max depth	87° 30.19' N	179° 47.89' E	3995.7
PS94/101-5	14.09.15	03:49:00	CTD/L	on ground/ max depth	87° 30.31' N	179° 50.78' E	3995.5
PS94/101-6	14.09.15	06:27:00	ISP	on ground/ max depth	87° 30.14' N	179° 52.45' E	3995.5
PS94/101-7	14.09.15	12:13:00	CTD/L	on ground/ max depth	87° 30.13' N	179° 49.96' E	3995.7
PS94/101-8	14.09.15	14:23:00	CTD/UC	on ground/ max depth	87° 30.15' N	179° 55.92' E	3995.5
PS94/101-9	14.09.15	16:15:00	CTD/L	on ground/ max depth	87° 29.95' N	179° 56.84' W	3995.2
PS94/101-10	14.09.15	17:46:00	MUC	on ground/ max depth	87° 29.70' N	179° 52.73' W	3995.2
PS94/102-1	15.09.15	07:50:00	ICE	on ground/ max depth	87° 15.92' N	164° 36.92' E	4006.2
PS94/103-1	15.09.15	09:40:59	XCTD	on ground/ max depth	87° 12.14' N	162° 2.13' E	3979.5
PS94/104-1	15.09.15	15:55:59	XCTD	on ground/ max depth	87° 2.99' N	153° 56.98' E	1925.5

Station	Date	Time	Gear	Action	PositionLat	PositionLon	Water depth [m]
PS94/105-1	15.09.15	22:34:00	CTD/L	on ground/ max depth	86° 58.66' N	146° 50.62' E	1000.7
PS94/105-2	15.09.15	23:54:00	GKG	on ground/ max depth	86° 58.61' N	146° 48.61' E	1001.0
PS94/106-1	16.09.15	06:03:59	XCTD	on ground/ max depth	86° 50.26' N	140° 16.06' E	2152.2
PS94/107-1	16.09.15	11:18:59	XCTD	on ground/ max depth	86° 39.89' N	134° 38.68' E	3380.7
PS94/107-2	16.09.15	13:47:59	ICE	on ground/ max depth	86° 37.66' N	133° 51.90' E	3701.7
PS94/108-1	16.09.15	17:28:59	XCTD	on ground/ max depth	86° 24.59' N	131° 2.67' E	4285.2
PS94/109-1	16.09.15	22:45:59	XCTD	on ground/ max depth	86° 3.11' N	126° 40.28' E	4381.2
PS94/110-1	17.09.15	04:11:59	XCTD	on ground/ max depth	85° 44.09' N	123° 37.91' E	4399.0
PS94/111-1	17.09.15	09:28:59	XCTD	on ground/ max depth	85° 24.82' N	120° 49.32' E	4417.7
PS94/112-2	17.09.15	13:22:59	XCTD	on ground/ max depth	85° 12.88' N	118° 23.83' E	4410.0
PS94/112-1	17.09.15	14:20:59	ICE	on ground/ max depth	85° 12.76' N	118° 25.59' E	4410.2
PS94/113-1	17.09.15	19:31:59	XCTD	on ground/ max depth	84° 54.26' N	115° 29.49' E	4425.0
PS94/114-1	17.09.15	23:42:59	XCTD	on ground/ max depth	84° 38.11' N	113° 22.67' E	4220.2
PS94/115-1	18.09.15	06:37:00	CTD/L	on ground/ max depth	84° 16.30' N	110° 41.30' E	4046.5
PS94/116-1	18.09.15	11:42:59	XCTD	on ground/ max depth	84° 24.76' N	112° 44.54' E	3181.2
PS94/117-1	18.09.15	18:24:00	ICE	on ground/ max depth	84° 33.80' N	115° 59.76' E	4380.7
PS94/117-2	18.09.15	20:06:00	CTD/L	on ground/ max depth	84° 33.62' N	115° 59.74' E	4400.2
PS94/117-3	18.09.15	23:37:00	CTD/UC	on ground/ max depth	84° 32.55' N	115° 57.65' E	4320.2
PS94/117-4	19.09.15	01:44:00	CTD/L	on ground/ max depth	84° 31.74' N	115° 53.22' E	4272.0
PS94/117-5	19.09.15	04:24:00	MN	on ground/ max depth	84° 30.88' N	115° 45.44' E	4240.2
PS94/117-6	19.09.15	07:28:00	CTD/L	on ground/ max depth	84° 30.41' N	115° 40.75' E	4217.2
PS94/117-7	19.09.15	09:31:00	ISP	on ground/ max depth	84° 29.84' N	115° 42.29' E	4214.7
PS94/117-8	19.09.15	11:50:01	HN	on ground/ max depth	84° 28.78' N	115° 42.70' E	4170.0

Station	Date	Time	Gear	Action	PositionLat	PositionLon	Water depth [m]
PS94/117-9	19.09.15	16:00:59	ICE	on ground/ max depth	84° 31.36' N	116° 8.95' E	4350.7
PS94/118-1	19.09.15	23:58:00	CTD/L	on ground/ max depth	84° 39.72' N	119° 47.53' E	4395.5
PS94/119-1	20.09.15	10:20:00	CTD/UC	on ground/ max depth	84° 48.77' N	123° 53.59' E	4385.5
PS94/119-2	20.09.15	13:42:59	ICE	on ground/ max depth	84° 51.64' N	124° 11.71' E	4385.5
PS94/120-1	20.09.15	17:59:59	XCTD	on ground/ max depth	84° 55.52' N	128° 23.42' E	4358.2
PS94/121-1	21.09.15	00:22:00	CTD/L	on ground/ max depth	85° 0.85' N	132° 55.90' E	4318.0
PS94/121-2	21.09.15	04:14:00	CTD/UC	on ground/ max depth	85° 0.74' N	132° 43.92' E	4322.0
PS94/122-1	21.09.15	12:35:59	XCTD	on ground/ max depth	85° 6.71' N	135° 21.88' E	4281.2
PS94/123-1	21.09.15	18:24:00	CTD/L	on ground/ max depth	85° 3.85' N	137° 38.09' E	4089.5
PS94/123-2	21.09.15	21:19:00	MUC	on ground/ max depth	85° 3.18' N	137° 33.08' E	4113.0
PS94/124-1	22.09.15	02:57:59	XCTD	on ground/ max depth	85° 5.12' N	140° 0.47' E	3904.2
PS94/125-1	22.09.15	04:07:00	ICE	on ground/ max depth	85° 4.96' N	139° 57.38' E	3913.0
PS94/125-2	22.09.15	05:44:00	CTD/L	on ground/ max depth	85° 5.13' N	139° 58.72' E	3906.0
PS94/125-3	22.09.15	09:40:00	CTD/UC	on ground/ max depth	85° 4.85' N	139° 54.12' E	3919.5
PS94/125-4	22.09.15	11:10:00	HN	on ground/ max depth	85° 4.87' N	139° 48.07' E	3923.0
PS94/125-4	22.09.15	11:13:00	HN	on ground/ max depth	85° 4.88' N	139° 47.88' E	3923.7
PS94/125-5	22.09.15	11:38:00	CTD/L	on ground/ max depth	85° 4.93' N	139° 46.37' E	3920.2
PS94/125-6	22.09.15	13:45:00	MN	on ground/ max depth	85° 5.37' N	139° 40.83' E	3910.0
PS94/125-7	22.09.15	16:30:00	CTD/L	on ground/ max depth	85° 5.87' N	139° 37.60' E	3904.5
PS94/125-8	22.09.15	18:53:00	ISP	on ground/ max depth	85° 5.86' N	139° 36.09' E	3905.5
PS94/126-1	23.09.15	06:22:59	XCTD	on ground/ max depth	85° 4.20' N	143° 1.86' E	3292.7
PS94/127-1	23.09.15	08:01:59	XCTD	on ground/ max depth	85° 4.67' N	144° 43.83' E	2595.7
PS94/128-1	23.09.15	11:19:00	CTD/L	on ground/ max depth	85° 3.84' N	146° 56.54' E	1252.0

Station	Date	Time	Gear	Action	PositionLat	PositionLon	Water depth [m]
PS94/129-1	23.09.15	16:50:59	XCTD	on ground/ max depth	85° 1.39' N	149° 13.40' E	1734.5
PS94/130-1	23.09.15	21:34:00	CTD/L	on ground/ max depth	85° 0.93' N	151° 45.35' E	860.5
PS94/130-2	23.09.15	22:45:00	CTD/UC	on ground/ max depth	85° 1.02' N	151° 41.23' E	868.0
PS94/130-3	23.09.15	23:47:00	MN	on ground/ max depth	85° 1.22' N	151° 38.00' E	867.0
PS94/130-4	24.09.15	01:05:00	MUC	on ground/ max depth	85° 1.58' N	151° 35.41' E	866.5
PS94/131-1	24.09.15	04:45:59	XCTD	on ground/ max depth	84° 58.40' N	153° 51.88' E	1614.2
PS94/132-1	24.09.15	07:26:00	CTD/L	on ground/ max depth	85° 1.37' N	155° 13.15' E	2509.2
PS94/133-1	24.09.15	12:34:59	XCTD	on ground/ max depth	84° 58.47' N	157° 14.15' E	2503.7
PS94/134-1	24.09.15	15:40:00	CTD/L	on ground/ max depth	84° 50.66' N	159° 1.48' E	3170.2
PS94/134-2	24.09.15	18:26:00	CTD/UC	on ground/ max depth	84° 50.53' N	159° 2.68' E	3180.7
PS94/135-1	25.09.15	06:26:00	ICE	on ground/ max depth	83° 30.07' N	154° 56.58' E	2779.0
PS94/135-2	25.09.15	06:45:59	XCTD	on ground/ max depth	83° 29.99' N	154° 55.75' E	2778.5
PS94/136-1	25.09.15	08:01:59	XCTD	on ground/ max depth	83° 19.66' N	154° 44.94' E	2785.5
PS94/137-1	25.09.15	10:06:59	XCTD	on ground/ max depth	83° 2.04' N	154° 11.40' E	2800.2
PS94/138-1	25.09.15	13:45:59	XCTD	on ground/ max depth	82° 41.05' N	151° 52.20' E	2790.2
PS94/139-1	25.09.15	15:44:59	XCTD	on ground/ max depth	82° 22.93' N	150° 31.22' E	2796.5
PS94/140-1	25.09.15	18:56:59	XCTD	on ground/ max depth	82° 1.03' N	148° 24.31' E	2665.5
PS94/141-1	25.09.15	21:23:59	XCTD	on ground/ max depth	81° 42.44' N	146° 59.68' E	2557.2
PS94/142-1	25.09.15	23:23:59	XCTD	on ground/ max depth	81° 21.32' N	145° 49.49' E	2291.7
PS94/143-1	26.09.15	01:28:59	XCTD	on ground/ max depth	80° 58.52' N	144° 31.91' E	1871.5
PS94/144-1	04.10.15	17:36:59	FLOAT	on ground/ max depth	74° 0.06' N	6° 21.61' E	2225.7
PS94/145-1	05.10.15	06:54:00	GLD	on ground/ max depth	75° 33.35' N	2° 39.66' W	3715.7
PS94/146-1	05.10.15	10:27:00	GLD	on ground/ max depth	75° 23.44' N	1° 8.56' W	3749.7

Station	Date	Time	Gear	Action	PositionLat	PositionLon	Water depth [m]
PS94/147-1	06.10.15	18:13:00	CTD/RO	on ground/ max depth	75° 0.46' N	24° 15.10' E	150.7
PS94/147-2	06.10.15	18:43:00	CTD/UC	on ground/ max depth	75° 0.39' N	24° 15.43' E	151.5
PS94/147-3	06.10.15	19:15:00	MN	on ground/ max depth	75° 0.37' N	24° 15.75' E	150.7
PS94/148-1	06.10.15	22:20:59	XCTD	on ground/ max depth	74° 36.04' N	23° 57.66' E	209.5
PS94/149-1	07.10.15	00:35:00	CTD/RO	on ground/ max depth	74° 19.14' N	23° 48.38' E	303.0
PS94/149-2	07.10.15	01:16:00	CTD/UC	on ground/ max depth	74° 19.40' N	23° 48.24' E	305.0
PS94/149-3	07.10.15	01:57:00	MN	on ground/ max depth	74° 19.37' N	23° 47.63' E	304.5
PS94/149-4	07.10.15	02:51:00	CTD/RO	on ground/ max depth	74° 19.28' N	23° 46.31' E	303.2
PS94/149-5	07.10.15	03:25:00	MUC	on ground/ max depth	74° 19.32' N	23° 45.25' E	301.5
PS94/149-6	07.10.15	03:54:00	MUC	on ground/ max depth	74° 19.43' N	23° 44.18' E	300.5
PS94/150-1	07.10.15	05:15:59	XCTD	on ground/ max depth	74° 9.81' N	23° 43.52' E	415.7
PS94/151-1	07.10.15	06:19:59	XCTD	on ground/ max depth	74° 0.45' N	23° 36.15' E	456.5
PS94/152-1	07.10.15	07:21:59	XCTD	on ground/ max depth	73° 51.38' N	23° 28.48' E	466.2
PS94/153-1	07.10.15	08:47:00	CTD/RO	on ground/ max depth	73° 42.44' N	23° 21.65' E	460.0
PS94/153-2	07.10.15	09:35:00	CTD/UC	on ground/ max depth	73° 42.45' N	23° 21.60' E	460.0
PS94/153-3	07.10.15	10:17:00	MN	on ground/ max depth	73° 42.42' N	23° 21.49' E	460.2
PS94/153-4	07.10.15	11:18:00	CTD/RO	on ground/ max depth	73° 42.42' N	23° 21.57' E	459.2
PS94/153-5	07.10.15	12:24:00	BN	profile start	73° 42.46' N	23° 21.74' E	459.0
PS94/153-5	07.10.15	12:24:01	BN	profile end	73° 42.46' N	23° 21.74' E	459.0
PS94/153-6	07.10.15	13:16:01	ISP	on ground/ max depth	73° 42.31' N	23° 21.82' E	461.7
PS94/154-1	07.10.15	18:06:59	XCTD	on ground/ max depth	73° 35.33' N	23° 18.21' E	450.2
PS94/155-1	07.10.15	18:48:59	XCTD	on ground/ max depth	73° 29.13' N	23° 13.72' E	445.5
PS94/156-1	07.10.15	19:33:59	XCTD	on ground/ max depth	73° 22.57' N	23° 8.74' E	427.2
PS94/157-1	07.10.15	20:43:00	CTD/RO	on ground/ max depth	73° 15.15' N	23° 4.27' E	415.0

Station	Date	Time	Gear	Action	PositionLat	PositionLon	Water depth [m]
PS94/157-2	07.10.15	21:28:00	CTD/UC	on ground/ max depth	73° 15.24' N	23° 4.42' E	415.2
PS94/157-3	07.10.15	22:17:00	MN	on ground/ max depth	73° 15.20' N	23° 4.34' E	416.7
PS94/158-1	07.10.15	23:30:59	XCTD	on ground/ max depth	73° 7.80' N	23° 1.14' E	409.5
PS94/159-1	08.10.15	00:18:59	XCTD	on ground/ max depth	73° 0.39' N	22° 57.57' E	410.2
PS94/160-1	08.10.15	01:17:59	XCTD	on ground/ max depth	72° 51.57' N	22° 53.23' E	405.5
PS94/161-1	08.10.15	02:32:00	CTD/RO	on ground/ max depth	72° 44.08' N	22° 49.27' E	395.2
PS94/161-2	08.10.15	03:18:00	CTD/UC	on ground/ max depth	72° 44.06' N	22° 49.30' E	395.0
PS94/161-3	08.10.15	04:03:00	MN	on ground/ max depth	72° 44.08' N	22° 49.22' E	394.2
PS94/161-4	08.10.15	04:48:00	CTD/RO	on ground/ max depth	72° 44.07' N	22° 49.24' E	395.0
PS94/161-5	08.10.15	10:03:00	ISP	on ground/ max depth	72° 44.09' N	22° 49.38' E	395.2
PS94/161-6	08.10.15	10:20:00	MUC	on ground/ max depth	72° 44.04' N	22° 49.56' E	394.7
PS94/162-1	08.10.15	11:30:59	XCTD	on ground/ max depth	72° 36.96' N	22° 46.35' E	382.2
PS94/163-1	08.10.15	12:43:59	XCTD	on ground/ max depth	72° 27.16' N	22° 41.11' E	333.5
PS94/164-1	08.10.15	13:46:59	XCTD	on ground/ max depth	72° 18.72' N	22° 35.99' E	317.2
PS94/165-1	08.10.15	15:19:00	CTD/RO	on ground/ max depth	72° 9.42' N	22° 29.81' E	328.7
PS94/166-1	08.10.15	17:02:59	XCTD	on ground/ max depth	71° 59.31' N	22° 24.28' E	372.0
PS94/167-1	08.10.15	18:10:59	XCTD	on ground/ max depth	71° 49.93' N	22° 18.58' E	374.5
PS94/168-1	08.10.15	19:13:59	XCTD	on ground/ max depth	71° 41.21' N	22° 13.46' E	372.5
PS94/169-1	08.10.15	20:36:00	CTD/RO	on ground/ max depth	71° 33.93' N	21° 54.44' E	357.5
PS94/169-2	08.10.15	22:29:00	CTD/RO	on ground/ max depth	71° 34.04' N	21° 54.75' E	358.2
PS94/169-3	08.10.15	23:11:00	CTD/UC	on ground/ max depth	71° 34.00' N	21° 54.57' E	356.7
PS94/170-1	09.10.15	01:02:59	XCTD	on ground/ max depth	71° 21.62' N	21° 52.01' E	315.5
PS94/171-1	09.10.15	01:53:59	XCTD	on ground/ max depth	71° 14.75' N	21° 38.76' E	299.7

Station	Date	Time	Gear	Action	PositionLat	PositionLon	Water depth [m]
PS94/172-1	09.10.15	02:46:59	XCTD	on ground/ max depth	71° 7.42' N	21° 25.91' E	218.0
PS94/173-1	09.10.15	03:56:00	CTD/RO	on ground/ max depth	70° 59.98' N	21° 11.96' E	174.5
PS94/173-2	09.10.15	04:27:00	CTD/UC	on ground/ max depth	70° 59.96' N	21° 11.57' E	175.5

Gear abbreviations:

Argo	Deployment of Argo float
CTD/L	Large Conductivity/Temperature/Depth and water sampler system
CTD/RO	Conductivity/Temperature/Depth system with water sampler caroussel
CTD/UC	Ultra-clean Conductivity/Temperature/Depth and water sampler system
CTD/UW	Towed Underway Conductivity/Temperature/Depth system
GKG	Box corer
Glider	Recovery of glider
HN	Hand net
ICE	Ice station
ISP	In-situ pumps
LOKI	Lightframe On-sight Key species Investigation system
MN	Multi-net
MOR	Mooring deployment
MUC	Multi corer
XCTD	Expandable CTD

Die **Berichte zur Polar- und Meeresforschung** (ISSN 1866-3192) werden beginnend mit dem Band 569 (2008) als Open-Access-Publikation herausgegeben. Ein Verzeichnis aller Bände einschließlich der Druckausgaben (ISSN 1618-3193, Band 377-568, von 2000 bis 2008) sowie der früheren **Berichte zur Polarforschung** (ISSN 0176-5027, Band 1-376, von 1981 bis 2000) befindet sich im electronic Publication Information Center **(ePIC)** des Alfred-Wegener-Instituts, Helmholtz-Zentrum für Polar- und Meeresforschung (AWI); see http://epic.awi.de. Durch Auswahl “Reports on Polar- and Marine Research“ (via “browse”/”type”) wird eine Liste der Publikationen, sortiert nach Bandnummer, innerhalb der absteigenden chronologischen Reihenfolge der Jahrgänge mit Verweis auf das jeweilige pdf-Symbol zum Herunterladen angezeigt.

The **Reports on Polar and Marine Research** (ISSN 1866-3192) are available as open access publications since 2008. A table of all volumes including the printed issues (ISSN 1618-3193, Vol. 377-568, from 2000 until 2008), as well as the earlier **Reports on Polar Research** (ISSN 0176-5027, Vol. 1-376, from 1981 until 2000) is provided by the electronic Publication Information Center **(ePIC)** of the Alfred Wegener Institute, Helmholtz Centre for Polar and Marine Research (AWI); see URL http://epic.awi.de. To generate a list of all Reports, use the URL http://epic.awi.de and select “browse”/ ”type” to browse ”Reports on Polar and Marine Research”. A chronological list in declining order will be presented, and pdf-icons displayed for downloading.

Zuletzt erschienene Ausgaben:

Recently published issues:

703 (2016) The Expedition PS94 of the Research Vessel POLARSTERN to the central Arctic Ocean in 2015, edited by Ursula Schauer

702 (2016) The Expeditions PS95.1 and PS95.2 of the Research Vessel POLARSTERN to the Atlantic Ocean in 2015, edited by Rainer Knust and Karin Lochte

701 (2016) The Expedition PS97 of the Research Vessel POLARSTERN to the Drake Passage in 2016, edited by Frank Lamy

700 (2016) The Expedition PS96 of the Research Vessel POLARSTERN to the southern Weddell Sea in 2015/2016, edited by Michael Schröder

699 (2016) Die Tagebücher Alfred Wegeners zur Danmark-Expedition 1906/08, herausgegeben von Reinhard A. Krause

698 (2016) The Expedition SO246 of the Research Vessel SONNE to the Chatham Rise in 2016, edited by Karsten Gohl and Reinhard Werner

697 (2016) Studies of Polygons in Siberia and Svalbard**,** edited by Lutz Schirrmeister, Liudmila Pestryakova, Andrea Schneider and Sebastian Wetterich

696 (2016) The Expedition PS88 of the Research Vessel POLARSTERN to the Atlantic Ocean in 2014, edited by Rainer Knust and Frank Niessen

695 (2016) The Expedition PS93.1 of the Research Vessel POLARSTERN to the Arctic Ocean in 2015, edited by Ruediger Stein

694 (2016) The Expedition PS92 of the Research Vessel POLARSTERN to the Arctic Ocean in 2015, edited by Ilka Peeken

693 (2015) The Expedition PS93.2 of the Research Vessel POLARSTERN to the Fram Strait in 2015, edited by Thomas Soltwedel

ALFRED-WEGENER-INSTITUT
HELMHOLTZ-ZENTRUM FÜR POLAR-
UND MEERESFORSCHUNG

BREMERHAVEN

Am Handelshafen 12
27570 Bremerhaven
Telefon 0471 4831-0
Telefax 0471 4831-1149
www.awi.de

HELMHOLTZ
GEMEINSCHAFT